Suspended Sediment and Light Attenuation Characteristics in Singapore Waters

MSc. Thesis

7 November 2012

Toh Han Loong

This MSc. thesis is submitted for the partial fulfilment for the award of the MSc. Hydraulic Engineering and Water Resource Management from National University of Singapore (NUS) and MSc. Civil Engineering (Hydraulic Engineering) from Technical University of Delft (TUD).

NATIONAL UNIVERSITY OF SINGAPORE (NUS)
DEPARTMENT OF CIVIL & ENVIRONMENTAL ENGINEERING, FACULTY OF ENGINEERING

(NUS Student Number: A0078711)

DELFT UNIVERSITY OF TECHNOLOGY (TUD)
FACULTY OF CIVIL ENGINEERING AND GEOSCIENCES

(TUD Student Number: 4131061)

SUPERVISORY COMMITTTEE:	*Dr. ir. J. C. Winterwerp (TUD)* *Dr. Liew Soo Chin (NUS)* *Dr. ir. Bas Van Maren (TUD/DELTARES)* *Dr.ir. P.J. Visser (TUD)* *Dr. Pavel Tkalich (NUS)*
CONTACT	*Toh Han Loong* *themole_7@msn.com*

Cover: Image of the sun, sea and sand, representing the three main components in this thesis. Photography courtesy of http://www.wallpaperseek.com/blog/tag/sun-rise-wallpaper/

Acknowledgement

The author would like to thank the supervisory committee for their guidance and for the flexibility to shape the direction of this thesis; Dr. ir. J. C. Winterwerp (TUD), Dr Liew Soo Chin (NUS), Dr. D. S. Van Maren (TUD and Deltares), Dr.ir. P.J. Visser (TUD) and Dr. Pavel Tkalich (NUS). Specifically, the author is indebted to Dr Liew Soo Chin for input on data analysis and underwater light field modelling ("the data will tell you something if you stared at it long enough"). Many thanks also to Dr. D. S. Van Maren for invaluable help on the visibility modelling and whom inspired the author on light and sediment dynamics as a subject ("you will repeat a few cycles of understanding and not' while modelling").

Thanks also to Dr. Chang Chew Wai and Boredin Saengtuksin from the Centre for Remote Imaging, Sensing and Processing (CRISP) for their support during field and laboratory investigation. Thanks similarly to A/Prof Vladan Babovic and the staffs from Singapore - Delft Water Alliance (SDWA) for all their support during the duration of the MSc. Double Degree Program. Likewise, thanks too to the research staffs in the Aquatic Science Centre of SDWA for the approval and assistance to use their facilities for chlorophyll analysis. Finally, special mention is reserved for those who make all that seems impossible possible - family and friends, for the direct and indirect help, support and motivations.

The author had travelled to the least travelled places in Singapore during the field measurement; it was an inspiring, although sometimes intimidating due to the occasional police queries. During the tail end of writing, one anonymous anecdote was always on the author's mind; when asked when he knows that he had finished polishing his woodwork, the carpenter says 'It's never done, one day they just came and take it away!' Similarly, instead of continuing to improve, the author realises that at some point this thesis must be ended to pursue a more challenging paths that awaits. Finally, the author hopes that this thesis will be beneficial and pleased that it is available to all since it is not under the guise of confidentiality due to its open source nature.

All the mistakes are from the author.

Toh Han Loong
7 October 2012

Abstract

Light is attenuated by materials present in the water column by scattering and absorption. The knowledge of light attenuation and its contributing factors influencing visibility/turbidity is unknown in Singapore waters. This MSc thesis consists of field measurement, laboratory experiment and numerical modelling in 3 parts; parameterisation of light attenuation coefficient K_d, numerical modelling of underwater light field and visibility. The objectives of this thesis are; a) to determine the dynamics of optical properties in Singapore waters, b) to investigate factors contributing to light attenuation in Singapore waters and c) to model underwater light field and visibility using Hydrolight and Delft3D WAQ. This first part addresses the dynamics of light attenuation (in relation to low/high tide), the spectral nature of optically significant constituents (water, CDOM, phytoplankton and sediment) as well as the effects of particle size distribution (PSD) to light scattering. For PSD with a higher slope j in $N(D) = KD^{-j}$, the d_{50} ranges from 7.11 to 9.90 µm in Singapore Strait representing sediment dominated environment. Higher TSS during low tide is advection dominated while lower TSS during high tide is suspension dominated. Relative contributions of CDOM, chlorophyll and sediment to light attenuation coefficient K_d is 1.4 – 6.5 % (average of 3.3 %), 1.3 – 62 % (average of 24 %) and 31.3 – 95.2 % (average of 70 %) respectively. Four (4) empirical equations to predict K_d was developed depending on its optical and physical characteristics. Underwater light field modelling shows that light attenuation depend mostly on the concentration of optically significant constituents and only weakly dependent on light structure, cloud cover and fluorescence. The modelled K_d from Hydrolight ranges from 1.2 to 2.3 m^{-1} with lower K_d in chlorophyll dominated waters while the empirical estimations underestimate $K_{d(PAR)}$ compared to the modelled K_d from Hydrolight. The modelled Secchi depth, S_d ranges from 0.6 – 1.4m corresponding to euphotic depth z_{eu} of 2.0 – 3.8 m with deeper z_{eu} for chlorophyll dominated waters. The modelled visibility is generally lowest during NE followed by SW monsoon and IM period with evidence of spatial homogeneity for all monsoons. The visibility model reproduces the recorded S_d reasonably well except for Johor Strait and sheltered areas in WCP due to the fact that some processes are not unaccounted in the model. The K_d variation coincides with SSC variation with no phase difference; the visibility is lowest during spring low tide and highest during neap high tide. Convective interaction between the diurnal and semidiurnal components is important in offshore locations while the non-linearity of tidal propagation contributes in the shallow water of Johor estuary. The residual turbidity in Singapore waters is due to tides (semi diurnal and diurnal spring neap interactions) and non-tides (monsoonal effect) in approximately equal magnitude during monsoons. The results from this thesis are applicable in coastal engineering, ecological and remote sensing.

Contents

List of Figures

List of Tables

List of Symbols

a	Absorption coefficient (m^{-1})
a_{w}	Seawater absorption coefficient (m^{-1})
a_{s}	Sediment absorption coefficient (m^{-1})
a_{p}	Phytoplankton absorption coeff. (m^{-1})
a_{g}	CDOM absorption coefficient (m^{-1})
a_c^*	Specific chlorophyll absorption coefficient (m^2g^{-1})
a_s^*	Specific sediment absorption coefficient (m^2g^{-1})
b	Scattering coefficient (m^{-1})
b_{w}	Seawater scattering coefficient (m^{-1})
b_{s}	Sediment scattering coefficient (m^{-1})
b_{p}	Phytoplankton scattering coeff. (m^{-1})
$\mathrm{b}_{\mathrm{TSS}}^*$	Particles mass-specific scattering coefficient (m^2g^{-1})
b_c^*	Specific chlorophyll scattering coefficient (m^2g^{-1})
b_s^*	Specific sediment scattering coefficient (m^2g^{-1})
b_b	Backward scattering coefficient (m^{-1})
β	Volume scattering function
c	Beam attenuation coefficient (m^{-1})
$\bar{c}$	Mean spectral beam attenuation (m^{-1})
δ	Solar declination (°)
D_{50}	Mean particle size (μm)
E	Irradiance (w m^{-2})
E_d	Downward irradiance (w m^{-2})
E_u	Upward irradiance (w m^{-2})
F	Form Number
H_s	Significant wave height (m)
I	Radiant intensity (w sr^{-1})
j	Slope parameter for Junge distribution
K_d	Light attenuation coefficient (m^{-1})
$\overline{K_d}$	Mean light attenuation coefficient (m^{-1})
$K_{d(PAR)}$	Attenuation coefficient (PAR range)
K_w	Partial light attenuation due to water (m^{-1})
K_s	Partial light attenuation due to sediment (m^{-1})
K_p	Partial light attenuation due to phytoplankton (m^{-1})
K_g	Partial light attenuation due to CDOM (m^{-1})
K_1	Lunar-solar declinational component
L	Radiance (W m^{-2} sr^{-1})
λ	Wavelength (nm)
μ_o	Angle between solar beam and the vertical
M_2	Semidiurnal lunar component
n	Refractive index of particles
N	Number of particles per unit volume
O_1	Principal lunar component
θ	Zenith angle (polar angle of a light beam and the upwards vertical)
p	Phase function
φ	Azimuth angle (the angle of a light beam and the vertical plane).
Φ	Radiant flux (W/J s^{-1})
Q_{abs}	Efficiency factor for absorption
$Q_{scat}.$	Efficiency factor for scattering
Q_{att}	Efficiency factor for attenuation
R	Reflectance (sr^{-1})
R^2	Correlation coefficient
S_d	Secchi depth (m)
S	Exponential slope for CDOM absorption (nm^{-1})
S_2	Semidiurnal solar component
T	Period (s)
γ^b	Exponent of power law for scattering spectrum
z_{eu}	Euphotic depth (m)

List of Notations

AOP	*Apparent Optical Properties*
CDOM	*Chromophoric Dissolved Organic Matter*
DOM	*Dissolved Organic Matter*
ECP	*East Coast Park (sampling location)*
EFDC	*Environmental Fluid Dynamics Code*
EMP	*Environmental Management Programs*
IM	*Inter monsoon*
IOP	*Inherent Optical Properties*
LCK	*Lim Chu Kang (sampling location)*
NE	*Northeast monsoon*
NEUTRO	*Eutrophication model*
NTU	*Nephelometric Turbidity Unit*
PAR	*Photosynthetically Active Radiation*
PSD	*Particle Size Distribution*
POC	*Particulate Organic Content (mg/l)*
POM	*Princeton Ocean Model*
RTE	*Radiative Transfer Equation*
SFU	*Standardised Fluorescence Units*
SRM	*Singapore Regional Model*
SRMRA	*Singapore Regional Model Refined and Aligned*
SSC	*Suspended Sediment Concentration*
SSM	*Suspended Sediment Module*
SW	*Southwest monsoon*
TSS	*Total Suspended Solids (mg/l)*
VSF	*Volume Scattering Function*
UV	*Ultraviolent*
WAQ	*Water Quality Model*
WCP	*West Coast Park (sampling location)*

Suspended Sediment and Light Attenuation Characteristics in Singapore Waters

CHAPTER 1.0: INTRODUCTION

Anthropogenic disturbances such as eutrophication, dredging/reclamation operation and soil erosion due to the deforestation of river catchments increases suspended and dissolved matter in coastal waters. This disturbance causes an increase in turbidity, which lead to the reduction in visibility. Turbidity increase causes benthic smothering to marine ecosystems, irritation of fish gills and transport of absorbed contaminants adversely affecting public health (Prandle, 2000) and recreational value of the coastal waters. The most important impact due to increased turbidity is related to its light attenuation potential, which reduces visual range in water and light availability for photosynthesis. The non-trivial relationship between turbidity and light attenuation is investigated in this thesis using combination of field measurement, semi-analytical calculations and numerical modelling. Specifically, the role of suspended sediment in attenuating light is a central theme in this thesis.

Previous studies (elaborated in Section 2.3) and anecdotal evidence points to the deterioration of the water quality in Singapore waters (i.e. increased turbidity corresponding to reduced visibility). However, processes responsible for the increased turbidity and its impact to light attenuation are poorly quantified. It is generally assumed that the increased turbidity is due to the apparent increase in suspended sediment concentration (SSC), but there is not a single study that quantifies the contribution of SSC to light attenuation. The deduction that the increase in SSC causes increased turbidity is an oversimplification of the natural system without a sound scientific basis. Increase in turbidity can also be caused by algal blooms, sewage discharge, bio-fouling of turbidity sensors etc. (Erftemeijer and Lewis, 2006). Therefore the presumption that suspended sediment is the single factor influencing visibility in Singapore waters is yet to be proven.

1.1 Research Motivation

This MSc thesis consists of 3 components. The first is the parameterisation of light attenuation coefficient while the second and third is the numerical modelling of underwater light field and visibility respectively. The quantitative study of underwater light fields in coastal waters has important applications in engineering, ecology and remote sensing. It is important to understand underwater light fields for:

a) *Monitoring/optimisation of dredging operations (to achieve minimum light attenuation during the dredging programme). Furthermore, underwater light field also influence visibility under water, which is important for underwater engineering operations.*
b) *Determining the rates of photosynthesis by phytoplankton and other organisms for Environmental Management Programs (EMP) which plays an important role in climate change/ecological studies.*
c) *Determine the volume reflectance of seawater which is important for remote sensing applications in coastal ecosystem surveying, monitoring and predicting.*

1.2.1 Thesis objectives

The main objective of this thesis is to investigate the factors contributing to light attenuation focusing on the role of suspended sediment. The following is the specific objectives:

a) To determine the dynamics of optical properties in Singapore waters
b) To investigate factors contributing to light attenuation in Singapore waters
c) To model the underwater light field and visibility using numerical model

1.2.2 Research questions

This MSc thesis was designed to test the following hypotheses: the suspended sediment is the single most dominant factor influencing light attenuation in Singapore waters. The following is the relevant research questions that this thesis will answer:

a) What is the relative importance of absorption and scattering in modifying light attenuation coefficient, K_d in Singapore waters?
b) Can turbidity be used to estimate scattering coefficient (b) of water samples?
c) Is SSC the single most dominant factor explaining the variation in K_d?
d) To what extent CDOM and phytoplankton play a role in light attenuation?
e) What is the effect of particle size distribution (PSD) to scattering coefficient and K_d?
f) How important is the physical forcing (i.e. tides) in determining visibility vis-a vis suspended sediment dynamics?

*The outline of this MSc thesis is as follows. Chapter 1 introduce the motivation for this thesis. Chapter 2 presents the literature reviews on hydrodynamics, suspended sediment and visibility in Singapore. Chapter 3 introduces the subject of physical optics and underwater light field focusing on Singapore waters. Chapter 4 discusses the methodology to achieve the study's objective in three main sections; decomposition of light attenuation coefficient, underwater light field and visibility modelling. Chapter 5 consist of parameterisation of light attenuation coefficient focusing on the effect of sediments (**Objectives a and b**). Chapter 6 models the underwater light field using Hydrolight (**Objectives b and c**) while Chapter 7 models visibility using Delft3D WAQ (**Objective c**). Finally, Chapter 8 contains the conclusions of this thesis and the recommendations for further research.*

The dynamics of light attenuation and its relation to suspended sediment remains unknown in Singapore waters although sediment is known to be an important factor in reducing light availability. This thesis is intended to fill this gap and provide framework for a broader research on sediment dynamics and light attenuation in the future. One of the realisations of this thesis is the quantification of the partial contribution of water (K_w), sediment (K_s), phytoplankton (K_p) and Chromophoric Dissolved Organic Matter (CDOM) (K_c) to light attenuation and predictive empirical equation for different locations in Singapore waters. Furthermore, the underwater light field and visibility will be modelled using Hydrolight and Delft3D-WAQ respectively, the first of its kind in Singapore waters. This interdisciplinary thesis is unique since its novelty lies in the combination of optics physics and hydraulic engineering for dredging, ecological and remote sensing applications.

CHAPTER 2.0: LITERATURE REVIEW

2.1 Study Area (Singapore)

Singapore is situated at latitude 1° N and longitude 104° E. It consists of a group of 60 islands spanning approximately 700km^2 at the southernmost tip of continental Asia (Figure 2-1). Singapore is located at the confluence of the Malacca Straits from the west, the South China Sea from the east and the Java Sea from the south. The climate is typically tropical and humid, with an average rainfall of 2000mm per year. The seas and weather systems is influenced by monsoon climate, connected to the changes in pressure belts of Asian and Australian land masses as a result of latitude dependent heating on earth (Bosboom and Stive, 2010). Generally, the Southwest (SW) monsoon occurs from June to September while the Northeast (NE) monsoon period occurs from November to March. April-May and October are inter-monsoon periods with relatively lower wind speed and varying wind direction.

The past four decades witnessed pressures along Singapore's 200km coastline to create more land areas for the expansion of the industrial and shipping activities (Figure 2-1). This had resulted in an imbalance between the economic progress and the ecologic/social costs to the people of Singapore. The challenge which Singapore faces is how to effectively manage the coastal impacts so that sustainable development is pursued. Increasing public awareness on environmental issues and political will from the authorities had forced dredging industries to reassess the role of suspended sediment in environmental degradation, especially to the increase in turbidity. These developments necessitate an understanding of the hydrodynamics and characteristics of the coastal system for better decision making especially for the management of dredging plumes.

Due to the confined nature of Singapore waters and the presence of a large number of patch reefs, reclamation and associated dredging activities often take place in very close proximity to coral reefs and seagrass areas (Doorn-Groen and Foster, 2007). This had necessitated the need to understand the natural system for effective management of sediment plume from dredging/reclamation activities. Traditional methods for environmental management of reclamation works in Singapore (and elsewhere in the region) have generally concentrated on arbitrary percentage of tolerance limit adopted from studies in European temperate climate. This is inherently flawed as meaningful criteria to limit the extent of suspended sediment from dredging plumes and their effects require site-specific evaluations and should take into account the natural variability of background turbidity (Erftemeijer and Lewis, 2006).

Besides climate change and increasing sea temperatures, increased sediment load is one of the most pertinent problems faced by coral reefs and sea grasses worldwide. According to Chou (2002), there used to be some 60 offshore islands and patch reefs around Singapore but major reclamation and dredging works since 1970's had severely reduced the numbers. It is the high turbidity waters that restrict light penetration and due to this reef life ends at a depth of only 6-8m, compared to more than 12-20m in the open ocean (Chou et al., 2004).In another study, sedimentation rates everywhere around Singapore had been increasing, resulting in average lost up to 65% of their live coral cover (Chou et al., 2004). Doorn-Groen and Foster (2007) who quoted (Waycott et al., 2004) noted high species diversity of sea grasses in Singapore; 12 out of 57 known species but its habitats and species composition is also on the decline primarily due to land reclamation.

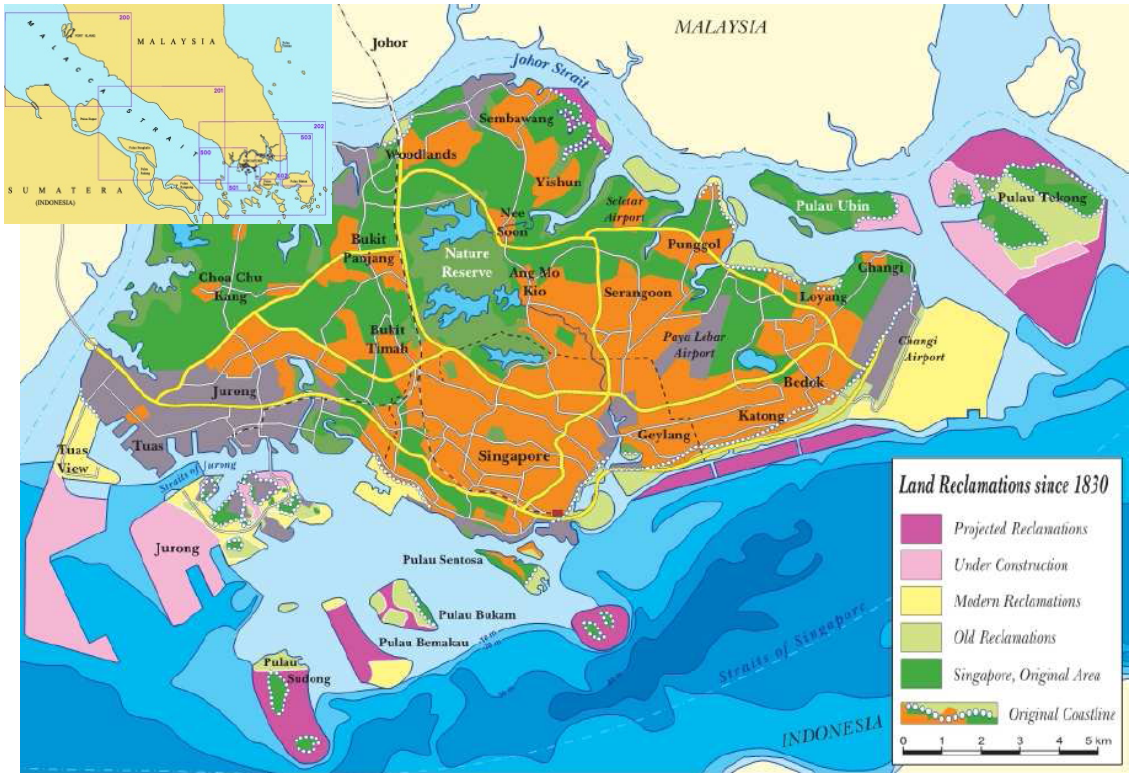

Figure 2-1: Singapore's extended coastline due to land reclamation since 1830's and future projects. Extensive reclamation work is on-going in Pulau Tekong and Tuas (Waterman, 2008)

2.2 Suspended Sediment Dynamics

Understanding sediment dynamics is pre-requisite for understanding light attenuation in Singapore waters. Suspended sediment dynamics can be attributed to four different time scales; high frequency event, infra tide, spring neap and seasonal. Nevertheless, full complexity involving all timescales to suspended sediment is too broad for this thesis; the sediment dynamics will only be investigated against intra tide and spring neap. It is reasonable to assume that suspended sediment variation will be partly attributed from the tides alone as postulated by Van Maren and Gerritsen (2012) and Hoitlink (2004).

2.2.1 Hydrodynamics of Singapore waters

<u>Large scale-coastal system</u>

Singapore Strait is one of the most important shipping lanes in the world. Suited to its strategic location in the middle of China and India's sea trade, the Singapore Strait likewise is influenced by South China Seas and Indian Oceans. The water levels and currents in the South China Sea (East of Singapore) are diurnal while water levels and currents in the Indian Ocean (West of Singapore) are semi diurnal (Chen et al., 2005; see Figure 2-1 from Van Maren and Gerritsen, 2012). In Singapore Strait, the tide is semi diurnal (two high and two low waters a day) due to the increase of the semi diurnal amplitude and corresponding decrease in diurnal amplitudes. The two contrasting tidal systems meet approximately at the western part of the Singapore Strait, resulting in a complicated tidal pattern and eddies (circular movement of water formed at the side of a main current) especially in the middle of the strait due to deeper and irregular bathymetry.

Singapore lies in low wave energy and is dominated by moderate to strong tidal environment (Cheong et al., 1993). Water levels are mixed, mainly semi-diurnal while the current velocities are mixed, mainly diurnal (one high and one low per day) due to the sharp transition in the tidal regime resulting in deviation of the tidal current from its local water level (Van Maren, 2010). The semi diurnal nature of water level is governed by principal solar component S_2 and the principal lunar component M_2 while the diurnal currents are governed by K_1 and O_1 constituents (related to moon declination). Tidal flows in Singapore Strait are generally strong (0.83 m/s on spring tides to 0.67 m/s on neap tides (Riddle, 1996). The strongest surface currents are found in the narrowest pass in the Singapore Strait, during both monsoon seasons, often in excess of 2 m/s (Zhang and Gin, 2000; Chen et al., 2005). Higher currents in Singapore Strait are also due to the narrow channel connecting separate basins with different tidal regimes (Pugh, 1987).

Tidal behaviour is classified using the Form number F (also known as Fromzhal number), which is the ratio of (K_1 + 0_1) to (M_2 + S_2). When F < 0.25, the tide is classified as semi diurnal with two tides of closely similar height and constant phasing relative to the moon; when 0.25 < F < 1.5, the tide is mixed, mainly semi diurnal; when 1.5 < 3.0, the tide is mixed, mainly diurnal; and if F > 3.0, diurnal with the second tide absent during the spring tide (Bosboom and Stive, 2010). The tidal constituents can be selectively amplified by local geography where shallow estuaries may favour amplification of semi diurnal constituents. The tides in Singapore are mixed with significant daily inequalities in both height and time at which they are phased (Mcgregor and Desouza, 1997). Mixed tides show both semi diurnal and diurnal tides. At certain times in the year, semi diurnal tide is produced, while at other times the tide is diurnal. The differences in moon and sun position can result in tides that exhibit only one high water and one low water per day (diurnal tides).

Two low and two high water per day are referred to as semi diurnal (with a maximum tide every 12 hour 25 min). Semi diurnal tides are more prevalent in the western end of Singapore compared to the eastern end since the semi diurnal tidal constituents are progressively weaker from the west to east. The spring range at the western end of the strait is about 2.7 m and with mean range of 1.9 m (Mcgregor and Desouza, 1997; Chen et al., 2005) to about 1.5 m to the east of Singapore (meso-tidal regime). The neap range is about 40 – 50 % of the spring range (Chen et al., 2005). The phase difference between the two ends is less than an hour with wave crest proceeding westwards. Generally, the wave conditions off the east coast of Singapore consist partly of wind generated waves caused by winds during the SW monsoon and partly of refracted swell penetrating from the South China Sea during the NE monsoon period (Cheong et al., 1993).

Chen et al. (2005) examined the circulation in Singapore Strait using 3D Princeton Ocean Model (POM). They proved that in addition to tidal forcing, circulation in the strait is governed by a strong hydrodynamic pressure gradient which reverses direction twice per year and coincides with seasonal monsoon changes. The water level in the model is reasonably reproduced, but the current velocity is not. Van Maren (2010) suggested that this is unavoidable since the model is forced by predominantly semi diurnal water level, underestimating the diurnal currents of K_1 and O_1 components. Furthermore, they found that strong current exists during most of the year and penetrates as deep as half of the water depth with maximum speed of about 2 m/s during the heights of both monsoon seasons in agreement with Zhang and Gin (2000).

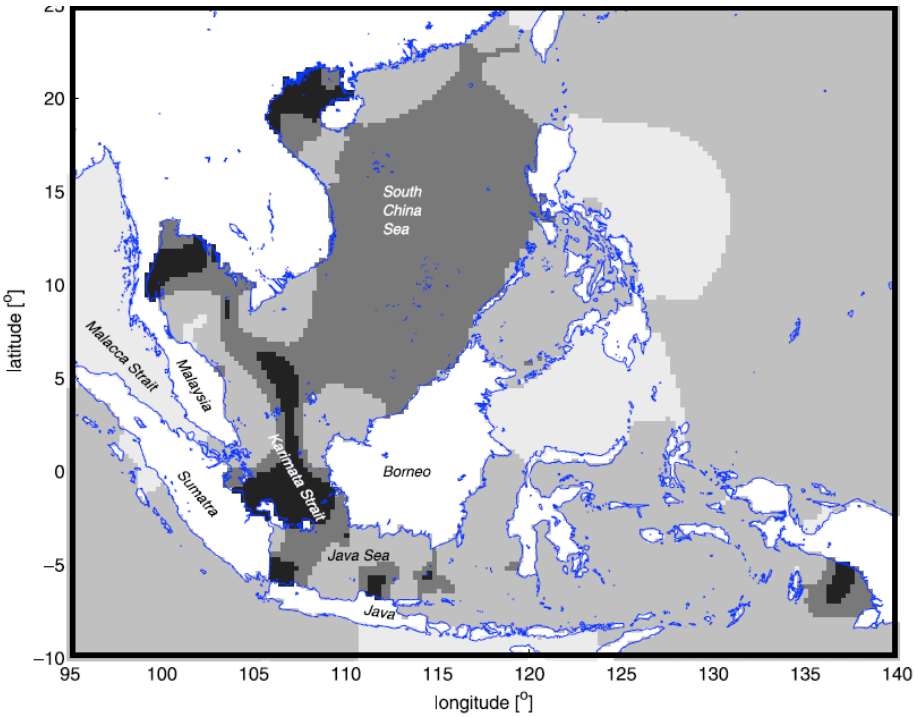

Figure 2-2: Water level regime in the Southeast Asia region, classfied as Form number, F. Tides are diurnal for F > 3 (black), mixed (grey) and semidiurnal for F < 0.25 (light grey).

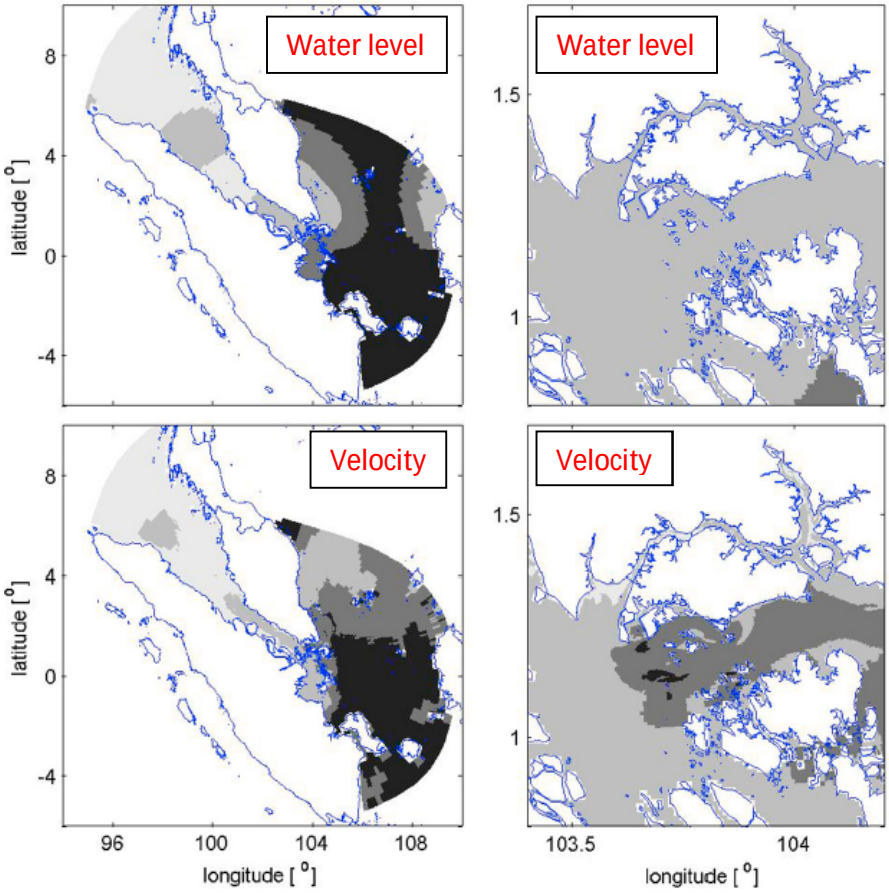

Figure 2-3: F number for water level (above) and current velocity (below). Note the semi-diurnal water level and mixed velocity in Singapore Strait (right pictures). Figure 2-2 and 2-3 were reproduced with permission from Van Maren and Gerritsen (2012).

The nature of water level and current velocity decoupling in Singapore is due to the presence of a diurnal amphidromic and a semidiurnal anti-amphidromic point nearby Singapore (for amphidromic point; water level variation are low but current velocities can fluctuate widely). Therefore, the currents are predominantly diurnal whereas the water level is predominantly semidiurnal in mixed tidal regime like Singapore waters (Pugh, 1987). The diurnal current velocity is strong because as they travel along Singapore Strait from the South China Sea, the diurnal tidal waves amplified as they reflect against the Sumatra east coast (Van Maren and Gerritsen, 2012). On the other hand, the diurnal water level signal is suppressed due to nearby amphidromic line located at the middle of Malaysian Peninsula and Borneo. Figure 2-2 shows Form factor for water levels and currents in Singapore.

Tidal asymmetry and residual flows

Tidal asymmetry can be identified in two ways; one is due to the duration of flood and ebb tide and secondly due to slack tide duration. Any one of the two phenomena will results in imbalance of material being transported since S, the amount of material being transported is non-linear function of the velocity u *(*$S=u^n$*). For example, if the flow velocity is higher during flood tide compared to ebb tide, more materials will be transported (or imported) during flood tide and vice versa. The occurrence of tidal asymmetry is normally associated with the non-linear interaction of the* M_2 *constituents. However, as reported by Hoitink et al. (2003), tidal asymmetry may also be caused by the interaction of various tidal constituents and particularly relevant to the residual sediment transport in diurnal tidal regimes. They developed an analytical expression for quantifying the residual transport using the phases and amplitudes of these constituents.*

Zhang and Gin (2000) applied a 3D multi-level hydrodynamic to model tidal motions in Singapore's coastal waters using a two-step Euler predictor–corrector algorithm. They showed that the residual flow pattern for spring tide is similar to the neap tide pattern, but the residual flows in the spring tide are slightly weaker than those in the neap. The residual flow strength is strongest in the western Singapore and progressively weakens towards the east while the large-scale eddy occurs near the southern tip of Singapore. Their numerical investigation of wind effects on currents shows that the velocities over the whole domain are significantly influenced by wind forcing and that the maximum velocities do not necessarily occur at the top level. Non tidal residual current arising from prevailing winds can attain a maximum speed of 0.4 m/s during the NE monsoon (Chen et al., 2005).

Residual current is due to the non-tidal contribution. Residual flows can be produced by wind drag on the sea surface (Zhang and Gin, 2000) or driven by density gradients due to salinity or temperature distributions, or by the non-linear interactions of the oscillating tidal streams (overtides). Zoelaeha (2010) found that the seasonal variation of current velocity in Singapore waters is influenced by residual flow, generated from the combination of tidal current and monsoon current. During NE monsoon, average residual flow ranges from 0.1 to 0.3 m/s westward with the peak of 0.8 m/s in January. During SW monsoon, residual flows range from 0.1 m/s to 0.2 m/s and relatively low during the inter monsoon period. Residual flow components are small but persistent and associated with easterly winds (due to pressure difference between western Pacific and eastern Indian Ocean), Stokes drift (residual discharge in the wave propagation direction) and locally generated vorticity (oscillating current on an undulating topography) (Van Maren, 2010).

Van Maren and Gerritsen (2012) investigated on the relative role of tidal asymmetry and residual flow in transporting sediment. They found that tidal asymmetry in mixed tidal regime is stronger than in temperate regions due to the contribution of triad interaction (O_1-K_1-M_2) instead of only overtides (interaction of tide constituent with itself i.e. M_2-M_2 interaction) in semi diurnal tidal regimes. They found that transport by tidal asymmetry is directed eastward (coarse sediment) while residual flow transport is directed westward (fine sediments) in equal magnitude since fine sediment are more sensitive to small change in velocity due to residual flow. Hence, transport of sediment may occur when there is asymmetry in the flow velocity, either due to tidal asymmetry or residual flow (Van Maren, 2010). Therefore, for mixed tidal system such as the Singapore Strait, residual flow plays major role to the fine sediment transport (Zoelaeha (2010); Van Maren and Gerritsen (2012)).

2.2.2 Sediment transport in Singapore waters

<u>Sediment sources and characteristics</u>

Sediment is particulate material, formed by the physical and chemical disintegration of rocks from the earth's crust and by various biological processes (i.e. organic, mostly plankton, zooplankton and detritus) (Deltares, 2011). Sediment also sometimes consists of detritus as the residual products of decomposed phytoplankton and zooplankton. The source of mineral particles (or triton, meaning non-living component) is from river discharge, shoreline (littoral drift and cross shore) and bed erosion (offshore sand banks) or atmospheric particulates. Mineral particles consist of clay, silt and sand, each with varying sizes, composition and chemical properties. Fine clay is about 5µm in diameter, silt particle are in the range of 5 to 40 µm and fine sand 40 to 130 µm while coarser grain sand is from 130 to 250 µm (Bosboom and Stive, 2010).

The sediment in Singapore coastal waters consist of mud, silt and sand in varying degree. In a study of heavy metal in Singapore marine sediment by Goh and Chou (1997), 20 sediment samples collected in Raffles Island shows 99 % of sand and coral rubble with only 1 % silt/clay fraction, this is similar to Chuang (1977) in Pulau Sudong (refer Figure 2-1 for location). Another sedimentation study in Pulau Semakau by Chou et al. (2004) found that on average, sediment consist of 30% coarse sand, 65-70% fine to medium sand and 5% silt. Cheong et al. (1993) found that similar characteristics from the sea bed samples around the east of Singapore (Changi) with less than 5% finer than 100 µm, 65-70% fine to medium sand and about 30% coarse sand with essentially non-cohesive material at the sea bed. In the upper Johor estuary, mud accumulates on the intertidal mudflats and near the embankments based on a dual frequency echo-sounding survey in Van Maren (2010).

Sedimentation rates (of predominantly sand with some silt) around Semakau (about 5km northeast from Raffles Island) are 10 to 90 mg/cm^2/day (Chou et al., 2004) while the sea bed material is essentially non-cohesive sediment with d_{50} of 0.25 - 0.70 µm. The northeast and south Semakau seems to have higher proportion of silt clay fraction in the bed samples, reaching as high as 47%. They also found that organic matter only occupied 4% to 10% of all the sediment. Organic to inorganic ratio ranged from 0.07 to 0.13 in trap sediment and from 0.03 to 0.14 in the bottom sediment showing prevalence of organic matter near the seabed. Excess sedimentation of as given above is higher than the threshold (absolute) value of 0.5 mg/cm^2/day recommended by Doorn-Groen and Foster (2007) to impart slight impact to the coral habitats with existing stress levels in Singapore waters.

The sediment load from Johor River is expected to be significant in modifying the suspended sediment variation in Singapore waters, especially in the eastern side of the Johor Strait due to its geographical proximity. This is plausible since sediment load from various small rivers in Singapore like Sungai Buloh and Sungai Kranji were negligible since they were all damned during the last decades. Van Maren (2010) estimated the sediment load into Singapore coastal waters using an average concentration of 150 mg/l and an average discharge of 37.5 m^3/s for the Johor River. He estimated the long-term sediment influx equal to 5.6 kg/s or 0.17 million ton per year. Extrapolation and comparison of similar catchment area resulted in 0.4 million ton per year for other rivers draining to Johor Strait. As such, a total of 0.6 million ton of sediment is annually supplied to Singapore's coastal waters.

<u>Previous studies on sediments modelling</u>

Studies on sediment transport in Singapore are more inclined towards the impact of the turbidity to the marine communities and not much on the suspended sediment linked to the mechanics of the hydrodynamic forcing. Dikou and van Woesik (2006), Chou et al. (2004) and Hoitlink (2004) among others investigated on the impacts of sedimentation on the marine communities in Singapore Southern Islands. The conclusions from all the studies points to deterioration of marine habitats; with sediment variation mostly attributed to the tides (Hoitlink, 2004); that rapid reclamation/construction activity affected the surrounding marine area by increasing the sedimentation rate and altering the sediment composition (Chou et al., 2004). Some of the limited studies on sediment transport modelling are linked to sediment dynamics; Van Maren (2010) and Van Maren et al. (in prep). Recent Delft3D transport modelling is by Van Maren and Gerritsen (2012). Limited information on sediment plume model is given in Doorn-Groen and Foster (2007).

Doorn-Groen and Foster (2007) advocated quantifiable compliance targets covering temporal and spatial scales during reclamation projects which include daily spill budget targets through feedback between measurement and simulation. Simulation was carried out on MIKE 21 nested grid with resolution of 675m to 25m in the finest resolution. Spill budget was integrated with specific habitat tolerance limits (from monitoring surveys) for varying magnitudes and durations of sediment loading from project records and measurements. Spill hindcast was carried out daily and are validated against the daily control samples from sites. Critical shear stress for erosion and deposition over coral reef were found to be 1.5 and 0.6 N/m^2 respectively. Van Maren et al. (in prep) however specified these values as 0.1 and 0.05 N/m^2 to account for higher sediments in the Johor estuary.

Van Maren (2010) shows that the Johor estuary and the Singapore Southern Islands region are characterised by two different sediment transport mechanisms. The former dominated by advection of very fine sediments and minor sediment resuspension by tidal currents while the latter involved almost equal contribution from advection of coarse sediments and resuspension. He postulated that higher suspended sediment concentration (SSC) levels in Southern Islands can result from advection (due to non-tidal residual flows) and resuspension (due to tides). He however did not completely rule out resuspension of coarser sediment, but maintained that tidal currents remain the dominant factor for resuspension. Recently, Van Maren et al. (in prep) found that although large sediment load enters Singapore Strait from Johor River, mixing in the Johor estuary and Singapore Strait dilutes the fluvial sediment source resulting in negligible impact in Singapore Southern Islands.

The intra-tidal, spring-neap, and seasonal variation in suspended sediment are found to be low in Johor estuary compared to the more pronounced intra-tidal and spring-neap variation in Singapore Southern Islands (Van Maren, 2010). Analysis of Johor River hydrodynamics by Hasan et al. (2011) shows the estuary is ebb-dominant. Van Maren (2010) explained this by suggesting that sediment movement is related to the stratified discharge level; sediment is imported into the Johor estuary during low discharge and by settling lag effects (longer flood slack periods) rather than estuarine circulation (Van Maren et al., in prep). Sediment is exported in the turbid surface plume during large discharge events, and by ebb-dominant maximum flow asymmetry caused by interaction of the O_1-K_1-M_2 constituents which generate a persistent asymmetry influencing sediment transport.

2.3 Visibility in Singapore

2.3.1 Review of previous studies

There is not much study documenting light attenuation in Singapore waters or its surrounding seas. However studies on visibility and/or turbidity using Secchi depth, S_d related to phytoplankton or coral reef ecological studies are available. However, these are only sporadically available from 1970's to relatively recently. Nevertheless, the results can be used to provide surrogate account on the light attenuation characteristics. However, even this is sparse and most were not systematically account for physical forcing like tides and seasons. The earliest study on visibility in Singapore waters is by Tham et al. (1970) in the eastern entrance to Johor Strait. They measured incident light using submarine illuminator from the surface reaching to a depth of 66m and concluded that on a bright day, 3.5% of the incident light is reflected at the surface. The author of this thesis calculated K_d from the above data to be 0.142 m^{-1}.

Monthly mean of S_d at the Johor estuary during high tide varied from 1.60 to 3 .02 m (Tham et al., 1970). About 7 years later, Chuang (1977) studied the Malayan and Singapore coral reef and recorded the fall of light intensity on a cloudy day in Pulau Hantu. He found that light attenuated rapidly as 33 % of the surface light is attenuated within the first 3m. At 10m and 16m depth, 95% and 99.7% of the light was attenuated respectively (works out to K_d of 0.323 m^{-1}). Thus, in about less than a decade, the visibility had more than doubled to the worse, assuming that both K_d are representative of the Singapore waters at that time. However, the general reduction trend in visibility seems to be consistent with Chou (2002) who pointed out that visibility was around 10m in 1960's but after extensive reclamation works since 1965 had reduced to less than 2m in recent times.

An ecological study of the Punggol estuary by Chua (1973) in the eastern Johor Strait using data from July 1965 to June 1966 shows that S_d varies from 0.2 - 3.0m depending on the distance from the land discharge and the tide condition (i.e. more turbid during low tide). Recent measurements by Chuah (1998) in the same location from December 1996 to July 1997 show that the temporal variations of S_d are within 1.0 – 2.0 m. The lowest and highest S_d are 0.7m and 3.2m respectively. Although the Chuah (1998) mentioned that the water sampling was conducted during similar tide condition, the exact tide condition was not stated making comparison with the former study difficult. However, it is certain that the visibility in the eastern Johor Strait had showed consistent deterioration. Assuming S_d is 1.7/ K_d, the mean K_d for Chua (1973) and Chuah (1998) are 0.68 m^{-1} and 1.13 m^{-1} respectively, almost double in the 20 years period.

The study by Dikou and van Woesik (2006) using data from October 1999 to February 2000 in Singapore Southern Islands is one of the more comprehensive evidence that point to reduction of light intensity. The light intensity data measured with a LI-COR light meter was linked to transect data of coral reef cover. The results of the study is twofold; firstly, there seems to be a reduction in available light measured compared to previous years, secondly the luxuriant coral cover had more than halved at all sites examined, and lastly the generic composition of coral fauna indicative of chronic sediment exposure. They concluded that clearly a reduction in both water clarity and live-coral cover has taken place since monitoring efforts began in the early 1970s, while benthic space was predominantly occupied by dead corals covered with sediment and filamentous algae.

Turbidity was measured using Secchi Disk and the S_d was used to calculate the light attenuation coefficient K_d using the relation K_d = 1.7 / S_d in Dikou and van Woesik (2006). It was found that the K_d ranges from 0.6 to 1.9 m^{-1} compared to 0.5 to 1.1 m^{-1} using the S_d from Tham et al. (1970). The K_d and percentage live coral cover (% LCC) showed a strong and inverse curvilinear relationship; % LCC = 13.6 $K_d^{3.40}$. Furthermore, they have shown that strong correlations existed between K_d and suspended solids, volatile particulate matter and Chl-a during inter monsoon season. The results also shows a tendency for more stable conditions (i.e. lower variance) in downward flux of suspended particulate matter, Chl-a, and K_d during inter monsoon. This is important because lower variability for these parameters during inter monsoon is proven in this study. Additionally, positive relationship between these parameters can also be expected.

Gin et al. (2000) based on S_d readings during the measurements in 2000 showed that the euphotic zone (depth at which the light falls to 1% of that at the surface) in Singapore waters were apparently between 4 and 9m. Visibility along the east coast was generally lower (average S_d of 3 m) than the south-west region around the Southern Islands (average S_d of 4.5 m). This pattern seems to correlate well with higher chlorophyll concentrations and suspended solids in those areas. Chang (2007) noted that the waters in the Southern Islands of Pulau Hantu and Pulau Semakau show considerably turbidity with characteristic attenuation length ranging from 0.25 m to about 0.4 m, with approximate K_d of 2.5 to 4m^{-1} (from the inverse of attenuation length). As such, in the years after 2000, K_d in Singapore waters has increased ten-fold from that in 1970's.

Chou et al. (2004) investigated the impact of sedimentation in Singapore Southern Islands also recorded light intensity measured using underwater light sensor. The reading ranged from 0.94 to 10.7 µmol m^{-2} sec^{-1} at all stations. However, during the subsequent surveys, the light intensity at most stations showed reduction, although few stations recorded higher intensity. Unfortunately, details like the tide condition and cloud cover during light measurement was not recorded. Nevertheless, they showed that light intensity dropped rapidly close to the construction area. Kuwahara et al., (2010) showed that the west coast of Malaysia was characterized by shallow mean UV-B (320 nm) penetration (1.68 ± 1.12 m), higher chlorophyll concentration (3.00 ± 4.72 µg/l) and CDOM (6.61 ± 3.31 ppb) compared to the East Coast. Maximum $K_{d(PAR)}$ recorded on the West Coast was 0.90 m^{-1}. Although $K_{d(PAR)}$ seems relatively low (indicating higher visibility), it is still high considering the light measurement were recorded in relatively pristine waters far from land.

Van Maren and Gerritsen (2012) showed that the visibility in Southern islands is influenced by seasonal variation, with lowest visibility around July and December (less than 0.5m) while the highest visibility is around March and April (exceeding 2m). Van Maren (2010) suggested that the seasonal variation in visibility is caused suspended sediment since the chlorophyll and CDOM is known to be relatively low in Southern Islands. Similar conclusion was derived for Johor estuary although the sediment mechanism in the latter is different from the Southern Islands (Van Maren, 2010). There is no study that quantifies the relative contribution of constituents (water, CDOM, chlorophyll and sediment) to light attenuation thus far in Singapore. It is therefore desirable that a scientific study with sound physical basis is formulated to conclusively prove that the theory.

2.3.1 Review of visibility modelling

Visibility is related to the variability in the underwater light field. Underwater light field in turn is determined by the distribution of optically significant constituents in the water column. Much of the impact while sediment remains suspended is related to its visibility vis-à-vis light attenuation potential. There is not much visibility modelling literatures in Singapore waters available at least in the public domain. Sediment dynamics studies which qualitatively link SSC and turbidity to describe visibility were discussed in Section 2.2.2. However, most of the studies model sediment coupled to the hydrodynamic model (the so called on-line model). There is no study yet on water quality-visibility modelling (off-line model) in Singapore waters as far as the author's limited awareness is concerned. Hence, the visibility modelling presented in Chapter 7 of this thesis is the first afford in this regard and can be assume to be an experimental exercise in earnest.

The difference between sediment transport with flow model and transport with water quality model is related to the transport mechanism of coarse sand and fine sediment (silt and clay) respectively. Sand is transported with the flow, depending on the transport capacity of the instantaneous flow condition. Fine sediments are also transported by flow but the erosion and deposition (settling velocity) is compounded by the advection-diffusion process. Furthermore, sand transport are modelled as bed low transport while fine sediment are modelled as suspended transport due to the difference in time and length scale variation. Sand transport responds almost immediately to flow variation while adaptation time for fine sediments is much smaller than the changes in the flow field (i.e. sediment concentration variation). This necessitates extra processes (diffusion and dispersion) to account for fine sediment transport (see Section 3.2.2).

The simulation of water quality parameters, especially in Johor strait has been carried out with 2D eutrophication model NEUTRO (Tkalich et al., 2001), Environmental Fluid Dynamics Code (EFDC) (Maznah, 2009) and 3D multilevel eutrophication model (Gin et al., 2001). The results of water temperature, salinity and DO generally showed fairly good agreement with observations for all three studies. Unfortunately, Maznah (2009) did not modelled suspended sediment in Johor River to allow comparison with Chapter 7. The model output of Tkalich et al. (2001) achieved baseline levels and is able to reproduce the general features of the Singapore coastal waters but the detail variation of nutrients, plankton, bacteria and SSC were not shown. Gin et al., (2001) conclude that Singapore waters are well mixed and differences in concentration with depth for all state variables are generally <20% with horizontal spatial differences for all the variables are generally <40%.

CHAPTER 3.0: DYNAMICS OF UNDERWATER LIGHT FIELD

This section will provide the theoretical framework for understanding the underwater light field. It starts by presenting an overview of the light spectra and the propagation of light from the atmosphere to the water surface in Section 3.1. This is followed by the introduction to various optical parameters to quantify the light fields in Section 3.2. The fate of light, once it is in the water will be detailed in Section 3.3. Physical processes responsible for light attenuation are discussed in Section 4.4 while the complexities of the optically significant constituents are elaborated in Section 4.5. Section 4.5 will deal with this complexity in general but with reference to the Singapore waters in particular. Finally, Section 4.6 presents previous studies on underwater light field in Singapore waters relevant to this thesis.

3.1 Physical optics of underwater light

3.1.1 Light and electromagnetic spectrum

Light is a form of electromagnetic radiation that travels as waves through space, air, water and even vacuum. Visible light waves forms part of the electromagnetic spectrum which contains all possible frequencies of radiation. Figure 3-1 shows the electromagnetic spectrum as a continuum of all electromagnetic waves with different frequency and wavelength. Visible light with the wavelength between 380 nm and 760 nm in the electromagnetic spectrum is the most important to human - it is the only electromagnetic radiation that a human eye can detect (Figure 3-2 a). Visible light waves have both magnetic and electrical properties, enabling it to transport energy from one location to another. Electromagnetic fields travel by oscillating perpendicular to the direction of wave while light oscillates in the direction opposite to the direction of wave (Figure 3-2 b).

The Infrared radiation (wavelength millions of a meter), lies before the visible light band. Longer wavelengths are microwaves (mm to cm wavelength) and radio waves (wavelengths of meters). After visible light band are the ultraviolent (UV), X-rays and Gamma rays. The visible range is important for many reasons: it warms the surface layers and facilitates ocean circulation from warmer seas to colder seas; provides energy required by phytoplankton for photosynthesis; and reflected light is used for mapping chlorophyll and sediment concentration in remote sensing. Visible lights, infrared and UV radiation are transmitted through the sun's radiation, but because the sun is about 6000 °C, approximately 45% of the sun's radiation consists of the visible light band (Figure 3-2a). Coincidentally, the visible light almost coincides with Photosynthetically Active Radiation (PAR; from 400 to 700 nm).

3.1.2 Nature of light

Aristotle and Democritus was the earliest to hypothesize that light is a disturbance in the air, composed of indivisible sub-components. Isaac Newton in Hypothesis of Light (1675) suggested that light was composed of particles which were emitted in straight lines, while the reflection and refraction demonstrated light's particle nature. In 1678, Dutch physicist Christiaan Huygens mathematically showed that refraction is explained as the medium-dependent propagation of light waves. James Maxwell later explained light as the propagation of electromagnetic waves using four equations that relate the electric field and magnetic field. In 1900 Max Planck suggested that although light is a wave, these waves can only gain or lose energy in finite amounts of the radiation called "quanta".

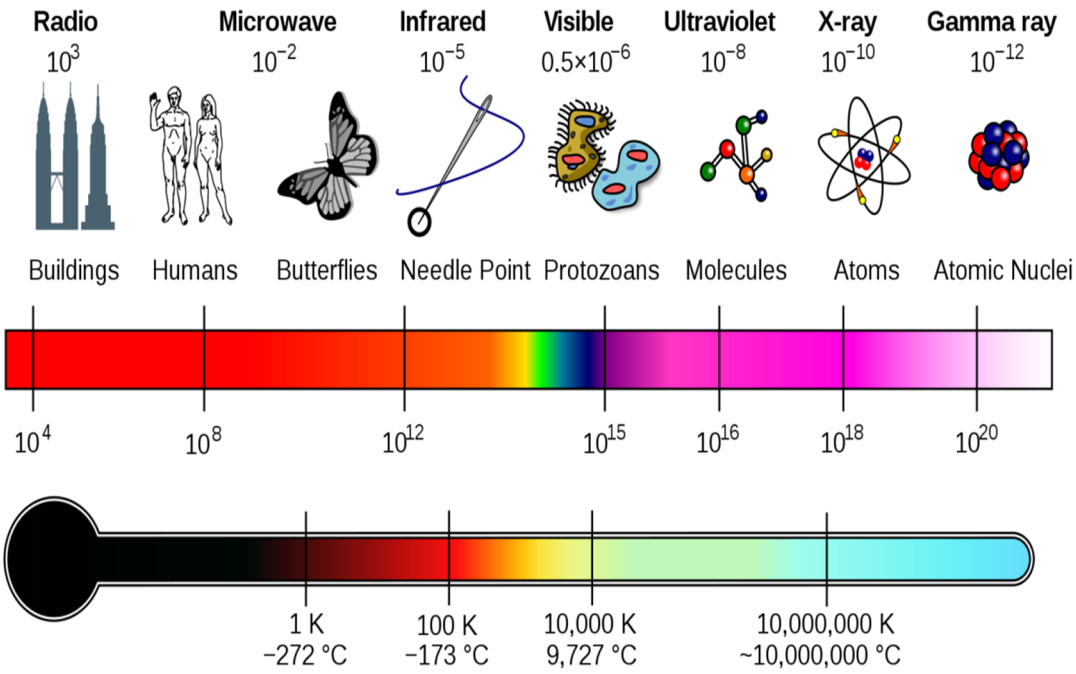

Figure 3-1: Electromagnetic spectrum and the approximate scale of wavelength and temperature at which the particular radiation is emitted. (From: http://www.edinformatics.com/math_science).

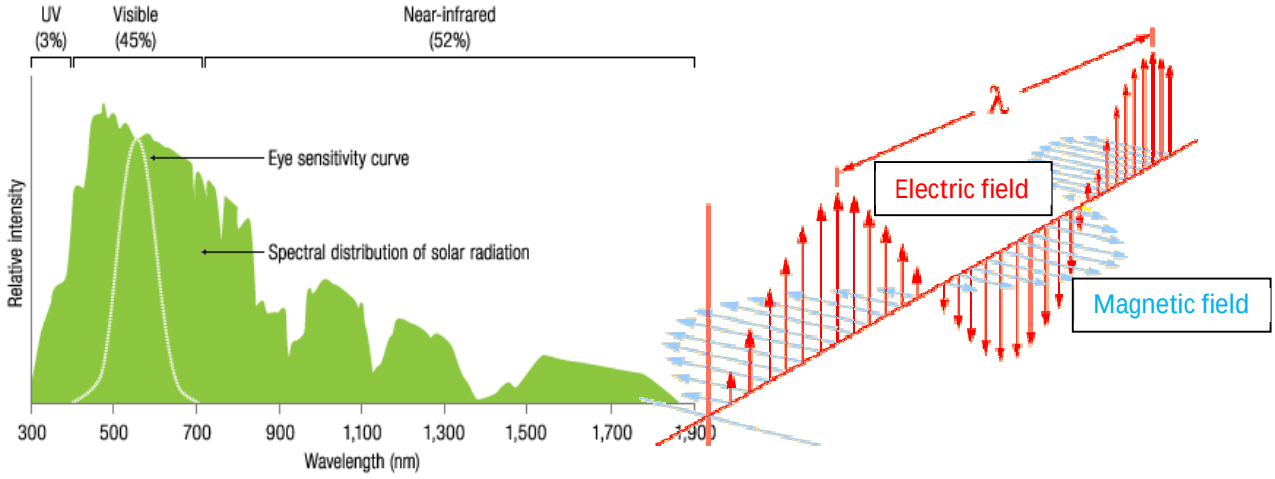

Figure 3-2: (a) The percentage of sun's electromagnetic radiation in the UV, visible and near infrared band. (b) The propagation of light exhibits in-phase sinusoidal variation of electric and magnetic field in space. (Figures modified from http://hyperphysics.phy-astr.gsu.edu)

The photon is the smallest amount of electromagnetic radiation that cannot be broken down further and moves at the speed of light with respect to all observers. They can be created and destroyed when interacting with other particles, but are not known to decay on their own and have both energy and momentum proportional to their frequency. Unlike other particles, photons have no mass; therefore Einstein famous $E = mc^2$ *does not work here, instead equations relating energy* (E)*, wavelength* (λ) *and speed of light* (c) *are:*

$$E = ch/\lambda \quad \text{(Wave like)} \qquad \text{(Eq. 3.1)}$$

$$E = cp \quad \text{(Particle like)} \qquad \text{(Eq. 3.2)}$$

Where:

- E *= energy, expressed in Joule*
- c *= 3 X* 10^8 *m/s is the speed of light in vacuum*
- h *= 0.663 X* 10^{-33} *is Planck's constant (Js)*
- $p = mv$ *(momentum) =* h/λ

Newton realised that light behaves in many ways like water waves. Light bends around obstacle in similar way to ocean waves around a harbour wall. Light beams can also be added together as overlapping wave groups does. However, when UV light shines on a metal, electron is emitted with a specific kinetic energy. This effect remained an obstacle to the acceptance of wave theory until Albert Einstein in 1905 concocted the idea of the light particle, or photon with particulate qualities. He showed how light could behave as a stream of photon pellets as well as continuous wave. This wave-particle duality is a central concept of quantum mechanics because it addresses the inability of classical concepts like 'particle' and 'wave' to fully describes the behaviour of quantum-scale objects of atomic size.

3.2 Property of ocean optics

Optics refers to a branch of physics concerned with interaction of light as it propagates through different medium. The property of underwater light field in the ocean waters is important in ocean optics. The proportion of radiation received at the water surface increases with decreasing solar elevation β, which depends on latitude and solar declination δ*. Light in the ocean travel at a velocity equal to the velocity of light divided by the refractive index* n*. Hence the velocity of light in water is about* 2.25×10^8 *m/s. Because light travels slower in water compared to in the air, some light is reflected at the sea surface. However, the proportion of incident light that is reflected by flat water surface is roughly 2% which shows that most of the sunlight propagates below the sea surface while only little is reflected (Kirk, 2011) back to the atmosphere.*

To understand the complete description of light field under the water surface, four parameters; Irradiance, direction, wavelength and polarisation (I, Q, U *and* W*) which form the so-called Stokes vector parameters of a light beam must be defined (Mobley, 1994). However in this thesis, the simpler system of point observation of radiance* L *as a function of* (θ, φ) *will be adopted. For the sake of simplicity, the spectral dependence of* λ *for all light units will also be omitted in the subsequent discussion of this thesis. The direction of light field is expressed as zenith angle* θ *(polar angle of a light beam and the upwards vertical) and azimuth angle φ (the angle of a light beam and the vertical plane).*

The two most important terms for understanding the behaviour of photon flux is radiance L *and irradiance* E*. These two terms are derived from the basic parameter called radiant flux Φ and radiant intensity* I*. The latter is one of the SI units called candela (lumen and lux are also SI units derived from the candela). The radiant flux* $\Phi = dQ/dt$ *(or radian power) is the time rate of radiant energy flow (Q) expressed in W (*Js^{-1}*). Radiant intensity* $I = d\Phi/d\omega$*, is the measure of radiant flux per unit solid angle in a specified direction (*$W\omega^{-1}$*). Irradiance* $E = d\Phi/dS$*, is defined as the radiant flux per unit area of surface (*Wm^{-2}*). Radiance* $L = I/A \cos\theta$ *is the measure of radiant flux per unit solid angle per unit area of a plane (*$W\omega^{-1}m^{-2}$*).*

Since the radiance L is both the function of zenith and azimuth angle, it is commonly written as $L(\theta, \varphi) = d^2\Phi / dS \cos\theta \, d\omega$ expressing the light field with the variation in θ and φ. Downward irradiance E_d and upward irradiance E_u are the values of the irradiance on the upper and lower faces respectively of a horizontal plane.

The net downward irradiance, $\bar{E} = E_d - E_u$, is the difference between downward and upward irradiance. Irradiance reflection $R = E_d / E_u$ is the ratio of the upward to the downward irradiance, widely used in remote sensing. The scalar irradiance E_o is the integral of the radiance distribution at a point over all directions about the point, which treats radiation from all direction equally. It has the same unit as irradiance. Similarly, the downward scalar irradiance, E_{od} and the upward scalar irradiance E_{ou} is the integral of the radiance distribution over the upper and lower hemisphere respectively.

$$E_{od} = \int_{2\pi}^{0} L(\theta, \varphi)\, d\omega \text{ and } E_{ou} = \int_{-2\pi}^{0} L(\theta, \varphi)\, d\omega \qquad \textit{(Eq. 3.3)}$$

The property of light field in the water column changes exponentially with depth corresponding to decrease in the case of irradiance or an increase in the case of reflectance. As the photons continue downwelling (or downward) propagation, at certain depth the intensity of the photon will reach zero indicating that radiance L is also a function of depth z (albeit a weaker dependence). However, L is also dependent on wavelength λ, due to the spectral nature of the photons and spectral dependencies of optically significant constituents (more on this in subsequent sections). Consequently, radiance, L is more accurately written as $L(\theta, \varphi, z, \lambda)$. Figure 3-3 shows the relation between various optical parameters.

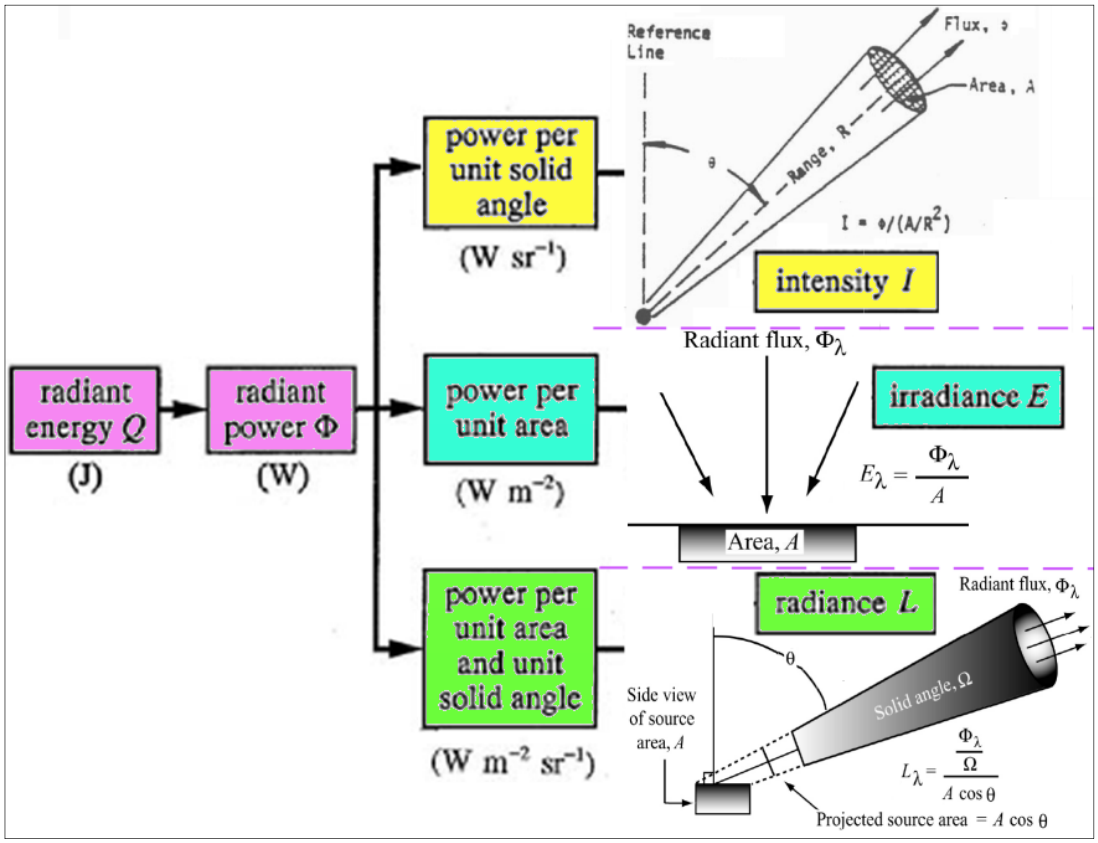

Figure 3-3: Hierarchy of optical properties and its interpretation (modified from Mobley, 1994).

3.3 Optical properties for underwater light fild

3.3.1 Inherent optical properties (IOP)

The propagation of light (or technically photon) in ocean water is reduced by either being absorbed or scattered by materials present in the water; these phenomena can be described by two coefficients: absorption coefficient a, and scattering coefficient b. Both absorption and scattering results in changes to the original underwater radiance distribution but scattering in itself does not remove light energy, it only increases the path length so that the chances of light being absorb or further scattered is increased. The beam attenuation coefficient c is given as the net effect of absorption and scattering ($a + b = c$). It is the fraction of the radiant flux lost from the incident beam by the combination of absorption and scattering.

The optical coefficients of a, b and c describe the exponential attenuation of light per unit path length, assuming an infinitely narrow beam of monochromatic light (light with one wavelength with all of the waves precisely in step) passing through an infinitely thin layer (or cross section) of water. Absorption coefficient a is defined as the incident flux that is absorbed divided by the thickness of the layer (It is also a measure of the conversion of radiant energy to heat and chemical energy). The amount of the incident flux (i.e. energy) absorbed by this layer, $\mathrm{d}\Phi_a$ will be proportional to the intensity of the beam Φ and the path length dr *as follows:*

$$\mathrm{d}\Phi_a = -a.\Phi.\mathrm{dr} \qquad \textit{(Eq. 3.4)}$$

This proportionality coefficient for the equation above is the absorption coefficient a. It is a characteristic of a given layer of medium (normally seawater). Likewise, scattering coefficient b and beam attenuation coefficient c has similar meaning. All three coefficients a, b and c have the dimension of L^{-1} and are measured in inverse distance (m^{-1}) which physically represent the fraction of light removed per unit distance. These coefficients (a, b and c) and the volume scattering function β is referred to as inherent optical properties (IOP) by Preisendorfer (1961) as quoted in Kirk (2011), because their magnitude depends on the optically significant constituents of the medium and independent of spatial distribution of the impinging radiation.

3.3.2 Apparent optical properties (AOP)

The apparent optical properties (AOP) are dependent upon the geometric structure of the prevailing light field since they are commonly derived with respect to the light quantity measured at the water surface. AOP changes approximately logarithmically with depth; examples of AOP are the vertical attenuation coefficient for upward irradiance K_u, downward irradiance K_d, scalar irradiance K_o and radiance $L(\theta, \varphi)$. The most important AOP in this thesis is the vertical attenuation coefficient for downwelling (or downward) irradiance, K_d to quantify the amount of underwater light field in the water column. It is defined as follows with E_d being the downward irradiance:

$$K_d = -\frac{d \ln E_d}{dz} = \frac{1}{E_d}\frac{d \ln E_d}{dz} \qquad \textit{(Eq. 3.5)}$$

Strictly speaking, although the values of K_d are a function of depth and changes according to environmental factors (light structure, tides and seasons) and IOP, they represent the average optical property belonging to the water. As noted by Kirk (2011), apparent optical properties are largely determined by the IOP of the aquatic medium and not altered by changes in the light structure such as change in solar elevation or cloud cover. This statement provides a basis to the first order assumption in this study which assumes that the particular body of water to have approximately the same K_d regardless of the time of the year, as long as the composition of the water remains about the same. However, this thesis will also investigate the second order nature of K_d variation with respect to tides (Chapter 5) and seasons (Chapter 7).

3.4 Physical processes of light attenuation

The rate at which sunlight reduces with depth in a water column determines the extent to which the water column is lighted and heated by the sun. When the sun's radiation reaches the sea-surface, the radiation is attenuated by the constituents present in the water. Therefore, light intensity decreases with depth. The decrease is also affected by the angle of the incoming irradiance. The radiant intensity I of light at various depths can be calculated using the Beer-Lambert Law. The law implies the following assumptions; a non-diffuse incident light field, zero surface reflectance loss and a perfectly flat water surface. Light intensity I attenuates with depth and is quantified with light attenuation coefficient (or light extinction coefficient) K_d (in m^{-1}) where I_o and I_z is the light intensity at the water surface and at depth z respectively.

$$I_z = I_o e^{-K_d(z)} \qquad \textit{(Eq. 3.6)}$$

Since optically significant constituents (be it water, CDOM, sediment or phytoplankton) in a beam of light will scatter a certain fraction of the incident beam, the scattered flux is equivalent to that in a certain cross sectional area of the incident beam. This is the specific scattering coefficient (or scattering cross section σ_{scat}) of the component in unit area (m^2). The efficiency factor for scattering Q_{scat} is the specific scattering coefficient divided by geometrical cross sectional area of the particle. Similarly, the specific absorption coefficient σ_{abs} has analogous (and equally important!) definition. Finally, the efficiency factor for attenuation is given by $Q_{att} = Q_{abs} + Q_{scat}$.

Absorption and scattering are often complicated since they are wavelength dependent and diffusive in character (Van Duin et al., 2001). They are the two physical processes that contribute to the visible appearance of objects. Coloured light does not change its properties regardless of whether it was reflected or scattered because the colour is the results of the light interaction between the object and light. The blue light of the sky is due to the sun's selective scattering of shorter wavelength, i.e. blue light compared to longer wavelengths like green and red. Similarly, the apparent blue colour of the sea is due to the absorption of longer wavelengths (red) by water molecules. Therefore, a red object will not appear red underwater; since the human eye perceive 'less' red in the reflected light due to the absorption, thus the object will appear 'greyish'. The following will describe both absorption and scattering.

3.4.1 Absorption

When the photons of the visible light are captured by a molecule, they caused sub-atomic transition from one energy level to another corresponding to the energy of the incoming photons. The electrons in the molecule are transferred from ground state to an excited state, shifting from the one rotational/vibrational level to another, belonging to the given energy level at that point (Jonasz and Fournier, 2007). It was also shown that these transitions lead to the formation of entire complexes of electron-vibrational absorption and emission bands with a highly intricate fine structure (Jonasz and Fournier, 2007). The details of the quantum mechanics are far beyond the scope of this thesis but the above is only meant to foster basic understanding with regards to the mechanics of these intricate fine structures.

For eutrophic (highly productive) and mesotrophic (moderately productive) coastal waters with high concentrations of suspended and dissolved material, the absorption coefficient is dominated by that material. As such, the wavelength of minimal absorption shifts to the green, lending green color to that environment. However, the presence of humic material in CDOM distinguishes coastal waters and accounts for their yellow or brown colouration (Shifrin, 1988). Other than light absorption, CDOM also has a broad fluorescence emission band in the blue region (Mobley, 1994). The euphotic depth is approximated as the depth where the irradiance is only 1 % of the surface irradiance, as the minimum sunlight required for photosynthesis. This depth is normally represented as z_{eu} *and is calculated as 4.605 /* K_d *(Kirk, 1994). Similarly, in remote sensing applications, the* $z_{90\%}$ *is the thickness of the layer just below the water surface from which 90% of the light originates.*

3.4.2 Scattering

<u>Scattering coefficient</u>

The second physical process responsible for attenuating light is scattering, scattering coefficient measures the amount of light scattered. Most of the light photons entering the sea are absorbed, but some can are scattered a few more times before they are eventually absorbed. Rather than making the photons 'disappear' as in the absorption, the scattering still allows the photons to be available in the water column for photosynthesis. However, the increased in total pathlengths that photon must travel to a certain depth increases the chances for the photons to be absorbed or scattered back upwards. As such, the net effect of scattering is to just intensify the light attenuation in the water column and leads to a more diffuse character of the underwater light field (Van Duin et al., 2001).

Technically, light scattering is the alteration of the direction and intensity of a light beam due to the combined effects of reflection, refraction, and diffraction (Mueller et al., 2002). The amplitude of scattered light at different angles (the scattering pattern) depends not only on concentration and particle size, but also on the ratio of the refractive indices of the particles to the medium in which the particle exists. The more their refractive indices differ from the medium, the more light will be scattered by the particles. At the other extreme, if there is no difference in refractive indices, no light will be scattered (Webb, 2000). The scattering coefficient of natural waters especially at mid to large angles depends weakly on wavelength, that dependence is further reduced with increasing turbidity.

Volume scattering and phase function

Although scattering is a process that doesn't change the total energy, the direction in which the radiation propagates may be altered. The proportion of incident flux that is scattered in all directions per unit wavelength is equivalent to the scattering coefficient b*. Rearranging* b *is also equal to the fraction of energy dispersed from a light beam per unit of distance travelled when the integral of the volume scattering function is from 0-180° (Jonasz and Fournier, 2007). The scattering coefficient* b *can be partitioned into forward scattering coefficient* b_f *(scattering at angles less than 90°) and backward scattering coefficient* b_b *(scattering at 90° to 180°). The relationship between scattering coefficient* b *and volume scattering function* $\beta(\gamma)$ *is:*

$$b = 2\pi C \int \beta(\theta,\varphi) \sin\theta \, d\theta = \int \beta(\gamma) \, d\omega \qquad \textit{(Eq. 3.7)}$$

The effect of scattering to the penetration of light is determined by the scattering coefficient and the angular distribution of the scattered flux from the primary scattering process (Kirk, 2011). The angular distribution of scattered flux from a beam by a water sample is called the volume scattering function β. The angle between this beam and scattered light rays is the scattering angle. The volume scattering function β is a is a function of the incident radiation (θ,φ)*, wavelength* (λ) *and combining the shape and refractive index of the particle into an average scattering cross section* σ_{scat}

$$\beta(\theta,\varphi,\lambda) = \int_0^\infty \frac{\bar{\sigma}_{scat}(\theta,\varphi,\lambda,r)}{2\pi} n(r) \, dr \qquad \textit{(Eq. 3.8)}$$

where θ *is the polar angle of scattering and* φ *is the azimuthal angle of scattering,* $n(r)$ *is the number of particles with the radius in the range of* r *to* $r + dr$ *per volume. The total scattering coefficient per volume is the integral of the volume scattering function over all angles as shown in Equation 2.8. It is also convenient to express the scattering properties of the medium as the phase function* p *since the form of the scattering function is more important than the magnitude (Jonasz and Fournier, 2007). This is because the total number of particles* $n(r)$ *varies more than the ensemble of the refractive index* n*. For example, when numerically integrated over 90 ≤ φ ≤ 180°,* p *for sediment gives a particle backscatter fraction* b_b *of 0.0183 from Kirk (2011) who quoted (Petzold 1972).*

$$p(\theta,\varphi,\lambda) = \frac{\beta(\theta,\varphi,\lambda)}{b(\lambda)} \qquad \textit{(Eq. 3.9)}$$

Interesting observation from phase function p *is that the angular behaviour of the reflected radiation by the particle is not dependent on PSD since only the geometric cross section and scattering efficiency is needed for the expression of scattering cross section. This seems to hold for all ensembles of randomly oriented convex particles (Jonasz and Fournier, 2007). Another simplification to the phase function of an ensemble of particles is that the wavelength dependence cancels out since the PSD can be approximated by inverse power* j *(Junge distribution). However, theoretically, the phase function is not entirely independent of wavelength, though the dependence is not as strong. The total scattering cross section will vary to first order as* $\lambda^{-\gamma}$ *where* λ *is wavelength and* $\gamma = j - 3$*.*

Light scattering theories

In 1906, Gustav Mie formulated a scattering theory which has no size limitations and converges to the limit of geometric optics for large particles. It predicts scattering intensity I_{scat} as a function of the angle at which light is scattered at the point of interaction with a spherical particle (Webb, 2000). The intensity of the scattered light I_{scat} is a function of the wavelength λ, the scattering angle θ, the particle size d, and the relative index of refraction n of the particle and the medium; $I_{scat} = I_{inc}(\theta, \lambda, d, n)$.

As summarised by Webb (2000) some limitations must be applied in order to accurately model scattering, it includes the assumption on the nature of the scattering itself which includes that only static light (scattering characteristics are independent of the motion of the particle) and single scattering effects are considered with isotropic assumption of scattering particle. Furthermore, all particles are considered to be spheres and have the same optical properties. Finally, the light nature of the field must consist of a single wavelength and light energy may also be lost by absorption by the particles rather than only scattering.

The refractive index n, of most phytoplankton is between 1.05 to 1.1 relative to water while for most sediment it is 1.12 (Kirk, 2011). Since the real part of refractive index n' is close to 1, the direction of light propagation is almost unchanged after travelling a particle at an arbitrary angle (Jonasz and Fournier, 2007). Although more can be said about scattering theories, no further attention is paid to them in this thesis.

3.5 Optically significant constituents

The underwater light field depends on:

a) *The inherent optical properties (IOP) of sea water: The IOP's are dependent upon the concentration and composition of various constituents like the water (c_w), suspended particulate material like minerals and organic detritus (c_s) and phytoplankton (c_p) as well as coloured dissolved organic matter or CDOM (c_g). The c_d is the linear summation of other constituents as follows:*

$$c_d = c_w + c_g + c_s + c_p \qquad \textit{(Eq. 3.10)}$$

b) *The conditions of illumination: The conditions of illumination depend on solar angle, the degree and type of cloud cover, and the state of the sea surface. As a result, underwater light fields show strong diurnal and seasonal variability.*

The constituents (water, CDOM, sediment and phytoplankton) are also called the optically significant constituents. These partial contributions will be discussed in the preceding sections by referencing on previous studies. The relative contribution of optically significant constituents to light attenuation will be discussed while the similarities and difference with Singapore waters will be highlighted. The studies assume a linear additive relation between the constituents stated. However, Kirk (2011) cautioned that the relationship is not truly linear, especially when certain factor dominates over all the other. However, studies have shown that the assumption of linearity seems to work reasonably well at least within a certain range of constituents' concentration (Van Duin et al., 2001, Blom et al., 1994).

Perhaps it is best at this point to introduce the definition of Case 1 and Case 2 waters. In locations where the local marine ecosystem is the only sources of substances affecting the optical properties of waters are known as Case 1 waters (autogenic). Most of the time this occurs in clear oceanic waters (say middle of South China Sea). Case 2 waters however, are affected by the inflow of various substances from rivers, shores, or other external sources (allogenic). For the latter, substances from external environment dominate the optical property and play a significant part in the highly complex interactions with light. All the waters investigated in this thesis falls under the Case 2 category where external influences are the norm. The terminology of Case 1 and Case 2 waters were introduced by Morel and Prieur in 1977. The following will discuss the optically significant constituents.

3.5.1 Waters

Attenuation due to pure water means that only absorption and scattering by water molecules are considered. Any land based impurities and atmospherically derived organic or inorganic matter is not part of the pure water. The absorption and scattering coefficient are normally referred from the table of Smith and Baker (1981), as the optical properties of very clear sea waters. The temperature and pressure dependence of optical properties are undetectable in most natural waters, especially in the visible light band (Pegau and Zaneveld, 1997). For λ > 580nm, scattering by water molecules becomes insignificant when compared to absorption by water molecules, where the attenuation due to water c_w can be considered to be due to water molecule absorption a_w only (Bukata et al., 1995, pg.118). For wavelength from 400nm to 500nm, scattering and absorption by water molecules are equally dominant.

Pure water absorbs strongly in the longer red wavelength of the visible light (and much higher in the Infrared band). Furthermore, due to the scattering being much smaller value in the shorter (blue) than absorption at longer (red) wavelength; pure water displays a blue hue, which gives it blue colour. The blue colour is more prevalent in oceanic water and pristine coastal water without land based loadings/nutrients (Mobley, 1994). For pure water also, scattering in the backward direction is equal to scattering in the forward direction (Rayleigh scattering) while the presence of other impurities in the water will alter this balance (Mueller et al., 2002). Recent measurements of distilled pure water absorption coefficients were carried out by Pope and Fry (1997) using integrating cavity absorption meter (ICAM) showed similar results to Smith and Baker (1981).

The presence of dissolved salts (Cl^-, Na^+, So_4^{2-}, Mg^{2+}*) and gases (oxygen, nitrogen) in seawater is not significant to affect the absorption and scattering in the visible light band. The effect of salt in seawater on the attenuation is lower than the precision of the measuring equipment. Apparently, the most significant absorption due to dissolved salts are observable at UV since the electronic absorption bands of dissolved inorganic salt are at wavelength < 300nm (Bukata et al., 1995, pg.121). For dissolved gases, the concentration of gases usually does not exceed 1 ml/l, while only oxygen absorbs light at visible wavelengths. However even in oxygen rich waters, its concentration is insufficient to produce consequential impact to the attenuation property of waters. Salts increases molecular light scattering in sea water, accounting to 30% of the total scattering, relative to pure water (Morel 1974). Alas, this is also negligible because the total scattering of water only ranges from 0.007 m^{-1} at 400nm to 0.001 m^{-1} at 700nm.*

3.5.2 CDOM

Coloured dissolved organic matter (CDOM, or sometimes called yellow substances, gelbsoff or gilvin) in natural waters is the results of phytoplankton degradation/microbial decomposition or from land based inputs. The former is autochthonic while the latter is allochthonic. The presence of CDOM distinguishes coastal waters compared to oceanic waters and accounts for their yellow/green colouration. The yellow brownish colour is due to the presence of multiple double bonds, conjugated and in aromatic nuclei. Kirk (2011) noted that the decomposition of phytoplankton in the former results in the creation of complex polymers (referred to as water humus) with variety of sizes and molecular weights, of soluble and insoluble fractions. The land based inputs are from rainfall draining through soils (and extracting humic materials) and rivers/lakes bringing these materials to the estuaries.

Factors governing the concentration of CDOM in natural waters are not entirely understood in view of the complexity of the chemical composition and associated volatility of CDOM. It seems that CDOM concentration is consistently higher in estuary which drains from nearby near peat swamps or humid tropical forests (Kirk, 2011). The lack of oxygen in those areas helps to build up partially decomposed organic matter in which CDOM is derived. CDOM is known to be chemically stable although it undergoes photodegradation by intense sunlight at the water surface. As such, it is plausible to assume that for a given water body, the variation of CDOM tend to be around a mean value and the water body can be regarded as typically high, intermediate or low CDOM concentration (Kirk, 2011).

Foden et al. (2008) investigated on CDOM contribution to light attenuation in UK water bodies (more than 15 estuaries, 30 coastal and 70 offshore sites) found that although CDOM was found to be less influential on K_d compared to suspended matter, but it is still statistically significance particularly in coastal waters of lower turbidity. They concluded that CDOM appears to be of terrestrial origin due to the inverse correlation of decreasing CDOM with increased exposure. The more sheltered water body and heavily influenced by rivers and lagoons had average CDOM concentrations more than 5.0 SFU (Standardised Fluorescence Units). CDOM distribution is also dominated by mixing with a strong negative correlation with salinity. CDOM absorption (a_g) was derived from fluorescence measurements and was in the range 0.02–2.2 m^{-1} with mean 0.15 m^{-1}.

McPherson and Miller (1987) found that CDOM attenuation in Charlotte Harbour was greatest in the brackish tidal rivers and decreased with increasing salinity and was positively correlated with water colour. Investigation on four natural lakes in Brazil found that that CDOM is the major component of K_d and explains 76% ($p < 0.001$) of its variation (Bezerra-Neto, et al., 2006). In Singapore, measurements have shown that the CDOM concentrations were relatively small with higher mean of 2.89 mg/l in the Johor Strait and lower 1.37 m/l in the Singapore Strait (Gin et al, 2003). The CDOM concentration in the Singapore Strait was about half of that in the Johor Strait mainly due to the higher levels of primary production and organic detritus in the Johor Strait (Gin et al., 2000). However, the contribution of CDOM to the optical properties in Singapore waters was not investigated until now. The following describes the suspended matters in the water column.

3.5.3 Suspended Inorganic Matter

Suspended particulate matter (SPM or Total Suspended Solids) in the natural waters consists of phytoplankton and non-phytoplankton particulate matter (which include inorganic mineral and organic detritus). This section deals with the latter under the broad heading of sediments. Absorption spectrum for sediment is highest at the blue end of the spectrum and reduces steadily to the red end, which is similar to the CDOM absorption spectra. Since the mineral particles are also brown in colour, it was thought that the humic substances from CDOM are sometimes bound to the inorganic/mineral particles, especially for clay particles which have higher surface area compared to its volume (Kirk, 2011). The light absorption and scattering by suspended particles depend quantitatively and spectrally on the chemical composition of the particles, their concentration in the water, and their physical properties (Jonasz and Fournier, 2007).

The partial effect of all the significant components on the optical properties in in 9 New Zealand estuaries was investigated by Vant (1990) using multiple linear regressions. It was shown that inorganic suspensions (3-11 g/m^3) comprised the major fraction (average 82%) of suspended particulates in the estuarine waters, and were the dominant cause of light attenuation (contributing 56% of beam attenuation on average). Phytoplankton biomass was relatively low (chlorophyll a; 0.5-5 mg/m^3) and caused 14% of the attenuation (Vant, 1990). In particular, since the inorganic mineral is the most dominant component in SPM compared to phytoplankton and detritus, the variability of the inorganic material (i.e. suspended sediment dynamics) and its relation to light attenuation will be elaborated in Section 4.1. This is valid assuming that sediment is the most dominant variable in governing SPM.

Smith (1981) investigated the relative importance of optically significant constituents off the coast of north-west Africa. He found that attenuation showed distinct cross-shelf variations, with highest attenuation at nearshore because of absorption by non-phytoplankton minerals from nearby desert. Similar purpose study in Charlotte Harbour, Florida shows suspended sediment accounted for an average of 72% of K_d, dissolved matter accounted for 21%, chlorophyll for 4% and water for the remaining 3% (McPherson and Miller, 1987). Similar to Smith (1981), attenuation by suspended matter was found to be greatest near the mouth of the tidal rivers and was variable over the rest of the estuarine system. Pierson et al. (2003) show that changes in suspended sediment concentration leads to both long-term and short-term changes in the attenuation of PAR. Blom, et al. (1994) have shown high contribution of sediment to light attenuation in Lake Veluwe, suggesting the effects of wave resuspension.

The contribution of non-phytoplankton particulate matter to the optical properties in Singapore waters is not known. There is evidence of decreasing visibility from limited studies but this has not been linked to suspended sediment, although Chou et al. (2004) points to visibility deterioration close to reclamation areas suggesting sediment as the main culprit. A more systematic approach to SPM measurement in Singapore was carried out by Gin et al. (2002) and found that the SPM concentration in the East Johor Strait was highly variable over the period of study (June 1997 to December 1998). TSS ranged from 2.0 mg/l to 28.8 mg/l (annual mean of 13.6 mg/l) in 1997 and from 7.0 mg/l to 72.6 mg/l (annual mean = 26.5 mg/l) in 1998. The sampling was conducted on a fortnightly basis during neap tide and showed mean contribution of 73.5% of inorganic sediments to the total dry mass of SPM.

3.5.4 Phytoplankton

Suspended particulate matter consists of highly pigmented phytoplankton, zooplankton, algae, bacteria, fungi and detritus (comprising fragments of decayed plant and animals along with their excretion). Phytoplanktons exist in various shapes (filaments, ribbon, stars, etc) and can vary in sizes from 5 to 200 µm (while zooplanktons vary from 30µm to 2mm). Phytoplankton pigments (chlorophyll, carotenoid and biliprotein) are the agent of energy during photosynthesis for plant growth and are an important indicator of the trophic state of natural waters. The amount of light harvested by the pigments depends on the amount of the pigments presence and the size of the algal cells. Lorenzen and Jeffrey (1980) analysed chlorophyll data from various regions and concluded that in regions with shallow euphotic zones most light absorption was due to phytoplankton. Zooplanktons are not considered to be significant in light attenuation studies due to its small concentration.

Absorption spectra of phytoplankton are determined by the composition and concentration of pigments. Pigments have unique absorption spectra with a range of spectral shapes to the respective absorption coefficients (Mobley, 1994). The major groups of pigments are the chlorophylls, carotenoids and phycobilipigments. Highest absorption of chlorophyll occurs in both blue and red region. The carotenoid absorption peaks is in blue region while biliprotein absorption peaks at green, yellow or red wavelengths depending on the algal species, age structure and composition (Kirk, 2011; Bukata et al., 1995). As such, chlorophylls appear green, carotenoid appears orange, and biliprotein appear either red or blue. In addition to the pigments above, there are also decomposed chlorophyll pigments (phaeophytin and phaeoforbid) that might alter the absorption spectrum of the chlorophyll, resulting in an apparent shift in the absorption bands (Bukata et al., 1995).

Gin et al., (2000) studied the spatial and temporal distributions of chlorophyll in Singapore's coastal waters from December 1996 to November 1999 with intermittent sampling scheme averaging 3-4 samplings per year. They found that the chlorophyll levels in the Singapore Strait is generally low ranging from 0.5 to 10µg/l, with an average of 1.7 µg/l with distinct seasonal variation; higher chlorophyll observed during the SW monsoon (averaged 2.3 µg/l) compared to NE monsoon (average 1.4 µg/l) attributed to higher precipitation and flow increase from Malacca Strait and Indonesian Seas. However, higher chlorophyll concentrations in the Johor Strait (averaging 21.5 µg/l) showed episodic elevated level and fluctuate widely (ranging from about 1 to 78 µg/l) compared to Singapore Strait. Chlorophyll a, Chlorophyll b, fucoxanthin and other major carotenoids were dominant in the Singapore Strait but were undetectable in the Johor Strait (Gin et al., 2003).

Only some of the phytoplankton species are available throughout the year. Gin et al., (2000) presented the size structure of the phytoplankton community; the dominant phytoplankton in the Singapore Strait is diatoms like Skeletonema, Chaetoceros and Eucampia representing 35 %, 15% and 10% of the cell counts respectively. In Johor Strait, Chaetoceros, Tintinnopsisa and Skeletonema was the three most abundant species, forming about 55% of the total phytoplankton community. Using ratios of chlorophyll a to pigment that were characteristic of the different algal classes; diatoms comprised 72% of the total chlorophyll in the Singapore Strait, whereas in the Johor Strait they comprised 88% (Gin et al., 2003). Total cell counts of phytoplankton (>10 µm) revealed that cell abundance in the Singapore Strait averaged 70 000 cells/l compared to 500 000 cells/l in Johor Strait.

In Singapore Strait, Gin et al., (2000) showed that during the NE monsoon, the dominant phytoplankton group is picoplankton and small nanoplankton (<8 µm diameter) contributing around 40% of total chlorophyll. For the very large size classes of >100 µm, the contribution was generally 6-20%. However, during the SW monsoon when chlorophyll levels are higher, cells in the <8 µm size contributes about 20% while the microplankton (20–100 µm size class) and >100 µm size contributes about 65% of the total chlorophyll. In Johor Strait, similar pattern was observed with contributions of about 60% for the larger size class while the smaller <8 µm contributed a mere 5%. On the whole, the pico- and small nanoplankton is significant to total chlorophyll in the Singapore Strait compared to the Johor Strait, whereas the reverse was true for the microplankton.

3.6 Underwater light field modelling

Specific studies on the underwater light attenuation are limited in Singapore waters. For instance, there are no known studies exist on the relative importance of CDOM, sediment and chlorophyll to underwater light field. However, studies to estimate the physical properties (SSC or chlorophyll concentration) of ocean water from its optical properties using remote sensing are relatively more abundant; Chang (2007); Heng et.al. (2011) and Liew (2009). Fundamental modelling works on ocean optics using statistical methods are also available (Narvada, 2005). This section will discuss on the radiative transfer model and some of the studies mentioned above.

There are three ways in which the light propagation can be calculated; the first is the Monte Carlo method, secondly semi-empirical methods and thirdly radiative transfer model. The essential characteristic of Monte Carlo is the use of random sampling techniques to arrive at a solution of the physical problem while the semi-empirical method are expressed by empirical relationships between upwelling (or upward) radiance or irradiance values measured at several wavelengths by inversion of the resultant system of equations (Narvada, 2005). Although all three ways are important but since the radiative transfer model is the heart of Hydrolight (to be employed in Chapter 5), only this will be briefly discussed here, without prejudice to the former two ways.

Narvada (2005) investigated remote sensing reflectance and the vertical structure of the oceans optical properties using Monte Carlo method. She showed that the reflectance of a stratified water column is the same as that of an equivalent homogeneous ocean for Case 1 waters (where the concentrations of the optical properties co-varied only with chlorophyll). It was also found that for some vertical structures of chlorophyll considered, the reflectance values for the stratified cases differed significantly from the homogeneous cases, especially for low surface chlorophyll concentrations.

Chang (2007) quantified the in-situ optical properties of surveyed water from Pulau Hantu and Pulau Semakau at various depths. It was found that higher absorption coefficients were from Pulau Semakau compared to Pulau Hantu but both shows low concentration of phytoplankton. Apparently the CDOM absorption in Pulau Semakau is higher (average concentration of CDOM is 6 times more to phytoplankton), but the notation of CDOM here comprise of both CDOM and sediment since it was not separated in the study.

CHAPTER 4.0: METHODOLOGY

4.1 Parameterisation of Light Attenuation Coefficient

4.1.1 Field and laboratory measurements

Field sampling

The author collected water samples at 9 locations around Singapore (Figure 4-1). Relevant information in the sampling location is shown in Table 4-1. The locations were chosen so as to amplify typical conditions for each site, facilitate comparison against previous studies and due to accessibility constraint. The samples were collected at 0.1-0.2m just below the water surface and stored in dark polyethylene bottles. The samples were kept cool during transport and subjected to five separate laboratory procedures; analysis on Total Suspended Solids (TSS) and chlorophyll, followed by turbidity, optical properties and PSD (particle size distribution) measurement. PSD from Serangoon and Tekong were obtained from CRISP while optical data from Semakau was from Chang (2007).

Samples from all other location were collected specifically for this thesis by the author during inter monsoon period (April – June). Water samples were collected using Van Dorn water sampler in the upper 0.5m water column during mid-day, when the sun is vertically positioned during a cloud-free day on a calm sea. Nevertheless, whenever this is not possible sampling was carried out within 2 hours before or after mid-day. Although it is desirable to collect water samples at the same tidal condition at all the sampling locations, it is not strictly possible due to various logistical and accessibility issues. However every care is taken to ensure that the collected samples represent the general condition at a particular location. Samples were mostly collected within 2-3 days after spring tide for consistency, unless otherwise stated.

To determine the influence of tidal forcing (high tide and low tide; spring and neap tide) to the dynamics of optically significant constituents like CDOM, phytoplankton and suspended sediment, a systematic sampling scheme was devised. There are three tiers in which this effect can be detailed. Firstly, 3 random sampling was carried out at East Coast Park (ECP) at different days while at Kranji, the samplings were carried on 4 tide conditions also on different days (during low tide, high tide and twice in between). Finally, sampling at West Coast Park (WCP) was conducted at hourly interval for 12-hr cycle during spring and neap tide. This approach will provide an indication of the influence of tide to the optical properties and suspended sediment dynamics; both as the central tenet of this thesis.

The water characteristics around the sampling location are the same with the sampling location with little difference due to spatial homogeneity. This extrapolation can be made assuming both locations have the same prevailing factors that govern the local characteristics at that particular time. Furthermore, the horizontal scales of significant optical variability (m to km) are usually much greater than the vertical scales (cm) (Mobley, 1994). Therefore, the composition and concentration of optically active substances does not vary over a certain distance from the sampling locations. This is what researchers refer to as a patch of waters having the same optical characteristics (Kirk, 2011; Mobley and Sundman, 2006) proven by recent measurement data in Singapore by Heng et al. (2011).

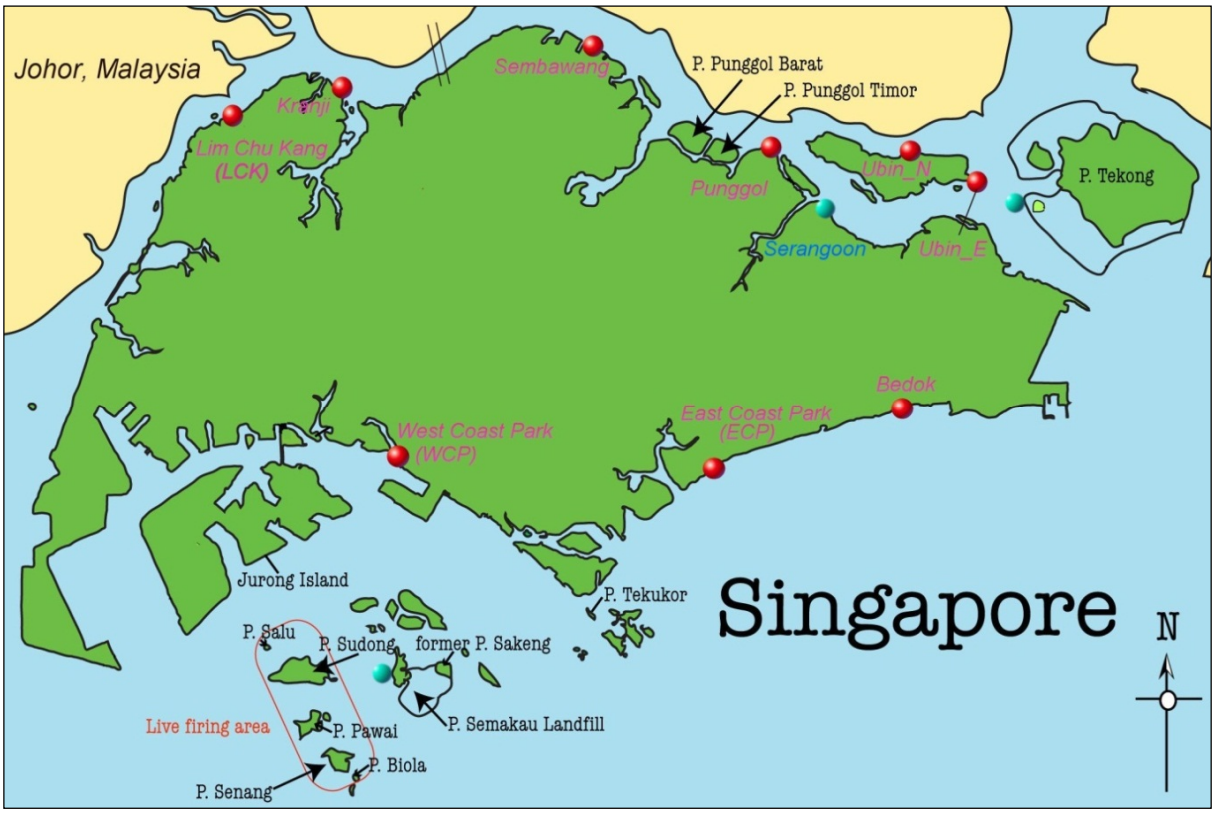

Figure 4-1: Sampling locations in red are collected during field measurements, the blue locations are data obtained from the CRISP database and Chang (2007). See Appendix A for site pictures of the sampling locations.

Table 4-1: Description on sampling date, water level and type of coastal zones in sampling locations

No	Location	Sample	Date	water level	Type of Zone	Remarks
1	Kranji	K04a	12-Apr-12	low tide (0.6m)	Sheltered bay	Calm water
		K04b	12-Apr-12	low tide (0.6m)		Tidal gate opening
		K04c	8-Jun-12	lowest tide (0.4m)		Calm water
		K13a	1-May-12	1.3m		Calm water
		K13b	1-May-12	1.3m		Calm water
		K19a	16-May-12	1.9m		Calm water
		K19b	16-May-12	1.9m		Murky water
		K11a	25-May-12	1.1m		Calm water
		K11b	25-May-12	1.1m		Calm water
		K26a	4-Jun-12	highest tide (2.6m)		Calm water
2	Poly Marina	PM	25-Apr-12	1.8m	Sheltered water	Jetty, oily murky water
3	East Coast Park	ECP1	26-Apr-12	1.4m	Exposed beach	Beach, wave ~ 0.3m
		ECP2	26-Apr-12	1.4m		Beach, near outfall
		ECP3	13-Jun-12	1.1m		Jetty, ~ 0.1m wave
4	West Coast Park	WCPa	3-May-12	2.2m (neap)	Sheltered water	Jetty, shipping
		WCPb	18-May-12	2.4m (spring)		Jetty, shipping
		WCP_N	20-Jun-12	Variable		Jetty, shipping
		WCP_S	5-Jun-12	Variable		Jetty, shipping
5	Punggol	Pgl	22-May-12	2.5m	Transition	Jetty, calm water
6	Pulau Ubin	Ubin_E	24-May-12	1.8m	Estuary	Jetty, high current, wave ~ 0.2m
		Ubin_N	24-May-12	2.0m	Sheltered strait	Calm water
7	Lim Chu Kang	LCK	25-May-12	1.5m	Stagnant water	Floating pantoon, boat waves
8	Sembawang	S	8-Jun-12	2.5m	Partially stagnant	Jetty, wave ~ 0.1m
9	Bedok	B	13-Jun-12	1.1m	Exposed jetty	Jetty, wave ~ 0.1 - 0.2m

Turbidity

Turbidity is described in Shifrin (1988) as "an expression of the optical property that causes light to be scattered and absorbed rather than transmitted in straight lines through the sample". The turbidity of the water samples were measured using Turbidimeter TN-100 (Eutech Instrument, Figure 4-2 a)) in Nephelometric Turbidity Unit (NTU). NTU is widely used as an index for light scattering by suspended particles. NTU relates directly to the optical effects of suspended matter than the mass concentration of particles in the water sample. Figure 4-2 b) shows the light source and a detector to monitor the light scattered at 90° with respect to the incident beam. The basic idea is that particles scatters off light in water and how the light scatters is a measure of the water murkiness. More particles will lead to murkier water and resulting in higher scattering, hence higher NTU.

The turbidimeter was calibrated relative to standards with known light scattering properties before measurement were taken. The water samples were filled into the glass chamber and the average NTU for 3 readings were recorded. The light beam interacts with the particles in the sample and scatters the light. A detector at 90° measures the intensity of the scattered light located at the side of the glass cell (Eutech Instruments, 2011). This is related to the average VSF centred on 90° which is equivalent to the scattering coefficient for a given water sample. Although NTU units are subjective and the turbidimeter does not provide information on intrinsic scattering property, its simplicity and its direct relation to the optical properties of water samples, especially in turbid coastal waters (Vant, 1990) makes this measurement a necessary component in this thesis.

Particle Size Analyser

The Particle Size Distribution (PSD) of the seawater sample was determined by using LISST-100X. LISST (Laser In-Situ Scattering and Transmissometry) uses laser diffraction technique to determine size distribution of an ensemble of particles. The collimated laser beam (parallel beams and minimally dispersed with distance) will be scattered by the particles before the 32 rings detectors (each ring measuring the scattering over a sub-range of angles) collects the total angular scattering distribution of the scattered light (Sequoia Scientific, 2009). The rings cover an angular range from 0.0017 to 0.34 radians which corresponds to the particle size range 1.2 to 250 μm (divided into 32 bins). The scattering intensity was recorded over a range of small angles using a specially constructed multi-ring detector shown in Figure 4-3. PSD was obtained by means of mathematical inversion of the 32-angle volume concentration of particle.

LISST records the volume scattering function β (see Section 3.2) by leveraging on the important small-angle scattering properties of particles in water. A collimated laser beam enters the water chamber and scattered by particles, sensed by a multi-ring detector behind a receiving lens. As the scattering of laser is observed at multiple small forward angles, light scattering is determined almost entirely by light diffracted by the particle (Sequoia Scientific, 2009). This is handy since other information on the particles can be ignored (i.e. laser diffraction is not depended on the composition of particles like refractive index. However, although light that was transmitted through the particle might change in character due to interaction with the particles; alas it is not so important since the transmitted light from the particle to the observed scattering is small.

About 60ml of distilled water was emptied into a chamber that mounts to the optics of the LISST-100X to obtain the background scattered light from pure water before starting the experiment. This background was subtracted from actual particle scattering measurements to obtain the true particulate scattering of the sample. Once the background scatter was obtained, 60 ml of seawater sample was added to the chamber while the interface was activated to communicate with the instrument and for monitoring the progress of the experiment. After the scattering data had been collected for 5 minutes, the raw data were offloaded and processed manually to invert the volume concentrations to obtain PSD. Figure 4-3 shows the LISST and the water sample chamber.

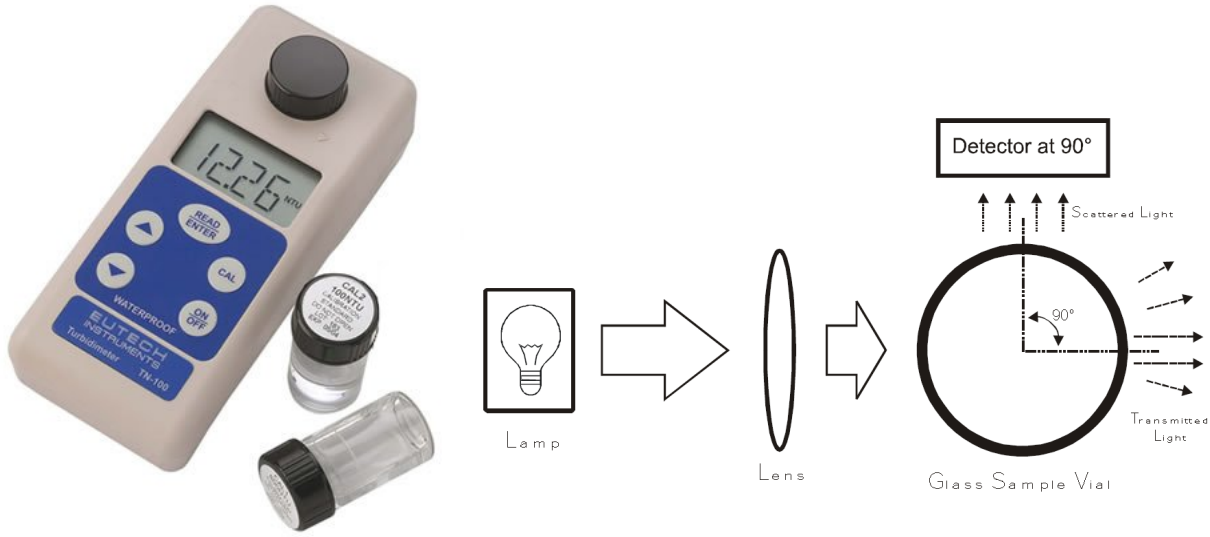

Figure 4-2: Turbidimeter (right) and basic Nephelometric arrangement for turbidity measurement (left). (Figures from Eutech Instruments, 2011)

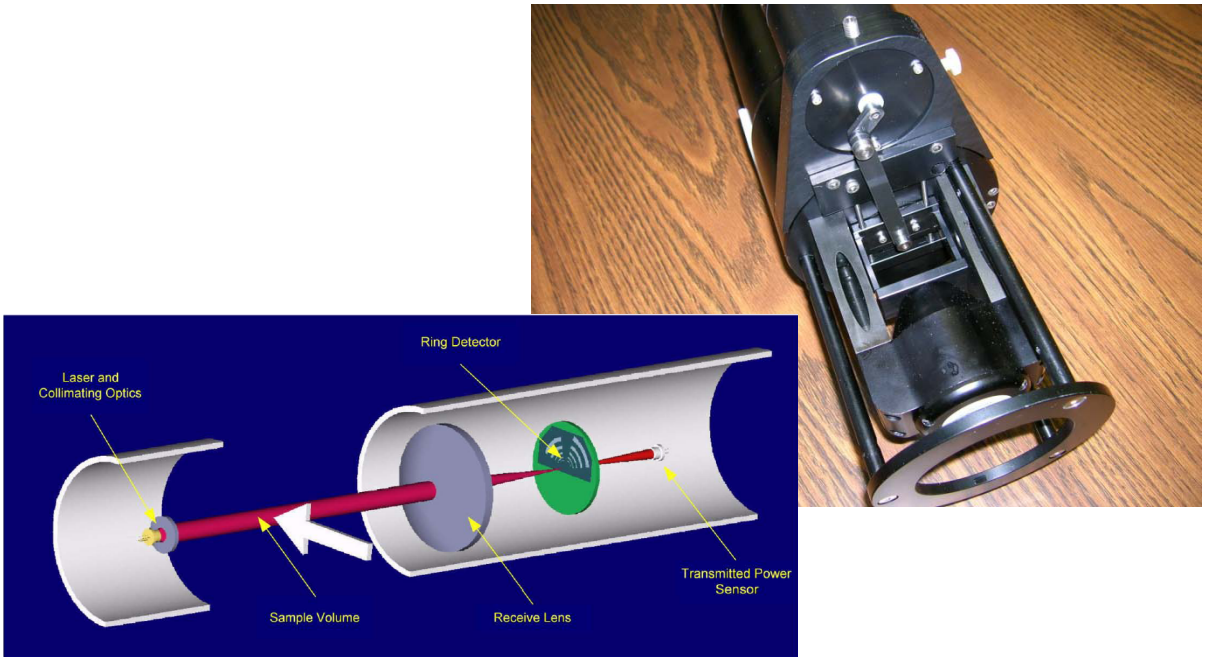

Figure 4-3: The LISST records the scattering intensity over a range of small angles using a multi-ring detector shown in the lower graphic (lower). The chamber for water sample (above) for PSD determination (Figures from Sequoia Scientific, 2009)

Since LISST only provides the volume concentrations of particles for different bin sizes, it was transferred to particle size distribution by assuming a homogenous sphere of particle of a certain radius, r depending on the bin sizes. The volume concentration for each bin was divided with volume of particle $V = 4/3\pi r^3$ to obtain the numbers of particles per cubic meter volume. Hence to find the number of particles for each bin, numbers of particles per cubic meter volume was divided with the difference of the upper and lower limit of bin size. Following this, the number of particles can be plotted against particle sizes which normally equals to Junge power law distribution. Finally, the mean particle size (D_{50}) can be estimated from the cumulative volume of particles against particle sizes.

Total Suspended Solids (TSS)

TSS analysis follows U.S EPA (1999) Method 160.2; Gravimetric, Dried at 103-105EC). The pre-weighed glass microfibre filter (GF/F 47mm, 0.7 µm pore size) was measured before and after the water sample filtration was carried out using filtering apparatus. The filter were then dried in a pre-heated 105 °C oven for 1 hour before placed in a desiccator for several hours and then weighed again with an analytical balance. The cycle of drying, cooling and weighing was repeated until a constant weight was obtained. The readings normally stabilized after one to two drying cycles. The calculation of TSS is as follows:

$$TSS\ (mg/L) = \frac{(Final\ weight - Initial\ weight) * 1000}{Filtered\ volume\ (L)} \qquad \textit{(Eq. 4.1)}$$

The same filter was also used to measure the suspended organic matter of the water sample TSS_{org}. The filter was placed in the oven for 3 hours at 300°C. Upon combustion, the particulate organic matter is oxidized, leaving behind the inorganic mineral and organic ash on the filter. The difference in weight before and after the burning TSS - TSS_{inorg} represents suspended organic matter, TSS_{org}. Calculation of the measured dry weight of TSS (after drying) and the organic content TSS_{org} (after burning) are as follows:

$$TSS_{org} = Final\ weight - Initial\ weight \qquad \textit{(Eq. 4.2)}$$

Once the value of TSS_{org} is obtained from the equations above, the Particulate Organic Content (POC) can be estimated using the relationship between POC and the suspended organic matter TSS_{org} from Babin et al. (2003) in which they referred to papers from Copin-Montegut (1980) and van Raaphorst and Melschaert (1996) as follows:

$$TSS_{org} / POC = 2.6 \qquad \textit{(Eq. 4.3)}$$

Chlorophyll analysis

The concentration of the photosynthetic pigment chlorophyll a (mg/m^3) is used as a proxy variable for phytoplankton biomass. The water samples were subjected to chemical analysis to estimate the chlorophyll concentration spectrophotometrically. Chemical extraction of chlorophyll and spectrophotometer measurement was in accordance to U.S. EPA Method 446.0 (1997); In Vitro Determination of Chlorophylls a, b, c_1 + c_2 and Pheopigments in Marine and Freshwater Algae by Visible Spectrophotometry. The following summarises the procedures followed by the equations to calculate chlorophyll pigment.

The sample bottle were shaken before filtering 300 to 500ml of seawater through a pre-weighed filter paper (47 mm, 0.7 µm pore size) using a magnetic filter funnel. The filter was then placed on a mortar for grinding while adding 4ml of 90% acetone solution. The content was then transferred to 15ml centrifuge tube before 6mL of 90% acetone solution was added. The centrifuge tube was allowed to steep for about 2-12 hours in a dark refrigerator at 4°C. The contents were subsequently centrifuged for 5 min at 10000 revolution/min. Finally, the supernatant fluid was analysed with a spectrophotometer (Genesys 10S UV-Vis). Chlorophyll concentration was then calculated using the equations developed by Jeffrey and Humphrey (1975) and Lorenzen (1967).

After the spectrophotometer has warmed up for at least 30 min, it was zeroed on a 90% acetone solution as a calibration blank at all of the selected wavelengths; 750nm, 664nm, 647nm and 630nm a for the determination of Chl a, Chl b and Chl c + c while 750nm, 665nm and 664nm are used for the determination of pheopigment-corrected chl a and pheo a. In subdued lighting, the supernatant fluid of the extracted sample was pipetted into the glass spectrophotometer cell. If the absorbance at 750 nm exceeds 0.005 AU, the sample was re-centrifuged again. For the determination of pheopigment-corrected chl a and pheo a, the samples was acidify to 0.003 N HCl using the 0.1 N HCl solution before the sample's absorbance at 750 and 665 nm were measured again.

The absorbance measurement at 750 nm is subtracted from the sample's measured absorbance values at 665, 664, 647, and 630 nm to account for the turbidity of the sample. The concentrations (mg/l) of Chl a, b, and c + c in the extract solution were calculated by inserting the 750 nm-corrected absorbance values into the Jeffrey and Humphrey's Trichromatic Equations:

$$C_a = 11.85\,(\text{Abs } 664) - 1.54\,(\text{Abs } 647) - 0.08\,(\text{Abs } 630) \qquad \textit{(Eq. 4.4a)}$$

$$C_b = 21.03\,(\text{Abs } 647) - 5.43\,(\text{Abs } 664) - 2.66\,(\text{Abs } 630) \qquad \textit{(Eq. 4.4b)}$$

$$C_c = 24.52\,(\text{Abs } 630) - 7.60\,(\text{Abs } 647) - 1.67\,(\text{Abs } 664) \qquad \textit{(Eq. 4.4c)}$$

where C_a, C_b and C_c are the concentration of Chlorophyll a, b and c respectively in the extract solution while the Abs (λ) *are absorption value from the spectrophotometer at the corresponding wavelength. Concentration of chlorophyll a and pheophytin a (common degradation product of chlorophyll a) in the extract solution can also be determined using the Lorenzen's Monochromatic equation (by inserting the 750 nm corrected absorbance values) into the following equations:*

$$C_a = 26.7(\text{Abs } 664 - \text{Abs } 665) \quad \textit{(Eq. 4.5a)}$$

$$P_a = 26.7\,[1.7\,X\,(\text{Abs } 665) - (\text{Abs } 664)] \quad \textit{(Eq. 4.5b)}$$

Where P_a is the concentration of pheophytin a in the extract solution. The concentration of pigment in the whole water sample was calculated using the following generalized equation:

$$C = \frac{c\,(a,b,or\ c) * extract\ volume\ (L)}{filtered\ volume\ (L) * cell\ length\ (cm)} \quad \textit{(Eq. 4.6)}$$

Where C is the concentration (mg/l) of pigment in the water sample while c (a, b, or c) is the concentration (mg/l) of pigment in extract measured in the cuvette. The method of chemical extraction using acetone allows the phytoplankton pigment absorption to be separated from sediment absorption that is also present in the filter paper. The results of chlorophyll analysis are presented in Section 5.2.1 of Chapter 5.

<u>Attenuation and Absorption meter (ac-9)</u>

Laboratory experiment to determine the optical properties of water samples was carried out using absorption and attenuation meter (ac-9). Light attenuation depends on the absorption and scattering, measured over nine wavelengths; 412, 440, 488, 510, 532, 555, 630, 676, and 715 nm. Ac-9 calculates the spectral absorption coefficient and attenuation coefficient at those wavelengths using optical theories in Section 3.3. Figure 4-4 shows the instrumentation of ac-9 composed of two housings separated by a frame. The monochromaticity is achieved through rotating filter wheel and propagates into 0.25m pathlength 'c' tube and 'a' tube containing water sample. Light reaching the end of the absorption tube is collected by a large area detector while light reaching the end of the attenuation path propagates into the second receiver housing and is refocused upon a small aperture and detector (WET Labs, 2005).

For the 'c'-beam, light from an incandescent source passes through a 1 mm aperture and is then collimated with a 38 mm lens followed by a 6 mm aperture (WET Labs, 2005). In the 'c' tube, scattered light that hits the blackened surface of the tube is absorbed and therefore does not contribute to the measurement of transmitted intensity. Light radiated through the 'c' beam is therefore subjected to both scattering and absorption by the water. For 'a' beam, beam splitter optics and apertures are identical with the 'c' beam expect for that the beam light is 45° out of phase from that of the c beam (WET Labs, 2005). Unlike the former, the 'a' beam is enclosed by a reflective flow tube so that the forward scattered light is reflected back into the water volume (although not all is reflected). The light is then collected by a diffused large area detector at the far end of both tubes.

Since the ac-9 measurements were referenced to pure water, the measured a and c were processed internally to exclude its contribution. However, since absorption and beam attenuation properties of pure water vary as a function of temperature and salinity, it must be ideally corrected (since temperature affects absorption while salinity affects absorption and scattering). Nevertheless, this effect is negligible since the temperature dependence on pure water absorption is 0 below 500nm and about 0.001 m^{-1} from 500 nm to 700 nm (Pegau and Zaneveld, 1997). Air and scattering correction was applied to the measured coefficients in the post-processing stage. Scattering correction of absorption is important to account for the error in the reflective tube due to the incomplete capture of scattered light.

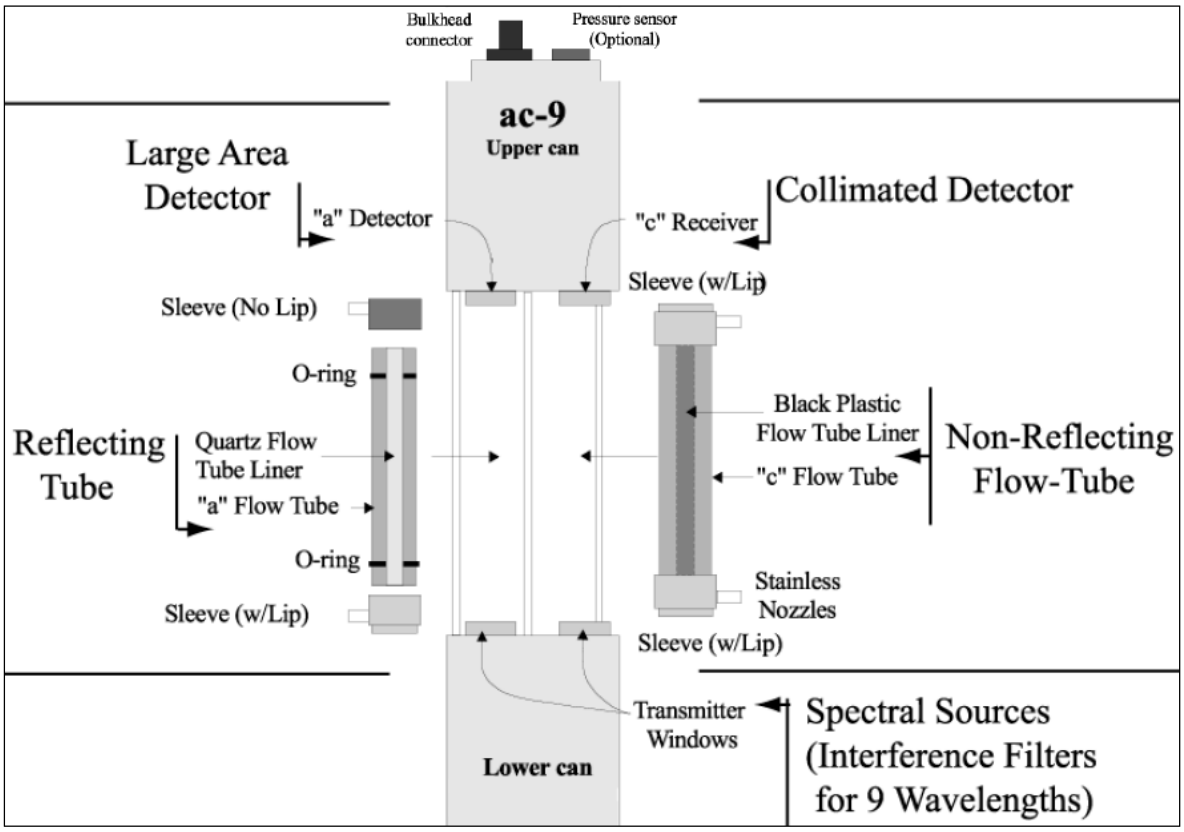

Figure 4-4: Schematic illustration of the attenuation and absorption meter (ac-9). The Quartz liner in the absorption tube reflects any scattered light back to the tube. Figure from Mueller et al. (2002).

Collimated light (parallel rays with minimal dispersion) will propagate through both the attenuation tube and the absorption tube. In the attenuation tube, both scattering and absorption effect was captured since the non-reflecting tube walls absorbs scattered light. However, in the absorption tube, light attenuation is only due to absorption of the in the tube since the tube wall is coated with quartz to prevent the wall from absorbing scattered light and reflect the light back to the tube. Despite this, small amount of scattered light (from 41° to 180°) will not be absorbed and consequently still be present in the absorption tube; hence the experiment was corrected to account for the scattering effect. Three methods used to correct this error are detailed below with higher level indicating higher accuracy:

a) *Level I: The reading at all other wavelengths was subtracted by the 'absorption reading' at 715nm, since it is assumed that any reading at 715nm is due to scattering only since absorption at 715nm is zero.*

b) *Level II: A fixed proportion of the scattering coefficient is removed from each reading, computed by subtracting absorption from attenuation. Kirk (1992) found that this fixed proportion varies from 0.14 for predominately biological particles in the open ocean (Case 1 waters) and increases to approximately 0.18 in waters were scattering is dominated by suspended sediments (Case 2 waters).*

c) *Level III: Combination of Level I and Level II correction. This correction uses the ac-9 reading at 715nm wavelength to determine the proportion of the scattering coefficient to be subtracted from the signal. Scattering is then computed by subtracting absorption from attenuation.*

Using the spectrum generated by ac-9, the light absorption and scattering characteristics per wavelength can be used to determine the relative importance of different factors to overall light attenuation. Since only K_w is estimated from previous studies, the remaining partial contribution of K_g, K_s and K_p will be determined from a scheme as follows; the unfiltered water samples and the filtered water samples (through 0.22µm membrane) represent CDOM (since only CDOM can pass through the filter at that size) will be analysed in ac-9. The subtracted attenuation and absorption readings between the unfiltered and filter water samples represents the TSS, which consist of inorganic (sediment) and organic (phytoplankton) materials. The method to decompose the attenuation due to TSS into sediment K_s and phytoplankton K_p will be described in Section 4.1.2.

4.1.2 Parameterisation of light attenuation coefficient

<u>Decomposition of attenuation spectrum</u>

*To ascertain the relative influence of CDOM, sediment and phytoplankton to the light attenuation potential, absolute value of irradiance I is not essential (see Equation 3.6 for definition). This is because since the IOP, absorption (*a*), scattering (*b*) and attenuation coefficient* (c) *does not vary with solar angle or the degree of cloudiness, they can be measured with reasonable accuracy. Consequently, AOP like the light attenuation coefficient K_d will be estimated by using the known relationship between IOP and AOP. Similar to Equation 3.10, the decomposition of light attenuation coefficient K_d is:*

$$K_d = K_w + K_g + K_s + K_p \qquad \textit{(Eq. 4.7)}$$

Where K_w , K_g , K_s , K_p are the partial contribution to light attenuation from water, CDOM, sediment and phytoplankton respectively. Each of the partial contribution above has combined absorption and scattering properties. The partial contributions also depend on the wavelength and the property of the material in absorbing and scattering lights. K_d is therefore theoretically possible to determine via readings from ac-9. K_w will be estimated from previous studies while K_g is quantified via filtered readings from ac-9. The contribution from both K_s and K_c are 'lumped' together; obtained from the difference reading between unfiltered (K_d) and filtered water sample (K_g). Finally, K_s and K_p will be separated via procedures as outlined in ocean optics protocols by Mueller et al. (2002).

Partial contribution of phytoplankton K_p is difficult to estimate. Specific chlorophyll absorption coefficient a_c^* therefore is normally used as proxy. However, a_c^* is not easily determined even for the well-researched water bodies which depend on the phytoplankton species at a particular time. Furthermore, it is also subjected to variability due to regions, phytoplankton composition and particle effect (Prieur and Sathyendranath, 1981). Even for the widely used spectrum of Prieur and Sathyendranath (1981), its applicability to a particular water body is not definite; at least a factor of five variances was measured for the value of a_c^*(440) between 0.02 and 0.1 m^2mg^{-1}. To complicated matters further, the techniques used to find a_c^* often varies from one publication to another, making comparison difficult. Some studies uses in-vivo absorption by mono-specific cultures while others uses in-situ spectrophotometry for phytoplankton in suspension. Nevertheless, despite the inherent variability, some similarities can be observed in the shape and magnitude of a_c^* as seen in Figure 4-5.

The chlorophyll absorption spectrum will depend on refractive index, size, shape and the chlorophyll content. The a_c^* (per unit of mass) are roughly proportional to the reciprocal diameter (Kirk, 2011) of the photosynthetic pigments. There are a multitude of studies on the specific absorption coefficient of phytoplankton and its variability with regards to environmental condition and taxonomic composition. Example includes Eduardo Millan et al. (1998) in the United States, Suzuki et al. (1998) in Japan waters and Prieur and Sathyendranath (1981) that presents systematic effort to estimate the mean values of a_c^* for application in underwater light field modelling. They iteratively identified the best fit using least square estimate for specific absorption curves for suspended matter (i.e. chlorophyll and sediment) by assuming an exponential absorption by CDOM.

Since the sediment and chlorophyll cannot be physically separated using filtering due to their similarity in size, the separation of partial contribution of chlorophyll K_p and contribution of sediment K_s must be empirically determined. The Chl-a concentration provides the physical basis to determine the relative contribution of chlorophyll and sediment to light attenuation in the empirical equation. Single-parameter model is used to decompose the TSS absorption spectrum by adjusting the values of the variables in the predictor–corrector model. The results from the simulated model will be compared against the measured TSS by minimising the error function. The phytoplankton pigment absorption coefficient is simulated using the model of the following scheme (Lee et al., 1998):

$$a_p(\lambda) = \left[a_o(\lambda) + a_1(\lambda)\ln(a_p(440))\right] a_p(440) \qquad \textit{(Eq. 4.8)}$$

Where $a_p(440)$ is the phytoplankton absorption coefficient at 440nm. The empirical coefficients for $a_o(\lambda)$ and $a_1(\lambda)$ were empirically determined for each wavelength by Lee (1994). This approach allows the $a_p(\lambda)$ curvature to change with $a_p(440)$, consistent with field observations. According to Lee (1994), Eq. 4.9 is valid if $a_p(440)$ is in the range of 0.01 to 1.0 m^{-1} (equivalent to 0.1 – 50 mg/m^3). Once the chlorophyll absorption spectrum $a_p(\lambda)$ is obtained, the absorption spectrum for sediment $a_s(\lambda)$ is obtained by subtracting the former from the total TSS absorption spectrum $a(TSS)$. $a_s(\lambda)$ is similar to the one for CDOM (Kirk, 2011); expressed as $a_s(\lambda) = a_s(440)\, e^{-S(\lambda-440)}$ with S in the range of 0.011–0.021. Because $a_s(\lambda)$ is due to suspended sediment instead of CDOM, S was chosen to be higher in the single parameter model (as compared to 0.012 for CDOM's absorption slope).

<u>*Predictive empirical equations*</u>

The beam attenuation coefficient c is the sum of the absorption coefficient a and scattering coefficient b. It represents the fraction of light attenuated from an infinite light beam in an infinitely small thickness of water. The 'c' will be transformed to the K_d using semi-analytical formula of Van Duin et al. (1992) and Kirk (1984). In the strictest definition, K_d is an AOP that depends on the prevailing light condition while the measured c is an IOP of the water. K_d is assumed to be a quasi-inherent parameter that can be described using the summation of partial K_d from the c terms of optically significant constituents. In Chapter 5, K_d is assumed to be the homogenous throughout the water column (a constant K_d is valid to the first order approximation) while Chapter 6 will investigate the depth variation of K_d followed by the temporal and spatial variation of K_d in Chapter 7.

4.2 Underwater Light Field Modelling

Underwater light field will be modelled using time independent 1D numerical model solving RTE that computes radiance distributions of a water body. The objectives of using Hydrolight are to provide vertical and spectral characterisation of the underwater light field. The following sub-section will deal with the methodology employed to model the underwater light field for IOP (Section 4.2.1) and AOP modelling (Section 4.2.2).

4.2.1 IOP Modelling

Although surface information on IOP was obtained from the field measurement, nevertheless IOP varies with depth, depending on the composition and concentration of optically significant constituents. Therefore, IOP modelling was carried out to model the vertical variation of IOP in the water column. The results of vertical variation in IOP will be used in the radiative transfer theory to compute the AOP in terms of irradiance and various K functions (see Section 3.2 for definition). The measurement of IOP is given precedence over AOP measurement because:

a) IOP can be measured with higher accuracy in the laboratory instead of laborious and not to mention uncertainty of AOP measurement in the field.

b) IOP is a less sensitive parameter compared to AOP. The spatial and temporal dynamics of IOP doesn't change much compared to changes in the AOP (light field) which might occur in shorter timescale (every minute).

c) IOP is independent of sample volume and is linearly correlated to concentration.

IOP modelling was carried out in 2 different models; ABACBB and ABCASE2. The former is for 2 constituents (water and everything else) while the latter is for 4 constituents (water, CDOM, sediment and chlorophyll). Measured a and c obtained from ac-9 are used to determine the IOPs of the second constituents (Mobley and Sundman, 2006) in ABACBB model. The input to ABCASE2 is the concentration of optically significant constituents (CDOM, sediments and phytoplankton), specified as a function of depth. This information was obtained from either field measurement or analytical model, in any case covered in the first component of this thesis in Chapter 5. The concentration of constituents in ABACBB model is not required since they are 'lumped' as one. The total IOPs of a water body are the sum of IOPs attributable to the various constituents in the water column as follows:

$$a_{total}\ (z,\lambda) = \sum_i^n a_i\ (z,\lambda) \qquad \textit{(Eq. 4.9)}$$

Where $a_i\ (z,\lambda)$ is the absorption coefficient of i $^{-th}$ component of the water which is a function of the depth z and wavelength λ. n is the number of components in the IOP model. Scattering phase function was specified for each component based on recommended values from Fournier and Jonasz (1999). This phase function is based on Mie theory and is parameterized by the real index of refraction of the particles and the slope of the Junge size distribution (Mobley, 1994). The following describes the equations used to model the absorption and scattering coefficient for the optically significant constituents.

Absorption

The pure water absorption is taken from Pope and Fry (1997) while the absorption for CDOM was modelled as an exponentially decaying function of wavelength.

$$a(\lambda) = a(\lambda_0)\, e^{-S(\lambda-\lambda_0)} \qquad \textit{(Eq. 4.10)}$$

Where $a(\lambda)$ and $a(\lambda_0)$ is the absorption coefficient at different wavelengths while S is the exponential slope. $a(\lambda_0)$ and S were extracted from the results of Chapter 5. The chlorophyll and sediment concentration was obtained from the field measurement data and converted to absorption and scattering coefficients using the specific absorption coefficient for chlorophyll (Eq. 4.11a) and sediment (Eq. 4.11b) respectively:

$$a_p(\lambda) = a_c^* * [\mathrm{Chl-a}] \qquad \textit{(Eq. 4.11a)}$$

$$a_s(\lambda) = a_s^* * \mathrm{TSS_{inorg}} \qquad \textit{(Eq. 4.11b)}$$

Here, $a_p(\lambda)$ and $a_s(\lambda)$ is the absorption coefficient for phytoplankton and sediment (in m^{-1}); a_c^* is the specific absorption coefficient for chlorophyll while a_s^* is for sediment (in m^2 mg^{-1}). $[\mathrm{Chl-a}]$ and $[\mathrm{TSS_{inorg}}]$ is the chlorophyll concentration in (mg m^{-3}) and sediment concentration in gm^{-3}. Information on chlorophyll specific absorption coefficient could not be found in the literature regarding the dominant phytoplankton species in Singapore waters; therefore the a_c^* as given in Prieur and Sathyentranath (1981) was used. Similarly, the mass specific absorption spectra for sediment a_s^* of Bukata et al. 1995 were used for the sediment absorption. Both these and other two spectrums are shown in Figure 4-5 for comparison. Note the similarities between and Lee (1994) and Prieur and Sathyentranath (1981).

The IOP modelling for ABCASE2 requires the vertical profile of CDOM, chlorophyll and sediment concentration. The vertical concentration of chlorophyll and sediment was estimated from the results of field measurement. However, since the measurement was only carried out at the near-surface, some extrapolation was required. The concentration of chlorophyll was approximated as the measurement value in the surface and linearly reduced with depth. The sediment profile was estimated from TSS_{inorg} in the water surface and reduced linearly throughout the water column but increased to a value of 1.3 times the surface value at the seabed. This is consistent with the observation of vertical sediment concentration in Johor estuary by Van Maren et al. (in prep). Linear reduction profile is a close approximation for logarithmic profile in reality. The CDOM concentration was estimated from the results in Chapter 5.

Scattering

The pure water scattering was obtained from Smith and Baker (1981). CDOM was assumed to not scatter in the model. Therefore, only scattering due to TSS is considered. Scattering coefficient for TSS is modelled by a power-law dependence on wavelength from the model of Gordon and Morel (1983) with the following relation:

$$b_p(\lambda) = b_0\left(\frac{550}{\lambda}\right)^r [\mathrm{Conc}]^1 \qquad \textit{(Eq. 4.12)}$$

Where [Conc] *represent chlorophyll or sediment concentration.* r *is an empirical value of 0.3, 1.0, and 5.0 to simulate a range from ocean to highly turbid waters. The value of* b_0 *(scattering coefficient at reference wavelength, 550nm) varies depending on the location and was extracted from the results of Chapter 5. The* b_0 *was 2.1m*$^{-1}$ *in Kranji and 0.4 m*$^{-1}$ *in WCP for chlorophyll scattering. For sediment scattering the* b_0 *was 5.2m*$^{-1}$ *in Kranji and 4.8 m*$^{-1}$ *in WCP respectively. The scattering phase function for chlorophyll and sediment was assumed to have a backscatter fraction of 0.005 and 0.025 respectively.*

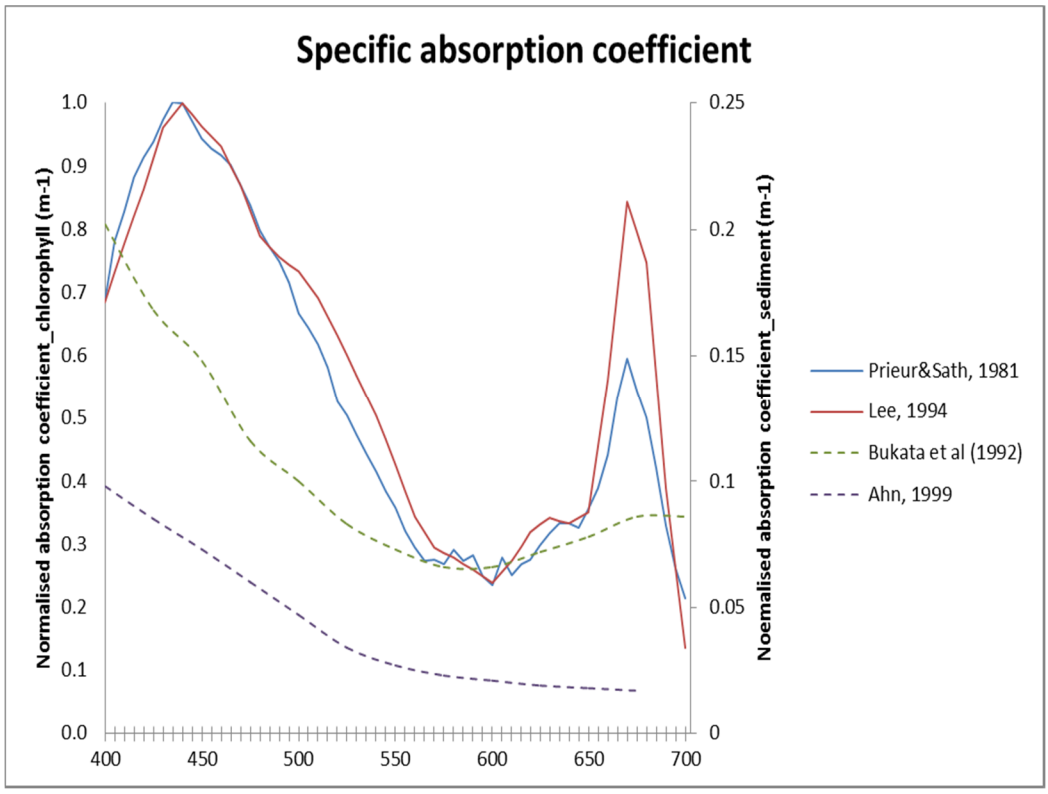

Figure 4-5: Comparison between non-dimensional specific chlorophyll (continuous line) and sediment absorption coefficient (dashed line) from various studies. Values of Lee (1994) will be used in Section 4.2.1 for TSS decomposition while Ahn (1999) represents absorption for brown earth.

4.2.2 AOP Modelling

The quantitative information of K_d *at various depths can provide information that is not possible from measurement alone since the measurements were obtained only close to the surface.* K_d *was modelled based on the IOP (from Section 5.1) and the concentration of optically significant constituents (from Section 5.2). The following describes the model setup for the AOP modelling.*

Model setup

- *Time independent*

Time-independent radiative transfer in Hydrolight is valid because the time scales for changes in environmental conditions (typically seconds to seasons) are much greater than the time required for the light field to assume steady state after a change in the optical properties or boundary conditions (typically seconds) (Mobley and Sundman, 2006).

- *Plane-parallel assumption*

The fundamental assumption in Hydrolight is the "plane-parallel assumption" that suggest limited variability of IOP within similar geographic position (recall spatial homogeneity concept during the field measurement in Section 4.1.1). Since horizontal gradients of IOP are weak, they are ultimately neglected in radiative transfer calculations of one dimensional light propagation. Water-leaving radiance and incident direct and diffuse sky radiance that is reflected upward just above the sea surface is also computed by Hydrolight.

- *Coordinate system*

Hydrolight uses an x-y-z Cartesian coordinate system with +x in the downwind direction and +z downward. Directions are specified via the polar angle θ and azimuthal angle φ, with θ = 0 being straight down and φ = 0 being downwind (Mobley and Sundman, 2006).

- *Numerical scheme*

The Hydrolight solves RTE numerically by discretising over direction and wavelength with specified boundary conditions to arrive at solution for spectral irradiance; a fundamental quantity that describes the light behaviour in depth z, *directional* (θ, φ) *and wavelength* λ. *The directional averaging divides the directions* $(0° < \theta < 180° \text{ and } 0° < \varphi < 360°)$ *into specified quadrilateral regions and polar caps, so called "quads" (Mobley, 1994). Similarly, the wavelength is divided into a number of contiguous wavelength "bands" of width* $\Delta\lambda$. *Hydrolight then computes the quads and bands averaged radiances at various depths. Radiances are thus quad and band averaged spectral radiances with units of W $m^{-2}sr^{-1}nm^{-1}$. Likewise, irradiances are spectral values with units of W $m^{-2}nm^{-1}$.*

To solve RTE, Hydrolight uses invariant imbedding technique which is more advantageous due to less computational time and reduced statistical noise compared to Monte Carlo method. The RTE for the propagation of radiance through the sea with horizontally homogeneous IOP is given by the following in unit μW $cm^{-2}nm^{-1}sr^{-1}m^{-1}$:

$$\frac{dL\,(\theta,\varphi,\lambda,z)}{dz}\,cos\theta = -c\,(\lambda,z)L(\theta,\varphi,\lambda,z) + \int_0^{2\pi}\int_0^{\pi}\beta(\lambda,z,\Psi)\,L(\theta,\varphi,\lambda,z)\sin\theta'_o\,d\theta'_o\,d\varphi'_o + L_r(\lambda,z) + L_f(\lambda,z) \qquad \textit{(Eq. 4.13)}$$

Where $L_r(\lambda,z)$ *and* $L_f(\lambda,z)$ *are inelastic scattering radiance emissions (assumed to be isotropic) due to Raman scattering by water and fluorescence by particles and CDOM. The first term on the right-hand-side of Equation 4.14 accounts for the radiance decrease per meter over path* $(dz/(cos\theta'))$ *due to absorption and scattering. The second term represents the increase in radiance over that path due to photons scattered into direction* (θ', φ) *from all other (source) angles* (θ'_o, φ'_o) *(Mueller et al., 2002).*

Model input and output

- *Sky radiance*

The input of sky radiance distribution was obtained from semi-empirical models that are built into Hydrolight. Information like solar zenith angle, time and location as well as cloudiness was specified as shown in Table 4-2. The angular resolution of the computed radiance was 10° in the polar angle and 15° in the azimuthal angle.

- *Phase function*

Fournier-Forand phase function was specified for all the optically significant constituents using the backscatter fraction. This closed-form, analytical phase function is based on Mie theory and is parameterized by the real index of refraction of the particles andthe slope of the Junge size distribution (Mobley and Sundman, 2006). The individual constituents phase functions are weighted by the respective scattering coefficients and summed in order to obtain the total phase function (Mobley and Sundman, 2006). The phase function specified in the model is shown in Table 4-2.

- *Bottom boundary*

The nature of bottom boundary was included in Hydrolight via bidirectional reflectance distribution function (BRDF; being the ratio of the reflected intensity to the energy in the incident beam) and depends on the type of bottom and wavelength. The bottom boundary is assumed to be infinitely deep, with homogenous water body below 5m depth. This depth was chosen because most of the light is attenuated beyond this depth. The bottom boundary of mathematically perfect opaque surface (flat mirror) was specified using the Lambertian surface of BRDF.

- *Boundary conditions*

The required boundary conditions to solve RTE are at the sea-air interface (to calculate the roughness of the sea surface) and at the sea-bottom. The effect of wind on sea surface can also be included using capillary wave slope statistics (azimuthal angle φ relative to the downwind direction is 0) to describe the transmission properties of the sea surface. Larger gravity waves and whitecaps are often neglected for computation of energy transfer through the air-water surface. Although wind speeds were not measured, historical wind data suggest average wind speeds from 4 to 8 m/s during the sampling period.

- *Output*

The AOP were modelled from 400 to 715 nm wavelength coinciding with the ac-9 band with 50nm band resolution. Output was saved every 0.5m between 0 and 5m depth. Hydrolight computes the radiance and other output (for a given set of input) more accurately than can be measured with standard instrumentation (Mobley and Sundman, 2006).

Table 4-2: Previous studies were used to supplement the model setup if the field/laboratory data is not available. Whenever available, values from field measurement were used as an input.

Parameters	Value
Water absorption	Pope and Fry, 1997
Chlorophyll absorption	Prieur and Sathyentranath, 1981
CDOM absorption	Exponential model with S=0.012
Sediment absorption	Bukata et al., 1995
Chlorophyll scattering	Gordon and Morel, 1983 (empirical values from field data)
Sediment scattering	Gordon and Morel, 1983 (empirical values from field data)
Water molecule phase function	Rayleigh phase function
Chlorophyll phase function	Based on backscatter fraction of 0.005 (Fournier and Forand, 1994)
Sediment phase function	Based on backscatter fraction of 0.028 (Fournier and Forand, 1994)
Sky condition	Based on the sampling time and date
Radiation	Incident sunlight (zero cloud cover)
Wind speed	4 m/s (consistent with average wind during inter monsoon)
Bottom	Bottom reflectance not considered
Water depth	5m (infinite depth assumed)
Fluorescence	Chlorophyll and CDOM fluorescence are not considered

4.3 SSC and Visibility Modelling

The coupled hydrodynamic and water quality model in DELFT3D WAQ allows the influence of tides and waves in modifying the turbidity to be determined (i.e. silt and clay variation, since sand do not play a significant role in water quality). In addition to tides, wave can also influence fine sediment transport by suspending sediment. Nevertheless, considering the magnitude of wave that can cause resuspension of fine sediment in shallow water (h = 10 H_s*), wave height of 0.3m can cause resuspension to the depth of 3 m. Furthermore, waves generated by high speed vessel and ships can cause resuspension of fine sediment along the vessel route. This is relevant in Singapore Strait due to the huge volume of ship traffic. However, due to low ambient wave height and the lack of ship wave data, wave contribution to sediment variation will not be investigated in this thesis.*

The coupled hydrodynamic and water quality modelled visibility by describing the transport of suspended sediment linked to light attenuation. Suspended sediment has been shown to be a dominant control on light attenuation in many shallow coastal waters (Smith 1981; McPherson and Miller, 1987; Pierson et al., 2003), but this link between suspended sediment and light attenuation is not yet modelled in Singapore waters. The modelled K_d *from AOP modelling (Chapter 6) will be qualitatively compared to* K_d *from water quality module in DELFT3D (Chapter 7). Section 4.3.1 will discuss the hydrodynamic model followed by Section 4.3.2 on water quality model.*

4.3.1 Hydrodynamic model

Hydrodynamic modelling was performed using the DELFT3D FLOW, simulating 3D unsteady flow and transport from tidal or meteorological forcing using model setup called SRMRA (Singapore Regional Model Refined and Aligned). This model provides description of water level and flow velocity in Singapore waters focusing on vertical stratification especially in the areas around Johor estuary. The SRMRA is built upon its predecessor 2D Singapore Regional Model (SRM) with some refinement in the model domain especially in the east

coast of Singapore and Johor estuary (see study by Hasan et al., 2011). SRM was developed in 2003 to simulate large-scale tidal and wind-driven flows in Singapore waters.

DELFT3D FLOW is based on 3D shallow water equations, the continuity equations and the transport equations for conservative constituents. The set of partial differential equations are solved with finite difference scheme. This model is implicitly solved but higher flow accuracy can be achieved if the Courant number is less than 4√2. For SRMRA, this criterion is fulfilled with a time step of 4 minutes (Hasan et al., 2011). All the terms in the model equations are solved in a consistent way with at least second-order accuracy in space (Hasan et al., 2011). The following describe relevant information of the model.

Bathymetry

The bathymetry in the SRMRA is based on Admiralty charts with the maximum depth of about 2000 m in the Andaman Sea and varies to over 150 m in the Singapore Strait. Deep waters are found along the Singapore's southern coast, especially the south western, with channels of over 20 m deep running through the Southern Islands (Tham et al., 1970). The inset in Figure 4-6 shows the bathymetry in Singapore waters; note the relatively deep waters along Singapore Strait and even deeper patch in the middle of the strait.

The hydrodynamic is influenced by the bathymetric variation of Johor Strait and Singapore Strait. Depths in the Johor Strait (50 km long and 1.3 km wide) range from about 0.5m to 20m (the western portion is narrower and deeper than the eastern portion). The depth at Singapore Strait ranged from 2m to 130m with average depth of approximately 40m. The middle part of Singapore Strait is only about 10 km wide. The strait has underwater canyons, sand banks located in the Malacca Strait, complicated coastline geometry (due to the small islands and open basins/bays) and sharply varying topography (Kurniawan et al., 2011).

Numerical grid

Due to the complex current pattern in the Singapore Strait due to the interaction of tidal waves from the Indian Ocean (through Andaman Sea) and Pacific Ocean, (through South China Sea) domain decomposition grids are established to capture the governing pattern of the regional flows while at the same time resolving the local flows in the Johor estuary.

The model consist of two (2) grids; outer and inner grid. Both grids are dynamically coupled and solved simultaneously by domain decomposition. The outer grid consist of boundary-fitted curvilinear orthogonal grid with 38,500 grid cells; varying from 200m around Singapore to 15 km at open boundaries (Hasan et. al., 2011) with the smallest grid size of 46m. The inner grid allows for grid refinement in the horizontal direction and vertical direction, capable of resolving the currents and the detailed flow patterns. The inner grid refinement follows the orientation of the deep channel in the Singapore Strait and in the Johor estuary area.

Simulation period

The simulation period for the DELFT3D FLOW was from 1 January 2004 to 31 December 2004. One-year simulation allows the model to capture the seasonal variations of the hydrodynamic conditions as follows:

- *Inter-monsoon period (approximately from April – June)*
- *North East (NE) monsoon (approximately from November – March)*
- *South West (SW) monsoon (approximately from July – September)*

The three scenarios approximate flow condition that occurs for some percentage of the year. Since the seasonal monsoons are variable; the "NE monsoon" scenario shall also be representative of some occurrences, which happen outside the NE monsoon season. This is also the case for the inter-monsoon (pure tide) and SW monsoon scenarios. As such, the labels of "NE monsoon" and "SW" monsoon" scenarios are applied in general terms.

Initial and boundary conditions

Open boundaries for the outer grid are located in the Andaman Sea (west of Singapore), in the South China Sea (the north-east boundary) and in the Jawa Sea (the south-east boundary). The whole of Malacca Strait, as well as Riau and Durian Strait and the numerous islands in Bintan are included in the model domain (Figure 4-6). Tide constituents, long-term average of ocean current set-up (dynamical topography) and frequent fluctuation of the mean sea level make up the three open boundaries components in SRM.

For all the open boundaries in the SRMRA, 8 tidal constituents (4 diurnal – Q_1, O_1, P_1, K_1 + 4 semidiurnal – N_2, M_2, S_2, K_2) have been prescribed based on global tide models while for the effect of dynamical topography; the South China Sea is prescribed to be about 15 cm higher than the Andaman Sea. Finally, the observed difference in level between the two seas is set at up to 0.2m; sometimes the Andaman Sea being higher and sometimes the South China Sea being higher, depending on the season derived from satellite altimetry data. The boundary for the inner grid is extracted along the specified boundary within the outer grid. Figure 4-7 shows the detail of the inner grid with discharge and observation points.

Calibration and verification

Readers are requested to refer to the following papers for details on SRM calibration; Ooi et al. (2010); Kurniawan et al. (2010); Sun, et al. (2009) and Hasan et al. (2011). Ooi et al. (2010) evaluated the sensitivity of the SRM to changes in tidal constituent forcing through single and multi-parameter optimization techniques. Using the results from multi-parameter optimization techniques, the optimisation of the SRM tidal calibration was continued with data assimilation techniques found in the OpenDA environment. OpenDA results improve the fit of M_2 and S_2 constituents for the model and suggest that that depth is more important than bed friction in model calibration (Kurniawan et al., 2010). Throughout the years the SRM had been further improved using sensitivity analysis (Kurniawan et al., 2011) and hybrid data assimilation technique (Sun et al., 2009). Using the former analysis, the vector difference error in tidal representation was reduced by 50%.

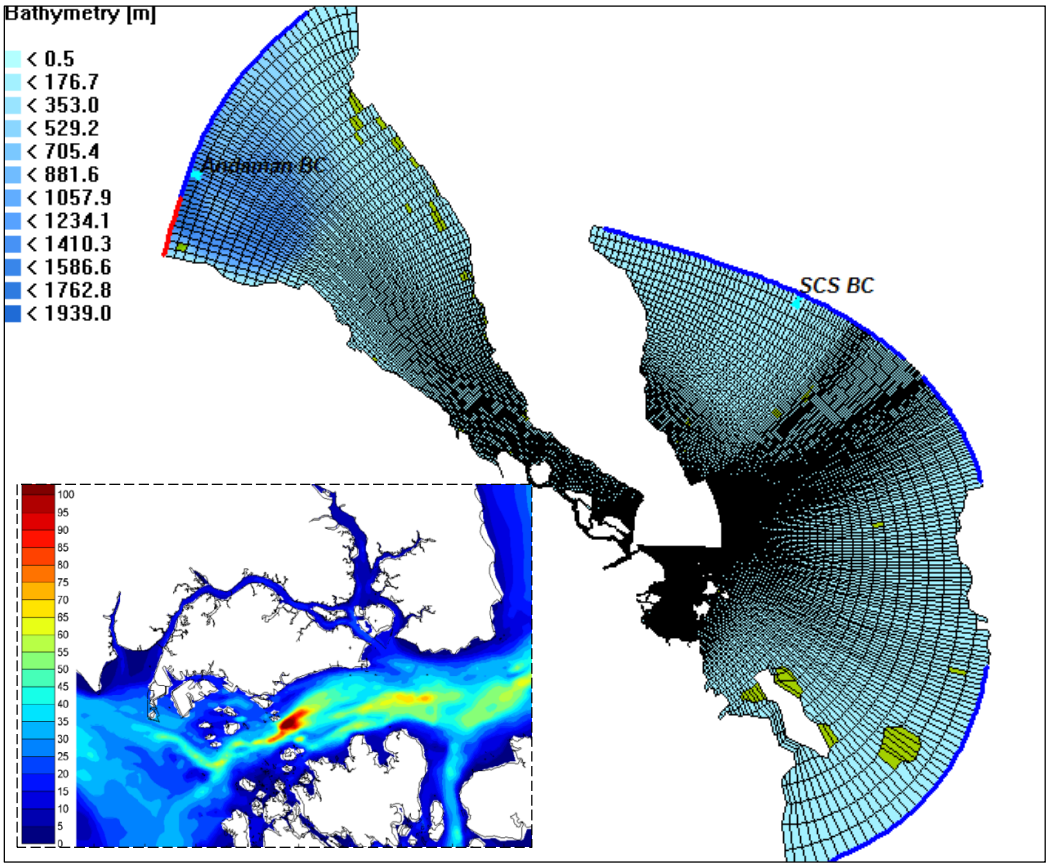

Figure 4-6: Open boundaries for the outer grid. Bathymetry in Singapore waters is shown in the lower left picture. Note the relatively deep waters along Singapore Strait, especially in the middle

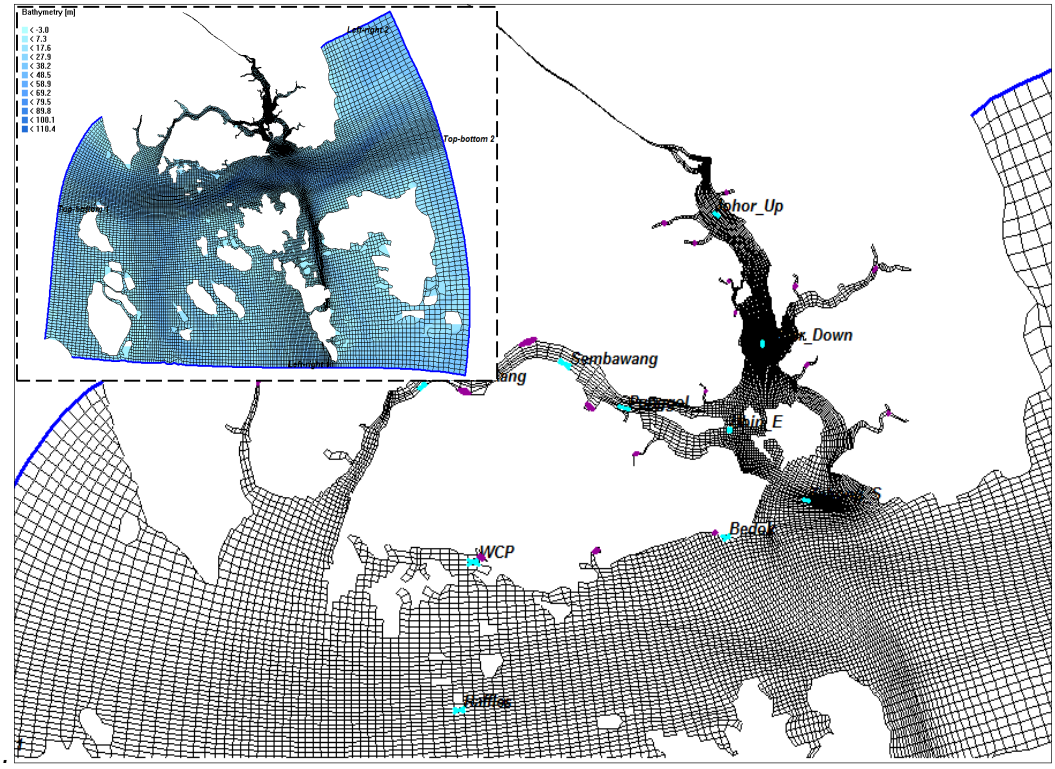

Figure 4-7: The open boundaries of the inner grid in the upper left and 10 observation points (light blue) and about 20 discharge points (purple) specified in the model.

4.3.2 Water quality model

Delft3D-WAQ is a 3D water quality model that solves the advection-diffusion-reaction equation for temperature, salinity, suspended sediment, nutrients and other biological parameters. This water quality model computes visibility vis-à-vis the erosion/sedimentation of suspended sediment. High sediment also limits the availability of light in the water column, hence decreasing the primary production. However, due to the complexity in modelling primary production, it will not be considered in the water quality model although some discussion on this will be provided in Chapter 6. The visibility variation can also be predicted spatially and temporally throughout the model domain in Chapter 7.

Interaction between physical and biological factors often complicates underwater light fields. For example, suspended sediment limit the light available for organisms, but the presence of those organisms may change the sediment stability/re-suspension and thus may also have effect on erosion/deposition processes. Furthermore, chemical composition and processes in the sediment are also influences by benthic organisms. This is both a direct result of their metabolic processes (production and respiration) and their behaviour (tube building, sediment reworking) (Deltares, 2011). Baker (2012) found that the effect of bioturbation on erodibility is a function of time with a factor of 3 to 18 after 8 days of bioturbation in Lake Markemeer. The following will describe the advection-diffusion-reaction equation, model setup and the suspended sediment module in DELFT3D-WAQ.

Advection-Diffusion-Reaction

In this section, the `advection-diffusion-reaction' equation which formed the backbone of Delft3D-WAQ is discussed from the numerical point of view. Delft3D-WAQ solves the transport and water quality processes by satisfying mass balance of active variables (in this case: sediment) for each computational cell. The mass balance accounts for all materials entering and leaving through direct and diffuse processes. The mass balance is computed by the time integration of the reaction equation as follows:

$$\frac{\partial C}{\partial t} = -u\,\frac{\partial C}{\partial x} - v\,\frac{\partial C}{\partial y} - w\,\frac{\partial C}{\partial z} + K_x\frac{\partial^2 C}{\partial x^2} + K_y\frac{\partial^2 C}{\partial y^2} + K_z\frac{\partial^2 C}{\partial z^2} + W + f \qquad \textit{(Eq. 4.14)}$$

Where W are sources and f is the water quality processes. The reaction equation include both advective and dispersive transport, that is the transport by flowing water and the transport as a result of concentration differences respectively (Deltares, 2008). Changes by sources represent any addition/reduction of mass in the system. Changes by processes include physical processes such as re-aeration and settling, (bio) chemical processes such as adsorption and de-nitrification and biological processes such as primary production and predation on phytoplankton (Deltares, 2008). However, only the sediment resuspension and sedimentation processes are included in the visibility model. The advective transport is:

$$T_{x_0}^{A} = v_{x_0} * A * C_{x_0} \qquad \textit{(Eq. 4.15)}$$

With $T_{x_0}^{A}$ as the advective transport at $x = x_0\,[g/s]$, v_{x_0} is velocity at $x = x_0\,[m/s]$, A is surface area at $x = x_0\,[m^2]$ and C_{x_0} is concentration at $x = x_0\,[g/m^3]$.

The dispersive transport across a grid is assumed to be proportional to the concentration gradient and to the surface area:

$$T_{x_0}^{D} = D_{x_0} * A * \left.\frac{\partial C}{\partial x}\right|_{x=x_0} \quad \textit{(Eq. 4.16)}$$

With dispersive transport at $x = x_0\,[g/s]$, D_{x_0} *is the dispersion coefficient at* $x = x_0\,[m^2/s]$, *A is the surface area at* $x = x_0\,[m^2]$ *while* $\left.\frac{\partial C}{\partial x}\right|_{x=x_0}$ *is the concentration gradient at* $x = x_0\,[g/m^4]$.

Model Setup

Delft3D-WAQ has been applied for studying eutrophication, dissolved oxygen depletion and transport of heavy metals through an estuary (Deltares, 2011). However, in view of the focus in the thesis; only the substances and processes involved in sedimentation and resuspension of an inorganic matter is modelled. This provides a link between the suspended sediment and visibility, as a central theme in this thesis. The model contains not only boundary and initial conditions to calibrate, but also many empirical coefficients. Selected parameters are based on field measurement data, previous studies or recommendations in various manuals in the absence of other information.

- *Communication files*

Delft3D-WAQ makes use of the velocities, water elevations, density, salinity, vertical eddy viscosity and vertical eddy diffusivity calculated in the Delft3D-FLOW module as input. The communication files from hydrodynamic and dispersion results were coupled and aggregated so that it will fit the format required by the water quality routines. The dispersion coefficient accounts for the transfer of energy or properties between the resolved scales due to the existence of non-resolved scales; horizontal diffusion and vertical diffusion were specified as 1 and 1^{-7} m^2/s respectively. The additional vertical diffusion was derived from the hydrodynamic simulation obtained from Delft3D FLOW.

- *Substances and processes*

Two variables were modelled in Delft3D-WAQ; Inorganic Matter 1 (IM1) and IM1S1 (fraction of IM1) while the resuspension and sedimentation flux was selected as process parameter. All these setups were from the Suspended Sediment Module (SSM).

- *Initial and boundary condition*

Initial conditions are the concentrations of substances at the start of the simulation. The initial condition of IM1 (in suspension) at the model boundaries was set to 10 mg/l while the initial condition for IM1S1 was specified as 0.5 (dimensionless) during inter monsoon simulation. Boundary conditions are the concentration at all open boundaries of the model grid. Since the open boundaries are far away from the area of interest, the boundary conditions were specified with different values for different monsoon seasons. The boundary conditions for IM1 and IM1S1 during monsoon seasons were higher than inter monsoon as shown in Table 4-3.

- *Simulation period*

To access the effect of seasonal forcing to the visibility, the time frame for water quality simulation was divided into 3 parts, each were set to 2 months where the monsoon prevails. The simulation for North East monsoon (NE) was carried out during November to December while for South West monsoon (SW) during July to August. The inter monsoon (IM) period were simulated from April to May (all the simulation was for the year 2004). The first month allows the model to spin up, while the visibility results from the second month will be analysed for both spring and neap tide condition, during low and high tide as representative condition for the particular monsoon.

- *Numerical scheme*

The numerical scheme to solve the advection-dispersion equation is an iterative, implicit (both in the vertical and in the horizontal) and centrally averaged in the vertical direction. This scheme is first order accurate in the horizontal and second order accurate in vertical direction. No dispersion transport is allowed if the flow is zero in tidal flats (areas that can be temporarily dry) and in the open boundaries. In order to prevent numerical oscillations (boundary reflections) at the boundaries, first-order advective transport was specified. This scheme is generally fast and efficient for stratified system, but the numerical dispersion may be large and positivity is not guaranteed.

- *Discharge*

Discharge of the active substances (i.e. inorganic matter, IM1) was also specified in the model setup. The highest flow rate and sediment concentration of the discharge is 57 m^3/s and 150 mg/l in the Johor River. Other smaller rivers like Pulai and Skudai have lower flow rate but its concentration was maintained at 150mg/l. In total, there were about 20 discharge points specified in the model domain from the upstream of Johor River to around south of Singapore mainland. The discharge of concentration was specified to be higher during both monsoon seasons to represent average wet season (Table 4-3).

- *Waves*

Wave forcing was not taken into account in the model as the wave climate is generally low in Singapore waters. Furthermore, the contribution of waves towards the resuspension of sediment is not considered to be significant. The influence of wind and wave on the sediment discharge in the study area is not significant due to the smaller bed shear stress induced by wind and wave effect compared to that induced by tidal currents.

- *Outputs*

Outputs were specified as time-series for the observation points and the spatial map plots of IM1 concentration (representing SSC) and visibility in Secchi depth S_d. 10 observation points were specified throughout the model domain coinciding with most of the sampling locations (Figure 4-7). The outputs for the time series were saved every 30 minutes while the outputs were saved every one-hour for spatial plots.

Suspended Sediment Module (SSM)

Suspended sediment is one of the most intuitive water quality parameters since its impact are not only physically visible (aesthetics and coloration) but also influenced by bio-chemical feedback (bioturbation from burrowing organism). Furthermore, as reiterated previously, the importance of suspended sediments in influencing water quality is expected to be the most dominant. The relation between sediment and water quality was investigated using the Suspended Sediment Model (SSM) in DELFT3D-WAQ.SSM calculates the Secchi depth and light attenuation coefficient to access the underwater light field.

SSM consists of a single suspended sediment fraction called IM1 (Inorganic Matter Fraction 1) in two state variables. The first layer is IM1S1, a thin suspension layer on top of the solid bed which actively accumulates and erodes. The second layer is IM1S2, a deeper layer in which sediment gradually accumulates but only eroded during energetic conditions (Van Maren at al., in prep). The suspended sediment in the water column (IM1) decreases when sedimentation occurs while resuspension (or erosion from bottom) increases the IM1 in the water column. All the variables form a closed mass balance with its suspended and sedimentation processes. Figure 4-8 shows the flow chart of the processes in SSM.

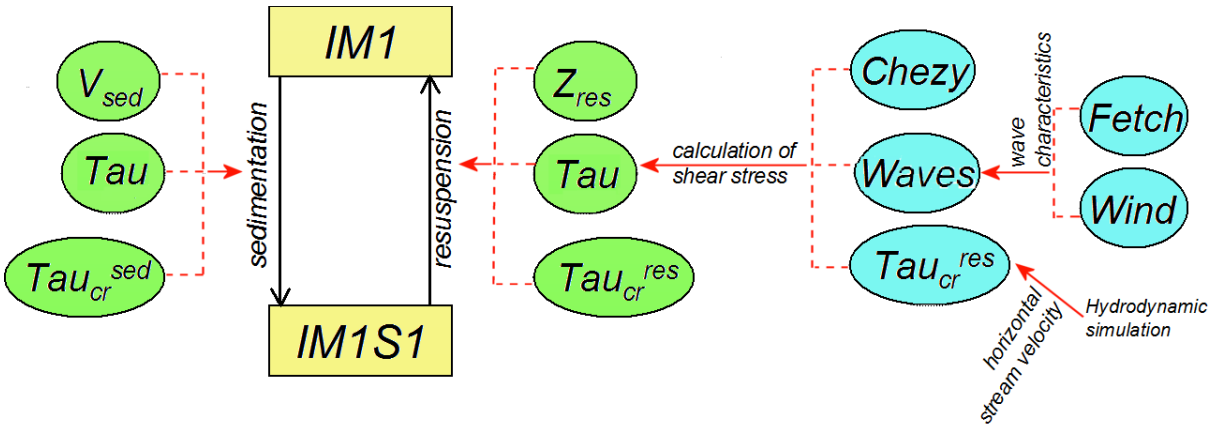

Figure 4-8: The connection between state variables, processes and process parameters in SSM of DELFT3D-WAQ (Deltares, 2008)

SSM simulate the dispersion of suspended sediment taking into account sedimentation and erosion using Partheniades-Krone formulations. The sedimentation of IM1 occurs when the ambient shear stress τ *is lower than the critical shear stress for sedimentation* τ_{cr}^{sed} ($\tau < \tau_{cr}^{sed}$). *Similarly, the resuspension (or erosion) occurs when the ambient shear stress is higher than the critical shear stress for erosion* $\tau < \tau_{cr}^{ero}$. *Sedimentation and erosion flux are calculated as follows:*

$$\text{Sedimentation flux } (gm^{-2}d^{-1}) = P_{sed} * V_{sed} * [IM1] \qquad \textit{(Eq. 4.17a)}$$

$$\text{Erosion flux } (gm^{-2}d^{-1}) = P_{ero} * Z_{ero} \qquad \textit{(Eq. 4.17b)}$$

Where V_{sed} *is the setting velocity (m/d) while* [IM1] *is the concentration of IM1 (g/m*^{3}*).* Z_{ero} *is the zero-order erosion rate (g/m*^{2}*d).* P_{sed} *and* P_{ero} *is the sedimentation and erosion probability respectively given as:*

$$P_{sed} = 1 - \frac{\tau}{\tau_{cr}^{sed}} \text{ if } \tau < \tau_{cr}^{sed} \text{ or } P_{sed} = 0 \text{ if } \tau_{cr}^{sed} \geq \tau \quad \textit{(Eq. 4.18a)}$$

$$P_{ero} = \frac{\tau}{\tau_{cr}^{ero}} - 1 \text{ if } \tau > \tau_{cr}^{ero} \text{ or } P_{sed} = 0 \text{ if } \tau \leq \tau_{cr}^{ero} \quad \textit{(Eq. 4.18b)}$$

The ambient shear stress τ depends on shear stress exerted by velocity τ_{vel} which depends on horizontal stream velocity and Chezy coefficient. Table 4-3 shows the specified values for active processes and boundary condition for inter monsoon and monsoon scenarios. Most of the values in the active processes were obtained from Van Maren et al. (in prep).

To access the underwater light field, SSM calculates the Secchi depth, S_d as follows:

$$S_d = \frac{PA_{constant}}{Ext_{total}} \quad \textit{(Eq. 4.19)}$$

Where $PA_{constant}$ is the Poole-Atkins constant while Ext_{total} is the total attenuation of visible light (or extinction coefficient). Total visible light attenuation, Ext_{total} is based on the summation of the background attenuation and the attenuation due to IM1 as follows:

$$Ext_{total} = Ext_{background} + (Ext_{IM1} * [IM1]) \quad \textit{(Eq. 4.20)}$$

Where $Ext_{background}$ is the background attenuation for visible light (specified as 0.6m^{-1} during inter monsoon to account for pure water attenuation plus background CDOM and chlorophyll concentration). Similar to Chapter 5, the specific attenuation of IM1 (Ext_{IM1}) is multiplied by the inorganic matter concentration in g/m^3 to arrive at the attenuation due to IM1.

<u>Summary of methodology</u>

This first component in Section 4.1 addresses three important issues to describe light attenuation; the dynamics of optical properties, the spectral nature of the underwater light field due to various constituents and the effects of sediment to light scattering. The Chl-a concentration was multiplied with the specific chlorophyll absorption coefficient a_c^* to determine the absorption spectrum due to phytoplankton alone. The contribution of sediment and phytoplankton to light attenuation is separated by subtracting the chlorophyll (phytoplankton) absorption from TSS absorption spectrum. Similar procedure was followed to separate chlorophyll and sediment scattering.

The second component (Section 4.2 and 4.3) will develop predictive capability for light attenuation characteristics and visibility using state of the art numerical modelling technique. Field measurement and process-based modelling will be combined to allow extension of field data temporally and spatially. Figure 4-9 shows the schematic of this thesis taking into account the link between Chapter 5, 6 and 7 against the main aspects as follows; NTU, IOP, AOP, K_d and S_d.

Table 4-3: Values specified in the model for the process parameters, initial and boundary condition for inter monsoon (IM) and Northeast (NE) and Southwest (SW) monsoon respectively.

Active processes	Dimension	IM	NE	SW
Sedimentation velocity	m/d	1.7	1.7	1.7
Critical shear stress for sedimentation	N/m^2	1000	1000	1000
Fraction IM1 in layer S1	-	0.5	0.6	0.55
Zeroth-order resuspension flux	g/m2/d	8640	8640	8640
First-order resuspension flux	1/d	0.0864	0.0864	0.0864
Critical shear stress for resuspension	N/m^2	0.1	0.1	0.1
Specific extinction coefficient for IM1	m2/g	0.08	0.08	0.08
Background extinction	1/m	0.6	0.65	0.7
Initial condition				
Inorganic Matter (IM1)	g/m3	10	10	10
Inorganic Matter (IM1) in layer S1	-	0.5	0.5	0.5
Boundary condition	g/m3			
Top Bottom 1 (Straits of Mallacca)		10	10	30
Left Right 1 (Jawa Sea)		10	10	30
Left Right 2 (South China Sea)		10	20	10
Top Bottom 2 (Pacific Ocean)		10	20	10
Discharge				
Flow rate	m^3/s	varies	varies	varies
Inorganic Matter (IM1)	g/m3	150	180	165
Inorganic Matter (IM1) in layer S1	-	0.5	0.6	0.55

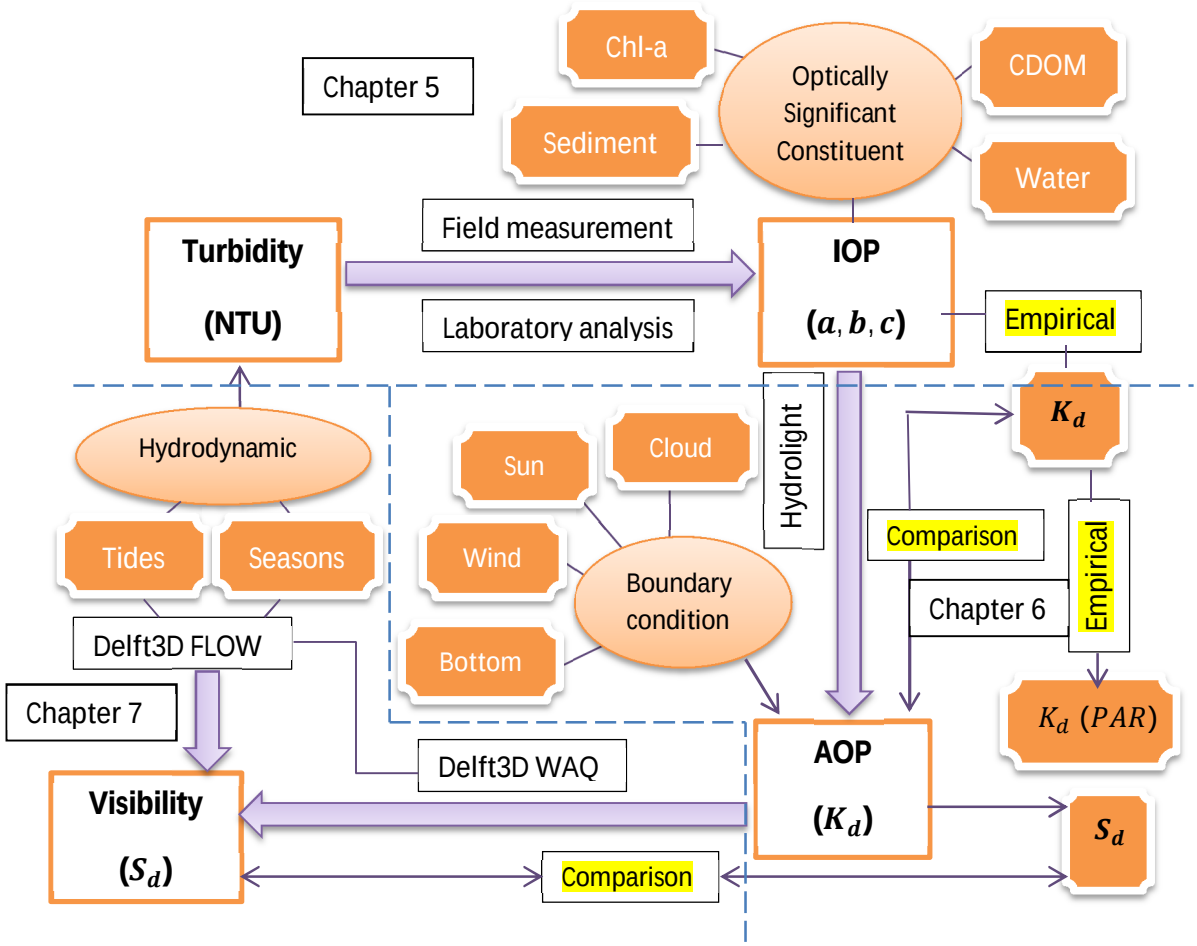

Figure 4-9: Flow chart describing the schematic of this thesis with respect to the methodology and the relations between the main aspects.

CHAPTER 5.0: PARAMETERISATION OF LIGHT ATTENUATION COEFFICIENT

Table 4-1 had provided information on the range of available sampling data corresponding to various types of coastal zones. These data constitute a reasonably good sampling of the diverse types of marine environment, from the near stagnant productive water in the Johor Strait (Lim Chu Kang, Kranji, Sembawang and Punggol) to the exposed beaches in the south of the mainland (ECP and Bedok). Pulau Ubin represents special case of highly anthropogenic waters due to the domestic and industrial discharges from Johor River for comparison against sheltered marine systems in West Coast Park (WCP) with minimal anthropogenic discharges. There are two sampling locations in Pulau Ubin; Ubin E and Ubin N, the latter represents stagnant water located at the north of Pulau Ubin while the former is situated directly at the mouth of Johor River, east of Pulau Ubin.

The optical properties of the sampling locations (which are considered as Case II waters) will be compared against the data from Chang (2007) representing quasi-Case I waters. Limited qualitative comparison will be drawn as the latter is only available at one location (Pulau Semakau). The results in this chapter are presented as follows; Section 5.1 will describe the light attenuation due to hydrodynamic forcing. Section 5.2 will then investigate the absorption and scattering spectrum of optically significant constituents. Section 5.3 will build on the results from earlier sections and will focus on the specific contribution of suspended sediment to light scattering. Finally, Section 5.4 decomposes the light attenuation coefficient to its constituent's (water, CDOM, sediment and phytoplankton) followed by the determination on the exact contribution of each in attenuating light.

5.1 Optical Properties and Hydrodynamic Forcing

Measurement during IM period (April-May) provided the best opportunity to investigate the dynamics of optical properties due to tidal forcing with minimal monsoon influence. The optical properties changes with respect to hydrodynamic forcing (high tide and low tide as well as spring-neap tide) as shown by Mobley (1994) and Lee et al. (1998). The optical properties due to CDOM will remain almost constant with the hydrodynamic forcing due to its limited concentration although it can vary considerably with river discharge (Pierson et al., 2003). Assuming average river discharge, this leaves phytoplankton and sediment as 'variable' optical properties that might vary with tides. However, further simplification can cancel either one depending on the nature of the water (chlorophyll or sediment dominated); leaving either one as the single variable that changes the optical properties of the water.

Strictly speaking, optical properties are not constant all the time; it shows variability related to prevailing environmental condition due to hydrodynamic or meteorological forcing. Although the field measurement is operating on the assumption that the local momentary sampling is a valid representation of typical condition, the fine variation during low/high tide can provide indication on the variability of optical properties outside the sampling time. As reference, physical and optical properties (represented as scattering coefficient at 555nm) from the West Coast Park (WCP) were investigated from hourly water samples for 12 hours during low and high tide for spring condition. Although the variation of TSS and $b(555)$ *also vary according to currents, it was not taken into account due to the complexities associated with measurement of currents. Nevertheless, light attenuation variation and its relation to current velocity will be analysed qualitatively in Chapter 7.*

The variation of physical property i.e. TSS with water level (Figure 5-1) is more straightforward than optical property i.e. $b(555)$ variation with water level (Figure 5-2). Firstly, highest TSS occurred during highest gradient in the water level (indicative of highest current velocity since the latter is a derivative of the water level gradient) and during low tide with no phase difference with the water level. This shows that TSS is advection dominated during low tide (convective effect from nearby discharge and/or ebb currents). Thirdly, lowest TSS occurs few hours after high tide slack suggesting that TSS settles down the water column and is suspension dominated.

The TSS concentration in Chuah (1998) was less than 16 mg/l while TSS concentration in this thesis rarely goes below 30mg/l, averaging around 50-60 mg/l. This shows that the TSS had increased at least two to three fold within the past 20 years at least in WCP, consistent with findings from other studies by Gin et al. (2002); Chou et al. (2004); Dikou and van Woesik (2006). For $b(555)$ however, a second order effect which is opposite from that of TSS variation can be observed due to the interplay of optically significant constituents. Figure 5-2 shows almost constant $b(555)$ of 6-8m^{-1} from low to high tide. Highest $b(555)$ occurs during low tide. But a $b(555)$ peak is observed after high tide slack, indicating resuspension. The phase of $b(555)$ with current is modulated by the suspension or deposition of SSC and is simulated in Chapter 7.

Variation in chlorophyll concentration due to low tide/high tide provides insights to the dynamics of light attenuation. In eutrophic, near stagnant bay like Kranji, measurement showed higher Chl-a concentration during high tide (about 66 mg/m^3) compared to 44 mg/m^3 during low tide. This is expected to correspond to slightly higher partial attenuation coefficient due to phytoplankton, K_p during high tide. However, K_p depends on the type and the concentration of chlorophyll pigment and its relative importance is site-specific and time-varying. Chuah (1998) found that the fluctuation in Chl-a concentration is higher during neap tide. The chlorophyll also seems to show overall increase during the end of monsoon and early inter monsoon (Chuah, 1998; Dikou and van Woesik, 2006). The increase in phytoplankton density in East Johor Strait is due to reduced salinity during low tide enhanced by river flow, bringing nutrients from the upstream of Johor River.

The higher Chl-a concentration during high tide is consistent to Tham et al. (1970) who reported higher cell count during high tide. However this is in contrast to Chuah (1998) who reported lower Chl-a concentration during high tide. But both these studies were carried out in East Johor while Chl-a concentration due to the tidal effect was only sampled in Kranji (West of Johor strait) for this thesis. Phytoplankton concentrations are likely to be more variable than was evident from the limited measurements, specifically in chlorophyll dominated waters. Phytoplankton experiences fluctuations due to incident light (minutes) to tides (hours), and variations in wind-induced resuspension (hours to days). Beyond the measurement data, larger time scales also affect the dynamics of light attenuation. For example, contribution to light attenuation often originates from phytoplankton on a seasonal basis (months–years), but from suspended solids on a smaller time scale (days–weeks) (Van Duin et al., 2001).

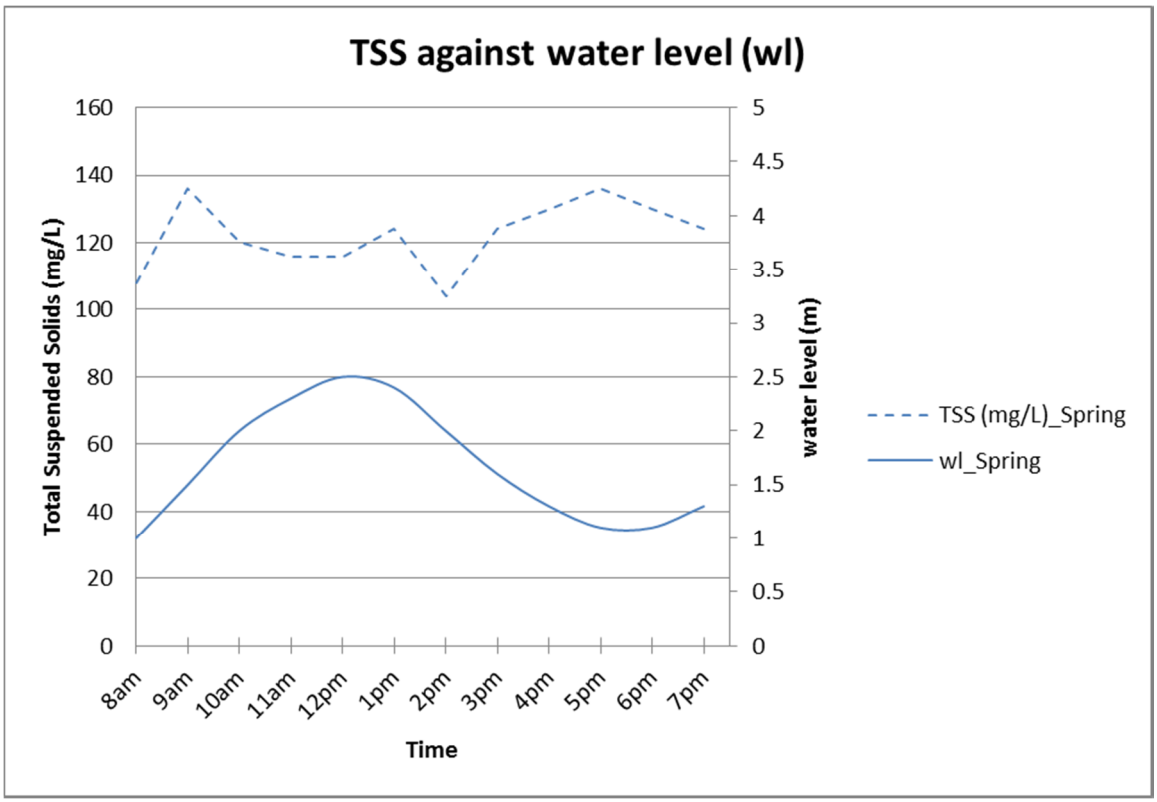

Figure 5-1: Variation of TSS in relation to low tide and high tide. The TSS during low tide and flood tide is consistently higher compared to high tide.

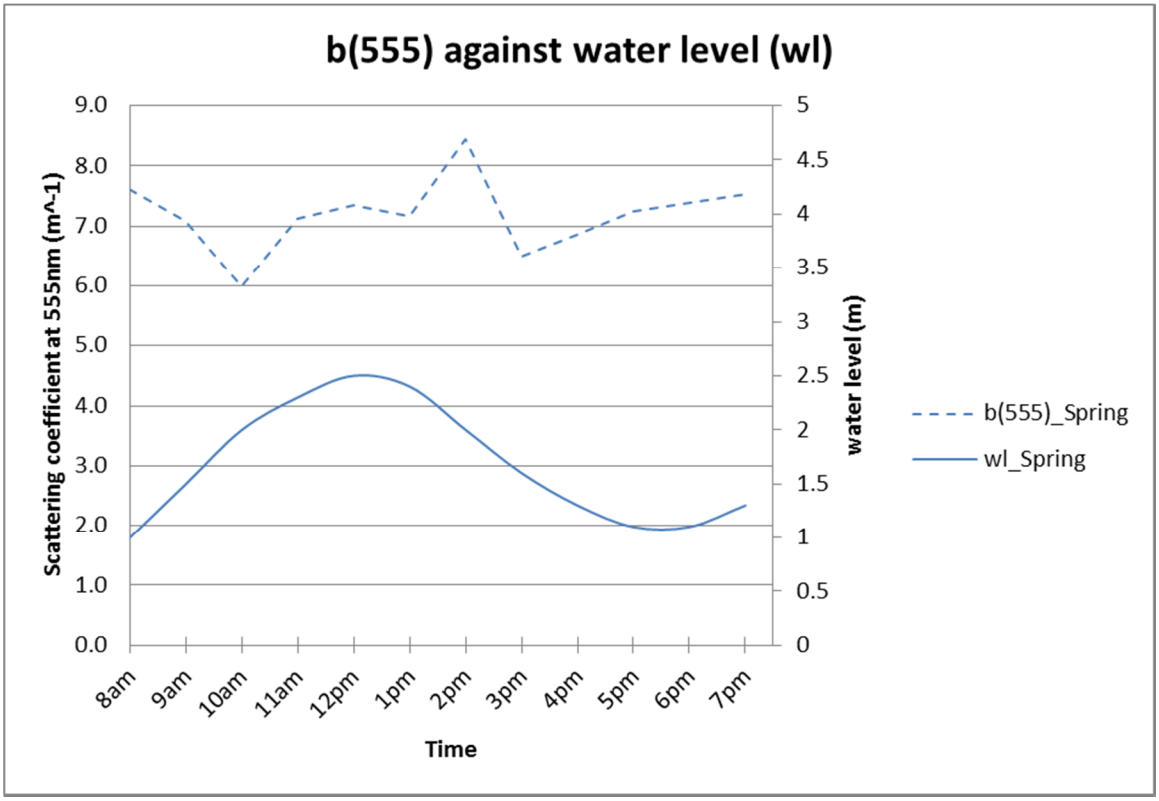

Figure 5-2: Variation of $b(555)$ in relation to low tide and high tide. $b(555)$ is higher during high tide and lowest during the highest gradient in the water level.

Owing to land runoff and tidal influences, coastal water properties changes rapidly (Lee et al., 1998; Vant, 1990). These properties may also include optical properties. Figure 5-3 shows the hourly variation of beam attenuation coefficient, c *in WCP during spring tide. Similar to the variation of* b(555) *in Figure 5-2, the variation in* c *during low/high tide is small (6 to 8.5m^{-1}). The highest attenuation was recorded few hours after the high water slack, while the lowest was recorded during flood tide. The results in this section show that optical properties vary slightly depending on the tides and follow the variation of the most important optically significant constituents in the local system (i.e. sediment in WCP and phytoplankton in Kranji). Assuming that WCP is representative of Singapore waters, the lowest and highest optical properties vary 31 %, with higher* c *occurring 2 hours after high tide.*

The optical properties of nine estuaries in New Zealand varied with a factor of about 3 during the ebb and flood tide (Vant, 1990). However, the effect of seasonal monsoon is unknown from the limited measurement data although it caused five to ten-fold increase compared to the intra-tide changes in New Zealand estuaries (Vant, 1990). The dynamics of light attenuation can also be caused by periodic increase in river discharge (Pierson et al., 2003) bringing with it high SSC and organic matter. The presence of floodwaters (high discharge) had caused an increase of at least five-fold increase in TSS compared to the ambient values in New Zealand (Vant, 1990). However, Van Maren at al. (in prep) showed that even large flood (10 year recurrence interval) from Johor River will only marginally influence the sediment dynamics in Singapore Strait (and by extension, towards WCP).

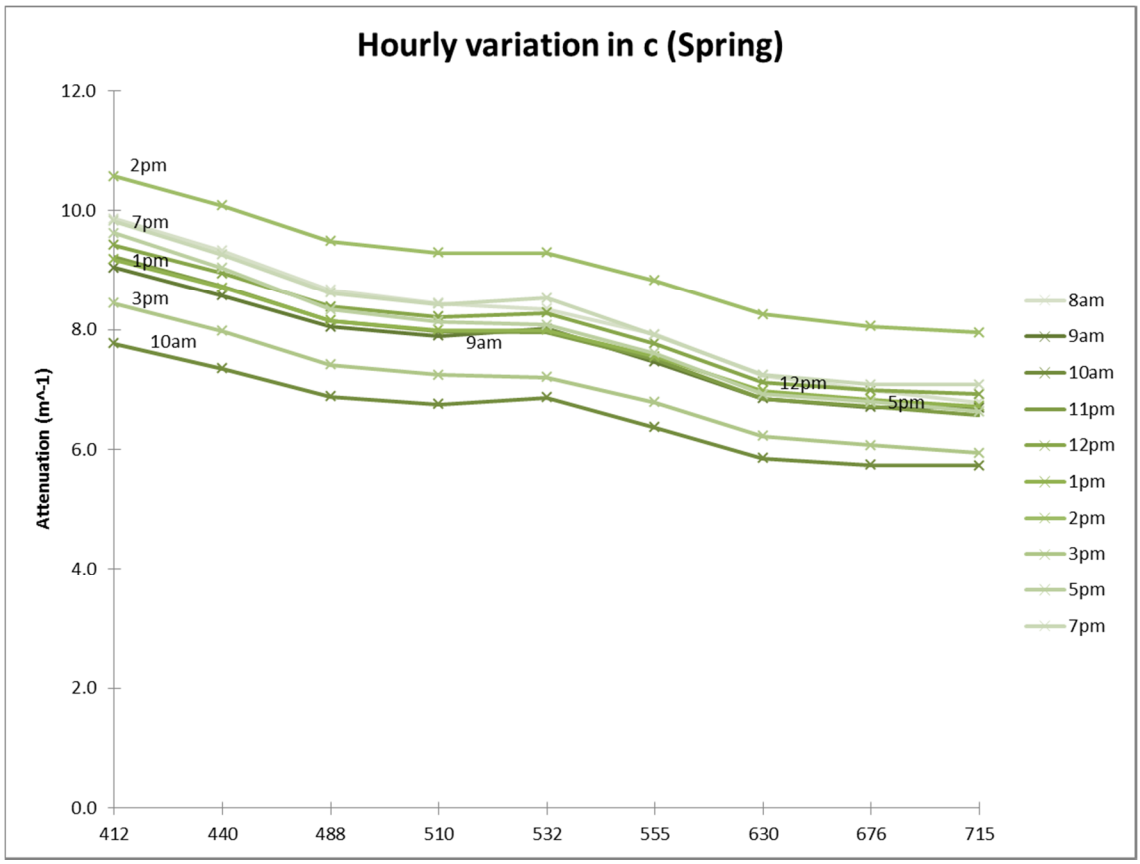

Figure 5-4: Hourly variation of beam attenuation coefificent in WCP. Small variation was oberved during low/high tide with the highest attenuation occuring 2 hours after high tide.

5.2 Attenuation Spectrum

This section will present the results of optical properties obtained from the ac-9 measurement. The optical properties are recorded as absorption, scattering and attenuation spectrum at specified wavelengths. The attenuation spectrum due to water is generally known and since this study intends to determine attenuation due to other dissolved and suspended substances, only brief attention is paid to pure water attenuation. Following this, the subsequent sections will discuss the absorption and scattering spectrum due to CDOM, sediment and phytoplankton. Some conclusion and remarks will be inferred from the various spectra obtained in two different sections; absorption and scattering. Absorption and scattering for pure water will be discussed together while for the CDOM, only absorption will be discussed as CDOM scattering is assumed to be negligible in the visible light band.

Figure 5-5 shows the beam attenuation spectrum from various sampling locations, which consist of both absorption and scattering effect. The highest attenuation is in Sembawang (mean spectral beam attenuation, $\bar{c}$ of 13.6m^{-1}) followed by Ubin E ($\bar{c}$ of 10.5 m^{-1}) and Ubin N ($\bar{c}$ of 8.9m^{-1}). All three locations have murky waters with high TSS content. Due to this, light scattering due to suspended sediment dominates over light absorption in these locations. For example, the ratio of a to b at 412nm varied from 0.13 to 0.22 in these locations indicating that scattering dominates over absorption. Bedok and Kranji have moderate attenuation in which the latter is probably dominated by phytoplankton absorption and scattering. In decreasing order, attenuations in Lim Chu Kang (LCK), ECP, WCP and Punggol are the lowest with the ratio of a to b ranging from 0.36 to 0.60, indicating that scattering still dominates over absorption but with relatively higher absorption.

Figure 5-5 also shows the attenuation spectrum from the data obtained from Chang (2007) in Semakau (Southern Singapore Islands) representing quasi-Case I waters. As expected for ocean water with minimal human influence, the mean attenuation spectrum $\bar{c}$ averages about 2.0m^{-1} from 412 to 715nm wavelength. Attenuation spectrum from Semakau is higher than attenuation spectrum obtained from clear ocean water, $\bar{c}$ ~ 0.1-0.2 m^{-1} from Kirk (2011). This value is considered to be on the higher range of clear waters with minimal suspended particles. The particles in clear waters generally consist of phytoplankton or decomposed detritus which together with water molecules dominate the attenuation (Prieur and Sathyendranath, 1981; Morel, 1988). However, the Chl-a concentration is expected to be low in Semakau, which means that sediment probably dominates attenuation.

5.2.1 Absorption spectrum for various constituents

Water

The partial contribution of water K_w to light attenuation K_d was referred from previous studies instead of formulating new experiment as the current knowledge on K_w is quite definitive. Furthermore, heroic effort needed to obtain pure water to sufficient degree requires sophisticated instruments. The absorption by pure seawater is practically the same as that of pure water in the visible/PAR band (400-700 nm) since absorption by dissolved salts is also known to be negligible in this band. Figure 5-6 shows the absorption and scattering property of pure water from the experiments of Pope and Fry (1997) using pure ionised distilled water compared to Smith and Baker (1981) using clear natural sea water in Bahamas. Both studies are widely accepted as the standard for pure water attenuation worldwide.

Pure water scattering is also sometimes called Rayleigh scattering because Raleigh scattering have a more balanced angular distribution of scattering in the forward and backward direction. VSF for turbid waters are characterised by intense scattering at small forward angle (Shifrin, 1988) due to the presence of suspended particles, similar to Mie scattering. Difference in VSF for pure water and turbid water can be seen in the angles between 100 to 180° in which the molecular scattering becomes significant in pure water (oceanic) but not in turbid water. The wavelength dependence of pure water scattering can be expressed in terms of a power law with γ^b ~ 4.3 *(Morel, 1974). While the magnitude of molecular scattering is negligible for total scattering, it plays considerable role in back-scattering especially in clear oceanic waters.*

Figure 5-6 shows the attenuation spectrum of pure water from various studies. The characteristic shape of absorption spectrum for both studies is as follows: from 400 to 500nm, the absorption is low with minima at 490nm (Morel and Prieur, 1977) compared to absorption minima at 560nm for chlorophyll absorption. The absorption then increases to 600nm with a small shoulder at 510nm. At 690nm, absorption increases rapidly until approximately 740nm before it decreases again beyond that wavelength (not shown in figure). Note that the scattering spectrums for pure water from both studies are similar. The scattering coefficient b *is insignificant with only 0.007* m^{-1} *400nm and reduces to 0.001* m^{-1} *at 700nm wavelength. The presence of other particles in turbid waters significantly increases the scattering coefficient as will be shown later in Section 5.2.2.*

<u>CDOM</u>

Short wavelength in the visible light band are greatly attenuated in water column that is rich in organic matter resulting in yellow or brown hue instead of blue, contrary to the role of water molecules in pure water which attenuate short wavelength only weakly. Purely from the color, waters in the Johor estuary are expected to be high in CDOM due to its brown hue. Experimentally, the imperfect reflectivity of the reflecting tube in the absorption tube causes CDOM absorption to be overestimated due. Level 3 correction was applied to account for the scattering error in CDOM absorption. It uses a reference wavelength to determine the proportion of the scattering coefficient to be subtracted from the measured absorption, assuming that the shape of the VSF to be independent of wavelength. As seen in Figure 5-7, the CDOM absorption after scattering correction is always lower than $1m^{-1}$.

CDOM especially at the east of Johor Strait is expected to play a considerable role in attenuating light due to the near-stagnant productive water and rich in organic matter, thanks to the anthropogenic discharges upstream of Johor River. Kirk (2011) indicated that the absorption spectrum for CDOM dominates over the scattering spectrum, hence CDOM scattering is neglected. This is further justified in view of the lower CDOM concentration (Gin et al., 2003) since the dissolved concentration is known to be an order of magnitude lower than the suspended concentration in Singapore waters. However, the optical impact of CDOM is greater compared to dissolved salts although the CDOM concentration is lower than the dissolved salts. CDOM absorption at the blue end is high but very low in the red end of the visible light band.

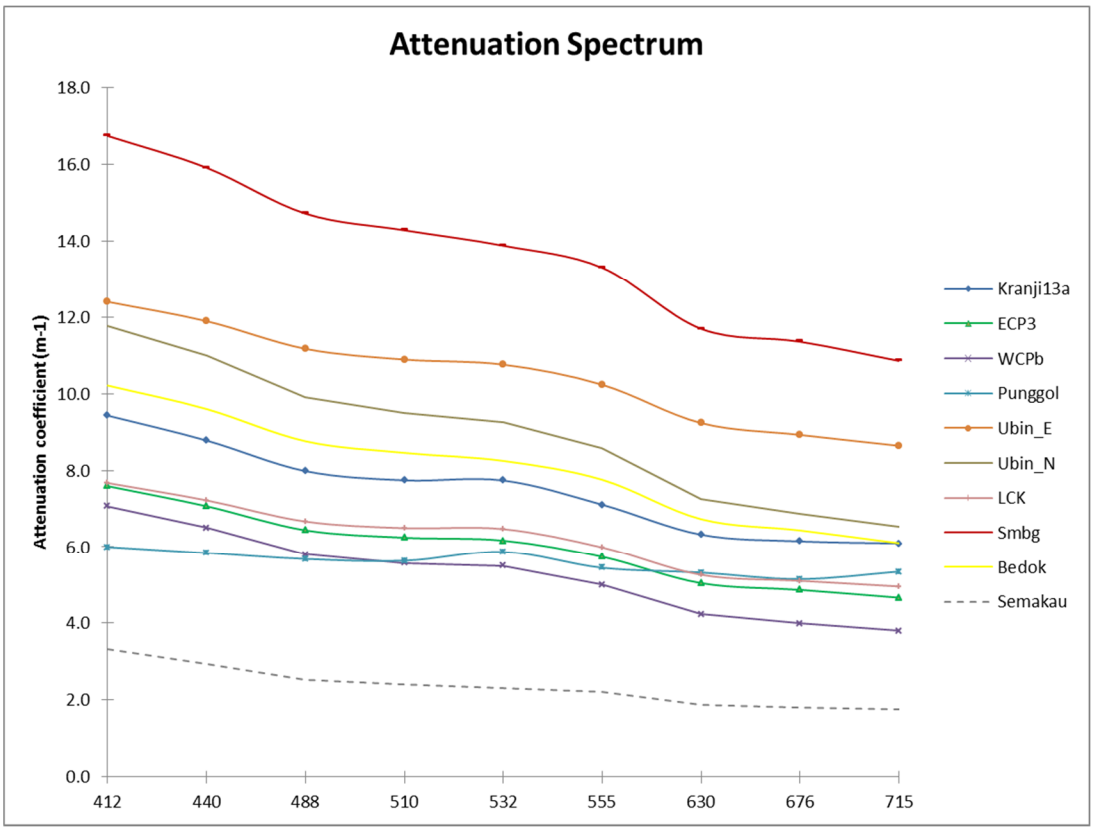

Figure 5-5: Attenuation spectrum from various locations as indicated. Highest attenuation is observed for Sembawang while the lowest are from WCP and Semakau.

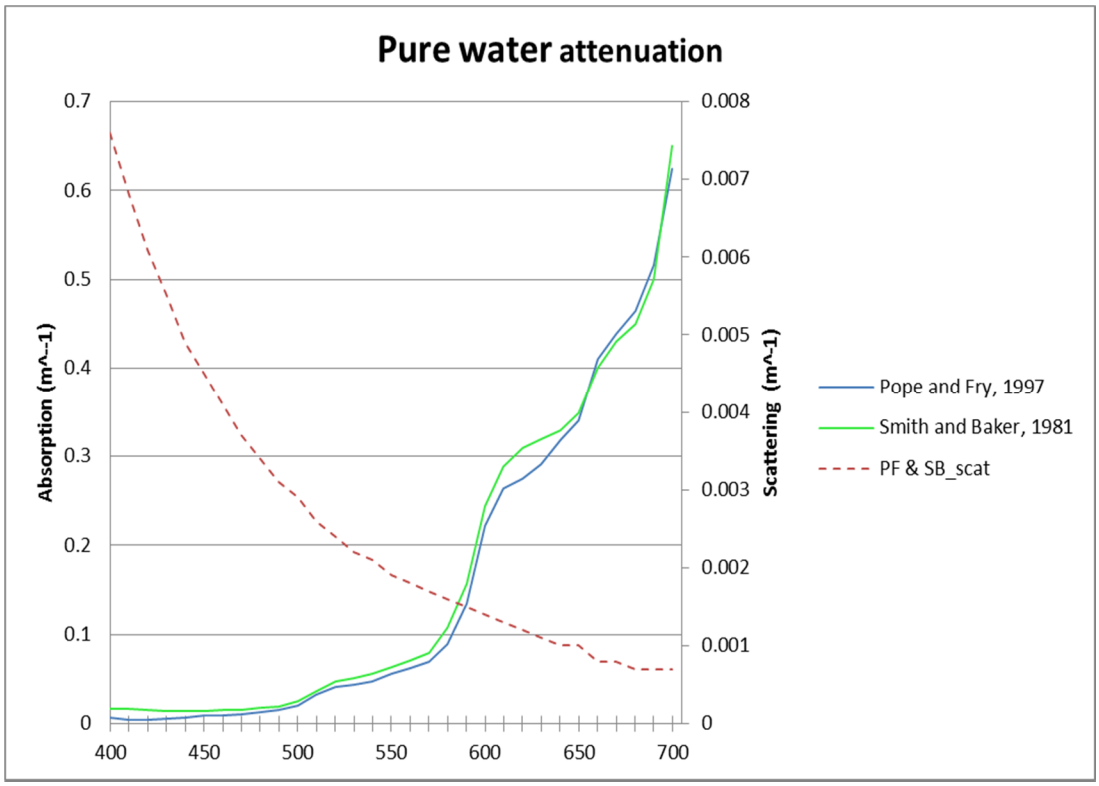

Figure 5-6: Attenuation (absorption and scattering) due to pure water; the primary vertical axis shows a while the secondary vertical axis shows b. Scattering spectrum from the two studies are similar.

Since CDOM scattering is assumed to be negligible, light attenuation from CDOM is only due to absorption. Therefore, the concentration of CDOM is proportional to the absorption coefficient at 440nm. Generally, the CDOM absorbance values at 320 nm are used to estimate the absorption coefficients of CDOM, a_g using equation: a_g = 2.303 / (a_{320} X 0.01). Unfortunately, CDOM absorption at 320nm was not measured for this study. However, a_g at 440nm can indicate the relative concentration of CDOM as shown in a table in Figure 5-7. Nevertheless, exact determination of CDOM is difficult due to the complexity of its molecular structures and its mostly unknown derivatives, especially from the less studied upstream of Johor River. Generally, CDOM absorption spectrum is normally described by the following relation by Bricaud et al. (1981):

$$a(\lambda) = a(\lambda_0)\, e^{-S(\lambda-\lambda_0)}$$

Where $a(\lambda)$ and $a(\lambda_0)$ are the absorption coefficients at wavelength λ and 440 *respectively, the latter is the reference wavelength. S is the coefficient describing the exponential slope, higher S means the more rapid CDOM degradation. In this thesis, S ranges from 0.010 to 0.015 nm^{-1} with a mean of 0.012 nm^{-1}. S was found to be 0.015-0.020 nm^{-1} for the lakes in New Zealand and 0.012-0.018 nm^{-1} for the lakes in Australia (Kirk, 2011). The mean S of 0.012 nm^{-1} compared to 0.014 to 0.019 nm^{-1} elsewhere may be attributed to the relative proportion of specific CDOM prevailing in Singapore waters since S is not related to locations (sediment or chlorophyll dominated waters). S from tropical climate does not seem to differ from the temperate values; Kuwahara et al. (2010) reported mean S values from CDOM absorption to be slightly higher on the west coast of Malaysia (0.0139 nm^{-1}) compared to the east coast (0.0124 nm^{-1}).*

Figure 5-7 shows the CDOM absorption spectra for Singapore waters corrected for scattering effect. The spectra decline exponentially with the highest S of 0.015 in ECP while the lowest S is 0.010 in LCK. CDOM absorption is highest in the near ultraviolet region (412nm) ranging from 0.4m^{-1} to 1.0m^{-1}, highest for Bedok, followed by WCP and LCK and the lowest in Ubin_E. CDOM absorption seems to be higher in the exposed beach of south Singapore (ECP and Bedok) compared to lower CDOM absorption in the east and west of Johor Strait (Punggol, Sembawang and Kranji). Furthermore, and quite ironically, CDOM absorption is apparently higher in WCP and ECP compared to Ubin_E and Ubin_N. The positive correlation between CDOM absorption with salinity and exposure is contrary to Foden et al. (2008) and McPherson and Miller (1987). Hence, CDOM in Singapore waters appears to be of marine origin.

CDOM absorption is inversely proportional to the Chl-a concentration (Figure 5-7). Kranji have higher Chl-a concentration but lower CDOM absorption while WCP, ECP and Bedok have higher CDOM absorption with lower Chl-a concentration. This is contradictory to Prieur and Sathyendranath (1981) who postulated that "absorption by CDOM is never negligible even at locations very rich in phytoplankton". Observation from CDOM absorption of Figure 5-7 showed that Johor River does not contain high concentration of humic material due to low CDOM absorption in all locations along Johor Strait and Pulau Ubin. Furthermore, the vertical variation of S should be higher for the surface water compared to the bottom due to increase photobleaching for the former. Nevertheless, this cannot be proven due to the lack of vertical readings data comparing CDOM absorption at different depths.

The $a_g(440)$ in this study is about two order of magnitude higher than $a_g(440)$ of oceanic water elsewhere inferred from Kirk (2011). The table in Figure 5-8 shows the $a_g(440)$ and the exponential slope S for all the sampling locations. Comparison of $a_g(440)$ in this study to the $a_g(440)$ of coastal waters elsewhere shows similarity especially in the Baltic Sea, Clyde River estuary in Australia ($a_g(440)$ = 0.72), Ganges estuary ($a_g(440)$ = 0.37) and Wadden Sea (extracted from the data compiled in Kirk, 2011). The average CDOM absorption coefficient ranged between 0.132 m^{-1} to 0.360 m^{-1} with the mean of 0.227 m^{-1} similar to 0.232 m^{-1} obtained by Lund-Hansen (2004) in Århus Bay (Denmark), which lies at the transition between North Sea saline waters and low-salinity, high CDOM waters of the Baltic Sea.

Although the CDOM absorption was corrected for scattering error, there remained some uncertainties in CDOM absorption measurement. Morel and Bricaud (1981) pointed out that storage can affect the absolute values of CDOM absorption, while its influence on the exponential slope would be less pronounced. In terms of experimental design, not all of the CDOM will pass through the 0.2 µm as colloidal CDOM are also known to be retained on the filter, thus underestimating the contribution of CDOM to light attenuation. Furthermore, the absorption by CDOM attached to suspended particle will overestimate TSS absorption spectrum but underestimate the CDOM absorption spectrum. Hence, since the definition of CDOM is fluid and not all CDOM were successfully filtered due to the presence of colloidal CDOM, it is fruitful to keep these limitations in perspective.

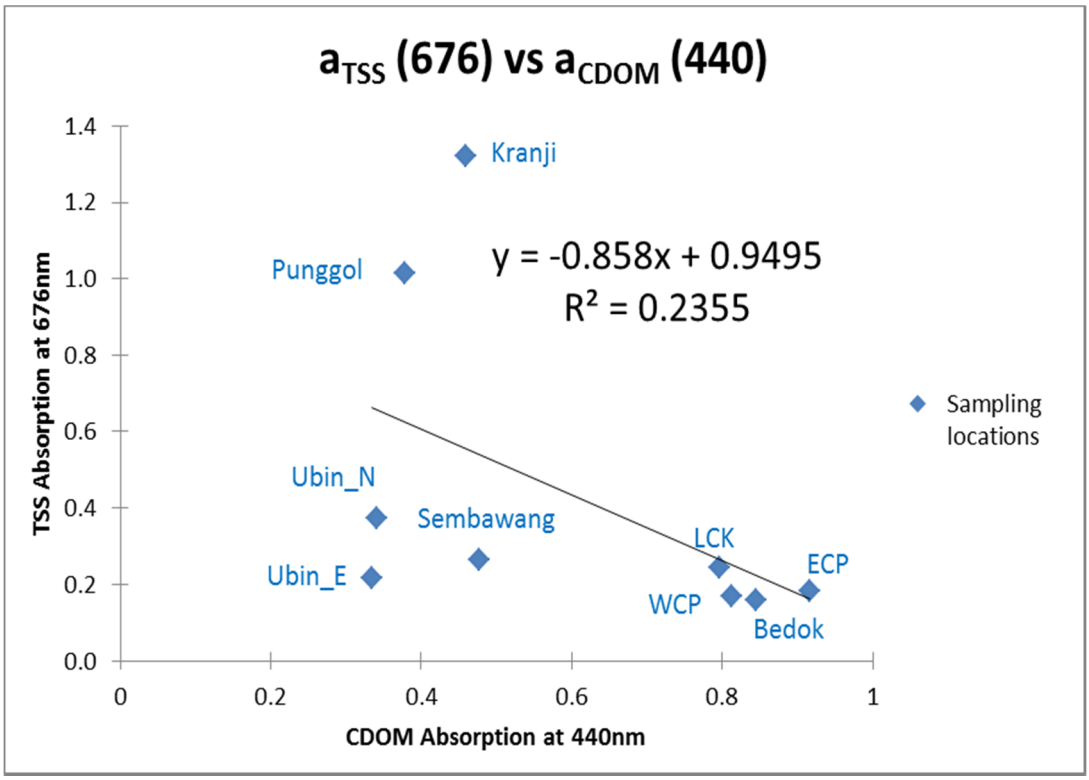

Figure 5-7: Scatter plots relating TSS absorption at 676nm and CDOM absorption at 440nm.The CDOM absorption is lower for chrolophyll dominated waters.

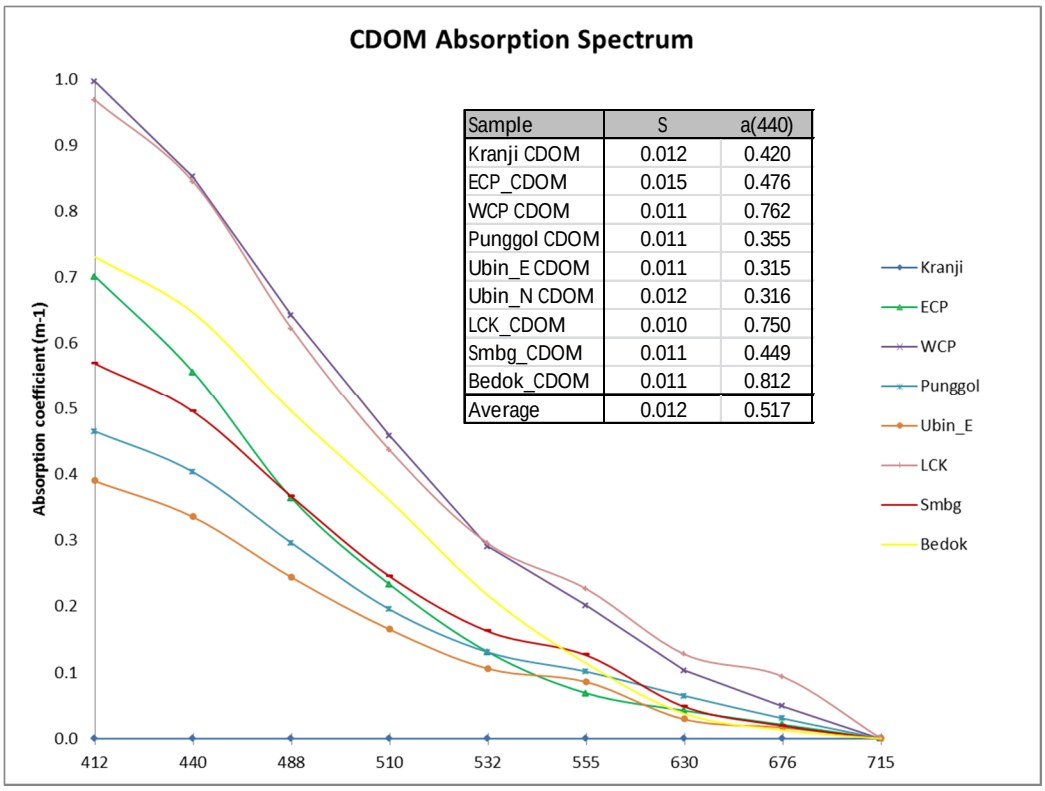

Sample	S	a(440)
Kranji CDOM	0.012	0.420
ECP_CDOM	0.015	0.476
WCP CDOM	0.011	0.762
Punggol CDOM	0.011	0.355
Ubin_E CDOM	0.011	0.315
Ubin_N CDOM	0.012	0.316
LCK_CDOM	0.010	0.750
Smbg_CDOM	0.011	0.449
Bedok_CDOM	0.011	0.812
Average	0.012	0.517

Figure 5-8: Absorption spectrum for CDOM corrected for scattering error. The spectrum shows exponential decrease with increasing wavelength, typical for CDOM. The table shows the exponential slope S and $a_g(440)$ for CDOM absorption.

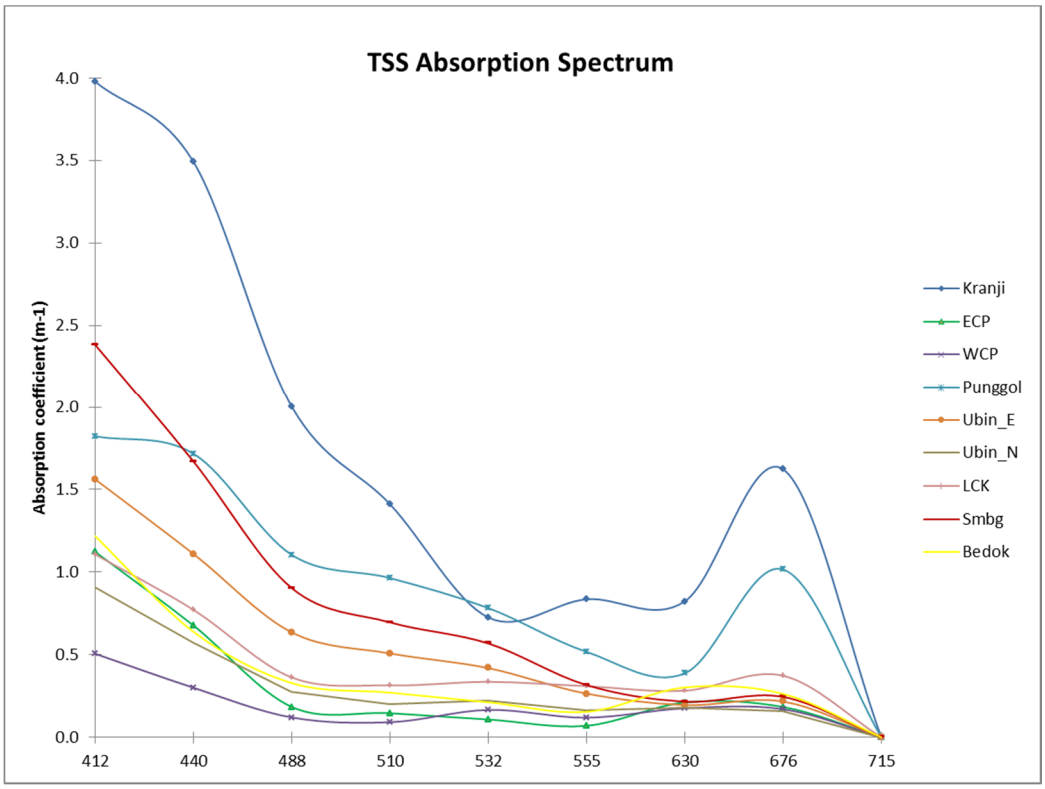

Figure 5-9: Absorption spectrum for TSS consisting of chlorophyll, sediment and detritus. Note the absorption peak in 440 and 676 in Kranji and Punggol. The shoulders above 440 nm are due to the presence of the accessory pigments, such as chlorophyll b, chlorophyll c and carotenoids.

Total Suspended Solids (TSS)

TSS fraction in the water column consists of non-phytoplankton particulate matter (sediment) and phytoplankton. Both are known to absorb and scatter light quite intensely although this section is limited to the results for TSS absorption decomposition to sediment and phytoplankton. Although theoretically detritus also makes up the TSS, but the lack of standard method to separate and measure detritus particles makes it difficult to analyse its optical properties. Detritus and phytoplankton (and their derivatives) play a dominant role in determining the optical properties of oceanic Case I waters (Morel and Prieur, 1977) as opposed to Case II waters for which sediment or CDOM, make an important contribution to the optical properties. TSS absorption spectrum was obtained by subtracting the total absorption spectra with the corrected CDOM absorption spectra. Relative contribution of suspended sediment and phytoplankton to K_d is presented in Section 5.4.

Figure 5-9 shows the absorption spectrum for TSS. The left-hand side of the absorption spectra has a nearly exponential form similar to that of CDOM, albeit steeper and probably reflects the effect of CDOM in colloidal form (i.e. bigger than the filter pore of 0.2 µm). Table 5-1 shows the Chl-a concentration for all the sampling locations. The result shows that Kranji and Punggol tend to be high in Chl-a compared to its adjacent water bodies. Some of the spectrums also show some 'bump' in the 440 and 676 wavelengths due to the presence of chlorophyll, coinciding with locations of high Chl-a concentration like Kranji and Punggol. However, the width of the peaks around 440 nm and 676 nm varies for different locations, due to the change in accessory pigments and the "package effect" (Morel and Bricaud 1981; Kirk, 2011). The package effect is the reduced pigments absorption in cells compared to the absorption potential of the same amount of pigment in solution.

Figure 5-10 shows the relation between Chl-a concentration and TSS absorption at 676nm. Kranji and Punggol showed the highest Chl-a concentration due to their stagnant productive waters. Not far from these locations; Chl-a concentrations in Lim Chu Kang and Sembawang are also considerable around 12 mg/m^3 followed by Bedok and WCP (~3 mg/m^3). Higher tidal/wave actions in ECP and Ubin_E seem to make the Chl-a concentration negligible. Unfortunately, Chl-a concentration for Ubin_N was not available due to measurement error. However, using extrapolation of results from other locations, the Chl-a is probably in the region of ~5 mg/m^3 in Ubin_N due to the partially stagnant water. The differences between Trichromatic equation and Lorenzen's monochromatic equation for the calculation of Chl-a are significant and can reach up to 30% in some locations, although the latter equation is preferred due to its simplicity and extra information on phaeophytin concentration.

Sathyendranath et al. (1987) observed that for low Chl-a concentration, the total absorption coefficient for chlorophyll, a_c at a given wavelength is linearly related as a product of specific chlorophyll absorption coefficient a_c^* and Chl-a concentration. For higher Chl-a concentration, the chlorophyll absorption is not linearly related to the concentration anymore. Such non-linearity is observed between optical properties and algal biomass (Morel, 1988) for eutrophic waters with Chl-a concentration in the order of 20mg/l (Morel and Bricaud 1981). The TSS absorption spectrum is parameterised and the results from Kranji and Sembawang are shown in Figure 5-11 and 5-12 as representative locations for waters dominated by phytoplankton and sediment respectively. The detailed decomposition of absorption spectrum for all locations can be viewed in Appendix B.

Table 5-1: Chlorophyll analysis showing the Chl-a concentration in mg/l from Monochromatic (M) and Polychromatic (P) equation and pigment concentration in mg/m^3

Location	Sample	Absorption					Concentration (mg/L)			Pigment Conc (mg/m3)
		630	647	664	665(b)	665(a)	ch-a (M)	ch-a (P)	Pheo a	ch-a
Kranji	K04	0.000	0.003	0.070	0.070	0.000	0.8	1.9	3.2	44.0
	K11	0.000	0.000	0.007	0.007	0.000	na	na	na	na
	K13	0.017	0.021	0.074	0.046	0.028	0.8	1.2	2.9	48.6
	K19a	0.035	0.041	0.157	0.113	0.070	1.8	2.3	6.2	73.9
	K19b	0.033	0.039	0.156	0.144	0.089	1.8	1.8	6.2	89.3
	K26a	0.012	0.018	0.157	0.158	0.048	1.8	2.9	6.8	65.7
West Coast Park	WCPb	0.002	0.003	0.007	0.006	0.004	0.1	0.1	0.3	3.0
Bedok	B	0.002	0.003	0.009	0.009	0.006	0.1	0.1	0.4	3.5
East Coast Park	ECP3	0.000	0.000	0.009	0.009	0.011	0.1	na	0.4	2.0
Punggol	Pgl	0.054	0.064	0.228	0.228	0.226	2.6	0.1	8.9	65.6
Pulau Ubin	Ubin_E	0.000	0.000	0.007	0.007	0.007	0.1	0.0	0.3	1.8
	Ubin_N	0.000	0.000	0.001	0.001	0.095	na	na	na	na
Lim Chu Kang	LCK	0.000	0.000	0.024	0.024	0.000	0.3	0.6	1.1	13.4
Sembawang	S	0.000	0.000	0.021	0.022	0.008	0.2	0.3	1.0	12.1

The dual peak representing chlorophyll absorption (440 and 676nm) can be seen in Figure 5-11 for Kranji, while Figure 5-12 shows relatively flat chlorophyll absorption at these wavelengths except for small peak at 676nm for Sembawang. The total TSS absorption in Sembawang also shows an exponentially declining absorption pattern, typical of sediment dominated waters. The exponential slope of sediment absorption in Sembawang is 0.015, slightly higher than the mean CDOM exponential slope of 0.012. With the exception of Kranji, the RMS errors for all other location range from 0.0206 to 0.0606 showing the close match of the modelled predictor-corrector model of Lee et al. (1998) and measured absorption spectrum. The relatively higher error in Kranji is probably due to the inaccuracy in determination of Chl-a concentration and/or the non-linear effect of absorption.

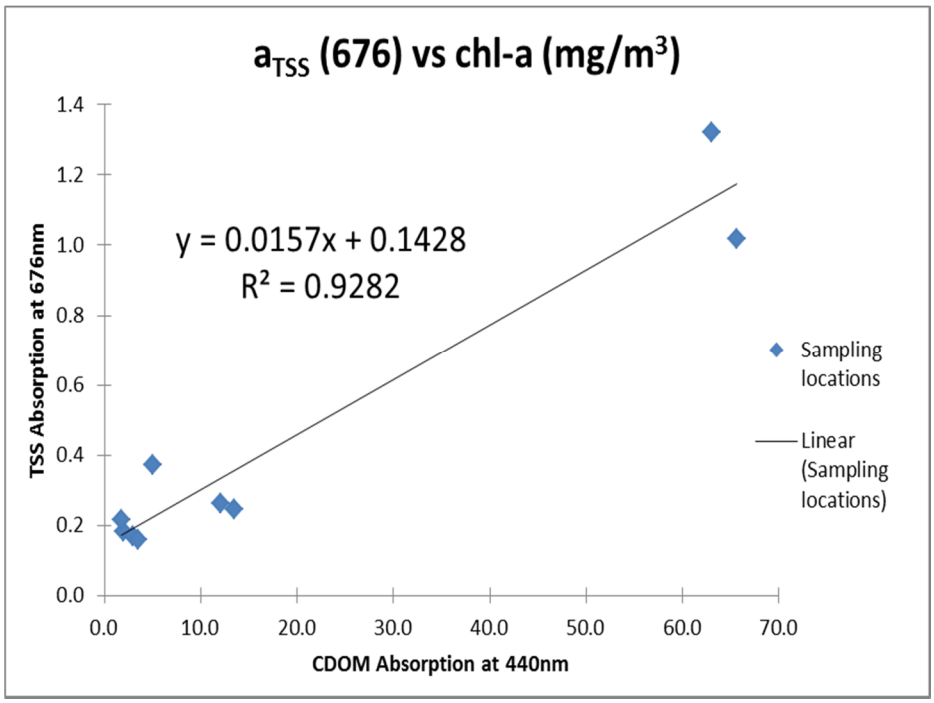

Figure 5-10: Scatter plot showing the positive linear relation between Chl-a concentration and TSS absorption at 676nm.This shows that the latter is a good optical indication for the former.

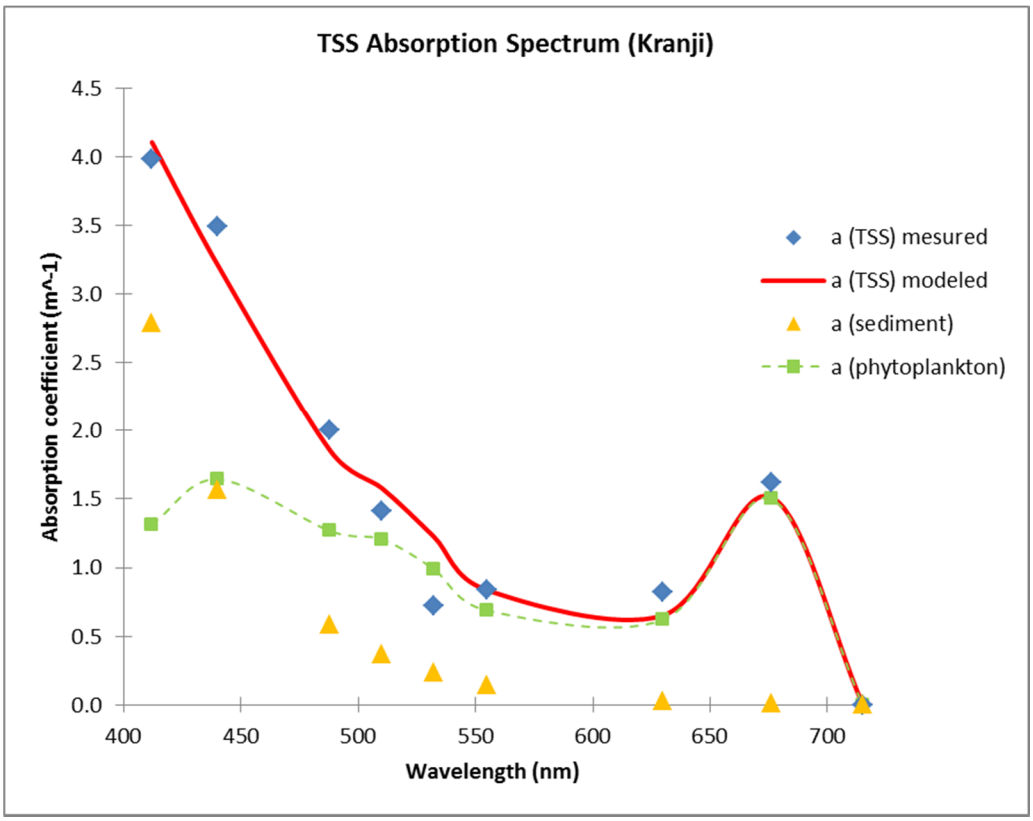

Figure 5-11: Decomposition of TSS absorption spectrum into sediment and phytoplankton (chlorophyll) contribution in Kranji. Note the dual peaks absorption for phytoplankton.

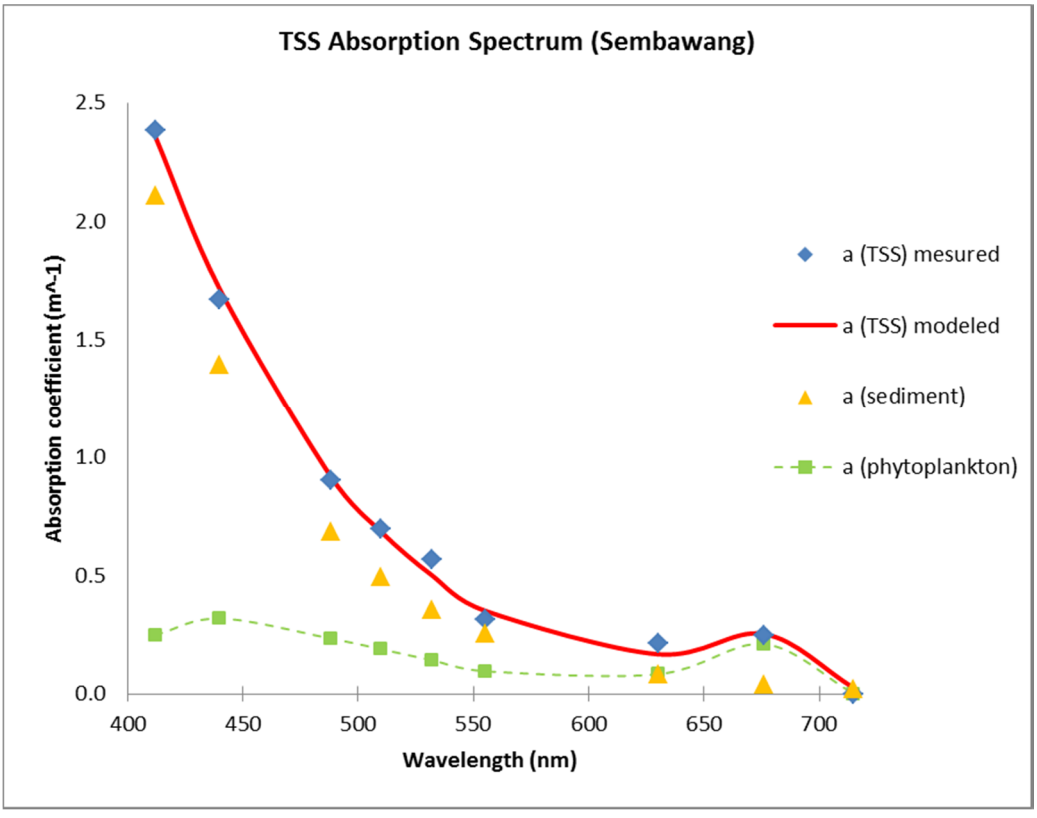

Figure 5-12: Decomposition of TSS absorption spectrum into sediment and phytoplankton (chlorophyll) contribution in Sembawang. Note the higher sediment contribution.

5.2.2 Scattering spectrum for various constituents

It is assumed that CDOM doesn't scatter light and since the scattering effects of water molecules were excluded from the ac-9 measurement, the remaining contribution to light scattering consists of TSS only (phytoplankton and suspended sediment). This section discusses the effect of phytoplankton and sediment to light scattering before the effect of sediment to light scattering is examined in Section 5.3. The causes for the observed variability in magnitude and spectral behaviour of scattering coefficient will be explained.

TSS scattering is less sensitive to wavelength compared to pure water molecular scattering due to density fluctuation scattering (Kirk, 2011). As shown in Figure 5-6, the wavelength dependence of molecular scattering is in the region of 4. Molecular scattering are more prevalent in oceanic or pure water and contributes greatly to the backscattering and makes large contribution to upwelling (or upward) light stream due to the lack of other impurities like sediment and phytoplankton. These impurities are enhanced in the coastal waters due to waves/currents stirring up materials and substantially increases light scattering. The turbid nature of all the sampling locations due to either high phytoplankton or suspended sediment makes the contribution of molecular scattering to the total scattering negligible.

Large particles (phytoplankton) scatter intensely at narrow angles while smaller particles (sediment) scatter intensely at large angles (Shifrin, 1988). However, with increasing angle, the effect of particle size is smoothed out due to the mixture of particles with various sizes (Jonasz and Fournier, 2007). If particle size and shape are assumed to be constant, the total scattering coefficient increases with increasing relative index of refraction (Gordon et al., 1980, James et al., 2002). Owing to this also, phytoplankton does not contribute greatly to backscattering (relative to sediment) but plays considerable role in light scattering. However, the efficiency of larger particles to attenuate light are low for they will not remain in suspension for long as they tend to settle rapidly in the water column, due to higher settling velocity especially in stagnant waters.

Figure 5-13 shows the scattering spectra assumed due to TSS. Scattering coefficient b *at 412nm ranged from 4 to 14m*$^{-1}$*, highest in Sembawang and lowest in Punggol. The scattering coefficient varies inversely with wavelength (i.e. lower wavelength, higher scattering) except for locations in which the phytoplankton dominates where the contrary is true. In locations dominated by sediment, all the spectra show a 'bump' in 555nm; where higher bump indicates more sediment, hence higher scattering in this domain. Scattering is high at the wavelength at which the absorption is low and vice-versa (Van Duin et al., 2001). Figure 5-14 shows the parameterizations of scattering spectra into contribution from chlorophyll and sediment respectively for Lim Chu Kang using* b_s^* *which is analogous to the specific chlorophyll absorption coefficient* a_c^* *in Section 5.2.1.*

In locations where phytoplankton dominates, scattering minima at 440nm and 676nm is seen corresponding to the blue and red absorption of Chl-a respectively. The scattering minima at both wavelengths are quite pronounced in Kranji and Punggol showing that scattering spectra is clearly affected by phytoplankton absorption. The minimum at 676 nm is deeper for Punggol, suggesting that phytoplankton particles in Punggol are more absorbing in the red wavelengths compared to Kranji. Scattering spectrums in both locations shows ascending slope towards smaller wavelength, in contrast to sediment dominated waters.

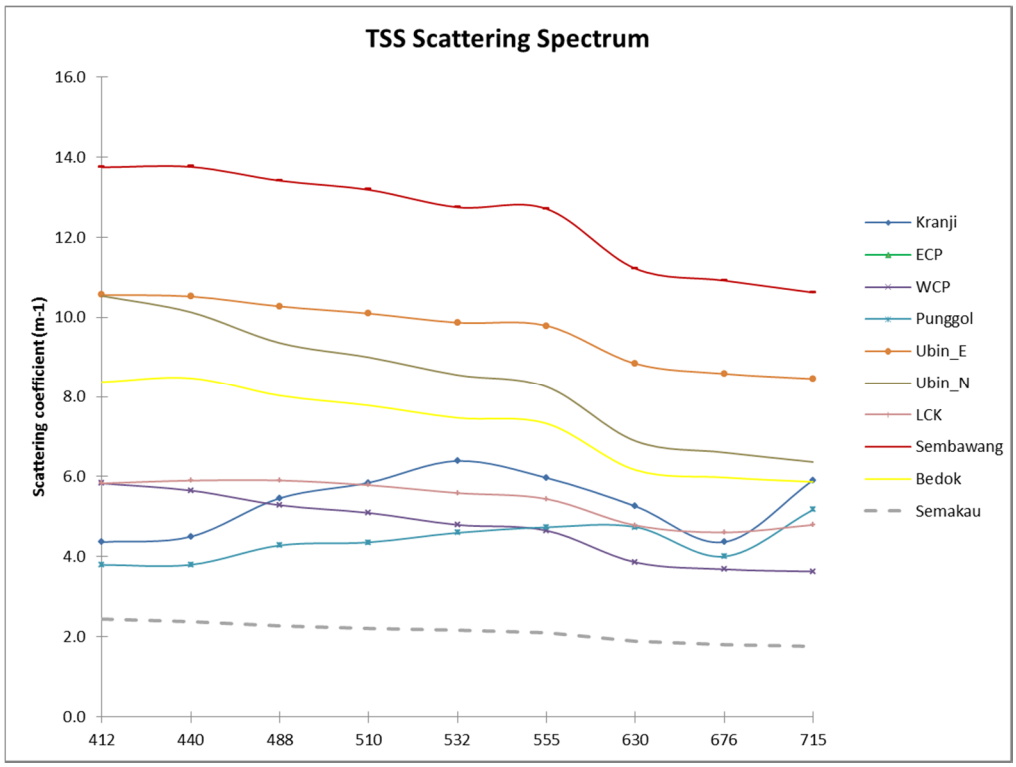

Figure 5-13: The scattering spectrum for sediment dominated waters decreases towards longer wavelengths with negative scattering slope (mean: -0.65) compared to the chlorophyll dominated waters with positive scattering slope (mean: 0.25)

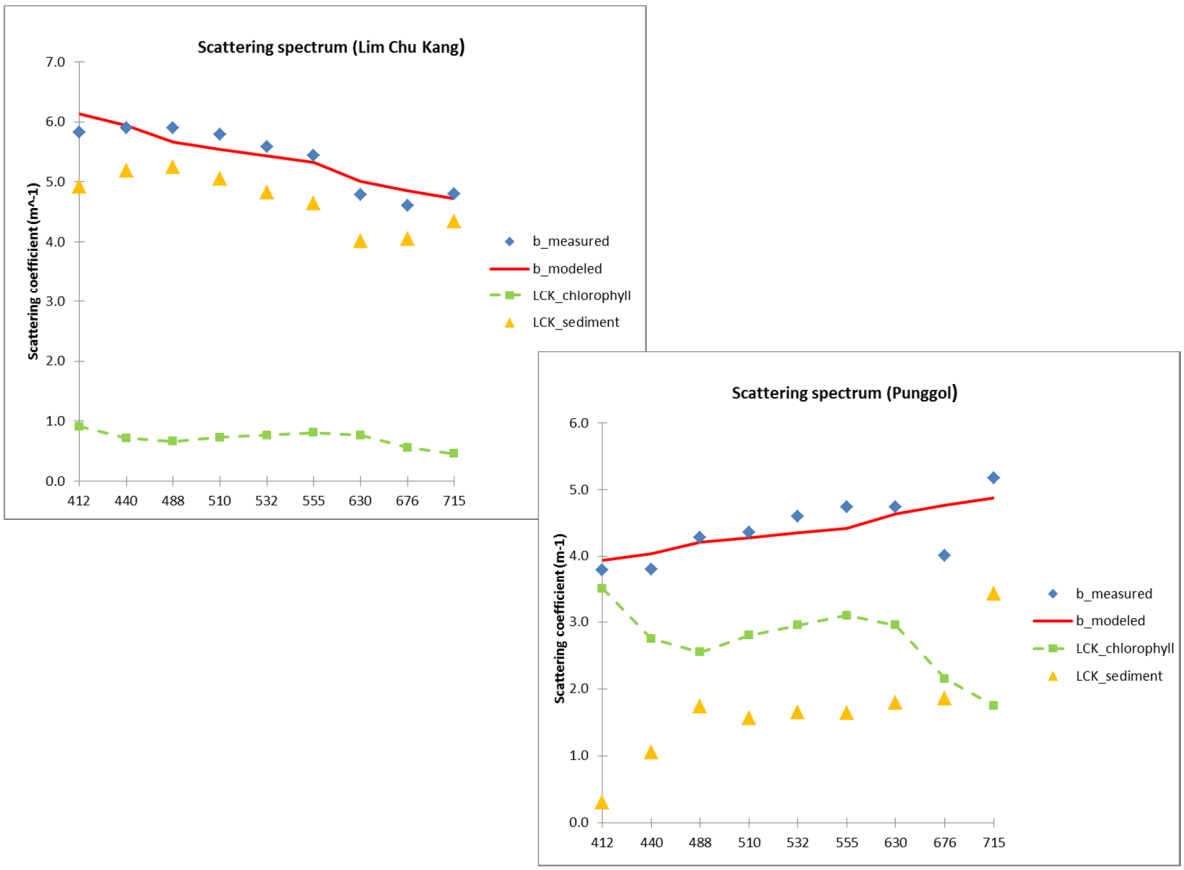

Figure 5-14: The measured and modelled scattering spectrum in LCK and Punggol. The contribution of sediment to the scattering spectrum is 5 times more than phytoplankton in LCK.

Analysis of scattering spectrum shows than when expressed as power law according to $b(\lambda) \propto \lambda^{-\gamma}$ *, scattering changes with spectral exponent* γ *ranging from -0.20 to 0.93. Scattering slope is higher for turbid water dominated by suspended sediment compared to water dominated by phytoplankton. However, the spectral exponent in waters dominated by suspended sediment seems to be inversely related to the sediment load; the higher the sediment load, the lower the power. As such, the magnitude of exponent provides an indication on the amount of suspended sediment; highest in Sembawang, followed by Ubin, Bedok, ECP and finally WCP. In contrast, the spectral exponent in Punggol is lower than Kranji due to higher chlorophyll concentration in the former.*

Despite the differences among the individual spectrums, mean spectra for both classes are as follows; for waters dominated by sediment, $b(\lambda) = \lambda^{-0.65}$ *with lower scattering towards longer wavelengths while the spectra dominated by phytoplankton* $b(\lambda) = \lambda^{0.28}$ *with higher scattering towards longer wavelengths. Mean spectra from both classes are gentler than dependency of* $b(\lambda) = \lambda^{-1}$*, expected for ocean waters. This gentler dependency is likely the result of increased absorption in the blue domain, which is characteristic for most particles. Assuming that refractive index is independent of wavelength, the scattering spectrum varies from* λ^{-4} *for small particles like water molecules (Section 5.2.1) to* λ^{-0} *for large particles like phytoplankton (Fournier and Jonasz, 1999). The data in this thesis is consistent with this result since scattering slope is lower in chlorophyll dominated waters (larger particles) compared to sediment dominated waters (smaller particles).*

Relationship between scattering and TSS/NTU

Figure 5-15 (a) shows linear relation between $b(555)$ *and NTU with is roughly 1.0 in chlorophyll dominated waters and increases to 1.5 for waters dominated by sediment (see Table 5-2). Since NTU is a better determinant of optical properties than mass concentration, a strong relationship between* $b(555)$ *and NTU (*$R^2 = 0.73$*) is observed compared to Figure 5-15 (b) between* $b(555)$ *and TSS (*$R^2 = 0.46$*). For a) however, some variation was also observed probably due to variation in the VSF of the suspended material, since chlorophyll scatters light at larger angle compared to the sediments. Hence, not all of the scattered light from chlorophyll is detected by the turbidimeter, which only detects light scattered at right angles (90°). This is partly the reason for lower NTU in chlorophyll dominated waters compared to sediment dominated waters. Liew at al. (2009) also showed linear relationship between NTU and the optical properties of backscattering.*

Figure 5-15 (b) are more scattered than Figure 5-15 (a) because $b(555)$ *is more closely related to the optical properties of particle (NTU) than the mass concentration of particles (TSS). Furthermore, NTU is more sensitive to the differences between specific locations (chlorophyll or sediment dominated), in contrast to* $b(555)$ *which shows lower variability between locations. This is proven with Figure 5-15 (c) which shows slightly better linear relation between inorganic matter of TSS (sediment) and* $b(555)$ *(*$R^2 = 0.78$*). The slope of the linear relation in b) is 0.09 which represents the mean particle mass specific scattering coefficient,* $b^*_{TSS} = b(555) / TSS$ *(Otto, 1966 who cited the article by Burt, 1954). Finally, experimental random error as suggested by Babin et al. (2003) could also explain some scatter. The wavelength 555nm is selected as a representative wavelength for* b *(Babin et al., 2003) because it corresponds to a minimal absorption by suspended solids.*

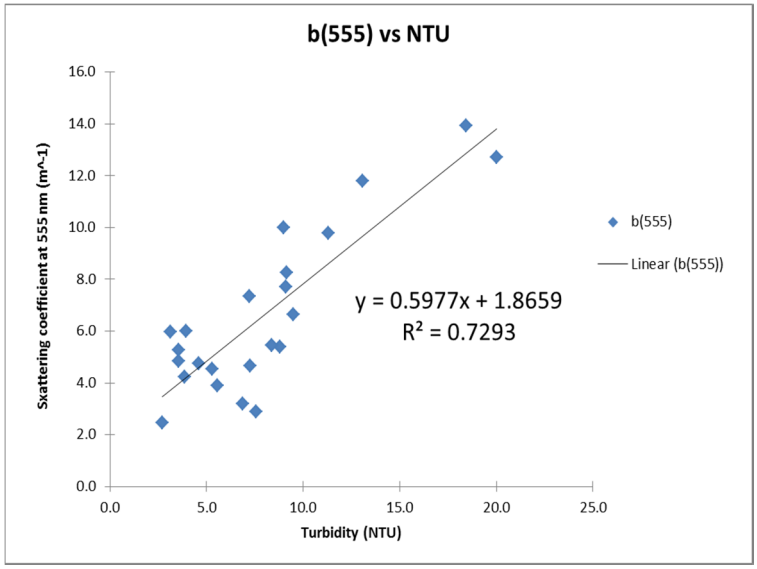

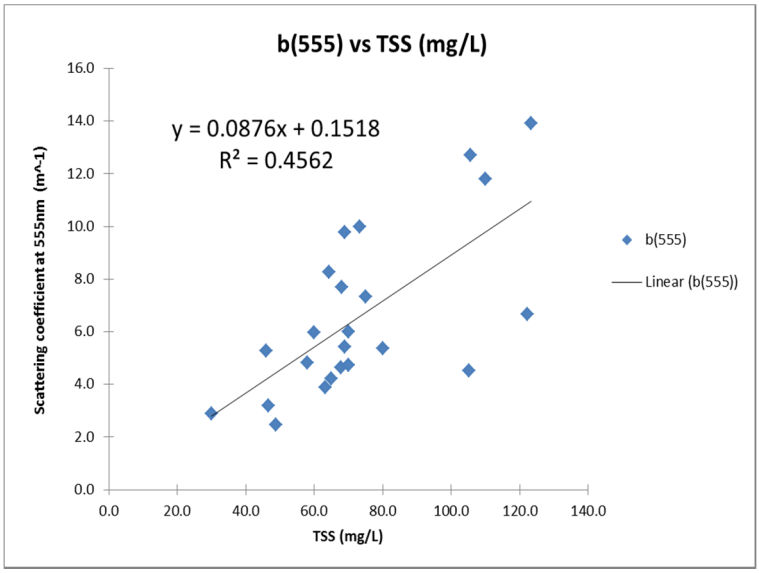

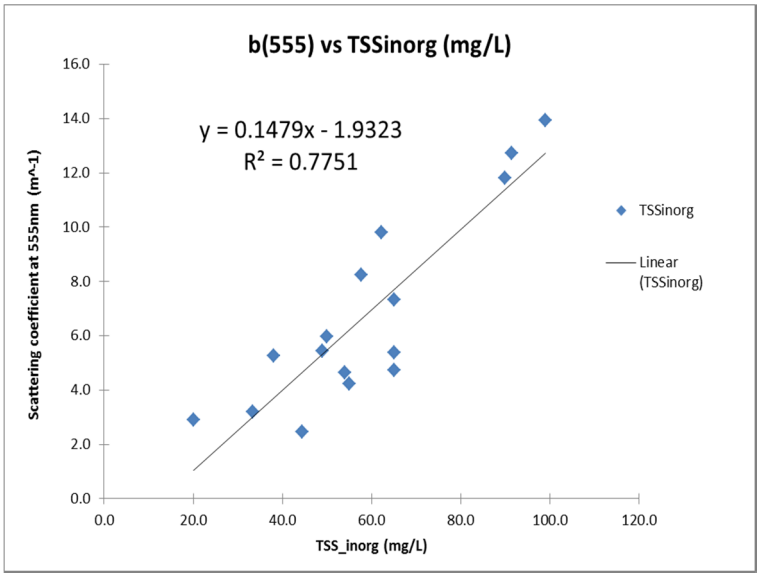

Figure 5-15: The relationship between b(555) *and NTU and TSS in a) and b) respectively. c) shows the relation between* b(555) *and inorganic matter of TSS.*

Table 5-2: The particle mass-specific scattering coefficient b^*_{TSS} and the comparison between theoretical and the measured slope from the field data for various locations.

Place	Samples	TSS (g/m3)	NTU	b(555) (m^-1)	b_TSS^* (m^2/g^-1)	γ_theoritical	γ_measured
Kranji	K04a	65.0	3.86	3.200	0.05	1.65	0.20
	K11a	48.9	2.70	2.457	0.05	Na	Na
	K13a	60.0	3.15	5.969	0.10	Na	Na
	K19a	58.0	3.56	4.827	0.08	Na	Na
	K26a	46.0	3.57	5.271	0.11	Na	Na
Poly Marina	PM1	73.3	9.00	9.992	0.14	1.99	Na
East Coast Park	ECP1	110.0	13.07	11.800	0.11	2.07	Na
	ECP2	123.3	18.45	13.925	0.11	2.04	0.35
	ECP3	80.0	8.80	5.378	0.07	1.72	0.52
West Coast Park	WCPa	63.3	5.56	3.900	0.06	Na	Na
	WCPb	63.3	7.26	4.653	0.07	2.81	0.93
WCP_Spring	WCP_S	105.2	5.28	4.524	0.04	Na	Na
WCP_Neap	WCP_N	122.3	9.50	7.190	0.06	Na	Na
Punggol	Pgl	70.0	4.60	4.734	0.07	0.97	0.38
Pulau Ubin	Ubin_E	68.9	11.29	9.791	0.14	2.25	0.44
	Ubin_N	64.4	9.16	8.254	0.13	1.24	0.96
Lim Chu Kang	LCK	68.9	8.38	5.443	0.08	2.54	0.47
Sembawang	S	105.7	19.87	12.710	0.12	2.11	0.50
Bedok	B	75.0	7.21	7.330	0.10	2.4	0.72

Babin et al. (2003) found that the average values of b^*_{TSS} are close to 0.5 m^2 g^{-1}, in coastal waters and increases to 1.0 m^2 g^{-1} for ocean waters due to differential scattering contribution of sediment and chlorophyll in coastal and ocean waters respectively. This means that b(555) is twice as high as TSS in coastal waters dominated by sediment, in contrast to almost equal ratio of b(555) and TSS in ocean waters dominated by chlorophyll.

The mean values for the mass-specific scattering b^*_{TSS} from the measurements are provided in Table 5-2. The b^*_{TSS} *ranges from 0.04 m^2g^{-1} in ECP to 0.12 m^2g^{-1} in Sembawang. The* b^*_{TSS} *in sediment dominated waters is slightly higher than chlorophyll dominated waters due to higher scattering effect of sediment. The* b^*_{TSS} *in Kranji and Punggol averages 0.08 m^2g^{-1} while sediment dominated waters elsewhere averages 0.1 m^2g^{-1}. This seems to indicate the occurrence of two kinds of suspensions (phytoplankton and sediment), each with a more or less constant composition as proposed by Otto (1966). However there is some exception because even in the sediment dominated waters of ECP and WCP, the* b^*_{TSS} *only averages to 0.06 m^2g^{-1}. This is probably due to an increase in TSS that is not in tandem with the magnitude of increase in b(555).*

The b^*_{TSS} is higher in Sembawang, Bedok and Pulau Ubin compared to ECP and WCP probably because the PSD are skewed towards smaller range (i.e. not randomly distributed) in ECP and WCP. Therefore, purely from particle size view, the b^*_{TSS} *decreases with decreasing sediment grain size especially in ECP and WCP. Because fine sediment has a greater surface area to volume ratio, a volume of fine sediment scatters more light than the same volume of coarser sediment. However, this is not seen in the field data and will be probed further in Section 5.3.2. Baker and Lavelle (1984) studied light attenuation by sediment and found a strong linear relationship between particle concentration and beam attenuation. They also found that the slope of this relationship* b^*_{TSS} *ranged from 0.041 to 0.67 m^{-1} consistent with the findings from this thesis with average* b^*_{TSS} *of 0.09.*

Previous studies have found for an infinite distribution of randomly orientated particles with a constant index of refraction, the spectral exponent γ is related to the PSD slope j by $j = \gamma + 3$ (Babin et al., 2003: Jonasz and Fournier, 2007). However, as shown in Table 5-2, the discrepancy between measured and theoretical γ is substantial. The discrepancy is perhaps due to the following; If the particle contains waters i.e. colloidal particles (smaller than 0.7µm) as expected in Kranji and Punggol, the γb would tend to increase slightly from λ^{-0} dependence for phytoplankton dominated waters. For sediment dominated waters, γ decrease from λ^{-1} dependence (for ocean waters) is expected if the sediments are absorbing. The latter is prevalent in Sembawang and Lim Chu Kang due to residual absorptivity of chlorophyll in altering the scattering spectra.

Furthermore, the inability of the measuring equipment in taking all the particle size into account when estimating the total particle volume is one of the major reasons for this discrepancy (further discussed in Section 5.3.2). Theoretical calculations of scattering with the measured size distributions overestimates observed scattering can also be attributed to the simplification in particle size assumption. The particles are assumed to be homogenously spherical particles but in reality the non-spherical shape and roughness typical of natural particles create an effective optical diameter larger than that for a sphere of equal volume (Baker and Lavelle, 1984). Otto (1966) cited Postma (1961) who defines the term "optical grain size" as the size that can be deduced from attenuation measurements, assuming that the particles behave as quartz spheres.

Although the magnitude of TSS in ECP is equivalent to Sembawang, but the b(555) are only 4.8 m^{-1} and 7.1m^{-1} during spring and neap tide respectively compared to twice higher (12.7m^{-1}) in Sembawang. This is somewhat perplexing since it is now observed that higher TSS does not necessarily lead to higher scattering coefficient, especially for sediments in ECP and WCP. This is probably due to the nature of fine sediments that tend to aggregate if present in large concentration. The proportion of organic matter in ECP and WCP are also higher compared to Sembawang (Section 5.3.1). Since ECP and WCP consist of organic matter, flocculation of fine sediment due to electromagnetic and chemical interaction (hydration effects, hydrophobic and polymer bridging) is likely to be exaggerated. One would expect that the flocculation impact to absorption and scattering properties is likely to be considerable as will be proven in Section 5.4.1.

5.3 Sediment and Light Attenuation

Light attenuation due to TSS not only depends on its concentration (previous section), but also on the particle type, size, shape, and refractive index as alluded previously. Although sediment also absorbs light, it was shown in Section 5.2 that absorption is mostly dominated by chlorophyll while scattering is dominated by sediment. Moreover since the positive relationship between suspended sediment and scattering coefficient are also shown in Section 5.1 and 5.2 and the focus of this thesis on the effect of sediment to visibility, this section will focus on the effect of sediment in scattering light. The relationship between scattering coefficient b and TSS depends mostly on the nature of the suspended particles (whether it is organic or inorganic) and its size distribution (PSD). Section 5.3.1 will focus on the nature of particle to the scattering spectrum while the effect of PSD to scattering spectrum will be examined in Section 5.3.2.

5.3.1 Nature of particles and light scattering

The relevant parameters describing the nature of particles including its organic and inorganic content, etc. are listed in Table 5-3. Some interesting features emerge from the examination of these data. First of all, they are ordered in the same way from location to location, which shows the consistency of the three data sets (TSS, POC and Chl-a concentration) although they were obtained independently. Secondly, the reduction in TSS concentrations with increasing chlorophyll concentration is also clearly noticeable. TSS ranges five-fold from 30 to 105 mg/l depending on the location, with lower TSS in chlorophyll dominated waters and higher TSS in sediment dominated waters. This is comparable to higher scattering slope in sediment dominated waters since higher TSS scatters more light, thus the increased slope as discussed in Section 5.2.2.

The TSS values correlates well with TSS_{inorg} (R^2 = 0.94). An average 80% of TSS is represented by TSS_{inorg} in waters dominated by chlorophyll which increases to 88% in waters dominated by sediment. However, it is recognised that the TSS_{inorg} percentage in waters dominated by chlorophyll is likely to be overestimated as the laboratory measurement did not manage to account for all the organic matter. It is reasoned that this is probably due to error where the organic portion were not sufficiently removed during burning and/or higher temperature needed to burn certain fraction of organic matter. However, neglecting the absolute value and concentrating on the relative pattern, the organic content of TSS, i.e. TSS_{org} is 6-30 % of the total TSS in chlorophyll dominated waters and reduces to less than 10% in sediment dominated waters.

Organic substances in seawater occur mainly as dissolved organic matter (DOM) with small traces of particulate organic carbon (POC). The POC were estimated from the water sample as describe in Section 4.1.1. A large proportion of TSS in Singapore waters, especially in semi enclosed (WCP) and coastal seas (ECP) is made up of inorganic particles (sediment) and high percentage of organic matter. Other locations like Sembawang and Lim Chu Kang also showed relatively considerable organic matter. The concentrations of the sediment are governed by physical factors connected with the tides (Section 5.1) and meteorological-seasonal forcing (Section 7.1).

Light scattering in seawater is due to particles varying in shapes, sizes, composition and refractive index interacting with the incident light. Multiple scattering in an ensemble of particles simplifies the complex features associated with a single particle scattering (Jonasz and Fournier, 2007). The averaging process of multiple scattering results in the VSF that characterises the angular pattern of the scattered light. Most of the particles are larger than the light wavelength; they scatter about half of the incident light into a 10° forward-directed cone and less than 3% in the backward direction (Jonasz and Fournier, 2007). Difference in VSF for ocean water and turbid water can be seen in the angles between 100 to 180° in which molecular scattering becomes significant in oceanic but not in turbid water.

Table 5-3: Relevant parameters derived from field measurement and empirical equations for investigating the nature of the particles. All the units are in mg/l unless otherwise stated.

Place	Samples	TSS	TSSorg	TSSinorg	POC	chl-a (mg/m3)
Kranji	K04a	46.7	13.3	33.4	5.1	44.0
	K04b	30.1	10	20.1	3.8	Na
	K04c	65.0	10	55.0	3.8	Na
	K11a	48.9	4.4	44.5	1.7	Na
	K13a	Na	Na	Na	Na	48.6
	K19a	Na	Na	Na	Na	73.9
	K19b	Na	Na	Na	Na	89.3
	K26a	46.0	8	38.0	3.1	65.7
East Coast Park	ECP3	80.0	15	65.0	5.8	2.0
West Coast Park	WCPb	Na	Na	Na	Na	3.0
WCP_Spring	WCP_S	105.2	12.0	93.2	4.6	Na
WCP_Neap	WCP_N	122.3	33.2	89.1	12.8	Na
Punggol	Pgl	70.0	5	65.0	1.9	65.6
Pulau Ubin	Ubin_E	68.9	6.7	62.2	2.6	1.8
	Ubin_N	64.4	6.7	57.7	2.6	Na
Lim Chu Kang	LCK	68.9	20	48.9	7.7	13.4
Sembawang	S	105.7	14.2	91.5	5.5	12.1
Bedok	B	75.0	10	65.0	3.8	3.5

5.3.2 Particle size distribution (PSD) and light scattering

Gordon et al. (1980) used Mie scattering model (developed by Gustav Mie, based on Maxwell's electromagnetic equations) to calculate particle scattering due to various parameters. They found that the change in particle size is the most influential variable describing light scattering. Therefore, this section determines the relative importance of particle size to light attenuation in Singapore waters. PSD were determined using LISST (as detailed in Section 4.1.1) for volumes in between 1 to 250 µm. Table 5-4 shows the relation between TSS, particle density and d_{50} while the full LISST data is appended in Appendix C. This section relates the spectral scattering slope to the PSD slope. Particle shape is assumed to be spherical.

The particle density (mg/m^3) in Table 5-4 was obtained by dividing the TSS mass (mg/l) over the total volume of particles (m^3/l). Most of the density is too high and are rendered meaningless. This is because the measurement of LISST is only for the finite interval of 1-250 µm, compared to PSD which is from 0 to ∞. The measurement also ignored particle smaller than 1µm, which are considerable in turbid waters with PSD slope $j > 4$ (Babin et al., 2003). The dry weight of particles less than 1 µm (from 0.2µm to 0.7µm) is not negligible (ranging from 37-60 % of the dry weight of TSS), with lower percentage in phytoplankton dominated waters compared to higher percentage in sediment dominated waters.

Table 5-4: Results from field and laboratory (LISST) measurement describing the PSD parameters. The data from Serangoon and Tekong was obtained from CRISP database.

Place	Samples	TSS (mg/L) (0.7 µm - ∞)	Particles (m3/L) (1 - 250µm)	density (kg/m3) (1 - 250µm)	d50 (µm) (1 - 250µm)	PSD slope (j)	TSS (mg/L) (0.2 -0.7µm)
Kranji	K04a	46.7	0.0103	4518	13.8	4.65	Na
	K11a	48.9	0.0101	4856	19.2	Na	Na
	K19a	58.0	0.0100	5773	16.3	Na	Na
	K26a	46.0	Na	Na	Na	Na	17.1
Poly Marina	PM1	73.3	0.0096	7657	9.9	4.99	Na
East Coast Park	ECP1	110.0	0.0233	4722	9.9	5.07	Na
	ECP2	123.3	0.0397	3105	9.9	5.04	Na
	ECP3	80.0	0.0119	6709	13.8	4.72	30.0
West Coast Park	WCPb	63.3	0.0060	10492	7.11	5.81	40.5
WCP_Spring	WCP_S	105.2	Na	Na	Na	Na	Na
WCP_Neap	WCP_N	122.3	Na	Na	Na	Na	Na
Punggol	Pgl	70.0	0.0168	4169	16.3	3.97	28.6
Pulau Ubin	Ubin_E	68.9	0.0247	2795	13.8	5.25	34.3
	Ubin_N	64.4	0.0117	5521	11.7	4.24	35.6
Lim Chu Kang	LCK	68.9	0.0188	3671	16.3	5.54	Na
Sembawang	S	105.7	0.0564	1874	13.8	5.11	33.0
Bedok	B	75.0	0.0174	4300	9.9	5.37	Na
Serangoon	Srgn	na	0.0266	na	22.7	4.9	Na
Tekong	Tkg	na	0.0760	na	5.72	6.2	Na

The PSD is assumed to follow the Junge distribution: $N(D) = KD^{-j}$ where K is the magnitude parameter and j is the slope of the distribution. $N(D)$ is the number of particles in the size interval from D to $D + dD$ per unit volume C. Typical values of j for most of the marine particle vary from 3 to 5. However, Junge distribution tends to overestimate small particles: $N(D) \to \infty$ as $j \to 0$ and underestimate larger particles: $N(D) \to 0$ as $j \to \infty$. Most of the previous studies underestimate the volume concentration for particles in between 0 to 1µm and overestimates particles > 250 µm (Babin et al., 2003). However, the error in the latter is not expected to be significant but the former can be quite substantial. Similarly, Babin et al. (2003) found that 80% of the scattering is related to fractions < 2 µm.

The PSD in seawater are hyperbolic (smaller particles are more numerous than the bigger particles). This is consistent with the data in this study that shows the number of particles per unit volume increases as the particle size decreases. The largest total particle volume (1 to 250 µm) was observed in Sembawang with 0.06 m^3/l. Total particle volume averages about 0.01 m^3/l for locations with higher d_{50}, corresponding to higher Chl-a concentration while the total particle volume for all other locations converges around 0.03 m^3/l. This shows bigger particle contributes less to the total particle volume than smaller particles. For PSD with a slope j > 5, the d_{50} ranges from 7.11 to 9.90 µm representing sediment dominated environment in Singapore Strait. For lower slope j of 3-5, the d_{50} are in the region of 13.8 to 16.3µm, indicating phytoplankton dominated environment along the Johor Strait.

Light scattering due to suspended sediment also depends on the scattering efficiency of particles. Single particle scattering efficiency is lower compared to the ensemble particles. The particle size of about 2µm (equivalent to the wavelength of visible light) is the most efficient in scattering light (Kirk, 2011). If 1.18 and 1.05 are considered as representative n

values for sediment and chlorophyll particles respectively, about half of the scattering is due to particles smaller than 1 µm when they are suspended sediment, whereas the most efficient particles in the scattering coefficient of phytoplankton are in the range of 1-10 µm (Babin et al., 2003). The scattering efficiency is assumed to be constant for all locations regardless of the PSD in this section although Baker and Lavelle (1984) pointed out that smaller particle in suspension attenuate more efficiently than bigger particles.

The number of undetected particles which are smaller than 1 µm is not negligible in areas with higher PSD slope j; especially in WCP and ECP. The higher slope indicate that more sediment are in the < 1µm fraction thus underestimate the total particle volume of the sample, producing worthless sediment density reading. For example, the sediment density in WCP is 10,000 kg/m^3 with particle volume concentration of only 0.006 m^3/l. In contrast, the total particle volume of 0.03 m^3/l in Sembawang and Pulau Ubin produce reasonable density reading. This is consistent with findings from Babin at al. (2003) that found that more than 95% of the particle volume is confined within the small-sized fraction when j approaches 5. This disproportionately large contribution of the smallest particles is greatest for higher j towards smaller particles.

In summary, smaller particles, especially with high refractive index, contribute significantly to scattering. Spectral dependency of scattering is lower in chlorophyll dominated waters compared to sediment dominated but both are less steep than λ^{-1} dependency for ocean waters. Parallel to the conclusion of Babin et al. (2003), it was found that scattering increases with j and for a given j increases with decreasing d_{50} value. This result also confirms that a large number of undetected small particles are important in explaining scattering. Figure 5-16 shows the PSD and its Junge distribution in WCP as representative example while PSD for other locations can be viewed in Appendix C.

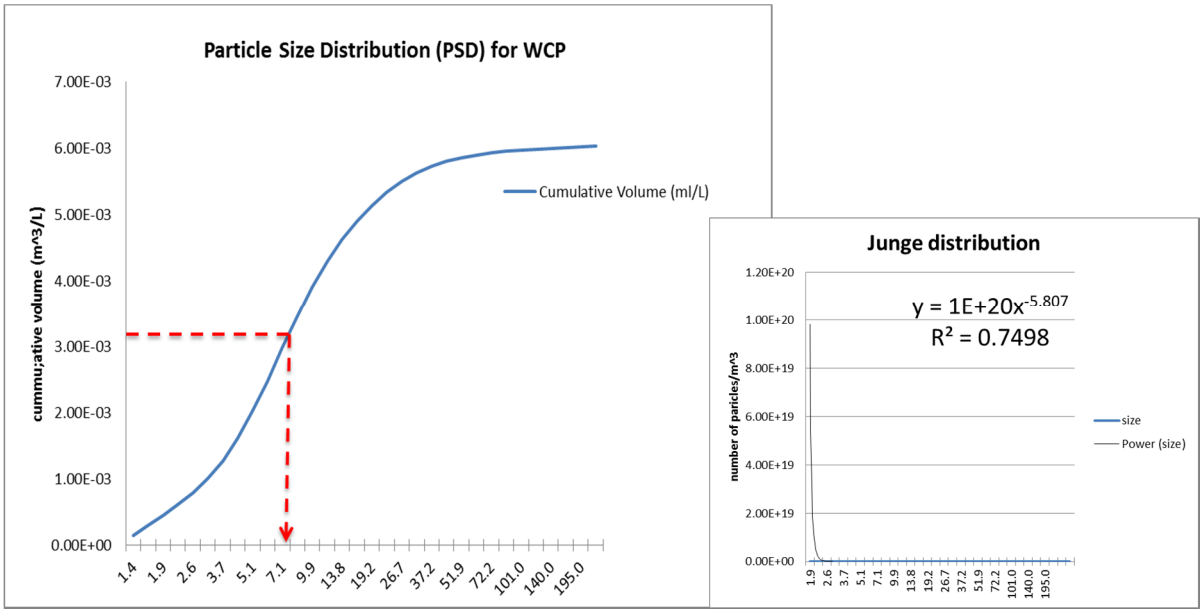

Figure 5-16: Example of PSD (left) and Junge distribution (right) for the particle volume concentration in West Coast Park (WCP), note the high j = 5.81 and small d_{50} of 7.11µm

5.4 Empirical estimation of light characteristics

5.4.1 Decomposition of K_d

The findings from all the preceding sections in Chapter 5 resulted in the culmination of Table 5-5 showing the partial contribution of optically significant constituent to light attenuation. The coefficients for each component are spectrally averaged from 412 to 715nm. The percentage error represents the percentage of attenuation not accounted for after adding up the contribution from various constituents. The error is less than 2% except for samples K04a, K19a and K26a from Kranji. The errors are more prevalent in the waters dominated by chlorophyll, most likely due to inaccuracy in Chl-a concentration determination and sensitivity of chlorophyll to light attenuation. The error for sample K04a is exceptionally high because only Level 1 scattering correction is carried out this sample. This is to illustrate that it is necessary to correct for scattering error at the highest level to minimise error.

The contribution of partial attenuation coefficient due to water, K_w and CDOM, K_g ranges from 3.4 to 8.9% to the total light attenuation coefficients K_d for all locations. The contribution is less than 4% in areas where sediment is dominant, for example in Sembawang and Pulau Ubin. However, in areas where chlorophyll is dominant, the attenuation due to water and CDOM seems to increase in tandem marginally, peaking to 9% in Kranji during low tide and 7% during high tide. For K_w and K_g, only absorption is the main mechanism in attenuating light since pure water and CDOM scattering is negligible. It is interesting also to suggest that perhaps the 'error' that is not accounted for is partly due to CDOM scattering although this cannot be proven from the existing data. Figure 5-17 shows the percentage contribution of the optically significant constituents from 8 locations in Singapore waters.

Table 5-5 shows that the partial light attenuation due to sediment K_s is the single most important factor in describing on average about 40-95% to K_d. K_s is increasingly important from chlorophyll dominated waters to sediment dominated waters, reaching the highest percentage in Pulau Ubin with an astounding contribution of 95% to total light attenuation. The contribution of sediment scattering b_s seems to govern K_s over sediment absorption a_s with the ratio of b_s / a_s averages about 10 in sediment dominated waters compared to 4 in chlorophyll dominated areas. However, in ECP and WCP, as the b_s / a_s ratio is only about 5, just slightly higher than in chlorophyll dominated waters. This is most probably due to the flocculation of the fine sediments that lowers the surface area to volume ratio, resulting in less efficient scattering due to higher settling velocity and lower b_s / a_s.

The partial contribution of chlorophyll K_p to K_d is higher in locations with higher Chl-a concentration, peaking from 50% up to 61% during low to high tide. This is significant because it quantitatively shows that chlorophyll contribute significantly to light attenuation, at least in the chlorophyll dominated waters. The data also shows inverse relationship between Chl-a concentration and light penetration as agreed by Lorenzen and Jeffrey (1980) especially during high tide when the K_p is higher compared to K_s. However, more balance contribution of K_s and K_p is seen during low tide. The Chl-a concentration is not linearly related to K_d as reported by Morel (1988) as 'non-linear biological effect' in Case I waters. Contrary to expectation, chlorophyll scattering dominates over absorption in K_p, also agreed by Van Duin et al. (2001) where the former is 5 times higher than the latter.

Table 5-5: Percentage contribution to absorption and scattering of optically significant constituents (K_w: water, K_g: CDOM,K_s: sediment and K_p: phytoplankton) to K_d

Place	Samples	% Kw		% Kg		% Ks		% Kp		% error
		a	b	a	b	a	b	a	b	
Kranji	K04a	3.79	0.03	5.02	0.00	3.99	37.20	7.73	42.24	10.47
	K13a	2.89	0.03	2.63	0.00	11.84	37.47	10.02	35.13	0.00
	K19a	3.55	0.03	4.51	0.00	5.66	24.60	6.53	55.11	8.40
	K26a	3.41	0.03	3.54	0.00	6.26	25.32	6.51	54.93	5.86
East Coast Park	ECP2	3.73	0.03	3.32	0.00	2.77	87.71	0.55	1.89	0.05
	ECP3	3.60	0.03	3.39	0.00	4.96	85.65	0.53	1.82	0.00
West Coast Park	WCPb	3.93	0.04	6.47	0.00	2.49	83.24	0.85	2.98	0.00
Punggol	Pgl	3.76	0.03	2.91	0.00	3.58	31.02	13.03	45.67	1.43
Pulau Ubin	Ubin_E	2.04	0.02	1.43	0.00	4.45	90.73	0.30	1.03	0.43
	Ubin_N	2.38	0.02	1.61	0.01	2.49	91.39	0.48	1.03	0.43
Lim Chu Kang	LCK	3.37	0.03	5.64	0.00	2.98	73.63	3.25	11.10	0.50
Sembawang	S	1.57	0.01	1.53	0.00	4.32	86.40	1.40	4.77	0.04
Bedok	B	2.65	0.02	3.15	0.00	3.94	87.21	0.69	2.34	0.02

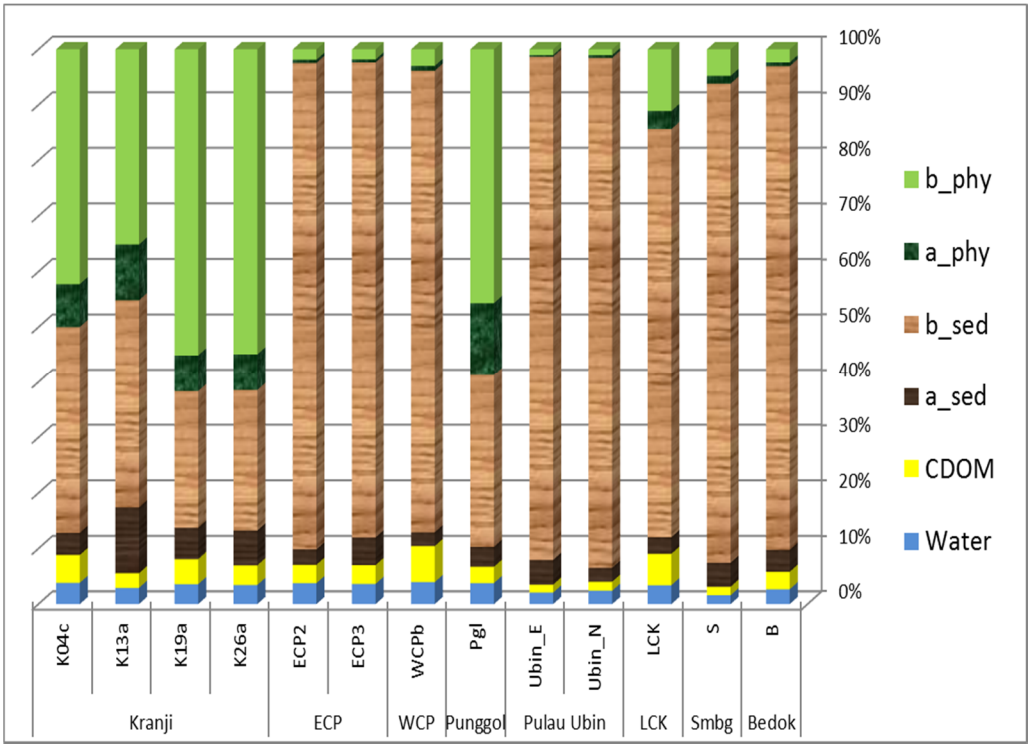

Figure 5-17: Percentage contribution of various constituents to the mean spectral downwelling attenuation coefficient, K_d in Singapore waters (a_sed means absorption due to sediment).

Evidently, phytoplankton contributes to scattering approximately as much as sediment in chlorophyll dominated waters. The proportional contributions of sediment and chlorophyll to light attenuation in Singapore waters are comparable to those reported by Lund-Hansen (2004) in the Århus Bay, Blom et al. (1994) in Dutch Lakes and Vant (1990) in New Zealand estuaries. However, they are in contrast to studies by McPherson and Miller (1987) and Smith (1981) who also shown greatest contribution from sediment but followed by CDOM and finally chlorophyll. Blom et al. (1994) and Pierson et al. (2003) found that light attenuation is largely governed by CDOM, with riverine input being the largest source.

5.4.2 Multiple linear regression of K_d

Equation relating the beam attenuation coefficients, c *of the optically significant constituents to light attenuation coefficient* K_d *will be presented before another equation relating* K_d *and physical properties is given. The physical properties of NTU and chlorophyll concentration are chosen because sediment and chlorophyll are the two most important contributors to light attenuation as seen in Section 5.4.1. In general, the most significant constituent is sediment but equal contribution from chlorophyll and sediment is observed in chlorophyll dominated waters. This is quite profound because even in chlorophyll dominated waters, sediment contribution rarely goes below 40%. Furthermore, NTU and Chl-a concentration are relatively conveniently measured from the field, hence it will be handy if these data can be plucked into an equation to estimate* K_d.

The contribution of partial light attenuation to K_d *can be determined using multiple linear regression equations (< 5% significance level). The results depicted in Table 5-5 are used to predict* K_d *value using the following regression for* n = 13 *and (*r^2*= 0.77,* $p < 0.05$*):*

$$K_d = 0.272 + 0.448 * \left((C_g)\right) + 0.134\ ((C_s)) + 0.357\ \left((C_p)\right) \qquad \textit{(Eq. 5.2)}$$

0.448, 0.134 and 0.357 are the regression coefficients for beam attenuation due to CDOM, sediment and chlorophyll respectively. These regression coefficients provide estimates on the effect of optically significant constituents to light attenuation coefficient K_d*. However, the above relation is not particularly useful since one has to perform elaborate laboratory experiments to determine the* c *(i.e. absorption and scattering coefficients for all the optically significant constituents). A more useful equation linking* K_d *directly to physical properties (not optical) of measured parameters are derived. The linear regression of* K_d *on NTU and chlorophyll concentration (Chl-a) produces an equation of the following form (for* n = 13 *and* $r^2 = 0.63, p < 0.05$*) because* $a_g(440)$ *was not significant:*

$$K_d = 1.08 + 0.033 * (\text{NTU}) + 0.009 * (\text{Chl} - \text{a}) \qquad \textit{(Eq. 5.3)}$$

In view of the different factors dominating the light attenuation at these locations and to partly improve the fit of the equations, the data are separated into chlorophyll and sediment dominated water respectively. The following is the improved relation for chlorophyll dominated water with n = 6 *and (*$r^2 = 0.98, p < 0.05$*):*

$$K_d = 1.64 + 0.01 * (\text{NTU}) + 0.004 * (\text{Chl} - \text{a}) \qquad \textit{(Eq. 5.4)}$$

However, the equation above is only statistically significant for Chl-a. No significant linear relations exist for the data in sediment dominated waters. This makes sense as the <u>Chl-a concentration is relatively more linearly related to K_d *then the NTU</u> as shown also by Van Duin et al. (2001) and Otto (1966). Although NTU represents the optical property, it is not intrinsically identifiable to any of the optically active constituents. The suspended solid contains both sediment and chlorophyll with various sizes (and possibly some traces of CDOM). All this fluctuates the scattering property (i.e. NTU), causing absence of correlation between NTU and* K_d*. Furthermore, the multiple linear regressions inherently assume linear relationship between the variables, which is violated for NTU and* K_d.

However, the multiple linear regressions with low r^2 shown for Equation 5.3 does not truly represents the data as the linear relation assumption is not fulfilled, especially for NTU against K_d. To produce a better relation that describes the non-linearity between the variables, a surface fitting linear model (TableCurve 3D's Automated Surface-Fit Processing) is used. This fitting tool uses a single step Gaussian Elimination matrix solution method for the coefficients to increase the effectiveness of the fit. Firstly, the distribution of the data is shown in Figure 5-18. Note the two separate regions in which the data are clustered together, showing the diabolic nature of the data. Chlorophyll dominated waters have extremely high Chl-a concentration and lower NTU while sediment dominated waters have lower Chl-a concentration and relatively higher NTU.

The regression equation relating NTU and Chl-a to K_d from the surface fitting tool shows an improvement from the multiple linear regressions equations. Apparently, the best fit was obtained if the contribution of Chl-a is not considered, therefore making it appropriate for sediment dominated waters. The inclusion of Chl-a in the equation yielded a lower r^2= 0.50 although the relation is still statistically significant. The lower r^2 with Chl-a inclusion is in contrast to the results from the multiple linear regressions (Equation 5.3) that shows both Chl-a and NTU are statistically significant with r^2= 0.63. The fitting result (Figure 5-19) shows that the K_d is dominated by non-linearity of NTU and is best approximated by the regression equation (r^2= 0.74, $p<0.05$):

$$K_d{}^{-1} = 0.71 - 3.49\, e^{-5}\,(\mathrm{NTU}^3) - 7.41\, e^{-(\mathrm{NTU})} \qquad \textit{(Eq. 5.5)}$$

It seems that non-linear surface fitting fits non-linear model of K_d and NTU quite well while multiple regressions fit linear model of K_d and Chl-a well. Contrary to initial expectation, the K_p is found to be statistically significant influence on K_d in all sampling locations. This is also probably the case for other locations with similar types of water bodies within the region. Although sediment are the greatest contribution to light attenuation in Singapore waters, it is also proven that CDOM still has a measurable (although not statistically significant) and positive correlation with K_d in Singapore waters. The importance of CDOM is apparently higher when neither chlorophyll nor sediment dominates the water. The fine detail of each partial contribution to K_d depends on prevailing local condition that governs the IOP (i.e. tides, currents, discharge) and the environmental factors like (atmosphere, nutrients and biological feedback). These factors will be investigated further in Chapter 6 and 7.

Due to the limited data sets, the relationship does not pretend to be final and accurate at all times. Comparison against previous studies/data in the vicinity is not possible due to the lack of light attenuation study in this region. However, these values should work well for Singapore waters, especially if the 'correct' equations are used to represent its local condition. It is recommended that Equation 5.4 is used for chlorophyll dominated waters (Chl-a concentration > 30 mg/m^3) while Equation 5.5 is used for sediment dominated waters. Equation 5.3 can be used in areas where neither chlorophyll nor sediment dominates. Finally, Equation 5.2 can be used if the IOP of the waters are available but the AOP are not available. The proposed relation can be improved with increased data sets and improved measurement techniques. In the future, some form of verification works to the established equation should be carried out.

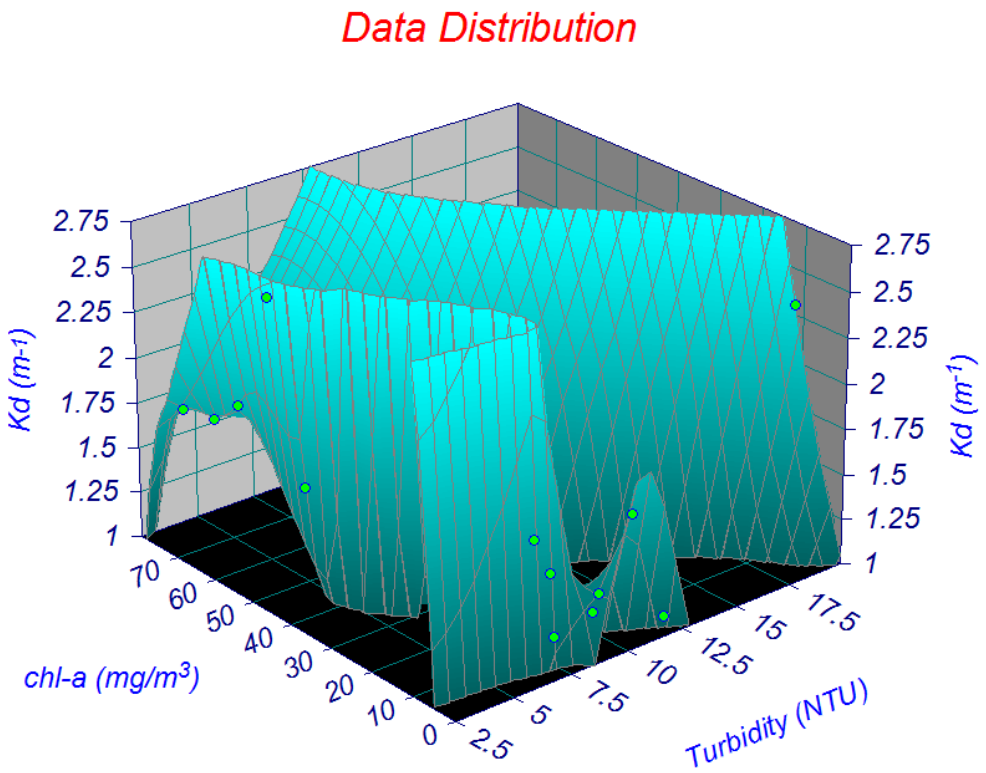

Figure 5-18: 3D plot of the data distribution showing 2 separate clusters with one 'extreme' point (representing Sembawang) with high NTU and relatively higher chl-a concentration.

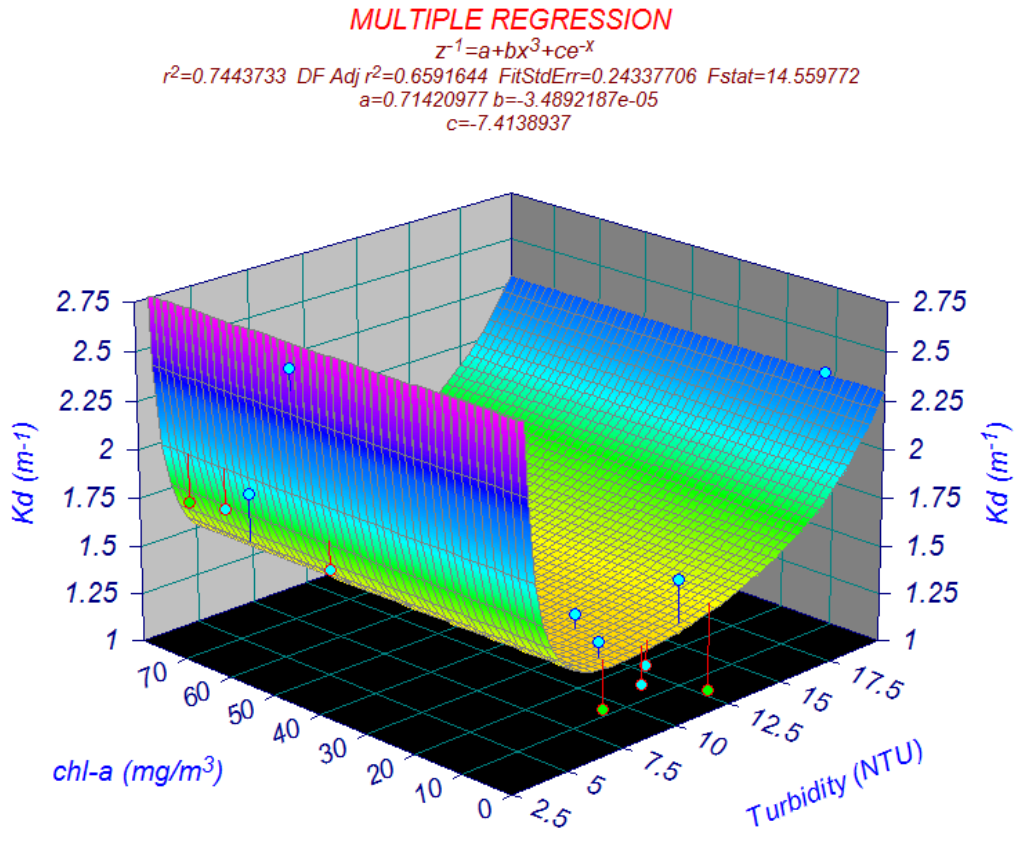

Figure 5-19: Multiple regressions function for 3 parameters (K_d, NTU and Chl-a) with one intercept (a) and two coefficients (b and c). Note that the term chl-a (or y) is not in the equation.

5.4.3 Theoretical K_d prediction

The beam attenuation coefficient c obtained from laboratory measurements describes the IOP of a water body yet it does not tell us much about light in the water column. Various efforts have been made to link the water's IOPs to AOP ever since optics research began in circa 1970's (Preisendorfer, 1976 as referenced by Kirk, 2011) since AOP is physically more representative parameter for underwater light field. Specifically, the vertical attenuation coefficient for diffuse downward irradiance, K_d and beam attenuation coefficient c *can be related through empirical equation. Such calculation circumvents the need for full simulation of underwater light field by expressing K_d as a function of IOP. Commonly used K_d approximation is the empirical equation of Sathyendranath et al. (1988):*

$$K_d(Z) = \frac{(a + b_b)}{\cos \mu_o} \qquad \textit{(Eq. 5.6)}$$

Where a *and b_b is the absorption and backscattering coefficient respectively. μ_o is the angle between the solar beam just below the surface and the vertical. The average cosine angle is normally chosen as 1 for incident/overhead sun (μ_o = 90) and 0.5 for diffuse/overcast sky (μ_o = 60). The following calculation assumes Peltzold's phase function b_b 1.8% of total scattering coefficient* b, (b_b = 0.018). *Kirk (1984a) found a simplified procedure for the calculation of light attenuation in absorption-scattering waters as follows:*

$$K_d = \frac{1}{\cos \mu_o} [a^2 + (0.425 \cos \mu_o - 0.19) a\ b]^{1/2} \qquad \textit{(Eq. 5.7)}$$

Assuming incident sun with $\cos \mu_o$ *of 1, the variable '0.256' (from 0.425 – 0.19) is chosen as the coefficient defining the relative contribution of b to K_d as proposed by Kirk (1984a). This equation was derived from the analysis of light field generated by Monte Carlo modelling of solar radiation in idealised water bodies (Kirk, 1984a) assuming incident light field with no cloud cover. Another equation by Kirk (1984b) for relatively high cloud cover condition (known as standard overcast/diffuse model) is given as:*

$$K_d = 1.168\ (a^2 + 0.168\ ab)^{1/2} \qquad \textit{(Eq. 5.8)}$$

Van Duin et al., (1992) compared measured vertical attenuation coefficients and laboratory-based beam attenuation coefficients c and derived the following linear relation based on 102 laboratory measurements (r^2 of 0.94):

$$K_d = 0.68 + 0.29\ c \qquad \textit{(Eq. 5.9)}$$

Table 5-6 shows the computed K_d from the above four equations. The $\bar{c}$ (in the first column) is averaged spectrally (412 to 715nm) from ac-9 measurement. The average $\bar{c}$ is assumed to be constant over the depth. The homogenous $\bar{c}$ estimation is approximately accurate to the first order as shown by Van Duin et al. (1992). The general trend describing the variation in K_d (lowest and highest K_d) agrees well for all four equations. The K_d varied between 1.2 to 4.5 m^{-1} for both Kirk (1984a and 1984b) equations while K_d for Sathyendranath et al. (1988) ranges from 0.8 to 4.2 m^{-1}. All equations showed <u>higher K_d for diffuse light compared to incident light</u> because the latter contains 'artificial' light from the diffuse downward flux from scattering instead of an infinite beam of light for the former.

Table 5-6: K_d as obtained from various empirical equations (the dimension of c and K_d is m^{-1})

Place	Samples	c from ac-9 (field data)	Van Duin, 1992	Sathyendranath et al. (1988) Kd=(a+bb)/cos(μ_o)		Kirk, 1984a	Kirk, 1984b
			Kd = 0.68 + 0.29c	cos(μ_o)=1	cos(μ_o)=0.5	Incident	Diffuse/Overcast
Kranji	K04c	5.67	2.32	1.25	2.49	1.64	2.39
	K13a	7.44	2.84	2.13	4.27	2.64	4.54
	K19a	6.07	2.44	1.32	2.63	1.74	2.60
	K26a	6.31	2.51	1.33	2.67	1.78	2.69
East Coast Park	ECP2	5.77	2.35	0.69	1.38	1.07	1.31
	ECP3	5.97	2.41	0.84	1.68	1.25	1.64
West Coast Park	WCPb	5.47	2.27	0.80	1.60	1.21	1.51
Punggol	Pgl	5.72	2.34	1.41	2.82	1.81	2.70
Pulau Ubin	Ubin_E	10.53	3.74	1.04	2.08	1.70	2.65
	Ubin_N	9.04	3.30	0.78	1.56	1.32	1.77
Lim Chu Kang	LCK	6.38	2.53	1.07	2.14	1.51	2.17
Sembawang	S	13.69	4.65	1.43	2.86	2.30	4.37
Bedok	B	8.13	3.04	0.98	1.96	1.52	2.20
Semakau	Smk	2.35	1.36	0.26	0.13	0.43	0.37

Kirk (1984b) overcast sky formula agrees quite well with Sathyendranath et al. (1988) for diffused light ($\cos \mu_o = 0.5$*) except in Sembawang witch shows substantial difference (2.86 in the former but 4.37 in the latter). The other Kirk's incident formula (1984a) overestimates incident K_d from Sathyendranath et al. (1988) with deviation of 0.38 to 0.87 m^{-1}. The overestimation seems to be lower in Kranji, Punggol, ECP and WCP compared to other sediment dominated areas (Bedok, Sembawang, Lim Chu Kang and Pulau Ubin). The Kirk's incident formula (1984a) agrees with Sathyendranath et al. (1988) if the value of* $\cos \mu_o$ *is about 0.72 (cosine angle in the region of 44°). However, the K_d estimation from Van Duin (1992) is on the higher side (since the coefficients are site specific), but does not deviate too much from Sathyendranath et al. (1988) and Kirk's (1984b) for overcast/diffuse formula.*

The most versatile equation seems to be the equations from Kirk (1984a, 1984b). One of the main reasons for this is the inclusion of both absorption and scattering in the formula compared to only absorption in Sathyendranath et al. (1988). This is important especially in waters dominated by sediment because the attenuation is mostly governed by scattering. Furthermore, the equations do not make any assumptions on the scattering phase function of the constituents in the water column. Contrast this with the equation Sathyendranath et al. (1988) which contains the b_b, thereby increasing the uncertainties associated with the use of the formula to estimate K_d. However, as Van Duin et al. (1992) pointed out attenuation coefficients estimated with this procedure often differ for the surface and bottom. Hence, the depth variation of K_d will be investigated in the next chapter.

The relative contributions of each optically significant constituent to K_d in this thesis are inferred from their percentage of contribution to beam attenuation c. However, strictly speaking, K_d cannot be expressed as a simple sum of the constituents. Minor discrepancies between K_d and K_w + K_g + K_p + K_s is due to the differential scattering for sediment which peaked in the forward direction. The forward scattered light does not deviate much from the incident beam (c) but the diffused K_d is contributed mostly by the backscattered light (b_b) which is only about 2% of the total scattered light (b). Nevertheless, the percentage contribution is assumed to be valid to the first order.

CHAPTER 6.0: UNDERWATER LIGHT FIELD MODELLING

Underwater light field is important for various coastal engineering, ecological and remote sensing application. The light field is normally estimated using empirical algorithms based on measurements and/or probabilistic methods. However, they are insufficient for understanding the light field variation and contain large uncertainties. Therefore, this chapter will model underwater light field using the well tested Hydrolight model as a platform for the discussion of the research questions. The purpose of this chapter is to gain more intuition with regards to the simulated optical properties, especially K_d. The modelled values were not intended to be compared against any measurement due to the lack of comparative data. The results from Kranji and WCP will be shown as representative location for chlorophyll and sediment dominated waters respectively.

Specifically, Hydrolight was used to spectrally resolve the light field and obtain point base information of the K_d at various locations. Underwater light field modelling was carried out using 2 different IOP models in Hydrolight (ABACBB and ABCASE2). The inputs for both IOP model is the concentration of optically significant constituents. The results from Kranji and WCP will be compared and analysed. IOP of all the optically significant constituents will be revisited in Section 6.1 while the AOP modelling will be presented in Section 6.2. Special attention will be paid to the diffuse attenuation coefficient for downwelling irradiance (K_d) as it is the single most important parameter describing the propagation of light in the water column. The modelled K_d will then be compared against the theoretical calculation of K_d from Section 5.4.2. Finally, other optical parameters like the Secchi depth and euphotic depth will be discussed in Section 6.3.

6.1 IOP modelling

It might seem counter intuitive to remodel IOP (i.e. absorption and scattering coefficient) again since the field measurement in Chapter 5 had provided detail insights of its characteristics. However, Chapter 5 assumes mean concentration for the optically significant constituents, hence constant absorption and scattering coefficient throughout the water column. This is similar to ABACBB model while the ABCASE2 model assumes vertical variation in the water column. In the former, the water is modelled by only two constituents: water and "everything else" (CDOM, chlorophyll and sediment). ABCASE2 model has four constituents: water, CDOM, chlorophyll and sediment. The figures in this section will show the absorption and scattering coefficient for all the optically significant constituents as a function of depth and selected wavelengths in Kranji and WCP.

The vertical concentration of optically significant constituents determines the vertical variation of IOP. This is not surprising as the routines in Hydrolight calculate the light propagation in the water column as a function of these concentrations. The concentration of chlorophyll and sediment was approximated as decreasing linear profile. The decreasing linear profile approximates the logarithmic profile observed in many coastal waters. The chlorophyll and sediment concentration in Kranji was specified as 65 mg/l and 38 mg/m^3 respectively in the surface. Similarly for other sampling locations, the value from the field measurement was also specified in the surface. The results were simulated for Kranji during high tide condition and WCP during mean sea level. Section 6.1.1 and 6.1.2 describes vertical variation of optical properties as modelled in ABCASE2 model.

6.1.1 Vertical variation in absorption coefficient

Figure 6-1 shows the absorption coefficient a for optically significant constituents as a function of depth at 415nm in Kranji and WCP. The absorption coefficient due to sediment is the highest, followed by Chl-a, CDOM and water in Kranji. However, CDOM absorption is higher than Chl-a absorption in WCP. Only the water absorption is constant with depth but other constituents like Chl-a vary as much as two-fold from surface water to bottom. The Chl-a concentration profile reduces linearly with depth, similar to Chl-a absorption which shows almost linear decrease but with a slight increase within the first 0.5m depth. This is attributed to photodegradation and self-shading effect at the water surface. Finally, the sediment absorption shows two peaks due to higher concentration at the surface and the resuspension at the bottom respectively.

Figure 6-2 shows the total absorption coefficient as a function of wavelengths for selected depths for both locations. There are no significant changes with respect to the depth as the simulated water depth is only 5m although the depth variation can be significant for deeper water in open oceans. For both locations, the absorption spectrum at the bottom is almost equivalent to the surface. Absorption is consistently high at blue wavelengths (~ 400 to 500nm) at all depths due to combined absorption by sediment, phytoplankton and CDOM and reduces in the green wavelength (~ 500 to 500nm) before picking up in red wavelengths (~ 600 to 700nm) due to higher absorption by water itself and Chl-a concentration in Kranji. The underwater light field bears the spectral "signature" of the water column constituents, especially for chlorophyll absorption at dual peak wavelengths (440 and 676 nm).The chlorophyll absorption at 440 and 676 nm is more prevalent in the surface water compared to the bottom indicating higher chlorophyll concentration in the former.

Figure 6-3 shows the total absorption coefficient as a function of depth for selected wavelengths. The absorption is highest at the blue wavelengths followed by the red and green wavelengths. The absorption at red wavelength (655 and 685nm) is higher than the green wavelength (595nm) due to significant absorption of water itself in the red wavelength. Consequently, the absorption of red light by water causes a relative increase in the fraction of blue photons that most efficiently drive photosynthesis (Van Duin et al, 2001). The absorption for WCP is slightly higher than Kranji because the latter lacked sediment. The difference between the surface and bottom absorption is more pronounced in the shorter wavelengths in WCP. Absorption is generally lower in the surface and increases towards the bottom. However, the absorption at surface and bottom for Kranji is similar because higher sediment at the bottom 'compensates' the lower chlorophyll absorption.

One constituent dominates over another to influence light attenuation depending on the depth and wavelength. Light attenuation especially in the upper layers of the water column is influenced by the chlorophyll concentration, especially in chlorophyll dominated waters. As presented in Section 5.4.1, the higher Chl-a in Kranji had light attenuation due to phytoplankton to be as high as 60% of the total light attenuation. Besides the self-shading effect due to increase concentration, variation in vertical chlorophyll distributions also leads to non-uniformities in absorption and consequently to variations in light available for chlorophyll absorption (Van Duin et al., 2001). Moreover, differential heating due to variation in chlorophyll absorption may also increase vertical mixing although this thesis does not aim to investigate these fine structures.

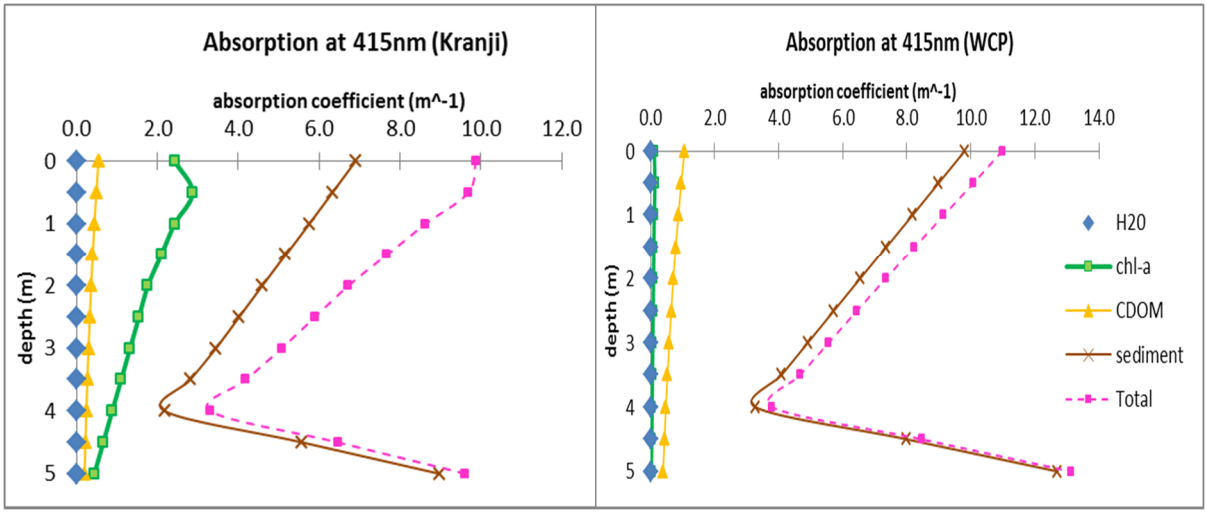

Figure 6-1: Optically significant constituents and absorption coefficient at 415nm in Kranji and WCP. CDOM absorption is higher than chlorophyll absorption in WCP.

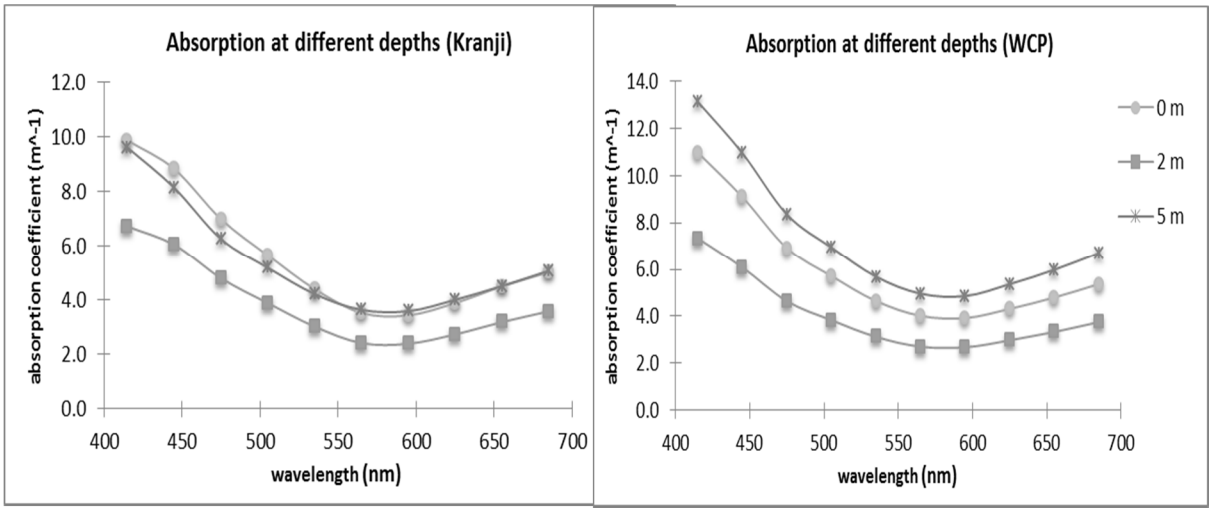

Figure 6-2: Total absorption coefficient at various depths for in Kranji and WCP. The difference between surface and bottom absorption is higher in WCP compared to Kranji.

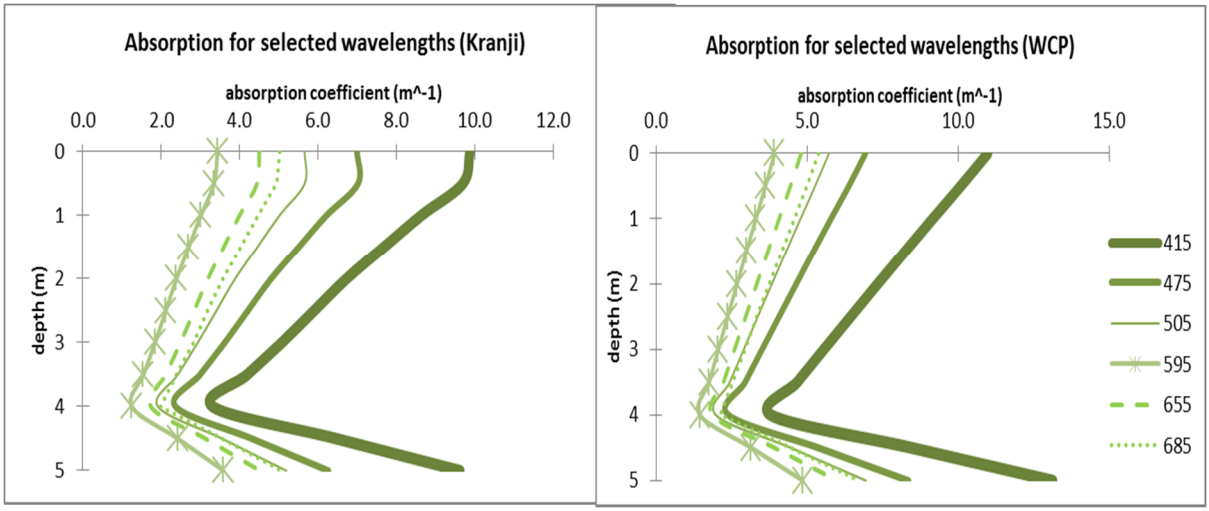

Figure 6-3: Vertical variation of absorption at selected wavelengths in Kranji and WCP. Absorption increases in the following order for both locations (green, red and blue).

6.1.2 Vertical variation in scattering coefficient

Figure 6-4 shows the scattering coefficient for optically significant constituents at 415nm in Kranji and WCP. The scattering coefficients are similar to the one for absorption coefficient but the former is about a magnitude larger than the latter. The scattering due to water itself is negligible while the chlorophyll scattering decreases almost linearly with depth and higher scattering at the surface and bottom. As observed for absorption, the scattering at near bottom is also relatively higher due to the increase of sediment concentration. The availability of more sediment near the bed is more pronounced in Kranji. This is probably due to the calm nature of stagnant water in Kranji (allowing sediment to settle) compared to higher vertical diffusivity due to turbulence, waves and current that enhance mixing and sediment resuspension in WCP.

Figure 6-5 and 6-6 shows the scattering coefficient at different depths and wavelengths respectively for Kranji and WCP. In Figure 6-5, the wavelength dependence $\lambda^{-\gamma b}$ of scattering spectrum reduces with wavelength (lower slope), especially at deeper depth at both locations. However, in contrast to the measured scattering spectrum in Section 5.2.2, the modelled spectrum in Kranji shows lower scattering at the longer wavelengths (as compared to Figure 6-10). Note that at all depth in Figure 6-6; the apparent importance of sediment to scattering is evident, since the vertical variation of scattering closely resembles that of sediment scattering. Furthermore, the scattering coefficient is highest at 415nm (blue wavelength) and reduces progressively towards the longer wavelengths (green and red).

6.2 AOP modelling

Underwater light field and its spectral distribution cannot be directly computed from the total IOP's of the constituents. Instead the AOP in terms of various diffuse attenuation coefficients (also known as K-functions) is needed to characterise a water body. To determine the amount of light attenuated in the water column due to absorption and scattering, vertical diffuse attenuation coefficient for downwelling irradiance or K_d is important. K_d and other AOP's are related to the IOP of a water body and the prevailing light structure by the use of RTE (Section 3.6). Hydrolight computes various AOP including K_d and radiance distribution, irradiance and reflectance as a function of depth, wavelength and direction in the water column. Section 6.2.1 discusses the spectral variation of K_d while Section 6.2.2 and 6.2.3 compares the model results against empirical calculation.

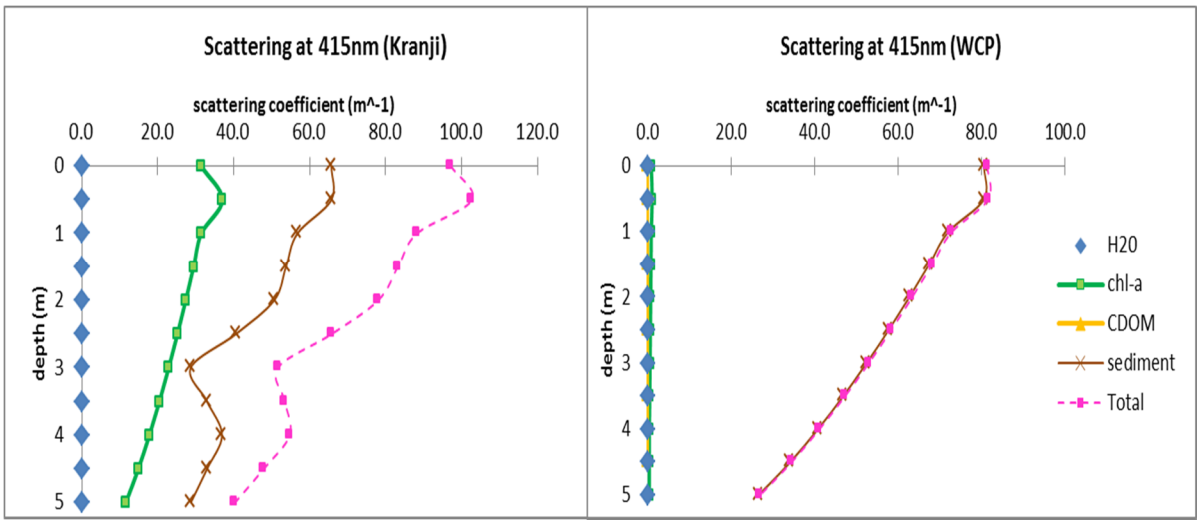

Figure 6-4: Optically significant constituents and total scattering coefficient at 415nm in Kranji and WCP. Total scattering in Kranji is higher than WCP.

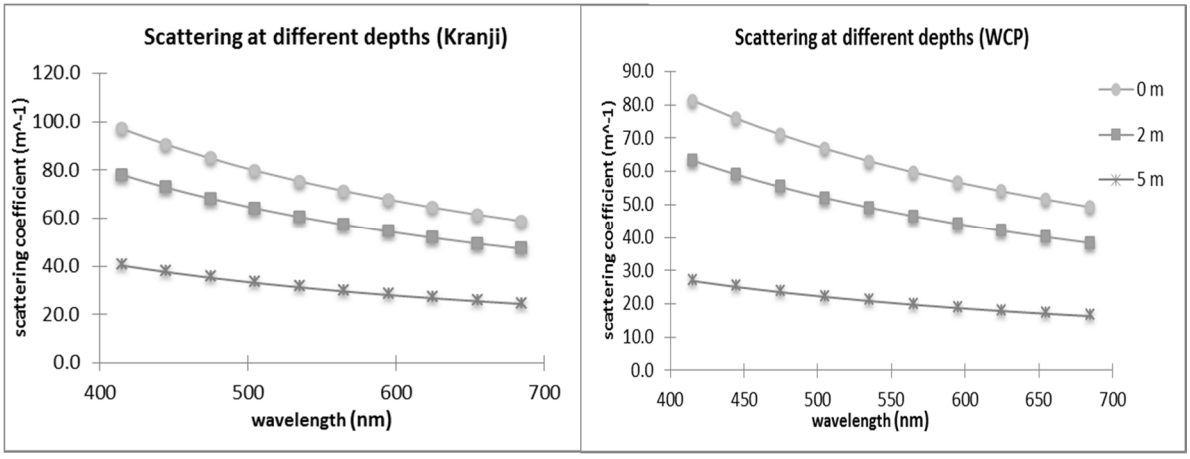

Figure 6-5: Absorption coefficient at various depths for wavelengths in Kranji and WCP. The difference of scattering spectrum at various depths is similar for both locations with reducing wavelength dependence (gentler slope) in deeper waters compared to surface.

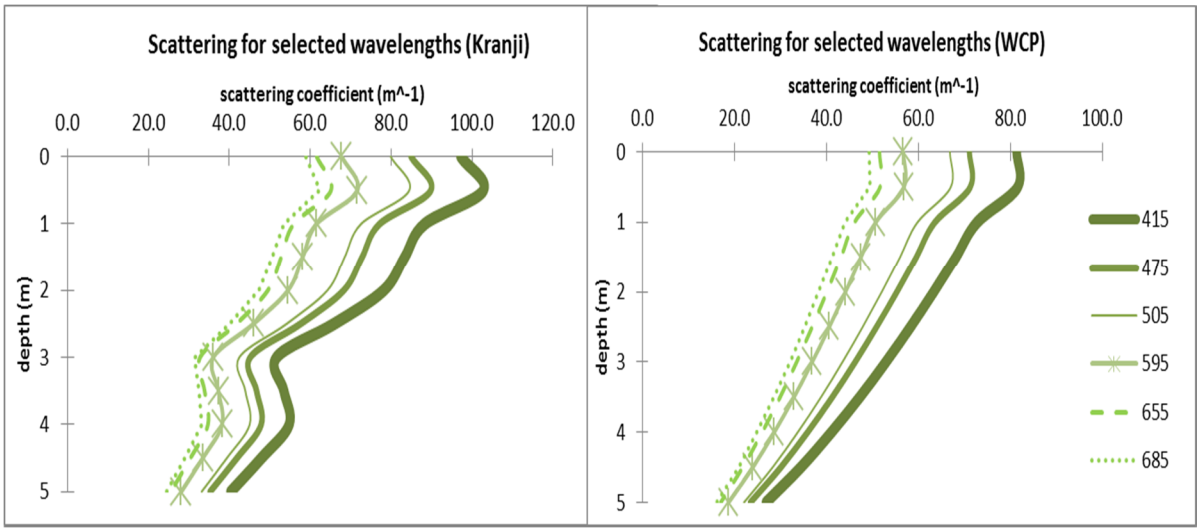

Figure 6-6: Vertical variation of scattering coefficient at selected wavelengths in Kranji and WCP. Scattering for WCP reduces exponentially with depth but the overall scattering in Kranji is higher.

6.2.1 Vertical and spectral K_d variation

Figure 6-7 shows the modelled results of K_d , K_u , K_{od} and K_{ou} at 415 nm in Kranji and WCP. The K_d indicates the amount of light propagated from the surface to the bottom (downwelling) while K_u indicate the measure of light propagated from the bottom to the surface (upwelling). The values K_{od} and K_{ou} are the scalar values of downwelling and upwelling irradiance respectively. Downwelling AOP's are higher than upwelling AOP's with the highest AOP of K_d, followed by K_{od}, K_u and finally K_{ou}. The values of all the K-functions are almost similar with small difference in the surface before reaching asymptotic value K_∞ at greater depths (Van Duin et al., 2001; Mobley, 1994). The $K_\infty(415)$ at Kranji is about 11.0m^{-1} and WCP is about 16.1m^{-1} suggesting that turbid coastal waters that have high sediment concentration should have higher K_∞ value.

Higher K_d physically means less light is propagated into the water column, as the exponential power of the light decrease is higher, hence the more rapid the light attenuation. This can be due to high light absorption and/or scattering within the water column. The K_d differs according to the wavelength and depth (to say nothing about the complexity of IOP variation and prevailing light structure). Since K_d governs underwater light field, the K_d value was averaged spectrally and in depth $\overline{K_d}$. This yielded $\overline{K_d}$ of 4.7m^{-1} in Kranji and 5.5m^{-1} in WCP for ABCASE2 model and 1.4m^{-1} and 1.2m^{-1} in Kranji and WCP respectively for ABACBB model. The K_d difference between both locations with the respective models are not big although one would expect different results since the main constituents for the waters differ remarkably (one is dominated by chlorophyll and the other dominated by sediment).

Figure 6-8 shows the K_d spectra computed between surface and various depths. The spectral K_d is similar for both locations, higher at the surface for the blue and red wavelengths compared to green wavelengths. This wavelength dependency is due to the CDOM, sediment and chlorophyll absorption which is higher at the shorter (blue) wavelengths and due to the absorption of water itself at the longer (red) wavelengths. The bottom K_d is highest in WCP, followed by the surface K_d and finally K_d at intermediate 2m depth, with considerable difference between all the depths. In contrast, the surface K_d and bottom K_d is similar for Kanji possibly due to 'compensation' by higher chlorophyll concentration in the surface equalling to mostly sediment contribution at the bottom. The bottom K_d at both locations are high, dominated by sediment scattering since the K_d spectrum seems to be unaffected by wavelengths, unlike in absorption spectrum.

Figure 6-9 shows the K_d as a function of depth for selected wavelengths. At both locations, K_d at 595 nm wavelengths (green) is low due to the lower light attenuating efficiency at these wavelengths. Although changes in AOP is related to the directional structure of the light field and other environmental factors (wave, sea surface, winds), ratios of AOP quantities are relatively constant and insensitive to those factors (Mobley, 1994). This is tested in which the directional structure of the light field was varied to incident light (sun is vertically positioned over the water surface) instead of 30°. The result for both simulations shows remarkable similarity. Furthermore, the inclusion of CDOM and chlorophyll fluorescence and Raman scattering for water in the model only change the results insignificantly. Therefore, the AOP is primarily governed by changes in the IOP by the presence of active constituents and its concentration.

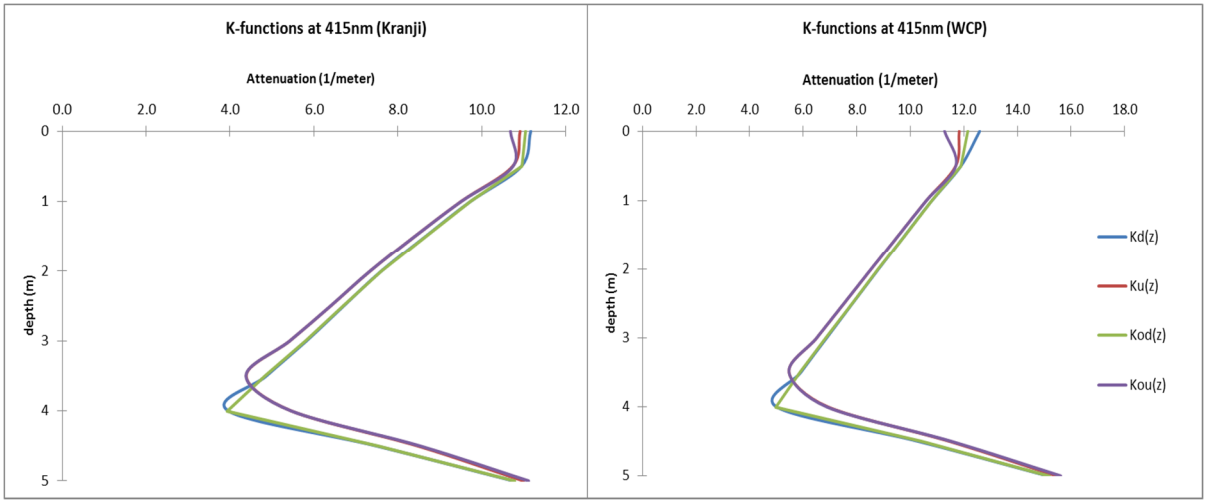

Figure 6-7: Diffuse attenuation for downwelling K_d and upwelling K_u with its scalar irradiance (K_{od} and K_{ou}) against depth in Kranji and WCP. Note asymptotic value K_∞ at greater depths.

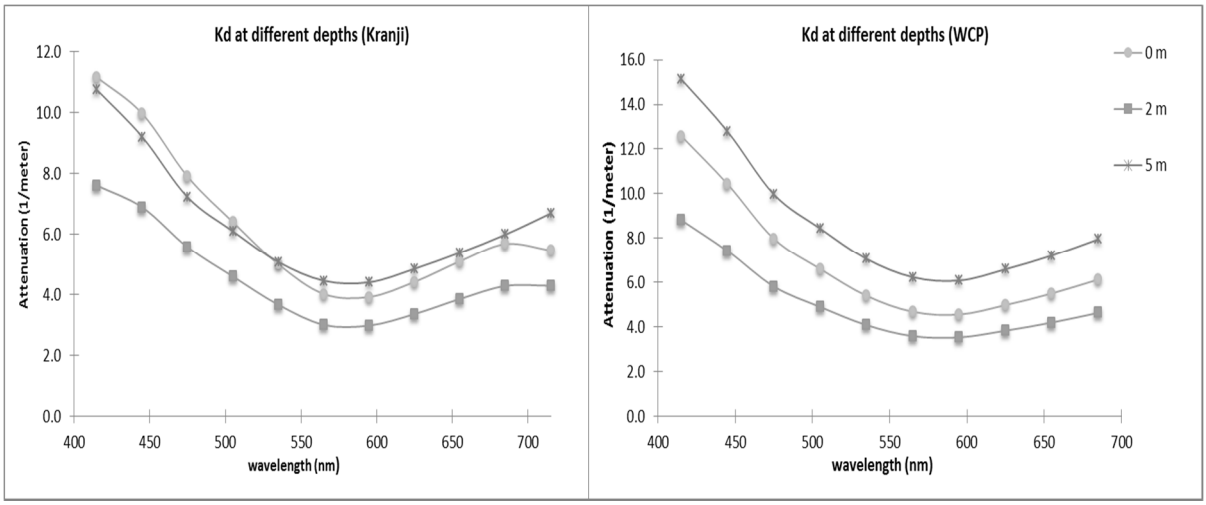

Figure 6-8: K_d at different depths computed in Kranji and WCP. K_d at the surface is dependent on wavelength compared to the bottom with higher attenuation at blue and red wavelengths.

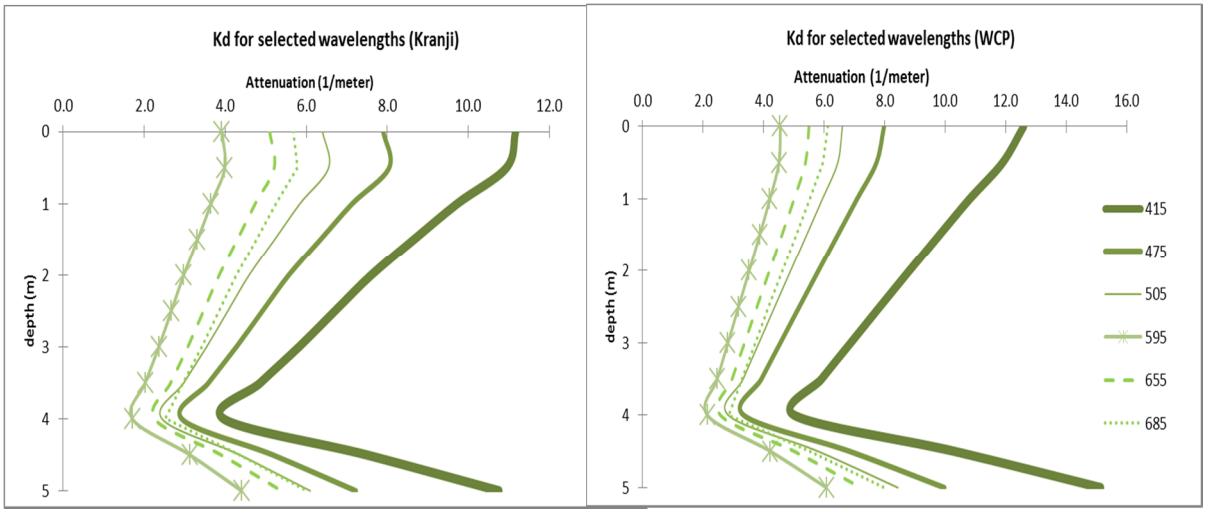

Figure 6-9: K_d as a function of depth for selected wavelengths in Kranji and WCP. K_d at 595 nm is the lowest due to the lack of optically signifcant constituents attenuating light at these wavelengths.

6.2.2 Empirical and modelled K_d

The modelled K_d from Hydrolight varies with wavelength and depth. Therefore, for comparison against the mean spectral K_d from Section 5.4.2, the modelled K_d was transformed to the depth and wavelength averaged $\overline{K_d}$. Table 6-1 shows the comparison between the calculated K_d and the modelled K_d from 2 different models (ABACBB and ABCASE2) in Hydrolight. The K_d from ABCASE2 is higher than ABACBB by a factor of 2.4 to 4.8, higher in sediment dominated waters. The most important reason is because K_d for the former is influenced by vertical variation of optically significant constituents, especially higher sediment at the bottom. Smith (1981) found that $\overline{K_d}$ is influenced by water depth, water colour and taxonomic composition of the phytoplankton, therefore scalar $\overline{K_d}$ may not necessarily represent the modelled K_d accurately. Other reasons for the discrepancy between the modelled and empirical K_d are:

- *The nature of prevailing light: 30° light angle and zero cloud cover were assumed in Hydrolight but it is impossible to simulate exact light during measurements.*
- *Assumption on the VSF used in RTE may not be accurate for each IOP's. For example, the phase function of sediment and chlorophyll may vary. However only one value can be specified in the Hydrolight model.*
- *Bottom reflectance was not assumed in Hydrolight but may play a role in sandy bottom by increased reflectance hence reducing K_d because more light is available.*
- *Surface irradiance in Hydrolight is overestimated, leading to higher modelled K_d. This is because Hydrolight computes K_d based on the computed downward irradiance E_d from the surface irradiance.*

The average $\overline{K_d}$ (spectral and depth) in Kranji during high tide (K26a) is 1.4m^{-1} and 4.7m^{-1} from ABACBB and ABCASE2 respectively. Table 6-1 shows K_d from ABACBB model is somewhere between Sathyendranath et al. (1988) for mean cosine between 0.5 and 1. The K_d agrees reasonably well with Sathyendranath et al. (1988) with incident light ($Cos\ \mu_0$ = 1). Specifically, the variation between empirical and modelled K_d in chlorophyll dominated waters is less than 7% but can reach up to 40% in sediment dominated waters. However, the variation is only less than 10 % using empirical equation of Kirk (1984a) for sediment dominated waters but up to 25% variation in chlorophyll dominated waters. This is likely because the equation of Kirk (1984a) accounts for relatively higher contribution of scattering to K_d in sediment dominated waters by the use of an adjustable coefficient instead of only absorption term in Sathyendranath et al. (1988).

The similarity between Sathyendranath et al. (1988) and ABACBB model for chlorophyll dominated waters is probably due to the accuracy of 0.018 for backscattering b_b of chlorophyll particles. Furthermore, since light attenuation in chlorophyll dominated waters is dominated by absorption, most of the attenuation is explained since the absorption term is prominent. The c from the ac-9 measurement is higher than the empirical and the modelled K_d because c consist of attenuation for incident beam of monochromatic light in an infinitely small layer of water while K_d is for diffuse light (Van Duin et al., 2001) from all the directions in the upper sphere). The forward scattered light still contributes to the radiant flux, supplying light in the water column, hence reducing the light attenuated (i.e. lower K_d). However, c seems to be close to the modelled K_d from ABCASE2 model in Hydrolight for c < 6.0 m^{-1}.

Table 6-1: Comparison between the empirical and modelled K_d. Hydrolight K_d (ABACBB) is between the Sathyendranath et al. (1988) for mean cosine between 0.5 and 1. Note the similarities between empirical and modelled K_d for chlorophyll (green) and sediment dominated waters (all units in m^{-1}).

Place	Samples	c from ac-9	Sathyendranath et al. (1988)		Kirk, 1984	Hydrolight (Avg Kd)	
		(field data)	cos(μ_o)=1	cos(μ_o)=0.5	kd = (a^2 + 0.256ab)^1/2	ABACBB	ABCASE2
Kranji	K04c	5.7	1.3	2.5	1.6	1.3	5.8
	K13a	7.4	2.1	4.3	2.6	2.3	5.7
	K19a	6.1	1.3	2.6	1.7	2.3	5.8
	K26a	6.3	1.3	2.7	1.8	1.4	4.7
East Coast Park	ECP2	5.8	0.7	1.4	1.1	1.2	5.7
	ECP3	6.0	0.8	1.7	1.3	1.4	6.3
West Coast Park	WCPb	5.5	0.8	1.6	1.2	1.2	5.5
Punggol	Pgl	5.7	1.4	2.8	1.8	1.5	6.8
Pulau Ubin	Ubin_E	10.5	1.0	2.1	1.7	1.8	6.6
	Ubin_N	9.0	0.8	1.6	1.3	1.4	6.1
Lim Chu Kang	LCK	6.4	1.1	2.1	1.5	1.6	5.3
Sembawang	S	13.7	1.4	2.9	2.3	2.3	9.5
Bedok	B	8.1	1.0	2.0	1.5	1.6	6.6

The K_d from Hydrolight (ABACBB model) ranges from 1.2 to 2.3 m^{-1} with lower K_d for chlorophyll dominated waters. The K_d from ABCASE2 model overestimates the K_d because it calculates the K_d to the seabed where the sediment concentration is high especially at the sampling locations adjacent to land. However, the K_d is expected to reduce further seaward from the land as shown by Smith (1981). This is also recorded in the offshore of Malaysian Peninsula when the maximum $K_{d(PAR)}$ was 0.90 m^{-1} from Kuwahara et al. (2010). The K_d in Table 6-1 agrees well with the K_d from the Ems-Dolland estuary (Netherland/Germany) in the region of 1 m^{-1}, Shaun estuary (Ireland) with K_d in the range of 1.7 to 4.5 m^{-1}, Chesapeake Bay with K_d of 1 to 2 m^{-1} and Swan river estuary (Australia) with K_d in range from 0.72 to 3.65 m^{-1}. All the K_d comparison was from Kirk (2011).

6.2.3 $K_d(PAR)$ prediction from K_d

This section will compare the vertical downwelling light attenuation K_d in the visible light band (390 to 750 nm) against PAR band (400 to 700nm). In practice, the difference between both bands is insignificant to the first order approximation. However, it is still interesting to know the specific relation between both bands so that the ecological discussion that follows is more insightful. The visible band is represented by the ac-9 measurements; even though the ac-9 spectrum (412 to 715 nm) does not entirely capture the visible light band.

Empirical equations to estimate $K_d(PAR)$ normally consist of IOP and AOP of the water body. The relationship between K_d(490) and the vertical attenuation coefficient of PAR $K_d(PAR)$ was investigated by various researchers due to the convenience of getting K_d(490) from satellite observations (Pierson et al., 2008). In this section, the K_d(490) will be estimated from the c(490) using Kirk (1984a). Pierson et al. (2008) developed a simple semi-analytical model to predict $K_d(PAR)$, as a function of the K_d(490) as follows:

$$K_d(PAR) = 0.6677\ [K_d\ (490)]^{0.6763} \qquad \textit{(Eq. 6.1)}$$

Morel (1988) presented a simple bio-optical model for $K_d(PAR)$ averaged over the euphotic zone which varies with chlorophyll concentration, $[Chl-a]$ (in mg/m^3) as follows:

$$K_d(PAR) = 0.121\,[Chl-a]^{0.428} \qquad \textit{(Eq. 6.2)}$$

Table 6-2: Comparison between $K_d(490)$ from Kirk (1984), Pierson et al. (2008) and Morel (1988) against the K_d from Hydrolight (representing K_d for visible light range).

Place	Samples	c (490)		Kirk, 1984	Pierson, et al 2008	Morel, 1988	Hydrolight (Kd)
		a	b	Kd (490)	Kd (PAR)	Kd (PAR)	ABACBB
Kranji	K04c	1.129	4.128	1.57	0.91	0.61	1.33
	K13a	2.278	5.463	2.89	1.37	0.64	2.33
	K19a	1.187	4.693	1.68	0.95	0.76	2.33
	K26a	1.215	5.299	1.77	0.98	0.73	1.44
East Coast Park	ECP2	0.615	5.799	1.14	0.73	0.16	1.18
	ECP3	0.502	5.530	0.98	0.66	0.16	1.35
West Coast Park	WCPb	0.471	5.286	0.93	0.63	0.19	1.20
WCP_Spring	WCP_S_h	0.583	3.340	0.92	0.63	0.19	1.20
	WCP_S_l	0.785	6.489	1.39	0.83	0.19	1.20
WCP_Neap	WCP_N_h	0.965	7.421	1.66	0.94	0.19	1.20
	WCP_N_l	0.858	7.482	1.54	0.90	0.19	1.20
Punggol	Pgl	1.355	4.283	1.82	1.00	0.73	1.51
Pulau Ubin	Ubin_E	0.858	10.274	1.73	0.97	0.16	1.81
	Ubin_N	0.467	9.358	1.16	0.74	0.18	1.41
Lim Chu Kang	LCK	0.889	5.904	1.46	0.86	0.37	1.62
Sembawang	S	1.225	13.411	2.39	1.20	0.35	2.33
Bedok	B	0.650	8.030	1.33	0.81	0.21	1.58

Table 6-2 shows the comparison between $K_d(PAR)$ estimation from Pierson et al. (2008) and Morel (1988). Since PAR is a subset of the visible light band, the K_d from the latter (represented as K_d from Hydrolight) should be slightly bigger than the empirical $K_d(PAR)$ estimations. Although this is true but the difference is too high since theoretically the $K_d(PAR)$ should not differ too much from the K_d. However, empirical $K_d(PAR)$ estimation from Pierson et al. (2008) is closer to K_d from Hydrolight than Morel (1988). Both estimations underestimate $K_d(PAR)$ compared to the modelled K_d from Hydrolight possibly because the empirical equations are site-specific. The latter underestimate the $K_d(PAR)$ especially in sediment dominated waters because the equation only contains Chl-a concentration. Although the K_d co-vary positively with Chl-a concentration (Section 5.4.1), contribution from other constituents cannot be neglected especially in sediment dominated waters.

$K_d(PAR)$ is significantly depth dependent because K_w (water's attenuation coefficient) is wavelength dependent and $K_d(PAR)$ reduces to wavelengths with less attenuation coefficients with increasing depth. Higher K_d from Hydrolight compared to empirical estimations of $K_d(PAR)$ is also due to depth dependency of K_d as shown in Section 6.2. The K_d is calculated to the whole depth compared to the depth where the irradiance is 1 % of the surface irradiance for $K_d(PAR)$. Therefore, K_d in Hydrolight takes into account the higher sediment at the bottom depths resulting in higher K_d. Furthermore, the sensitivity of the empirical equations will be dependent on variations in CDOM absorption (Pierson et al, 2008). This is proven because the deviation of $K_d(PAR)$ and K_d is consistently higher in ECP and WCP due to higher CDOM absorption.

Higher $K_d(PAR)$ means more light is attenuated in the PAR range, thus intuitively, the lower $K_d(PAR)$ is 'better' for marine ecosystems since more light is available. Yet, higher $K_d(PAR)$ may not be necessarily associated with lower productivity since higher $K_d(PAR)$ might also be due to phytoplankton. However, lower $K_d(PAR)$ for sediment dominated waters are most certainly associated with lower productivity. Moreover, $K_d(PAR)$ estimation using a scalar value like $K_d(490)$ in Pierson et al. (2008) underestimates the $K_d(PAR)$ and overestimate light availability. Therefore, the measure of scalar K_d (using only one value) to estimate PAR in turbid waters may overestimate light availability for photosynthesis, relative to a spectrally-weighted approach (Van Duin et al., 2001). Lund-Hansen (2004) found that $K_d(PAR)$ varied between 0.15 and 0.56 m^{-1} with an average of 0.29 m^{-1} in Århus Bay (Denmark).

6.3 Secchi Depth

Secchi depth, S_d is the most convenient, if arbitrary way to 'measure' visibility; the deeper the S_d, the higher the visibility. It is the depth at which the circular white disk just disappeared from the viewer above the water surface. It is associated with the depth at which the light intensity (or irradiance) decreased to 1% of its incident light intensity. Although S_d is prone to human error and are not related to any optical properties, it is one of the simplest ways to get an impression of the water quality. Moreover, previous records on visibility are mostly available in S_d which is normally related to light attenuation coefficient K_d as follows:

$$S_d = \frac{k}{K_d} \qquad \textit{(Eq. 6.3)}$$

The denominator k is not a 'constant' and the range between 1 to 2 is considered an 'average' value. Applying Eq. 6.3 to the data in this thesis, the k vary slightly depending on the K_d used (empirical or modelled). Taking the S_d and K_d from the Hydrolight model ABACBB, k is 1.60. However, k reduced to 1.46 if the K_d from Kirk (1984a) is used (while maintaining S_d from Hydrolight). Therefore, the average k in Singapore waters is 1.5. This method for estimating K_d from S_d or vice versa is useful when in situ measurement cannot be performed because of logistical or adverse weather conditions. Table 6-3 shows the modelled S_d from Hydrolight together with its euphotic depth from the formula $z_{eu} = 4.605/K_d$ (Kirk, 2011).Transmittance (Tr) were converted from the beam attenuation $c = (-1/x)\ ln\ Tr$ with x = pathlength. Transmittance is around 0.2 m^{-1} except in Pulau Ubin, Bedok and Sembawang coinciding with lower range of S_d.

S_d ranged from 0.6 – 1.4m with corresponding euphotic depth of 2.0 – 3.8m. These values are comparable to other estuarine environments like New Zealand estuaries with S_d of 1.2-4.4 m (Vant 1990); Pierson et al. (2003) found that the change in z_{eu} corresponds to a change in $K_d(PAR)$ of 1.8 to 4.6 m^{-1}. Figure 5-10 shows the inverse linear relation between K_d and NTU against S_d. However, S_d is more linearly related to K_d (R^2 = 0.53) than to NTU (R^2 = 0.14). Similarly, Otto (1966) and Foden et al. (2008) found that significant relationship between S_d and K_d can be a useful predictor of light attenuation while Pierson et al. (2008) suggest uncertainties related to greater influence of scattering on S_d estimates. However, S_d is not strongly related to Chl-a and TSS. This is perhaps due to inherent variability in the spectral absorption and scattering properties combined with normal uncertainty associated with sampling and laboratory analyses.

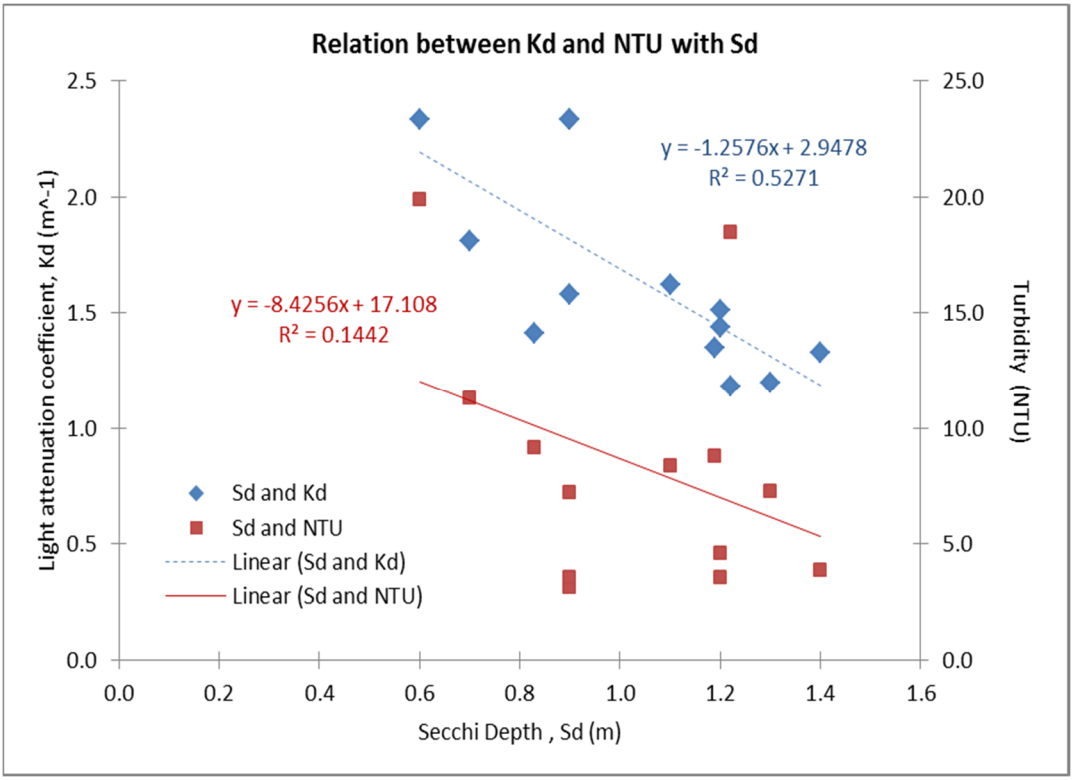

Figure 6-10: Inversed relation between K_d and NTU with Secchi depth S_d. Both K_d and S_d were simulated in Hydrolight (K_d was from ABACBB model). Better inversed relation was obtained for K_d with S_d compared to NTU with S_d.

Table 6-3: The modelled K_d and S_d for ABACBB model, euphotic depth z_{eu} and transmittance Tr

Place	Samples	Hydrolight Kd (m^-1)	Pierson et al 2008 Kd (PAR) (m^-1)	Hydrolight Sd (m)	Eup depth (m) 4.605/Kd	Transmittance c = (-1/x) ln Tr
Kranji	K04c	1.3	0.91	1.4	3.5	0.24
	K13a	2.3	1.37	0.9	2.0	0.16
	K19a	2.3	0.95	0.9	2.0	0.22
	K26a	1.4	0.98	1.2	3.2	0.21
East Coast Park	ECP2	1.2	0.73	1.2	3.9	0.24
	ECP3	1.4	0.66	1.2	3.4	0.22
West Coast Park	WCPb	1.2	0.63	1.3	3.8	0.25
Punggol	Pgl	1.5	0.63	1.2	3.0	0.24
Pulau Ubin	Ubin_E	1.8	0.83	0.7	2.5	0.07
	Ubin_N	1.4	0.94	0.8	3.3	0.10
Lim Chu Kang	LCK	1.6	0.90	1.1	2.8	0.20
Sembawang	S	2.3	1.00	0.6	2.0	0.03
Bedok	B	1.6	0.97	0.9	2.9	0.13

The light field calculated by Hydrolight is based on IOP at a single instantaneous point the prevailing condition at that point; therefore it cannot capture the light variability outside the sampling period. Furthermore, because Hydrolight relies on measured attenuation coefficients from ac-9, it would be difficult to apply them in a predictive sense to any scenario simulations. As the importance of seasonal variation and tides in determining SSC must be accounted, Chapter 6 models the visibility using water quality model. This allows extension of field data temporally and spatially to represent light attenuation.

CHAPTER 7.0: NUMERICAL MODELLING OF SSC AND VISIBILITY

This final chapter on analysis investigate the relation between suspended sediment concentration (SSC) and visibility using water quality module (WAQ) in Delft3D. In many ways, this section is the culmination of this thesis utilising findings from previous chapters. The particle mass-specific scattering coefficient b^*_{TSS} and background attenuation obtained from Chapter 5 was used as input to the visibility model. Suspended sediment and its relation to visibility is complicated and encompasses many complex processes such as flocculation, settling and mixing, deposition, re-suspension and consolidation, etc. (Bosboom and Stive, 2010). However, only resuspension and sedimentation, as the two most important processes are modelled in the visibility model as alluded to in Section 3.3. With this limitation in mind, this chapter presents the first attempt in modelling visibility in Singapore waters and the results does not pretend to be an accurate representation of reality in its entirely.

Field measurements are important for understanding baseline conditions and explaining point based variation, but they are not useful for analysing temporal and spatial variation of optical properties. Since the sediment was found to be the most dominant contributor to light attenuation in Chapter 5 and the vertical variation of K_d was explained in Chapter 6, the temporal and spatial variation of K_d is analysed in this chapter. James et al. (2002) shown that for suspended sediment, the clay and silt fractions exhibited the greatest K_d values and had the greatest impact to the underwater light field. Thus, water quality model describing resuspension/sedimentation of fine sediment was undertaken to assess the visibility via suspended sediment, extending both the temporal scales (tides and seasonal) in Section 7.1 and the spatial scale in Section 7.2. Qualitative comparison against the modelled K_d from Hydrolight will also be presented at the end of this chapter.

7.1 Temporal Variability in Visibility

Temporal variability in visibility will be assessed using the modelled timeseries for a year and will be discussed in 2 parts; variation due to tidal forcing (Section 7.1.1) and non-tidal forcing (Section 7.1.2). The visibility output of DELFT3D WAQ consist of K_d and S_d. However only the results of S_d is analysed in Section 7.2 because S_d is physically more meaningful representation of visibility compared to K_d. However, firstly, both the modelled result of current velocity, SSC and K_d is subjected to Fourier analysis using signal processing tools in Matlab. The modelled signals are decomposed into tide constituents components due to (a) tidal (semi-diurnal-diurnal, spring neap) and (b) non-tidal (low and high frequency events, residual) constituents from its respective unique frequencies.

Joseph Fourier demonstrated that any periodic/non-periodic signal can be described by a sum of harmonic components called Fourier series. Fourier analysis is a mathematical method in which a signal is unravelled into simpler constituents - sines and cosines and complex exponentials as building blocks of the Fourier series (Bosboom and Stive, 2010). These building blocks can be used to determine the spectral density (spectrum) of the time series. It is possible to identify the principal harmonic components of the time series because they always appear with larger amplitudes. Frequencies corresponding to principal harmonic components are the frequencies of the constituents present and are identified with its period T. Furthermore, once the influence due to tidal forcing is filtered, the signal from non-tidal forcing can be determined using low pass filter as presented in Section 7.1.2.

Figure 7-1, 7-2 and 7-3 shows the Fourier spectrum for the current velocity, SSC and K_d signals in Pulau Ubin and Bedok respectively. Pulau Ubin and Bedok are chosen because the latter are influenced by the large-scale hydrodynamics of Singapore Strait while Pulau Ubin shows more local behaviour with complicated bathymetry and river discharge. As shown in Figure 7-1, semidiurnal and diurnal contributions are almost equal in Bedok, while the semi diurnal constituent is three times higher than the diurnal in Pulau Ubin. There is a peak at about 170 hours in both locations (7 days: half of the spring-neap constituent) representing movement from east to west or vice-versa (Van Maren and Gerritsen, 2012).

7.1.1 Visibility variation due to tides

Intra tide

Figure 7-2 shows the Fourier spectrum for SSC. The frequencies present in the semidiurnal and diurnal bands in both locations are almost similar in amplitude and clustered as tightly packed groups. The diurnal band shows three distinct peaks; the highest is lunar declinational diurnal O_1 constituent (period of 25.82 hours) followed by lunar–solar declinational diurnal K_1 constituent (period of 23.93 hours). The K_1 and O_1 constituents have similar amplitude and work as a pair so that diurnal tide is greatest when the two are in phase and near zero when they are out of phase (Bosboom and Stive, 2011). The third peak in diurnal band is solar declinational diurnal P_1 constituent. The highest semidiurnal amplitude is at 12.42 hours representing semidiurnal lunar constituent M_2 followed by the semidiurnal solar constituent S_2 with a period of 12.00 hours and second lunar harmonic constituents N_2 with period of 12.66 hours.

Diurnal and higher frequency constituents appear to be less significant in Pulau Ubin while the diurnal constituents prevail only slightly more in Bedok. This shows that SSC in Bedok is more related to the current velocity compared to Pulau Ubin. SSC variation follows cyclic pattern coinciding with current velocity variation. However, the second order effect of higher harmonics are important for sediment dynamics and mixing (Prandle, 2009) which causes ebb and flood asymmetry and double high or low water occurrence. The higher harmonics in Pulau Ubin shows high contribution from the quarter diurnal constituents in decreasing amplitude of M_4 (M_2+M_2), MS_4 (M_2+S_2) and MN_4 (M_2+N_2) with the period of 6.21, 6.10 and 6.27 hours respectively. The M_4 and MS_4 contribution equals that of the semi-diurnals while the contributions of third diurnal bands (SK_3, M_3, and $2MK_3$) with period of ~8 hours and sixth diurnals bands ($2MN_6$, M_6, and $2MS_6$) with period of ~4 hours are negligible.

The existence of higher order harmonics in the SSC spectrum of Pulau Ubin is due to the shallow water frictions and/or resonance in the Johor estuary. The existence of similar amplitudes of M_4 and MS_4 constituents in the spectrum tend to cancel each other out during neap tide and thereby reduce the overall quarter diurnal signals (Prandle, 1997). This will result in a false indication of higher amplitude for semi-diurnal constituents. The presence of 'overtides' in the higher frequency bands like M_4, M_6, etc. in Pulau Ubin which have no counterpart in the tide-generating forces indicates non-linear effects (Bosboom and Stive, 2010). The non-linear effects originate through the interaction of locally generated tidal currents and can affect the tidal asymmetry. The presence of M_4 and MN_4 indicate that convective term $u\,du/dx$ and the non-linear effects (Bosboom and Stive, 2010) are more important than quadratic friction term in the momentum equations.

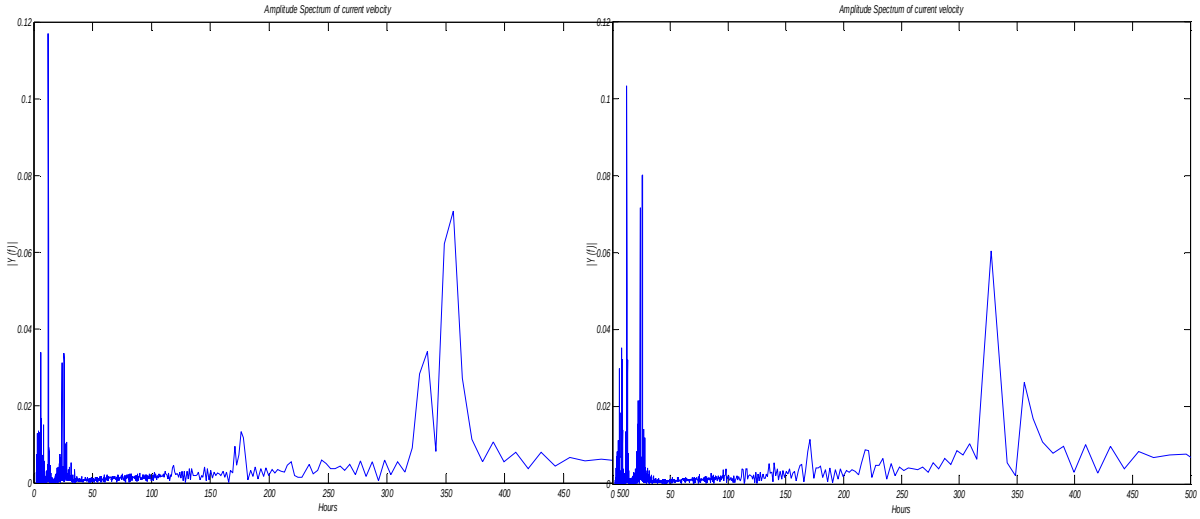

Figure 7-1: Fourier spectrum of current velocity for a year in Pulau Ubin (left) and Bedok (right). Note the dominant semidiurnal over diurnal and spring-neap constituents in the both locations.

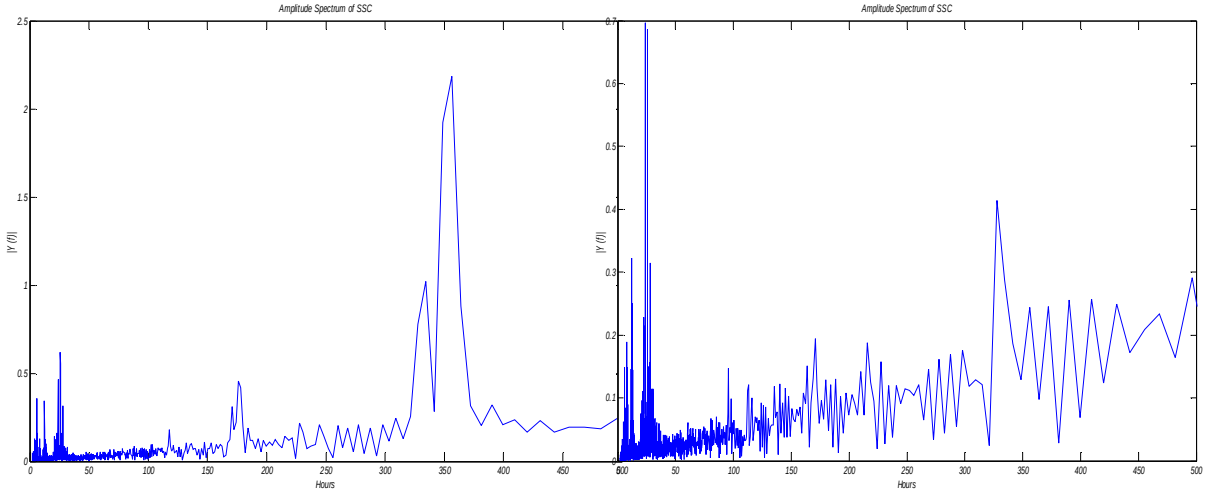

Figure 7-2: Fourier spectrum of SSC for a year in Pulau Ubin (left) and Bedok (right). Spring-neap constituent is more dominant in Pulau Ubin compared to Bedok.

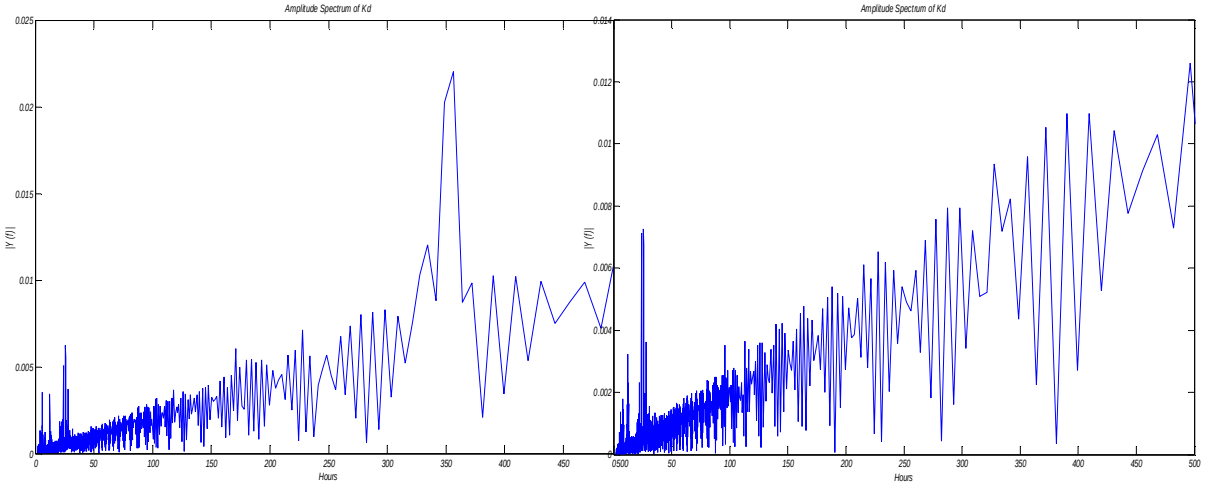

Figure 7-3: Fourier spectrum of K_d for a year in Pulau Ubin (left) and Bedok (right). Diurnal constituent are dominant in both signals while only spring neap constituent is dominant in Pulau Ubin.

Figure 7-3 shows the Fourier spectrum for K_d signal. The contributions from semidiurnal and diurnal bands are equally important in Pulau Ubin and Bedok. This will cause higher convective interaction between the diurnal and semidiurnal constituents and friction resulting in higher order harmonics and non-linear flux as also seen in the spectrum. However, non-linear effects which originate through the interaction of the tidal currents are important in shallow depths where the water level displacements have non-negligible amplitude compared to the mean depth. Therefore, SSC and K_d in Pulau Ubin is dominated by water level-induced tidal flooding/ebbing in the cross shore direction. Both these processes are at work in Pulau Ubin due to the geometry and bathymetry variation of Johor estuary compared to the importance of convection processes in zones of rapidly changing currents like Bedok (Chen et al., 2005).

Current velocities in Singapore Strait range from 0 m/s during slack tide up to 2 m/s during high tide and low tide. This highly fluctuating water velocity and corresponding bottom shear stress induce a periodically varying shear stress resulting in a cyclic pattern of sedimentation and resuspension (Van Maren, 2010). This causes higher SSC at the bottom compared to surface SSC as seen in Figure 7-4 for a representative location in Tekong. The bottom SSC is higher during neap tide as also concurred by Van Maren et al. (in prep). Moreover, the difference between surface and bottom SSC is more pronounced during neap compared to spring tide. The bottom SSC is large because the diffusivity is large due to ripple-generated eddies (Bosboom and Stive, 2010). The SSC decrease upwards to the water column because eddies dissolved rapidly to the water surface.

Spring neap tide

The spring neap modulation in Pulau Ubin is five times higher than in Bedok for SSC spectrum. The semi diurnal spring neap constituent MS_0 (M_2-S_2) with period of 14.76 days is higher than the diurnal spring neap constituent KO_0 (O_1-K_1) with period of 13.66 days in Pulau Ubin, and vice-versa in Bedok. The frequency of MS_0 and KO_0 equals that of MS_F and M_F in equilibrium tide suggesting compound tide origin (Van Maren and Gerritsen, 2012). The SSC spring neap variation follows the current velocity spring neap, with higher SSC during spring tide as evident in Figure 7-5. As a result, the SSC follows current velocity with little or no phase variation; low SSC during lower velocity and high SSC during higher velocity. It seems that the dynamics of optical properties can be explained by the variation in SSC, if all other factors being equal. SSC in Pulau Ubin also responds to water level instead of only current velocity while in Bedok, the SSC only responds to current velocity.

The spring neap constituent is apparently not important in K_d signals, although relatively it is twice higher in Pulau Ubin compared to Bedok. Figure 7-2 and 7-3 also show more 'noise' compared to Figure 7-1. This high frequency transient noise hampers the ability to resolve the longer period variations from shorter period variations. This is probably because firstly, K_d is more strongly influenced by interaction of various constituents at tidal frequencies. Secondly, K_d is more sensitive to changes in depth (i.e. vertical variation of IOP). Thirdly, due to the complex response function between tidal constituents of current velocity and SSC and lastly the uncertainties in the boundary condition for the model. Moreover, this 'noise' is apparently more prevalent in Bedok compared to Pulau Ubin because the spring neap constituent is damped due to large scale coastal effect and higher meteorological forcing compared to the local effect of Pulau Ubin.

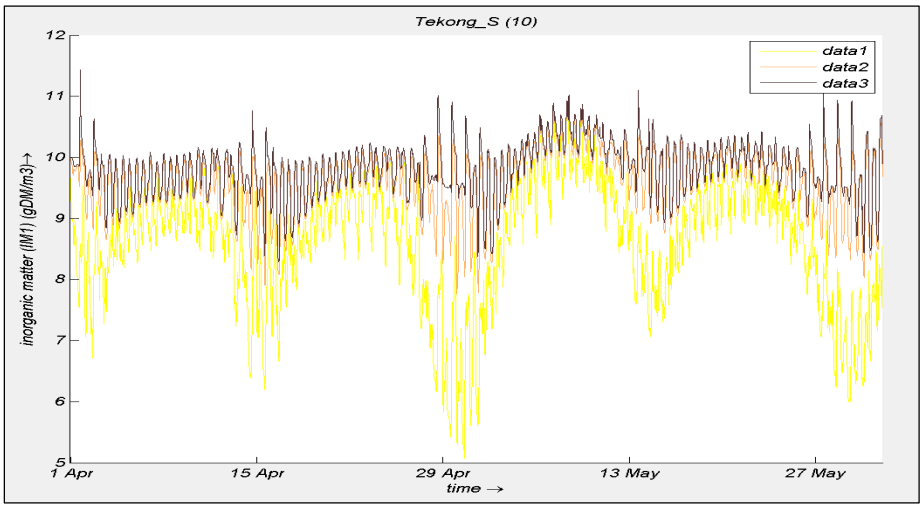

Figure 7-4: Vertical variation of inorganic matter (IM1) representing SSC in south of Tekong during IM period from WAQ SSM. Data 1, 2 and 3 signifies SSC in surface, middle and bottom respectively.

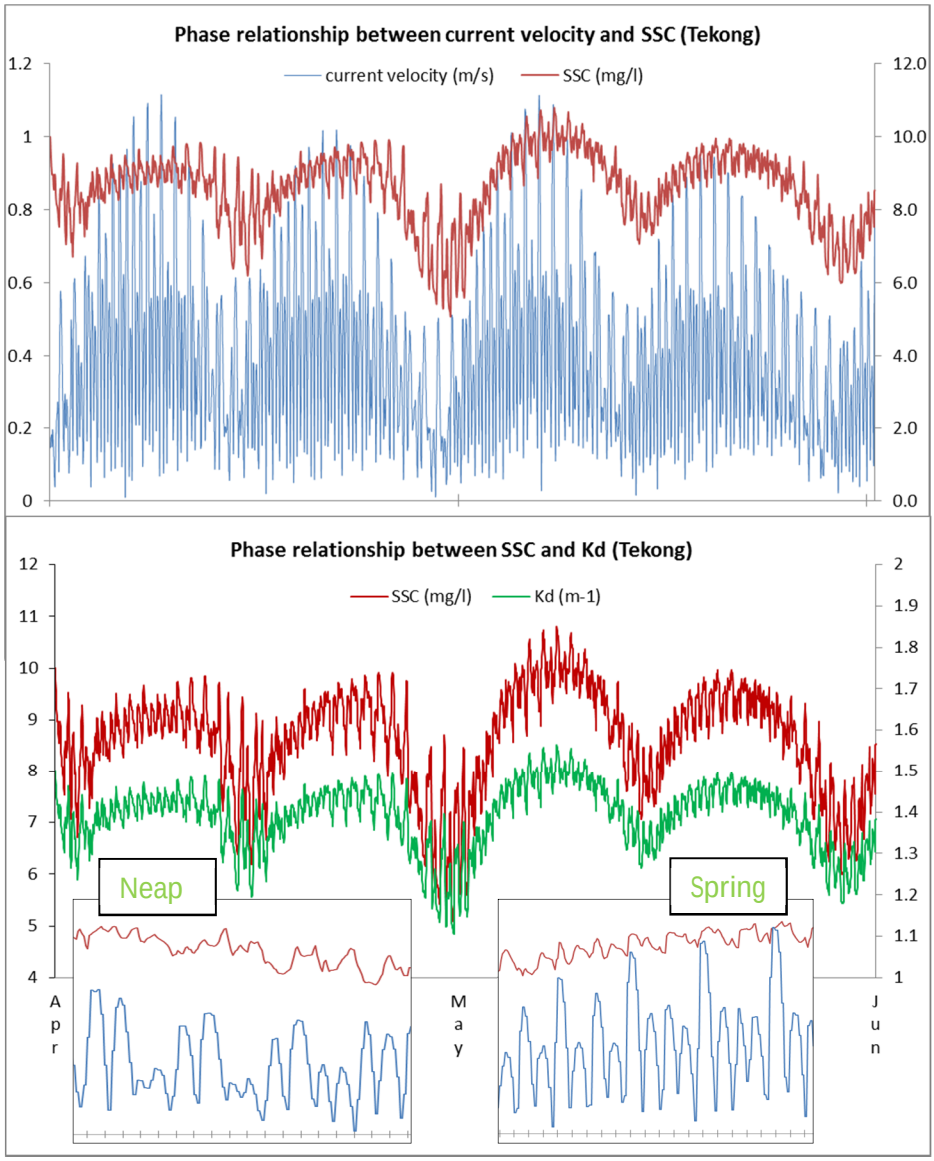

Figure 7-5: The phase relationship between current velocity and SSC (above) and SSC and K_d (below) in south of Tekong during IM period. The two boxes below shows zoom view of the latter.

7.1.2 Visibility variation due to non-tides

High frequency events

High frequency events cause the time series signal to oscillate rapidly. Besides the higher harmonics explained in Section 7.1.1 due to tide constituents with frequencies at multiples of each other, non-tidal events can also cause high frequency variability in the signal. The variability is highest for the current velocity signal, followed by K_d and SSC signals. High frequency event causes high variability of SSC especially due to short term influence sediment clouds related to high frequency velocity (Hoitlink, 2003). However, the variability in K_d is considered to be transient and does not influence the optical properties of the water to impart a meaningful effect to the overall light attenuation. These events are 'random' in nature and cannot be determined exactly in the time domain after spectral analysis.

Low frequency events

The low frequency events are the long term averaged signal which is represented by the residual signal due to factors other than tide constituent's interactions. Zoelaeha (2010), Van Maren and Gerritsen (2012) and Chen et al. (2005) have shown that the sediment dynamics, especially fine sediment can be significantly influenced by residual flow, density gradients and overtides (due to non-linear shallow water effect and/or complex bathymetry). The residual signal remains after the tidal influence from the SSC signal was separated using the low pass Godin filter $A^2_{24}A_{25}/24^2.25$ (Van Maren and Gerritsen (2012) who quoted Godin, 1972). A^2_{24} represents twice the 24 hour averages while A_{25} represents 25 hour average. This process applies three moving averages; 12-1-11, 11-1-12 and 12-1-12 hour. The result for residual current velocity, residual SSC and residual K_d is shown in Figure 7-6 to 7-8.

The residual current velocity in Figure 7-6 oscillates at frequencies of the fortnightly cycles. The fortnightly constituents have a (compound) tide (MS_0 and KO_0) and monsoon (S_A and S_{SA}) induced component. Highest residual velocity in April and October coincide with the time when the spring MS_0 overlaps with spring KO_0 (Van Maren and Gerritsen, 2012). The SSC increase twice yearly can also be partly attributed to the monsoon induced residual velocity (advection dominated) and is equally important as the compound tides during monsoon periods. Residual velocity from prevailing winds can attain a maximum speed of 0.4 m/s during the NE monsoon (Chen et al., 2005). During inter monsoon in June, the residual velocity is 0.35 m/s and 0.20 m/s respectively during spring and neap tide. This is due to the contribution from the out of phase compound tides since the residual due to monsoon (S_A and S_{SA}) is low.

The residual time series for SSC (Figure 7-7) and K_d (Figure 7-8) is similar to Figure 7-6 with two peaks yearly. It shows that the residual due to compound tides are more important than the monsoons in Pulau Ubin and vice-versa in Bedok. There is also large energy in 5400 hours band (225 days) for SSC spectrum in Pulau Ubin, although it may also be due to annual tide constituent, S_A with a period of ~200 days. However, exact contribution cannot be ascertained as the energy is too diffuse because one-year data is not sufficient to distinguish the amplitudes and phases of long period constituents. Prandle (1997) showed if the residual currents increase to 10% of the M_2 amplitude, the spectrum will show M_2 and S_2 constituents of similar magnitude to those for M_4 and MS_4, as seen in Figure 7-1.

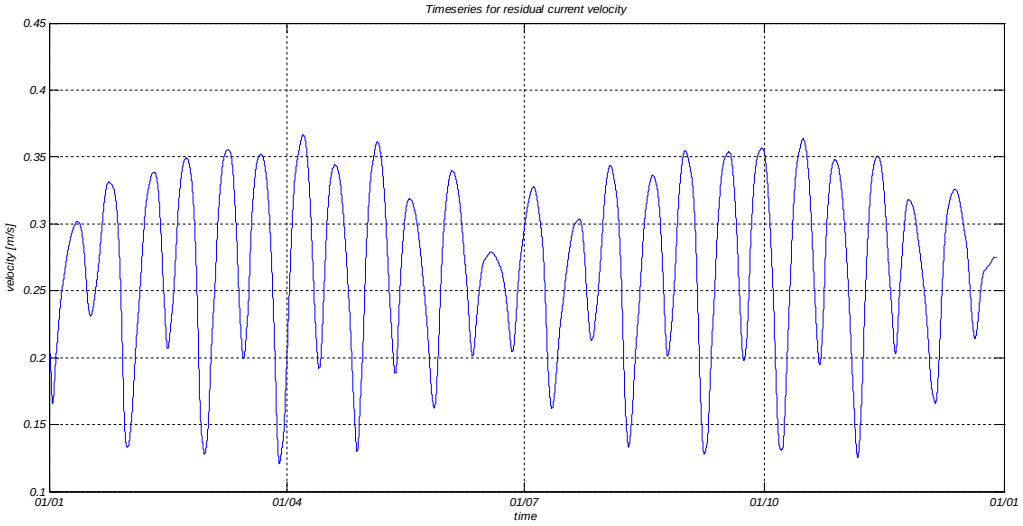

Figure 7-6: Residual current velocity after the 1 year signal is subjected to Godin low pass filter.

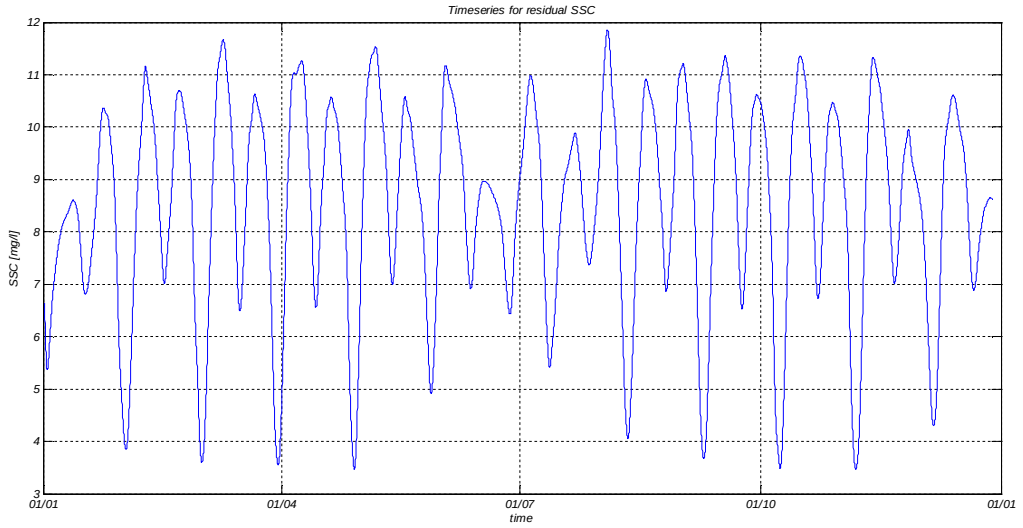

Figure 7-7: Residual SSC after the 1 year SSC signal is subjected to Godin low pass filter.

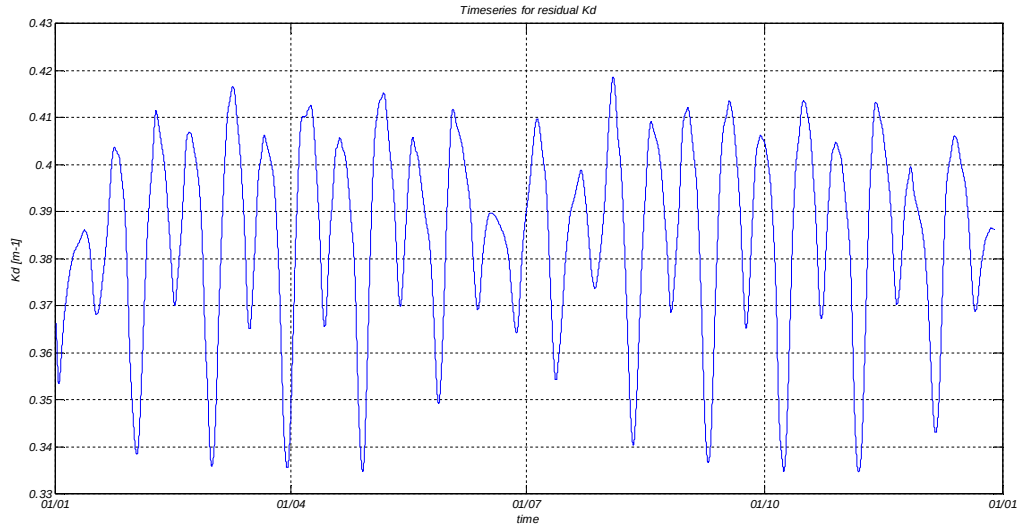

Figure 7-8: Residual K_d after the 1 year modelled K_d signal is subjected to Godin low pass filter.

7.2 Spatial Variability in Visibility

Section 7.2.1 will discuss the vertical variation of SSC with tides for IM period while Section 7.2.2 will present the spatial variability of visibility for various scenarios. In addition to the hydrodynamic regime, the seasonality in the model was reflected by modifying the background chlorophyll) and SSC concentration at the inner boundaries to coincide with the known concentration of that season. The boundary information was collated from previous studies and field measurements (Table 4-3). The background K_d was 0.6m^{-1} during inter monsoon consisting of 0.2m^{-1} contribution each from water, CDOM and Chl-a respectively. However, chlorophyll concentration during NE and SW monsoons is higher than during IM period (Dikou and van Woesik 2006). Furthermore, the chlorophyll concentration is typically higher during Southwest monsoon (SW) compared to Northeast (NE) (Gin et al., 2001).

The SSC at all the inner boundaries was specified as 10 mg/l during IM and was increased during monsoons, similar to the seasonal chlorophyll distribution. During SW monsoon, huge freshwater influx from Eastern Sumatra consisting of large sediment load drains into the Singapore and Malacca Strait. This is reflected in the model by specifying the top bottom 1 boundary (Straits of Malacca) to 30 mg/l during SW. Higher SSC were also specified in top bottom 2 boundary (South China Sea) to 20 mg/l during NE to reflect the stronger sediment resuspension from South China Sea. Sediment from all the discharges were higher during monsoons (NE > SW) to reflect the increased rainfall during wet season. The fraction of IM1 in layer S1, IM1S1 was also increased marginally (NE > SW > IM).

7.2.1 SSC dynamics

Figure 7-9 shows the difference between SSC at the surface (layer 1) and bottom (layer 10) during neap tide (for low and high tide) while Figure 7-10 shows the SSC difference during spring tide for both low and high tide condition. SSC in the model domain varies depending on the tides with higher SSC during spring compared to neap tide. For intra tide variation, the SSC is generally higher during low tide compared to high hide. As modelled in Hydrolight (Section 6.1), pronounced vertical variation is observed as the bottom SSC is higher than the surface SSC at all times. The difference is more distinct during high tide. During low tide, it seems the surface and bottom SSC are almost comparable. Spring conditions are characterised by vertically mixed water column but with a considerable turbidity difference during intra tide. However, during neap tide there is pronounced vertical stratification in SSC but the turbidity variation during intra tide is low.

The SSC during IM is considered as representative condition occurring during most of the year. SSC is highest in the upper reaches of Johor River and reduces to its ambient concentration of about 10 mg/l around Tekong. Van Maren (2010) suggested the downstream decrease in SSC may be related to turbid buoyant river plumes propagating downstream or from increased tidal resuspension during spring tides. The transition area in Johor estuary (north of Tekong) is more turbid, with SSC of 10-20 mg/l. Qualitative comparison of the modelled SSC in WCP against the field measurement of TSS in WCP (from Section 5.1) shows similarity in intra tide variability; lower SSC at high tide and higher SSC at low tide during spring and vice versa during neap (Figure 7-11).

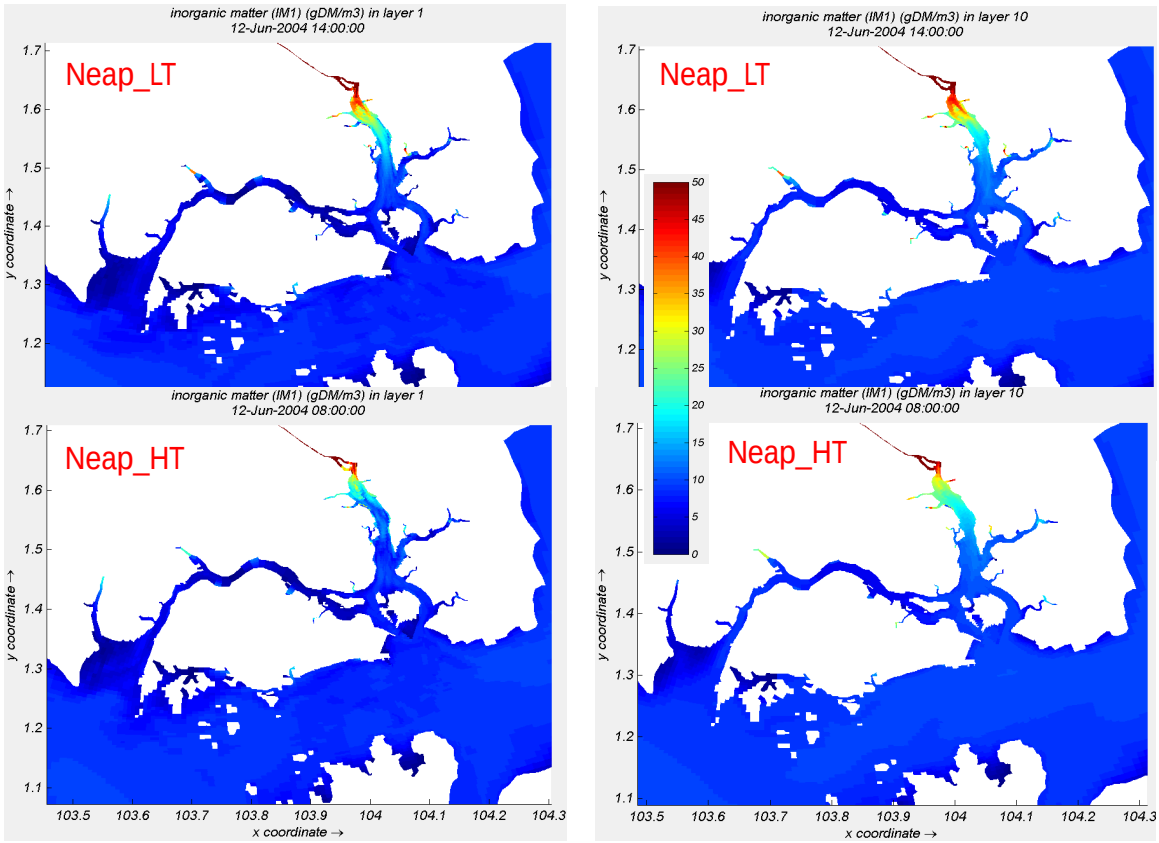

Figure 7-9: SSC during neap tide, the first two is during low tide while the bottom two during high

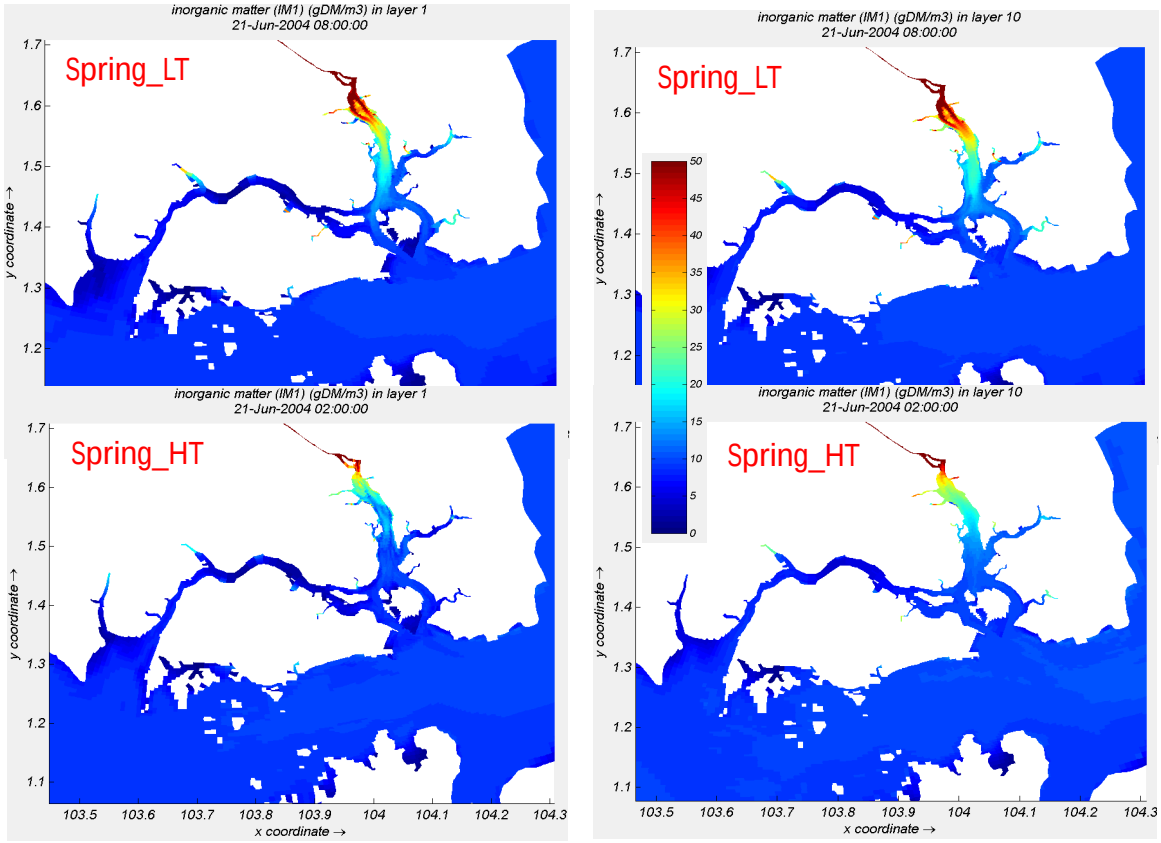

Figure 7-10: SSC during spring tide, the first two is during low tide while the bottom two during

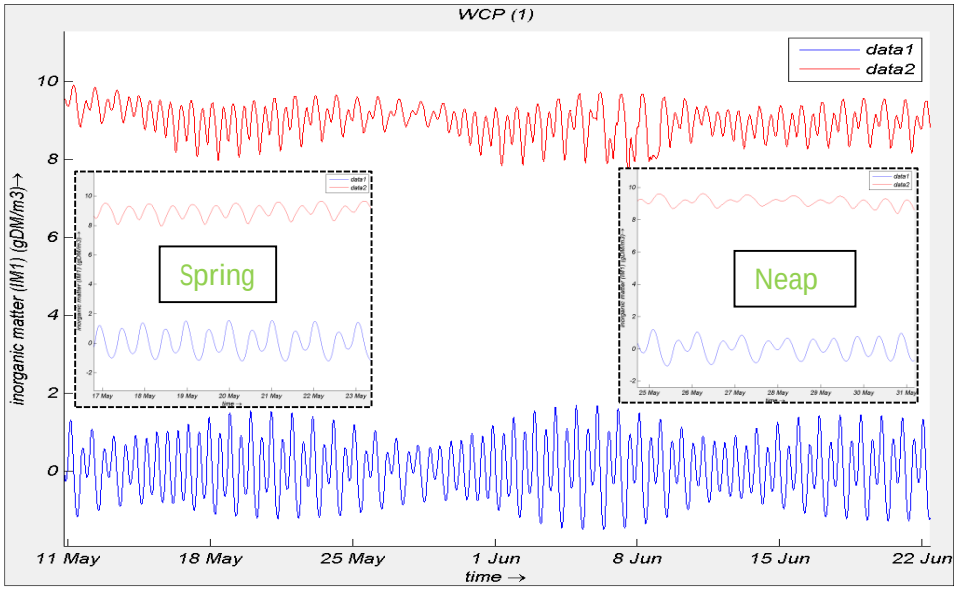

Figure 7-11: Modelled results in WCP during IM period. Data 1 is the water level while data 2 is SSC. The SSC variation is similar to the TSS variation in Section 5-1 during low and high tide (intra tide).

Comparison of the model results against the measured SSC from Van Maren et al. (in prep) shows that the modelled results are lower, except in the immediate vicinity of the Johor estuary, where the model is able to produce high SSC accurately. It is rather difficult to reproduce high SSC because the model cannot resolve all the relevant processes. One of the following; a source (large river with low refresh rates), converging sediment pathways (as occurs in estuaries) or processes (dredging, flocculation) is needed to create higher concentrations (Van Maren, pers. com). Since there is no converging pathway and the sources are limited, the higher SSC should result from the processes. Nevertheless, not much is known about the processes making its application to the model difficult.

7.2.2 Spatial visibility map

The seasonal effect to visibility was modelled and the visibility map for each simulation period (IM, SW and NE) will be extracted during spring tide and neap tide respectively during high tide and low tide. The discussion that follows is the general conclusion for all the spatial visibility maps and is applicable for all seasons.

Inter-monsoon

The model setup during IM was considered as dry season condition occurring most of the year with discharge Q of 57 mg/l and sediment concentration, C of 150 mg/l. Figure 7-12 shows the S_d for IM period during spring and neap condition for low and high tide.

Monsoons

NE monsoon represents average wet season with Q of 84 m^3/s and C of 180 mg/l. SW monsoon represents "in between" condition between wet season and dry season with Q of 65 m^3/s and C of 165 mg/l. Figure 7-13 and 7-14 shows the S_d for NE and SW monsoon during spring and neap for low and high tide.

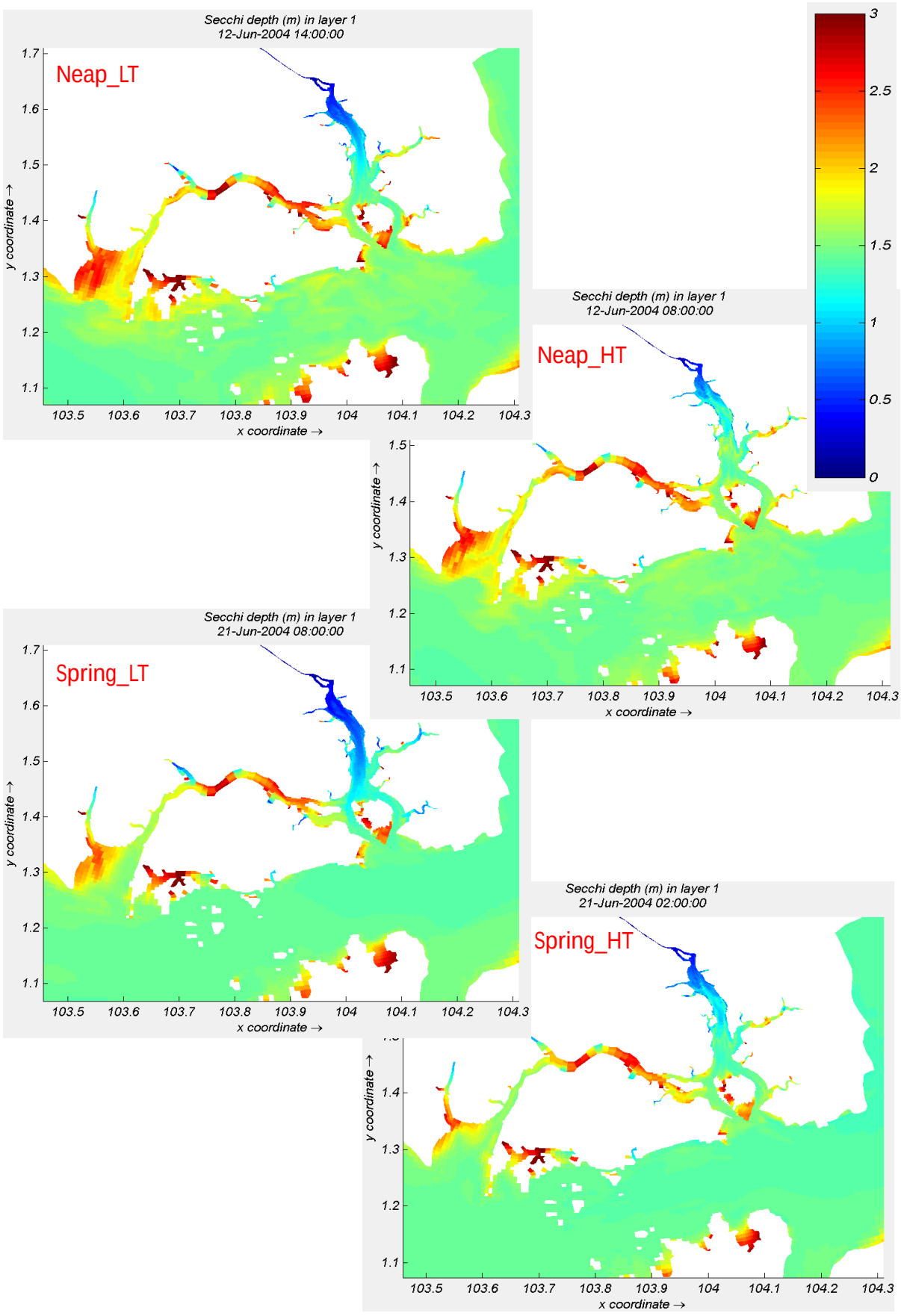

Figure 7-12: S_d for inter monsoon (IM) during spring and neap condition for low (LT) and high tide (HT). The first diagram is during neap low tide (Neap_LT), the second neap high tide, the third is during spring low tide and the last is during spring high tide.

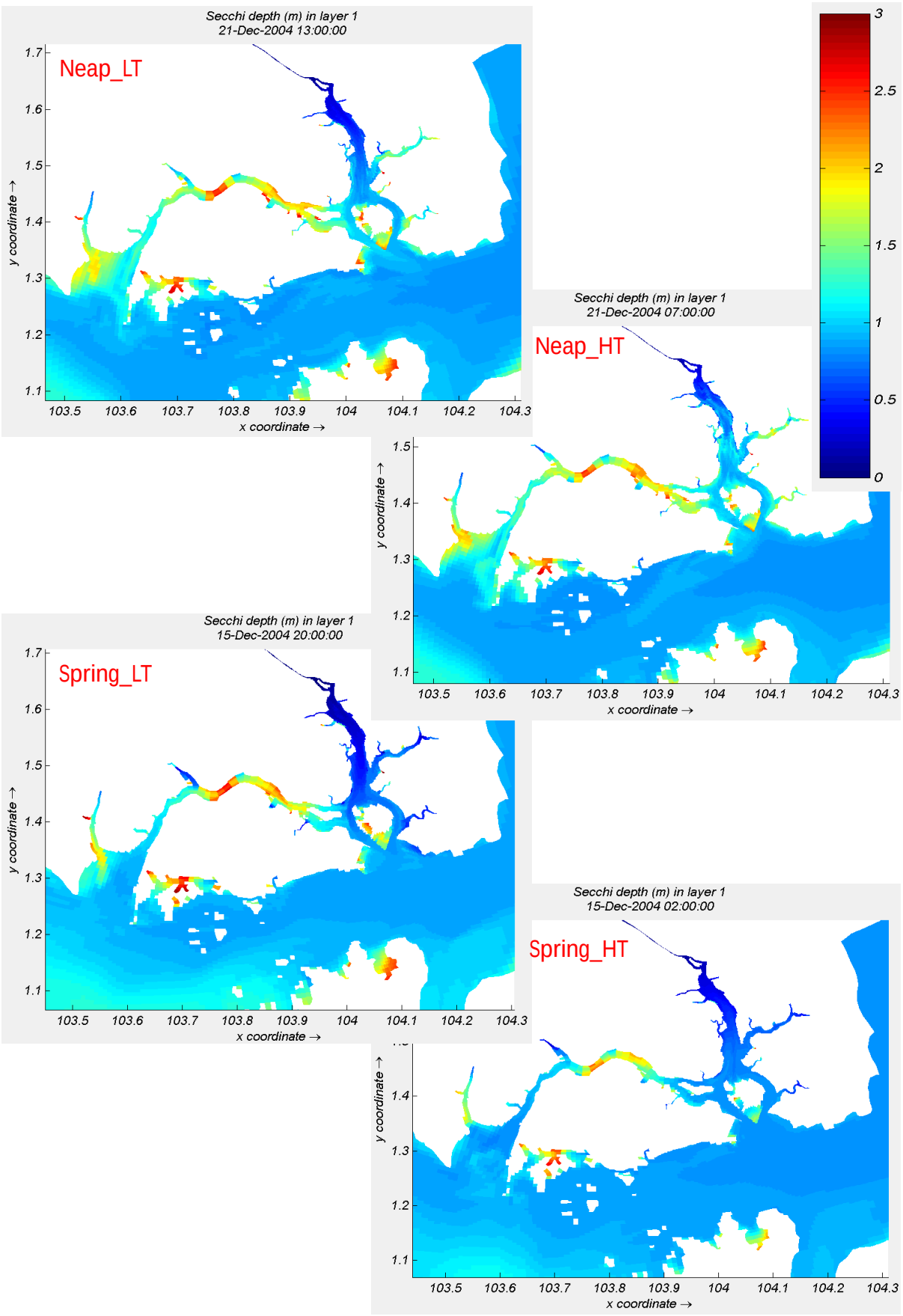

Figure 7-13: S_d for Northeast monsoon (NE). The first diagram is during neap low tide (Neap_LT), the second neap high tide, the third is during spring low tide and the last is during spring high tide.

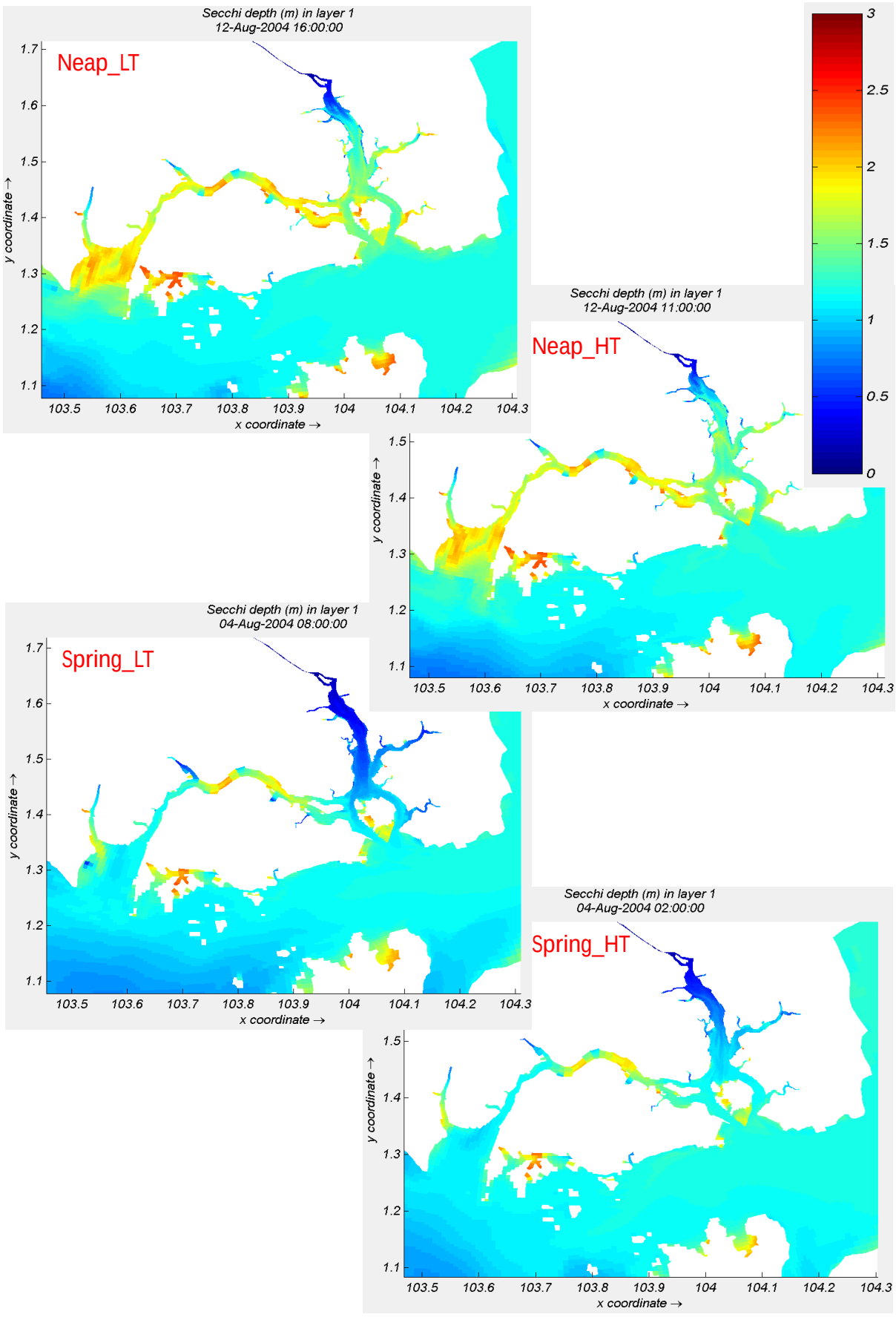

Figure 7-14: S_d for Southwest monsoon (SW). The first diagram is during neap low tide (Neap_LT), the second neap high tide, the third is during spring low tide and the last is during spring high tide.

By and large the SSC and by extension the K_d and S_d, from the upstream of Johor River to the south of Tekong Island appears to be well defined for all three monsoons. In the upstream of Johor River, SSC and S_d are "flashy", exhibiting large changes over short distance. In the estuary (north or Tekong), the SSC are spread out over a relatively larger distance and damped in concentration until they are barely noticeable at the south of Tekong. Similar decrease in SSC can also be seen in Figure 7-9 and 7-10. Regardless of the tide condition, higher visibility was observed along Johor Strait with S_d of 2-3m while visibility is lower in Singapore Strait with S_d of 1-1.5m. The modelled S_d can be divided into 5 main areas with approximately the same S_d; upper Johor River, Johor rivermouth, Johor Strait, Singapore Strait and the sheltered waters around Jurong Island.

The visibility does not seem to vary differently throughout the model domain. Upper rivers show lower S_d due to higher SSC from the upstream of Johor River. However the high fluvial contribution fades in the mouth of Johor River where higher mixing and dilution in the transition area allows the spread and thinning out of SSC around Pulau Ubin and north of Tekong. All the spatial visibility maps show evidence of spatial homogeneity in horizontal direction. This appears to answer the uncertainties in Heng et al. (2011) who found some variation in the spectral volume scattering coefficients. It is likely that the variation is due to SSC dynamics given that scattering are mainly governed by SSC (Chapter 5). Indeed, modelling results in this section proven that the variation observed is attributed to changing SSC with tides and have little to do with spatial differences.

Concurrent with SSC variation, the visibility is lowest during spring low tide followed by neap low tide, spring high tide and neap high tide. The most dynamic area for visibility changes are the Johor River and the Johor estuary areas. Visibility in Johor Strait however, is always higher than the Singapore Strait which seems to be rather unusual since the latter is relatively free from human influence and is expected to have higher visibility. Furthermore, previous studies and circumstantial evidence shows the contrary. The visibility in Singapore Strait averages 1.5m with higher visibility during neap tide. The visibility throughout the model domain is generally lowest during NE compared to SW monsoon indicating the importance of sediment concentration from Johor River over the boundaries modification. Visibility in the Singapore Strait during NE is only about 0.5m while visibility during SW is approximately 1.0m. Similarly, the areas around Tekong show S_d of 0.5 to 1m during NE and increases to about 1.0 to 1.5 during SW monsoon.

The visibility results in the Johor Strait and the sheltered waters around Jurong Island must be treated with caution. Visibility in Johor Strait (especially the eastern part) is consistently above 2.5 to 3.0m while the visibility in Jurong Island is 3m for all tide condition and monsoons. Although the water level around Jurong Island (WCP) is reasonable, the current velocity and bed shear stress is unrealistically low allowing the fine sediment to settle and accumulate at the bed layer resulting in higher visibility. However, in reality even low current velocity can suspend the fine sediment. Moreover, the SSC is low because of limited erodible bottom material due to consolidation of bottom layer in the model. The most important reason for this is the unaccounted processes in the underlying assumption of the sediment transport model; human influence i.e. shipping, pollution, reclamation (Maznah (2009) quoting Syamsidik and Koh (2003)) etc. and large scale transport (i.e. external sources, erosion elsewhere, etc.) as postulated also by Van Maren et al. (in prep).

Flood discharge

The scenario for flood discharge is modelled during IM period by modifying the discharge and sediment concentration of the Johor River. A flood with a 10-year recurrence interval with Q of 300m^3/s and C of 1g/l as estimated in Van Maren et al. (in prep) was specified in the model. Figure 7-15 shows the visibility map during flood discharge. The visibility is low with S_d of less than 0.5m along the Johor River extending to the transition zone around Tekong for all tide condition. Lower visibility extends furthest to the entrance of the Singapore Strait during low, spring tide. Flood discharge apparently does not influence the visibility in the Johor Strait much, except marginal reduction around Pulau Ubin extending to Punggol only during spring tide. However, the visibility in Singapore Strait remains relatively the same even during flood discharge, similar to during average discharge in Figure 7-9. This agrees well with Van Maren et al. (in prep).

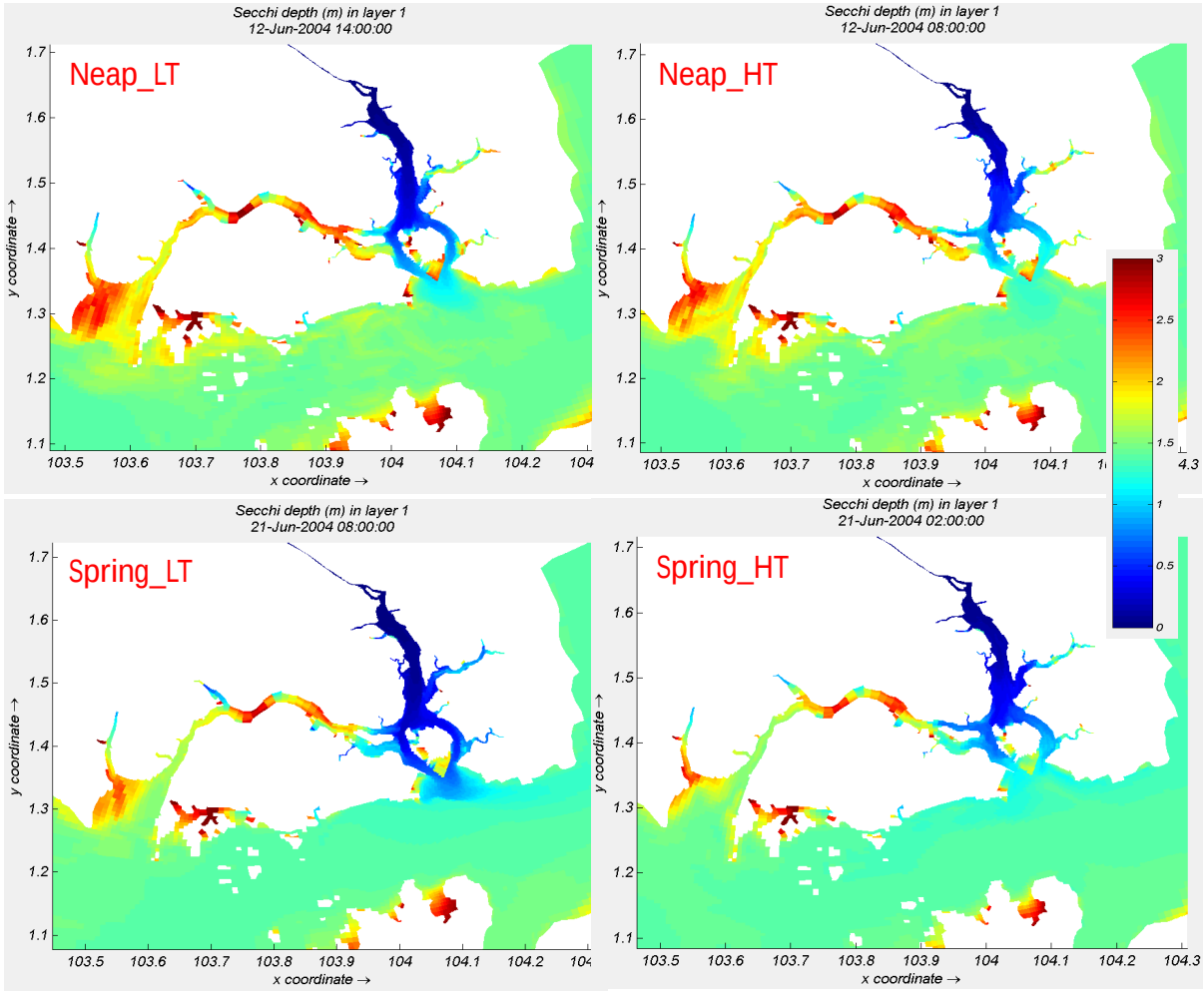

Figure 7-15: S_d for flood discharge during inter monsoon. The first two diagrams are during neap low (Neap_LT) and high tide. The second two is during spring low tide and spring high tide.

6.3 Discussion on Visibility Model

For an experimental model for deriving visibility, generally, the behaviour of the model was reasonable in describing the sediment transport and visibility in the model domain. Note that this is despite some processes like aggregation and disaggregation of particles and time lag effect are not included. Furthermore, only one sediment fraction and layer with uniform physical properties is modelled. As to the K_d*, it appeared that model trends and absolute values were simulated properly, in that they were similar to the relatively scarce measured values and Hydrolight results (Table 6-3). The SSC is lower during neap tide compared to spring tide, with higher SSC during low tide compared to high tide which agrees well with Van Maren et al. (in prep). The* S_d *shows limited spatial variability in the spatial scale. It is also proven that a flood discharge in Johor River does not influence the visibility along the Singapore Strait while only limited impact can be observed in the east of Johor Strait.*

The modelled SSC at the near shore grid cells is 3 to 5 times lower than the measured TSS in the shallows near land. As explained in Section 7.2.1, the higher SSC were not reproduced due to the unaccounted processes since the transport model is based on rather straightforward gradient transport from the upper river to the open sea. Higher SSC during measurement is most likely due to human impact or processes (shipping, dredging, etc.) that were not included in the model. Moreover, stochastic variability of climatological processes can potentially overestimate measurement data. However, although there are uncertainties in the specification and the processes in the model, the results seem to partially agree with satellite images and previous studies. This is true in the regions along the Johor River and Johor estuary (see turbidity map from Liew et al., 2009). However, satellite images from Van Maren (2010) show slightly higher SSC along the Singapore Strait.

High visibility in the Johor Strait is also due to the low background attenuation. Since only constant background attenuation was specified throughout the model domain, a 'balanced' value is needed. However, this balanced value may underestimate the background attenuation in the Johor Strait due to the higher chlorophyll concentration. Visibility is mostly dominated by the concentration of SSC (specified at the boundaries and discharge) followed by $\mathrm{Ext}_{\mathrm{IM1}}$ *, IM1S1 and background attenuation. The IM1S1 indicates the availability of sediment to be suspended from the layer and is relatively less important. The change in IM1S1 changes the SSC magnitude and not the SSC variation itself; higher IM1S1 will lead to higher SSC. Lowering of the settling velocity also reduced the magnitude of SSC, although the spring neap and intra tidal variation are still reproduced.*

In a mixed tidal regime like Singapore, SSC variation is partly dictated by the semi-diurnal and diurnal spring neap cycle (Section 7.1.1). The interaction between semi diurnal and diurnal spring neap cycle plays an important role in seasonal variation of SSC and visibility, strengthening and cancelling each other twice a year (Section 7.1.2). The occurrence of residual flow due to monsoon (westward flow due to easterly wind) at about the same time superimposed on the compound tides interactions. Therefore, the turbidity variation in Singapore waters is due to tides (semi diurnal and diurnal spring neap interactions) and non-tides (monsoonal effect) in approximately equal magnitude during monsoons period. Van Maren and Gerritsen (2012) goes a step further, suggested that residual flow (monsoon and tide induced) and tidal asymmetry are approximately evenly important in sediment transport, and by extension to visibility.

CHAPTER 8.0: CONCLUSIONS AND RECOMMENDATIONS

8.1 Summary of Results

8.1.1 Parameterisation of light attenuation coefficient

The areas around the Johor estuary including the east of Pulau Ubin and Tekong are expected to be reclaimed in the future, compelling the need to understand the hydrodynamics and its implication to sediment transport and turbidity. More than that, the factors governing turbidity are also poorly known and its relation to various forcing like the tides and monsoons remains elusive. This study is intended to fill the gap and provide framework for a broader research on sediment dynamics and light attenuation in the future. As part of the field measurement, more than a dozen of water samples were collected from 9 locations around Singapore with diverse range of zones. Singapore waters are tidally energetic with currents exceeding 2 m/s in meso-tidal regime (mean spring tidal range of 2-4m) and low to moderate wave exposure. The most important fluvial sediment supply is Johor River, consisting mostly of fine sediment with some silt and clay fraction.

The light attenuation characteristics are determined by means of field measurement, laboratory analysis, empirical relations and numerical modelling. Chapter 5 had investigated the physical forcing mechanism (i.e. tides) to light attenuation. The changes in optical property against tidal forcing were investigated for low/high tide. Firstly, highest TSS occurred during highest gradient in the water level (indicative of highest current velocity since the latter is a derivative of the water level gradient) and during low tide with no phase difference with the water level. This shows that TSS is advection dominated during low tide. Thirdly, lowest TSS occurs few hours after high tide slack suggesting that TSS settles down the water column and is suspension dominated. The results in this section show that optical properties vary slightly during low/high tide with 31% variation.

Chlorophyll analysis revealed that the Johor Strait showed higher chlorophyll concentration compared to estuarine waters of Johor River and coastal waters of Singapore Island. This is partly due to favourable hydrodynamic condition and relatively abundant nutrient inputs especially in Kranji and Punggol. For intra tidal variation, higher chlorophyll concentration seems to occur during high tide in Kranji. The CDOM concentration (estimated to be proportional to the CDOM absorption at 440nm) is higher in some of the coastal waters at Singapore Strait especially in Bedok, ECP and WCP compared to the low CDOM concentration in the Johor Strait and estuarine waters. This shows that CDOM absorption is inversely related to chlorophyll concentration and probably of marine origin. CDOM absorption is highest in the near ultraviolet region (412nm) ranging from 0.4m^{-1} to 1.0m^{-1}. The CDOM absorption spectra decline exponentially with the highest S of 0.015 in ECP while the lowest S is 0.010 in LCK. The average exponential slope S is 0.012.

Absorption spectra for TSS were decomposed into chlorophyll and sediment based on specific chlorophyll absorption coefficient using a single parameter model. The scattering spectrum was obtained by subtracting the absorption spectrum from the attenuation spectrum. Both light attenuation processes — absorption and scattering by optically significant constituents depend quantitatively and spectrally on the chemical composition of the particles, their concentration in the water, and their physical properties. Attenuation due

to sediment is dominated by scattering while chlorophyll attenuation shows almost equal contribution of absorption and scattering.

The optical properties of seawater depend on the composition and concentration of the optically significant constituents and on the physical conditions prevailing at any given time (Morel and Prieur 1977; Shifrin 1988; Kirk 2011; Mobley 1994). The most important constituents in the water column are water, CDOM, phytoplankton and sediment. Relative contributions of CDOM, chlorophyll and sediment to light attenuation coefficient K_d were found to be 1.4 – 6.5 % (average of 3.3 %), 1.3 – 62 % (average of 24 %) and 31.3 – 95.2 % (average of 70 %) respectively. The remaining 3 % are average contribution from water molecules itself. Light attenuation is mostly dependent on sediment while chlorophyll is shown to be statistically significant influence to K_d. However, these values may slightly vary depending on the method for K_d decomposition and the empirical formula used to convert c to K_d. The scattering contribution dominates over absorption for K_d, as agreed by Van Duin et al. (2001), especially in sediment dominated waters.

To understand the observed variations in light scattering due to TSS; the nature of the particles and PSD were investigated assuming constant refractive index. The organic content of TSS, i.e. TSS_{org} is 6-30 % of the total TSS in chlorophyll dominated waters and reduces to less than 10% in sediment dominated waters. An average 80% of TSS is represented by TSS_{inorg} in waters dominated by chlorophyll which increases to 88% in waters dominated by sediment. However, it is recognised that the former percentage is likely to be overestimated due to experimental error. For PSD with a slope j > 5, the d_{50} ranges from 7.11 to 9.90 µm representing sediment dominated environment in Singapore Strait. For lower slope j of 3-5, the d_{50} are in the region of 13.8 to 16.3µm, indicating phytoplankton dominated environment along the Johor Strait.

Sediment absorbs light poorly but scatters light effectively and fairly evenly across all wavelengths. Scattering spectra for Kranji and Punggol indicate features due to phytoplankton at 440 and 676nm wavelength. The scattering spectrum at chlorophyll dominated waters shows higher scattering towards longer wavelength compared to vice-versa for sediment dominated waters. However, the increase of the scattering coefficient with increasing wavelength is nearly flat for the former, with mean slope of $\gamma b \sim -0.28$. For sediment dominated waters, the mean slope is higher with $\gamma b \sim 0.65$, but with higher scattering at shorter wavelengths. The b^*_{TSS} is as low as 0.04 in ECP to 0.12 m^2g^{-1} in Sembawang. The b^*_{TSS} in chlorophyll dominated waters averages 0.08 m^2g^{-1} while sediment dominated waters averages 0.1 m^2g^{-1}. This seems to indicate the occurrence of two kinds of suspensions as also agreed by Otto (1966).

ECP and WCP show characteristics of flocculation such as very high suspended sediment (~100 mg/l), high organic contents and high PSD slope (j > 5) indicating more fine sediments. The amount of fine sediment in ECP and WCP and its flocculation potential will affect the light attenuation because light attenuation by particles is related to the cross sectional area of particles (Kirk 2011) instead of the volume. Hence, the light attenuation of a certain mass of smaller particles will be relatively larger than the attenuation of the same mass of larger particles. But due to its size, flocculated sediment has a lower surface area to volume ratio and has higher settling velocity than fine sediment. The interaction of fine sediment generates flocculation which lowers light scattering efficiency as also implied by

Baker and Lavelle (1984). Therefore, the net effect of fine sediment and flocculation are negative resulting in lower overall scattering properties (low b, b^*_{TSS} and b_s/a_s).

Assuming K_d is a quasi-inherent parameter that can be described using the summation of IOP for all the optically significant constituents, empirical equation is used to predict K_d from the measured optical or physical properties. While certain limitations exist in predicting the underwater light field purely from the measurements of optically significant constituents, it is still possible to construct an equation that predicts at least 70% of the variation in light attenuation solely from the NTU alone. NTU and chlorophyll concentration together explains more than 90% of K_d. Specific relationship between K_d and physical parameters (NTU and Chl-a concentration) are shown in Table 8-1. However, the equations must be applied specific to its location derived formula depending on whether it is chlorophyll or sediment dominated waters. For example, the K_d for the latter is dominated by non-linearity of NTU.

Table 8-1: Predictive empirical equations for K_d estimation for various locations

Criteria	Equation	R^2
Chlorophyll dominated waters	Kd = 1.64 + 0.01*(NTU) + 0.004*(Chl-a)	0.98
Sediment dominated waters	Kd^-1 = 0.71 - 3.49 e^(-5)(NTU^3) - 7.41 e^-NTU	0.74
Unknown/sediment-chlorophyll waters	Kd = 1.08 + 0.033*(NTU) + 0.009*(Chl-a)	0.63
If IOP is available	Kd = 0.272 + 0.448*(Cg) + 0.134 (Cs) + 0.357 (Cp)	0.77

The occurrence of other inhomogeneity, such as gas bubbles, oil droplets, and turbulence in the seawater means that seawater absorbs and scatters light quite erratically (Shifrin, 1988). Furthermore, the convention that seawater contains only four classes of optically significant constituents tends to conceal the fact that there can be considerable variability in specific optical properties within each class of constituent. For example, there are various species and pigments within the 'phytoplankton' constituent which are often present in differing proportions, and, as their absorbing properties are slightly different, the specific absorption curve of each group is also subject to certain variability (Prieur and Sathyendranath, 1981). The K_d is also assumed to be linear addition of partial attenuation coefficients, which does not hold in waters in which one of the constituents significantly dominates over others.

Light attenuation is mostly dependent on sediment while chlorophyll is shown to be statistically significant influence to K_d. However, it is important to put the percentage contribution to K_d in perspective. Firstly, the measurement of optically significant constituents is subjected to reasonable margin of error, especially for the sensitive chlorophyll analysis. Secondly, the average 70 % sediment contribution to K_d is considered an upper bound since the measurement were conducted at the near shore location where the sediment (SSC) is the highest due to the cross shore gradient in SSC. Therefore, the percentage of phytoplankton contribution K_p is only expected to increase moving further offshore. Last but not least, the percentage are considered an 'average' value for the diverse range of coastal zone in Singapore waters and might differ especially in waters dominated by large chlorophyll or sediment concentration.

8.1.2 Underwater light field modelling

Underwater light field modelling was carried out in Chapter 6 using Hydrolight, a 1D time independent model solving RTE. Hydrolight was used to spectrally resolve the light field and obtain point base information of the IOP and AOP at sampling locations. One constituent dominates over another to influence light attenuation depending on the depth and wavelength, especially in vertically inhomogeneous water. Hydrolight also computes various AOP including K_d as a function of depth, wavelength and direction in the water column. The modelled K_d from Hydrolight ranges from 1.2 to 2.3 m^{-1} with lower range of K_d in chlorophyll dominated waters. Empirical estimations underestimate $K_{d(PAR)}$ compared to the modelled K_d from Hydrolight. The modelled Secchi depth, S_d ranges from 0.6 – 1.4m corresponding to euphotic depth, z_{eu} of 2.0 – 3.8 m.

The vertical concentration of optically significant constituents is important in determining the vertical variation of IOP which in turn dictates the vertical variation of K_d. The modelled scattering spectrum in Kranji shows lower scattering at the longer wavelengths, in contrast to the measured scattering spectrum in Chapter 5. Light attenuation in the upper layers of the water column is influenced by chlorophyll concentration. Besides the self-shading effect due to increase concentration, variation in vertical chlorophyll distributions also leads to non-uniformities in absorption and consequently to variations in light available for chlorophyll absorption (Van Duin et al., 2001) Differential heating due to variation in chlorophyll absorption in the water column increases vertical mixing. Therefore, the water columns in all locations are well mixed and exhibited very little thermal stratification.

The AOP is governed by changes in the IOP (presence of active constituents and its concentration) and weakly dependent on the changes in the light structure and internal light production by fluorescence. Downwelling AOP's are higher than upwelling AOP's with the highest AOP of K_d, followed by K_{od}, K_u and finally K_{ou}. The values of all the K-functions are similar with only small difference in the surface before reaching asymptotic value K_∞(415). The results from the two models in Hydrolight differ with K_d from ABCASE2 model recorded higher K_d than ABACBB with a factor of 2.4 to 4.8, higher for sediment dominated waters. The K_d from ABACBB model agrees well with Sathyendranath et al. (1988) with incident light ($Cos\,\mu_0$ = 1) with the modelled K_d larger than those obtained from the empirical estimation due to scalar $\overline{K_d}$, nature of prevailing light, VSF assumption, underestimation of bottom reflectance and overestimation of surface irradiance.

Beam attenuation c is larger than the K_d due to the diffuse nature of the latter. In any way $K_d(PAR)$ is a subset of the visible light band, as such K_d > $K_d(PAR)$. This was evident as the K_d from Hydrolight is bigger than $K_d(PAR)$ estimations of Morel (1988) and Pierson et al. (2008). However, even after allowing some allowance, both the empirical estimations seem to underestimate $K_d(PAR)$ compared to K_d from Hydrolight, although Pierson et al. (2008) is more closely related to $K_d(PAR)$ from Hydrolight than Morel (1988). Higher $K_d(PAR)$ from Hydrolight compared to empirical estimations (Table 6-2) is also due to depth dependency of $K_d(PAR)$. The modelled Secchi depth, S_d ranges from 0.6 – 1.4m corresponding to euphotic depth Z_{eu} of 2.0 – 3.8 m, lower than Z_{eu} of 4-9m by Gin et al. (2000). Finally, Chapter 6 also found that the measure of scalar K_d in estimating PAR may overestimate light availability for photosynthesis by underestimating the light attenuation $K_d(PAR)$.

8.1.3 Visibility modelling

There has been little systematic assessment of the relation between suspended sediment and visibility in Singapore waters. Chapter 7 investigated the relation between SSC and visibility using water quality module (WAQ) of Delft3D. The backbone of Delft3D WAQ is the advection-diffusion equation, conserving mass for substances in the water column entering and leaving through direct and diffuse loading. The Fourier spectrums of yearly SSC signal showed that the most significant constituents in the current velocity signal are semidiurnal-diurnal followed by the spring-neap constituent. Semidiurnal and diurnal contributions are almost equal in Bedok, in contrast to Pulau Ubin where the former is higher. As such, convective interaction between the diurnal and semidiurnal components is important in Bedok while the non-linear flux term contributes in the shallow water of Pulau Ubin, where the current velocity is dominated by water level-induced tidal flooding/ebbing.

The offshore (Bedok) spring-neap cycle in current velocity is lower from that in the estuary (Pulau Ubin). The SSC spring neap variation follows exactly the current velocity spring neap with higher SSC during spring tide. Furthermore, the visibility in terms of K_d is also closely related to SSC with little or no phase variation. The fortnightly variation in the low-frequency signal in SSC and visibility is generated by both meteorological effects (monsoon) and by compound tides, producing 2 peaks yearly. SSC in the model domain varies depending on the tides with higher SSC variability during spring compared to neap tide. For intra tide variation, the SSC is higher during low tide compared to high hide. Greater 'noise' (i.e. variability) in the K_d signal compared to the SSC and current velocity signals is because of the interaction between optically significant constituents and the influence of environmental changes (sea surface, waves and incident light).

SSC is highest in the upper reaches of Johor River and reduces to its ambient concentration of about 10 mg/l in Singapore Strait due to higher mixing and dilution in the estuary area allows the spread of SSC around Tekong. In the upstream of Johor River, SSC and S_d maxima are ''flashy,'' exhibiting large excursions over short periods. In the estuary (north of Tekong), the excursions are spread out in time and damped in amplitude until they are barely noticeable at the south of Tekong. The SSC varies depending on the tide with higher surface SSC during spring compared to neap tide and vice-versa for bottom SSC. For intra tide variation, the SSC is generally higher during low tide compared to high hide. During low tide, the surface and bottom SSC are almost comparable. Higher SSC as measured were not reproduced by the model since the SSC is most likely due to human impact or processes (shipping, dredging, etc.) that was not included in the model.

Generally, the behaviour of the model was reasonable in describing the sediment transport and visibility in some areas of the model domain. By and large the SSC and by extension the K_d and S_d from the upstream of Johor River to south of Tekong Island appears to be well defined for all three monsoons. Concurrent with SSC variation, the visibility is lowest during spring low tide followed by neap low tide, spring high tide and neap high tide. Moreover, the visibility showed spatial homogeneity in horizontal direction. Flood discharge in Johor River does not influence the visibility along the Singapore Strait while only limited impact can be observed in the east of Johor Strait. The turbidity variation in Singapore waters is due to tides (semi diurnal and diurnal spring neap interactions) and non-tides (monsoonal effect) in approximately equal magnitude during monsoons.

8.2 Recommendations

The availability of good long term oceanographic data in Singapore waters is a limiting factor for effective risk assessments of dredging/reclamation operations. Lack of systematic data coupled with the reluctance to share them made research much harder. The author circumvented this issue by conducting independent field measurement so that the results from this study can be used by anyone. The optical properties of Singapore waters were determined from this thesis. With this and data from future measurements programs, considerable number of datasets can be compiled. Such dataset can be used to produce a detailed map of optical properties in Singapore for various engineering, ecology and remote sensing applications. The main challenges will be to collect as much water samples/optical data as possible to produce a statistically significant dataset especially in the Singapore where the institutional inertia regarding data proprietary is especially high.

The visibility model that includes the transport of multiple size classes of cohesive sediments and one that accounts for other physical processes and biotic interactions is a formidable challenge in the future. The dredging and reclamation processes must be embedded in the model in a sensible way so that future prediction on sediment processes and visibility is more accurate. Moreover, by improving the sedimentation rate, the sedimentation in the approach channels to port worldwide can be assessed more effectively to minimise dredging cost. Furthermore, uncertainties exist in the sediment sources due to various non-point sources loading into the Johor River and must be quantified. However, the desire to do something, rather than nothing, produced the present modelling approach. As presented in Chapter 7, this approach has been fruitful in producing visibility map for various monsoon seasons and flood condition. The results from this study can be used to optimise dredging operation by understanding the sediment dynamics and its impact to light attenuation.

Optical constituents varied with tidal, seasonal, and external forcing. Although the modelling efforts in this thesis represent the state of the art in the use of a water-quality model, some improvement is necessary. To effectively guide the management of visibility in Singapore waters, incorporation of long-term monitoring data for calibration and verification of model results (Chapter 7) and predictive empirical equations (Chapter 5) are necessary to bring visibility modelling results up to the levels achieved in the flow modelling. This is especially pertinent in Johor Strait where the modelled result seems to overestimate the visibility. Furthermore, numerical models on visibility are also versatile as they can also be used to design and assess the effectiveness of measures to reduce turbidity like deep pit and silt trap, especially in areas with pronounced 3D structures (layers with high SSC near the bed or secondary flow due to tidal currents interacting with local bathymetry).

REFERENCES

1) *Bricaud A, A. Morel and L. Prieur (1981). Absorption by dissolved organic matter of the sea (yellow substance) in the UV and visible domains. Limnology and Oceanography 26:43-53.*

2) *Babin M., A. Morel, Vincent Fournier-Sicre, Frank Fell and Dariusz Stramski (2003). Light Scattering Properties of Marine Particles in Coastal and Open Ocean Waters as Related to the Particle Mass Concentration. Limnology and Oceanography, Vol. 48, No. 2, pp. 843-859.*

3) *Bosboom J. and M.J.F. Stive (2011). Coastal Dynamics I. Technical University of Delft, VSSD.*

4) *Blom G., E.H.S. Van Duin and J.E. Vermaat (1994). Factors contributing to light attenuation in Lake Veluwe in W. van Vierssen (eds), Lake Veluwe, a Macrophyte-dominated System under Eutrophication Stress, pp. 158-174. Kluwer Academic Publishers.*

5) *Bukata, Robert P., John H. Jerome; Kirill Ya Kondratyev, Dimitry V. Pozdnyakov (1995). Optical Properties and Remote Sensing of Inland and Coastal Waters, CRC Press, 384 pages.*

6) *Bezerra-Neto, J.F., Barbosa, P.M. and Barbosa, F.A.R. (2006). Temporal variation of attenuation of the visible radiation in four lakes of Parque Estadual Brasil, Acta Limnol. Bras. 18(1):39-46.*

7) *Baker, Edward T. and J. William Lavelle (1984). The Effect of Particle Size on the Light Attenuation Coefficient of Natural Suspensions. J. Geophys. Res., 89 (C5), pp. 8197-8203.*

8) *Baker, M. (2012). The effect of Bioturbation on the Erodibility of Fine Sediments in Lake Markermeer. MSc. Thesis, Technical University of Delft.*

9) *Chang, C.W. (2007). Inverse modelling for retrieval of optical properties of sea water and atmospheric aerosols from remote sensing reflectance. PhD thesis, NUS.*

10) *Cheong, H.F., N. Jothi Shankar, R. Radhakrishnan and Ah-Cheong Toh (1993). Estimation of sand transport using tracers along reclaimed land at Singapore. Coastal Engng. 19, 311-325.*

11) *Chou, L.M., Yu, J. Y. and Loh, T. L. (2004). Impacts of sedimentation on soft-bottom benthic communities in the southern islands of Singapore. Hydrobiologia 515: 91–106*

12) *Chou, L.M. (2002). Singapore Reefs Report, Report of the Global Coral Reef Monitoring Network (GCRMN) Regional Workshop for the East Asian Seas. Ishigaki, Japan, pp 85- 95.*

13) *Chua T. E. (1973). An Ecological Study of the Ponggol Estuary in Singapore. Hydrobiologia Vol. 43, 3-4 pp. 505-533.*

14) *Chuah, A. L. (1999). Water quality study of the East Johor Strait. MSc Thesis, NUS.*

15) *Chen, M., K. Murali, Boo-Cheong Khoo, Jing Lou and Kurichi Kumar (2005). Circulation Modelling in the Strait of Singapore. Journal of Coastal Research, Vol. 21, No. 5, pp. 960-972*

16) *Chan, E. S., P. Tkalich, Gin K. Y. H., and Obbard, J. P. (2006). The physical oceanography of Singapore coastal waters and its implications for oil spills. In: The Environment in Asia Pacific Harbours, Chapter 23, edited by: Wolanski, E., Springer, The Netherlands, pp. 393–412.*

17) *Dikou, A. and R. van Woesik. (2006). Survival under chronic stress from sediment load: Spatial patterns of hard coral communities in the southern islands of Singapore. Marine Pollution Bulletin 52, pp. 1340–1354.*

18) *Doorn-Groen S. M. and T.M. Foster (2007). Environmental Monitoring and Management of Reclamation Works Close to Sensitive Habitats. Terra et Aqua, pp 3-18.*

19) *Erftemeijer, Paul L.A. and Roy R. Robin Lewis (2006). Environmental impacts of dredging on seagrasses: A review. Marine Pollution Bulletin 52, 1553–1572.*

20) *Eutech Instruments (2011). Instruction Manual, TN-100/T-100 Portable Turbidimeter, Rev. 6*

21) *Deltares (2008). Delft3D-WAQ Technical Reference Manual, 2.03 ed.*

22) *Deltares (2011). Delft3D-WAQ User Manual, Delft Hydraulics, Delft, the Netherlands, 4.03 ed.*

23) *Eduardo Millan, Nunez, J. Ruben Lara-Lara and Joan S. Cleveland (1998). Variation in specific absorption coefficient and total phytoplankton in the Gulf of California. CalCOFI Rep., Vol. 39.*

24) *Foden J., D.B. Sivyer, D.K. Mills and M.J. Devlin (2008). Spatial and temporal distribution of chromophoric dissolved organic matter (CDOM) fluorescence and its contribution to light attenuation in UK water bodies. Estuarine, Coastal and Shelf Science 79, 707–717.*

25) *Goh B.P.L. and L.M. Chou (1997). Heavy Metal Levels in Marine Sediments of Singapore. Environmental Monitoring and Assessment. Volume 44, Numbers 1-3, pp. 67-80.*

26) *Gordon H. R. and A. Morel (1983). Remote Assessment of Ocean Color for Interpretation of Satellite Visible Imagery: A Review. Springer-Verlag, New York, pg. 44.*

27) *Gin, K.Y.H., Lin, X. and Zhang, S. (2000). Dynamics and size structure of phytoplankton in the coastal waters of Singapore. Journal of Plankton Research 22: 1465-1484.*

28) *Gin, K.Y.H., S. Teck Koh, I. I. Lin and E. S. Chan (2002). Application of Spectral Signatures and Colour Ratios to Estimate Chlorophyll in Singapore's Coastal Waters. Estuarine, Coastal and Shelf Science 55, pp. 719–728.*

29) *Gin, K.Y.H., Zhang, S. and Lee, Y.K. (2003). Phytoplankton community structure in Singapore's coastal waters using HPLC pigment analysis. J. of Plankton Res. 25, pp. 1507-1519.*

30) *Gin K. Y. H., Q. Y. Zhang, E. S. Chan and L. M. Chou (2001). 3D Multilevel Ecological-Eutrophication model for Singapore. Journal of Environmental Engineering, Vol. 127, No. 10.*

31) *Hasan, G.M.J., Van Maren D.S. and H.F. Cheong (2011). Improvement in hydrodynamic modelling of an estuary in a mixed tidal regime by grid aligning and refining. Ocean Dynamics, 62 (3), pp 395-409.*

32) *Hoitink A.J.F. (2004). Tidally-induced clouds of suspended sediment connected to shallow-water coral reefs. Marine Geology 208, pp. 13– 31.*

33) *Hoitink A.J.F., Hoekstra P. and van Maren D. S. (2003). Flow asymmetry associated with astronomical tides: Implications for the residual transport of sediment. J. Geo. Res., 108 (C10), 3315.*

34) *Heng, A. W. C., C. W. Chang, J. He, N. Dewkurun, and S. C. Liew (2005). Inherent optical properties of water measured in situ and from multispectral imageries: A case study on waters south of Singapore. Proc. ACRS 2005, 26th Asian Conference on Remote Sensing, 7 - 11 Nov 2005, Hanoi, Vietnam, Paper No. CSZ1-4.*

35) *James, W.F., E.P.H. Best, and J.W. Barko (2002). Suspended sediment dynamics and light attenuation characteristics in Peoria Lake, Illinois: can submersed macrophyte communities improve water quality in this ecosystem? US Army corps of Engineers, ERDC/EL TR02-2, 35 p.*

36) *Jonasz, M. and G. Fournier (2007). Light Scattering by Particles in Water: Theoretical and Experimental Foundations. Academic Press, 714 pages.*

37) *Jeffrey S. W. and G. F. Humphrey (1975). New spectrophotometric equation for determining chlorophyll a, b, c1 and c2. Biochem. Physiol. Pflanz., 167, 194-204*

38) *Kirk J.T.O. (1984a). Attenuation of solar radiation in scattering absorbing waters: A simplified procedure for its calculation. Appl. Opt. 23: 3737-3739.*

39) *Kirk J.T.O. (1984b). Dependence of relationship between inherent and apparent optical properties of water on solar altitude. Limnol.Oceanogr. 29: 350-354.*

40) *Kirk J.T.O. (1992). Monte Carlo study of the nature of the underwater light field in, and the relationships between optical properties of, turbid yellow waters. Australian Journal of Marine and Freshwater Research 32(4) 517 – 532.*

41) *Kirk J. T.O. (2011). Light and Photosynthesis in Aquatic Ecosystems (Third Edition). Cambridge University Press, 662 pages.*

42) *Kuwahara V. S., R. Nakajima, B. H. R. Othman, M. R. M. Kushairi and T. Toda (2010). Spatial variability of UVR attenuation and bio-optical factors in shallow coral-reef waters of Malaysia. Coral Reefs 29:693–704.*

43) *Kurniawan, A., Ooi S.K., Hummel, S. and Gerritsen, H. (2011). Sensitivity analysis of the tidal representation in Singapore Regional Waters in a data assimilation environment. Ocean Dynamics 61:1121–1136.*

44) *Kurniawan A., Ooi S.K., Gerritsen H. and Twigt D.J. (2010). Calibrating the Regional Tidal Prediction of the Singapore Regional Model using OpenDA. In: Tao J, Chen Q, Liong S-Y (eds) Proc. 9th Int. Conf on Hydroinformatics, Tianjin, 7–11 September 2010, Vol. 2. Chemical Industry, Beijing, pp 1406–1413.*

45) *Lee Z. P., K. L. Carder, C. D. Mobley, R. G. Steward and J. S. Patch (1998). Hyperspectral remote sensing for shallow waters: A semianalytical model. Appl. Opt. 37, 6329–6338.*

46) *Lee Z. P. (1994). Visible-infrared remote-sensing model and applications for ocean waters, Ph.D. dissertation, Department of Marine Science, University of South Florida.*

47) *Liew S. C., B. Saengtuksin, and L. K. Kwoh (2009). Monitoring turbidity and SSC of coastal and inland waters using satellite data, Proc. IEEE 2009 International Geoscience and Remote Sensing Symposium (IGARSS'09), 13 - 17 July 2009, South Africa, Vol. II, pp. 837-839.*

48) *Lund-Hansen, L. C. (2004). Diffuse attenuation coefficients* K_d (PAR) *at the estuarine North Sea - Baltic Sea transition: time-series, partitioning, absorption, and scattering, Estuarine, Coastal and Shelf Science 61, 251-259.*

49) *Lorenzen, C.J. (1967). Determination of chlorophyll and phaeopigments: spectrophotometric equations. Limnol. Oceanogr., 12:343-346.*

50) *Lorenzen, C. J., and S. W. Jeffrey (1980). Determination of chlorophyll in seawater. UNESCO Tech. Papers Mar. Sci. 35: l-20.*

51) *Maznah Bt Ismail (2009). Application of a Hydrodynamic Water Quality Model in Sg Johor Estuary. MSc thesis, Universiti Teknologi Malaysia.*

52) *McGregor, R.C. and Desouza, W.E.R. (1997). On the analysis of tidal energy schemes with large diurnal variations with application to Singapore. Renewable Energy, Vol 10, (2–3), 331–334.*

53) *McPherson, B. F. and R. L. Miller (1987). The Vertical Attenuation of Light in Charlotte Harbor, a Shallow, Subtropical Estuary, Florida. Estuarine, Coastal and Shelf Science 25,721-737.*

54) *Mueller J., Fargion G., McClain C. (eds), Scott Pegau, J.Ronald V. Zaneveld, B. Gregg Mitchell, James L. Mueller, Mati Kahru, John Wieland and Malgorzat Stramska (2002). Ocean Optics Protocols for Satellite Ocean Color Sensor Validation, Revision 4, Volume IV: Inherent Optical Properties: Instruments, Characterizations, Field Measurements and Data Analysis Protocols. NASA Goddard Space Flight Center, Greenbelt, Md.*

55) *Mobley, C. D. (1994). Light and Water: Radiative Transfer in Natural Waters. Academic Press, San Diego, 592 pages.*

56) *Mobley, C. D. and Lydia K. Sundman (2006). Hydrolight 4.3, Technical Documentation. Sequoia Scientific, Inc. Bellevue, WA 98005*

57) *Morel, A. and A. Bricaud (1981). Theoretical results concerning light absorption in a discrete medium, and application to specific absorption of phytoplankton. Deep-Sea Research, 28, 1375-1393.*

58) *Morel, A. and L. Prieur (1977). Analysis of variations in ocean color. Limnology and Oceanography, 22 (4) pp. 709-722.*

59) *Morel, A. (1988). Optical modeling of the upper ocean in relation to its biogenous matter content (Case 1 water). J. Geo. Res., Vol. 93, (C9) pp 10,749-10,768.*

60) *Morel, A. (1974). Optical properties of pure water and pure seawater. In: Jerlov and E. Steeman Nielsen (ed). Optical aspects of oceanography. Academic Press, pp. 1-24.*

61) *Nervada, D. (2006). Monte Carlo simulation of light in stratified water. MSc Thesis, NUS.*

62) *Otto L. (1966). Light Attenuation in the North Sea and the Dutch Wadden Sea in relation to Secchi Disk visibility and suspended matter. Netherlands J. of Sea Res. 3, 1, pp. 28-51.*

63) *Ooi S.K., Gerritsen, H., Kurniawan, A. and Twigt, D.J. (2010). Parameter optimization and data assimilation to improve the tidal prediction of the Singapore Regional Model. Proc. 17th IAHR-APD Congress 2010, Auckland, New Zealand, Session 5.*

64) *Pegau, W.S., D. Gray and J.R.V. Zaneveld (1997). Absorption and attenuation of visible and near-infrared light in water: dependence on temperature and salinity. Apl.Opt., 36(24):6035-6046.*

65) *Pierson, Donald C., Hampus Markensten and Niklas Strömbeck (2003). Long and short term variations in suspended particulate material: the influence on light available to the phytoplankton community. Hydrobiologia 494: 299–304.*

66) *Pierson, Donald C., Susanne Kratzer. Niklas Strömbeck, Bertil Håkansson (2008). Relationship between the attenuation of downwelling irradiance at 490 nm with the attenuation of PAR (400 nm–700 nm) in the Baltic Sea. Remote Sensing of Environment 112: 668–680.*

67) *Pope R.M. and E.S. Fry (1997). Absorption spectrum (380-700 nm) of pure water, integrating cavity measurements. Appl. Opt. 36: 8710-8723.*

68) *Prandle, D. (2009). Estuaries: dynamics, mixing, sedimentation and morphology, Cambridge University Press, 236 pages.*

69) *Prieur, L. and S. Sathyendranath (1981). An optical classification of coastal and oceanic waters based on the specific spectral absorption curves of phytoplankton pigments, dissolved organic matter, and other particulate materials. Limnol. Oceanogr., 26(4): 671-689.*

70) *Pugh, D.T. (1987). Tides, surges and mean sea level. John Wiley & Sons, 472 pages.*

71) *Riddle A.M. (1996). Uncertainties in modelling of tidal flows off Singapore Island. Journal of Marine Systems 8, 133-145.*

72) *Sathyendranath S., Lazzara L. and Prieur L. (1987). Variations in the Spectral Values of Specific Absorption of Phytoplankton. Limnology and Oceanography 32: 403-415.*

73) *Sathyendranath, S., and T. Platt (1988). The spectral irradiance field at the surface and in the interior of the ocean: A model for applications in oceanography and remote sensing. J. Geo. Res., 93, 9270–9280.*

74) *Sequoia Scientific Inc. (2009). LISST-100X Particle Size Analyser, User's Manual, Version 4.65, Bellevve, Washington, 108 pages.*

75) *Shifrin K. S. (1988). Physical optics of ocean water. Springer, 285 pages.*

76) *Smith, R.C. and K.S. Baker (1981). Optical properties of the clearest natural waters (200-800 nm), Appl. Opt. 20 (2): 177-184.*

77) *Sun, Y.B., Sisomphon, P., Babovic, V. and Chan, E.S. (2009). Efficient data assimilation method based on chaos theory and Kalman filter with an application in Singapore Regional Model. J. of Hydro-environment Res. 3, 85-95.*

78) *Suzuki K., Motoaki Kishino, Kousei Sasaoka, Seiichi Saitoh and Toshiro Sainoi (1998). Chlorophyll-Specific Absorption Coefficients and Pigments of Phytoplankton off Sanriku, Northwestern North Pacific, Journal of Oceanography, Vol. 54, pp. 517 - 526.*

79) *Tham, A. K., Khoo, H. W. and Chua, T. E. (1970). A study of the plankton in Singapore waters in relation to the environment. In: The Kuroshio: A symposium on the Japan Current, Honolulu. East West Centre Press 361-376.*

80) *Tkalich P., Pang W.C. and P. Sundarambal (2002). Hydrodynamics and Eutrophication Modelling for Singapore Straits. The Seventh OMISAR Workshop on Ocean Models.*

81) *U.S. Environmental Protection Agency (National Exposure Research Laboratory) (1997). Method 446.0: In Vitro Determination of Chlorophylls a, b, c + c and Pheopigments in Marine And Freshwater Algae by Visible Spectrophotometry. Revision 1.2, Cincinnati, Ohio 45268.*

82) *U.S. Environmental Protection Agency (National Exposure Research Laboratory) (1997). Method 160.2: Total Suspended Solids (TSS) Gravimetric, Dried at 103-105°C.Revision 1.2, Ohio 45268.*

83) *Van Duin E. H. S., G. Blom, L. Lijklema and M. J. M. Scholten (1992). Aspects of modelling sediment transport and light conditions in Lake Marken. Hydrobiologia, 235/236: 167-176.*

84) *Van Duin E. H. S., G. Blom, F. Johannes Los, Robert Maffione, R. Zimmerman, Carl F. Cerco, MarkDortch and Elly P.H. Best (2001). Modeling underwater light climate in relation to sedimentation, resuspension, water quality and autotrophic growth. Hydrobiologia, 444:25–42.*

85) *Van Maren, D.S. and H. Gerritsen (2012). Residual flow and tidal asymmetry in the Singapore Strait, with implications for resuspension and residual transport of sediment. J. Geo. Res. Vol. 117, C04021.*

86) *Van Maren, D.S. (2010). Fine sediment dynamics in Singapore's Coastal Waters. Deltares Report 1202920-001.*

87) *Van Maren, D.S., Liew. S.C. and Hasan, G.M.J. (in prep). Estimating the role of Johor River on turbidity around Singapore.*

88) *Vant W. N. (1990). Causes of Light Attenuation in Nine New Zealand Estuaries. Estuarine, Coastal and Shelf Science 31, 125-137.*

89) *Waterman, R. E. (2008). Integrated Coastal Policy via Building with Nature. 500 pages.*

90) *Webb, Paul A. (2000). Particle Sizing by Static Laser Light Scattering. Technical Workshop Series: Introduction to the Latest ANSI/ISO Standard for Laser Particle Size Analysis Micromeritics Instrument Corp.*

91) *WET Labs, Inc. (2005). Ac-9 Protocol Document, Revision J.*

92) *Zhang, Q.Y. and Gin, K.Y.H. (2000). Three-dimensional numerical simulation for tidal motion in Singapore's coastal waters. Coastal Engineering 39, 71–92.*

93) *Zoelaeha, B. Dian (2010). Fine sediment transport near coral reefs islands in the Singapore Strait. MSc Thesis, Delft University of Technology.*

APPENDIX A: SAMPLING LOCATIONS

Kranji

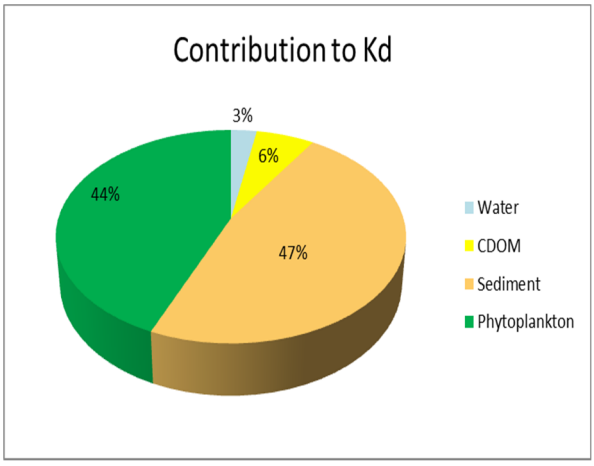

WCP

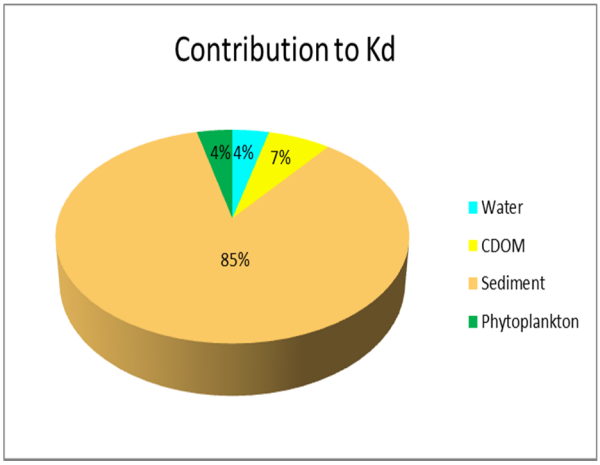

ECP

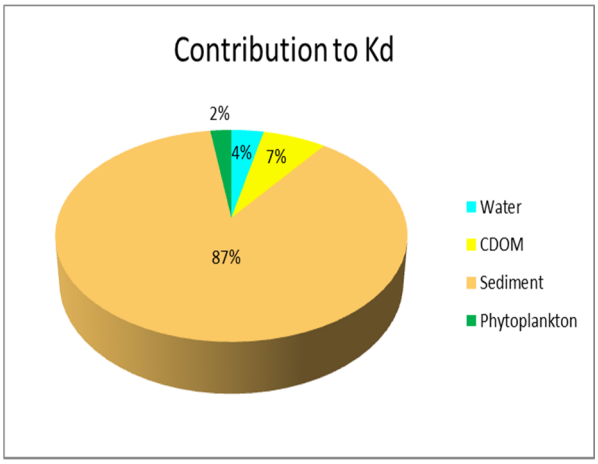

Punggol

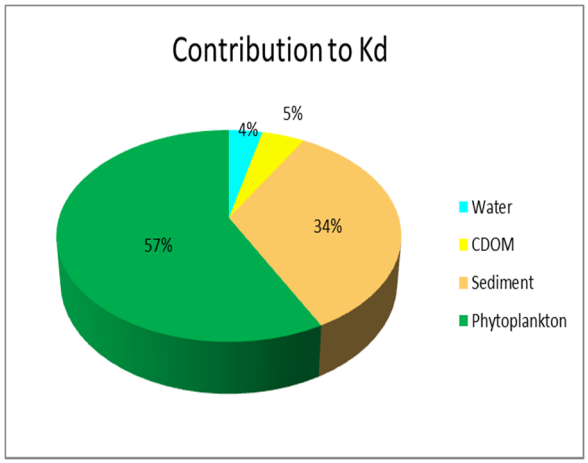

Ubin_East

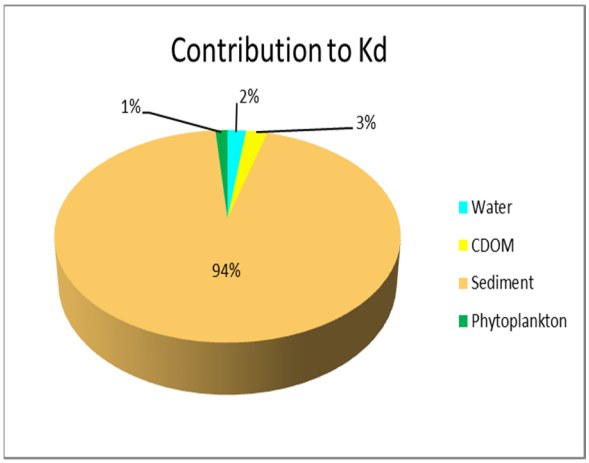

Ubin_North

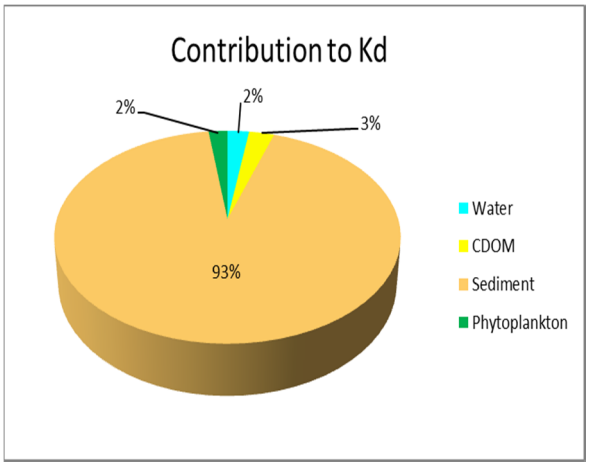

Lim Chu Kang (LCK)

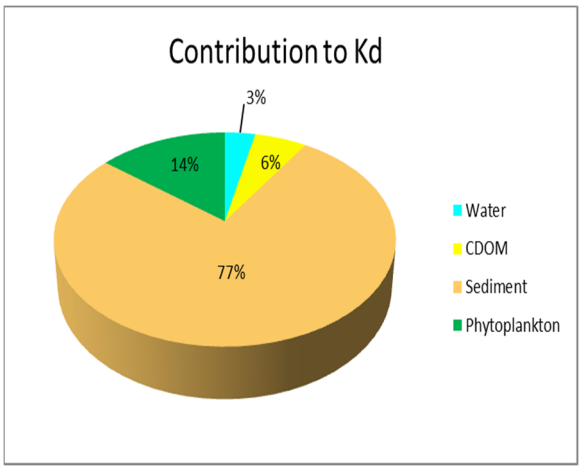

Bedok

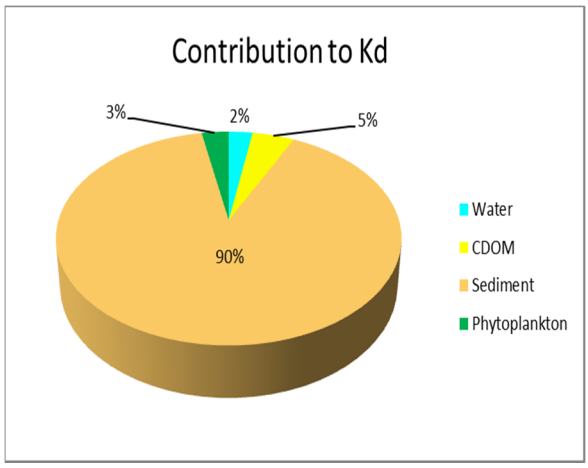

Sembawang

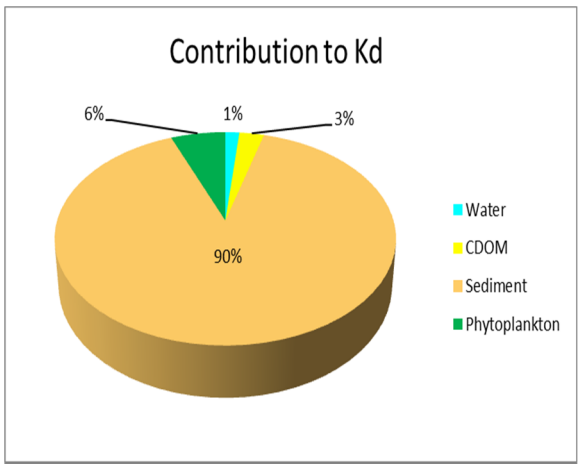

APPENDIX B: PARAMETERISATION OF K_d

K13a					uncorrected		corrected		**Scattering slope**				b0	5.36373	n	-0.2001	rms	0.696
	c (total)	c (CDOM)	c (TSS)	a (total)	a (CDOM)	a (TSS)	a (CDOM)	a (TSS)	b (TSS)	b_model	residue	residue^2						
412	9.432	1.088	8.343	4.606	1.258	3.349	0.627	3.979	4.364	5.053	-0.689	0.475						
440	8.781	0.786	7.995	3.819	0.857	2.962	0.327	3.492	4.502	5.120	-0.618	0.382						
488	7.984	0.518	7.466	2.278	0.537	1.742	0.276	2.003	5.463	5.227	0.236	0.055						
510	7.744	0.484	7.260	1.635	0.467	1.168	0.224	1.411	5.849	5.274	0.575	0.331						
532	7.739	0.622	7.117	0.875	0.456	0.419	0.150	0.726	6.391	5.318	1.073	1.151						
555	7.108	0.303	6.805	0.910	0.336	0.574	0.075	0.836	5.969	5.364	0.605	0.366						
630	6.323	0.241	6.083	0.877	0.270	0.607	0.054	0.823	5.260	5.501	-0.242	0.059						
676	6.150	0.160	5.990	1.650	0.220	1.430	0.027	1.623	4.367	5.580	-1.213	1.471						
715	6.095	0.181	5.914	0.000	0.234	-0.234	0.000	0.000	5.914	5.643	0.271	0.073						

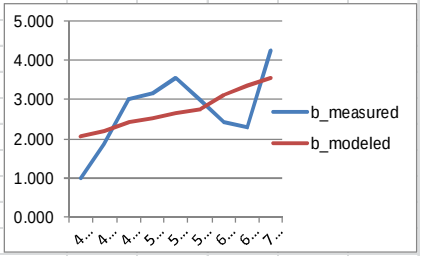

CDOM absorption				
	rms err			0.05192
	G	0.460		
	Sg	0.010		
	a (CDOM)	a (CDOM)	residue	
412	0.627	0.61318	-0.014	0.00018
440	0.327	0.45994	0.133	0.01771
488	0.276	0.28094	0.005	3E-05
510	0.224	0.22413	0.000	9.1E-08
532	0.150	0.1788	0.029	0.00086
555	0.075	0.14118	0.066	0.00441
630	0.054	0.06535	0.012	0.00014
676	0.027	0.04075	0.014	0.00019
715	0.000	0.0273	0.027	########

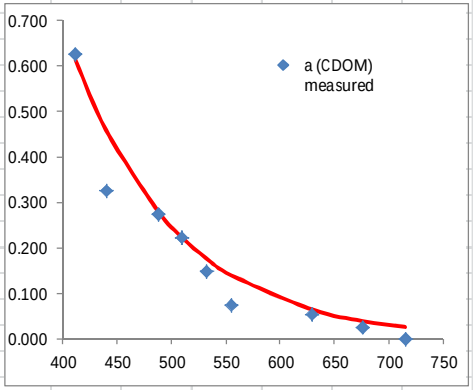

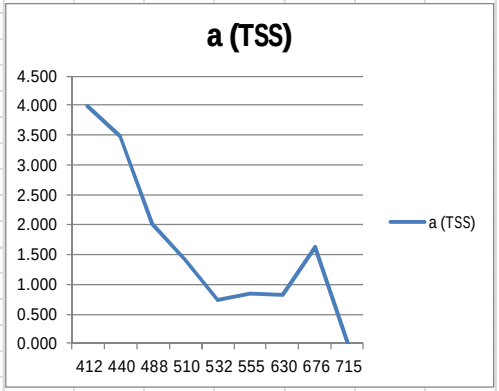

TTS decomposition (Lee, 1994)									
	rms err			0.22098	a_ss(440	1.56942	a_chl(44	1.6439	
					S_ss	0.02053			
	a (TSS) mesu	TSS) mode	residue		a (phyto)	(sedimen	hytoplank	a0	a1
412	3.979	4.10508	0.126	0.01581	1.190	2.789	1.316	0.795	0.011
440	3.492	3.21331	-0.279	0.07792	1.923	1.569	1.644	1.000	0.000
488	2.003	1.85255	-0.150	0.0226	1.417	0.586	1.267	0.760	0.022
510	1.411	1.57959	0.168	0.02834	1.038	0.373	1.207	0.691	0.087
532	0.726	1.22918	0.504	########	0.488	0.237	0.992	0.556	0.096
555	0.836	0.83573	0.000	2.7E-09	0.688	0.148	0.688	0.383	0.072
630	0.823	0.65277	-0.170	0.02905	0.791	0.032	0.621	0.342	0.072
676	1.623	1.51339	-0.110	0.0121	1.611	0.012	1.501	0.836	0.155
715	0.000	0.00554	0.006	3.1E-05	-0.006	0.006	0.000	0.000	0.000

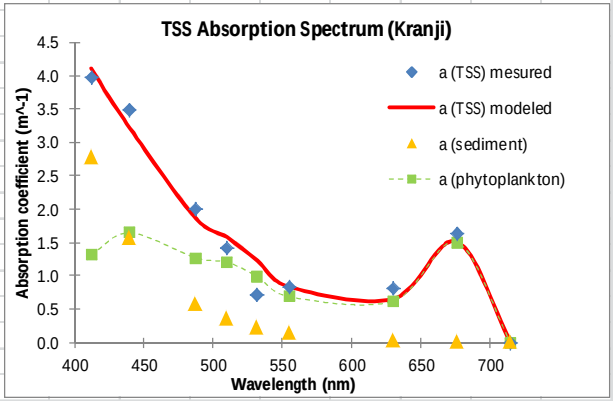

ECP3					uncorrected		corrected		**Scattering slope**				b0	5.16895	n	0.5233	rms	0.224
	c (total)	c (CDOM)	c (TSS)	a (total)	a (CDOM)	a (TSS)	a (CDOM)	a (TSS)	b (TSS)	b_model	residue	residue^2						
412	7.593	0.805	6.788	1.824	1.054	0.770	0.701	1.123	5.665	6.041	-0.376	0.142						
440	7.067	0.602	6.465	1.170	0.949	0.222	0.493	0.677	5.788	5.837	-0.049	0.002						
488	6.438	0.455	5.983	0.615	0.761	-0.145	0.282	0.184	5.799	5.529	0.270	0.073						
510	6.244	0.442	5.802	0.433	0.590	-0.157	0.177	0.146	5.656	5.403	0.253	0.064						
532	6.168	0.595	5.572	0.405	0.435	-0.030	0.087	0.108	5.465	5.285	0.180	0.032						
555	5.735	0.287	5.448	0.286	0.337	-0.051	0.042	0.070	5.378	5.169	0.209	0.044						
630	5.044	0.249	4.794	0.242	0.211	0.031	0.031	0.211	4.584	4.837	-0.254	0.064						
676	4.867	0.178	4.689	0.196	0.109	0.086	0.012	0.184	4.506	4.662	-0.157	0.025						
715	4.665	0.221	4.444	0.000	0.000	0.000	0.000	0.000	4.444	4.527	-0.084	0.007						

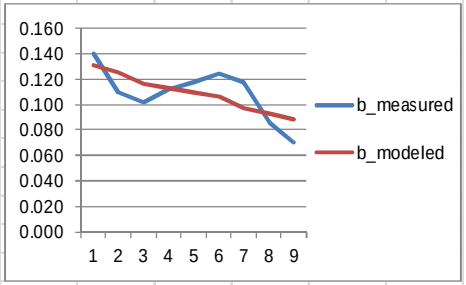

CDOM absorption				
	rms err			0.02641
	G	0.476		
	Sg	0.015		
	a (CDOM)	a (CDOM)	residue	
412	0.701	0.71713	0.016	0.00026
440	0.493	0.47598	-0.018	0.00031
488	0.282	0.23574	-0.046	0.0021
510	0.177	0.17083	-0.006	3.7E-05
532	0.087	0.1238	0.037	0.00134
555	0.042	0.08841	0.046	0.00215
630	0.031	0.02949	-0.002	2.3E-06
676	0.012	0.01504	0.003	9.2E-06
715	0.000	0.0085	0.008	########

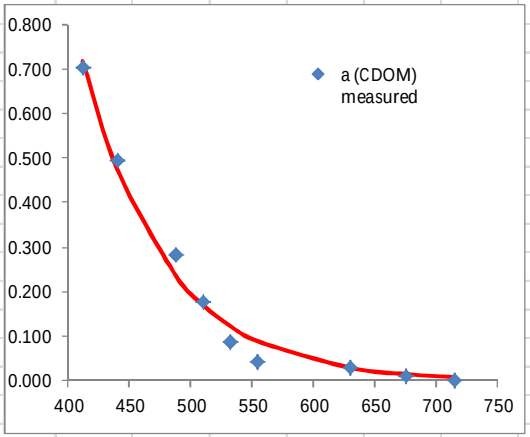

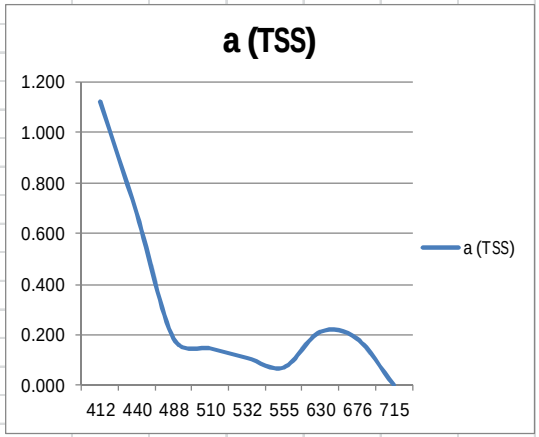

TTS decomposition (Lee, 1994)									
	rms err			0.06045	a_ss(440	0.35234	a_chl(44	0.26783	
					S_ss	0.0346			
	a (TSS) me	a (TSS) me	residue		a (phyto)	a (sedime	a (phytop	a0	a1
412	1.123	1.13722	0.014	0.0002	0.195	0.92828	0.20894	0.795	0.0113
440	0.677	0.62017	-0.057	0.00323	0.325	0.35234	0.26783	1	0
488	0.184	0.26275	0.079	0.00623	0.117	0.06695	0.19581	0.7598	0.0218
510	0.146	0.18586	0.040	0.0016	0.115	0.03127	0.15459	0.6911	0.0865
532	0.108	0.12961	0.022	0.00048	0.093	0.01461	0.11501	0.5557	0.0959
555	0.070	0.08388	0.014	0.0002	0.063	0.00659	0.07729	0.3828	0.07155
630	0.211	0.06679	-0.144	0.02074	0.210	0.00049	0.0663	0.3421	0.0718
676	0.184	0.16949	-0.014	0.0002	0.183	0.0001	0.16939	0.8362	0.1547
715	0.000	2.6E-05	0.000	6.8E-10	0.000	2.6E-05	0	0	0

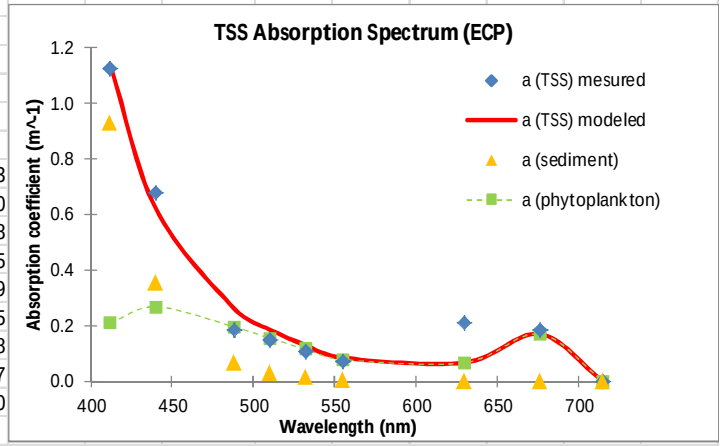

WCPb					uncorrected		corrected		**Scattering slope**				b0	4.55912	n	-0.9298	rms	0.126
	c (total)	c (CDOM	c (TSS)	a (total)	a (CDOM)	a (TSS)	a (CDOM)	a (TSS)	b (TSS)	b_model	residue	residue^2						
412	7.062	0.725	6.337	1.502	0.996	0.506	0.996	0.506	5.832	6.014	-0.183	0.033						
440	6.496	0.543	5.953	0.937	0.852	0.085	0.790	0.300	5.653	5.658	-0.005	0.000						
488	5.805	0.399	5.406	0.471	0.642	-0.171	0.553	0.120	5.286	5.138	0.148	0.022						
510	5.574	0.390	5.184	0.385	0.458	-0.073	0.379	0.091	5.093	4.932	0.161	0.026						
532	5.504	0.543	4.961	0.385	0.291	0.094	0.219	0.166	4.795	4.742	0.053	0.003						
555	5.010	0.238	4.772	0.282	0.201	0.081	0.163	0.119	4.653	4.559	0.094	0.009						
630	4.237	0.202	4.034	0.236	0.103	0.133	0.061	0.175	3.859	4.052	-0.193	0.037						
676	3.987	0.133	3.855	0.196	0.049	0.147	0.026	0.170	3.685	3.795	-0.111	0.012						
715	3.802	0.173	3.629	0.000	0.000	0.000	0.000	0.000	3.629	3.602	0.026	0.001						

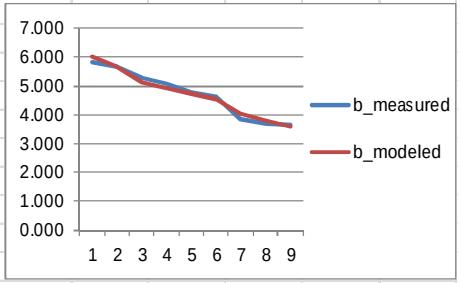

CDOM absorption				
	rms err			0.05084
	G	0.762		
	Sg	0.011		
	a (CDOM	a (CDOM	residue	
412	0.996	1.03807	0.042	0.00176
440	0.790	0.76247	-0.027	0.00075
488	0.553	0.44926	-0.103	0.01068
510	0.379	0.35254	-0.027	0.00072
532	0.219	0.27664	0.058	0.00332
555	0.163	0.2147	0.052	0.00267
630	0.061	0.09395	0.033	0.0011
676	0.026	0.05659	0.030	0.00091
715	0.000	0.03682	0.037	########

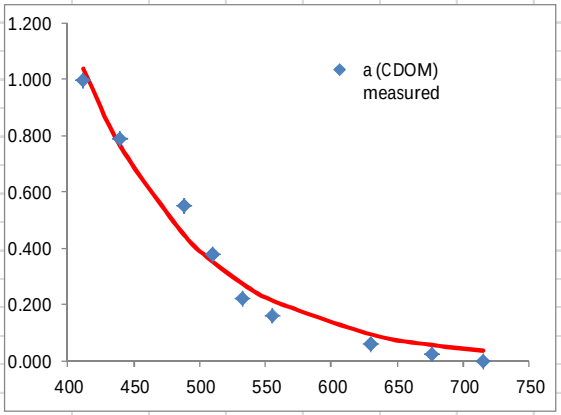

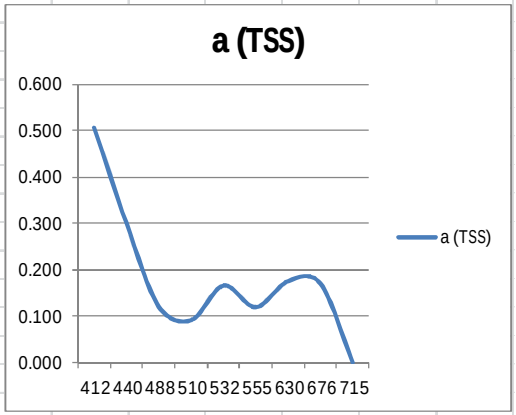

TTS decomposition (Lee, 1994)									
	rms err			0.05367	a_ss(440	0.03535	a_chl(44	0.25919	
					S_ss	0.07686			
	a(TSS) m	a(TSS) m	residue		a (phyto	a (sedim	a (phyto	a0	a1
412	0.506	0.50618	0.000	1.6E-07	0.202	0.30408	0.2021	0.795	0.0113
440	0.300	0.29454	-0.005	3E-05	0.265	0.03535	0.25919	1	0
488	0.120	0.19019	0.070	0.00493	0.119	0.00088	0.18931	0.7598	0.0218
510	0.091	0.14903	0.058	0.00337	0.091	0.00016	0.14886	0.6911	0.0865
532	0.166	0.11051	-0.055	0.00306	0.166	3E-05	0.11048	0.5557	0.0959
555	0.119	0.07419	-0.045	0.00199	0.119	5.1E-06	0.07419	0.3828	0.07155
630	0.175	0.06355	-0.112	0.01249	0.175	1.6E-08	0.06355	0.3421	0.0718
676	0.170	0.16261	-0.007	5.4E-05	0.170	4.7E-10	0.16261	0.8362	0.1547
715	0.000	2.3E-11	0.000	5.5E-22	0.000	2.3E-11	0	0	0

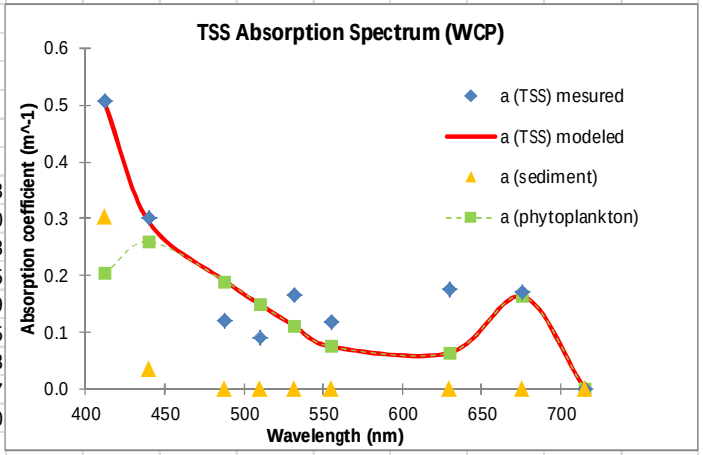

Punggol					uncorrected		corrected		**Scattering slope**				b0	4.41747	n	0.38449	rms	0.323
	c (total)	c (CDOM	c (TSS)	a (total)	a (CDOM)	a (TSS)	a (CDOM)	a (TSS)	b (TSS)	b_model	residue	residue^2						
412	5.998	0.379	5.619	2.288	0.465	1.823	0.465	1.823	3.796	3.939	-0.143	0.020						
440	5.839	0.322	5.517	2.094	0.403	1.691	0.377	1.717	3.800	4.040	-0.240	0.058						
488	5.678	0.290	5.388	1.355	0.296	1.059	0.250	1.105	4.283	4.204	0.079	0.006						
510	5.631	0.308	5.323	1.117	0.195	0.921	0.152	0.964	4.358	4.276	0.082	0.007						
532	5.868	0.486	5.382	0.886	0.131	0.755	0.103	0.783	4.599	4.346	0.252	0.064						
555	5.446	0.194	5.252	0.606	0.101	0.505	0.089	0.517	4.734	4.417	0.317	0.100						
630	5.321	0.192	5.130	0.436	0.065	0.372	0.049	0.387	4.742	4.638	0.104	0.011						
676	5.150	0.127	5.023	1.032	0.030	1.002	0.016	1.017	4.006	4.765	-0.759	0.576						
715	5.347	0.171	5.175	0.000	0.000	0.000	0.000	0.000	5.175	4.869	0.306	0.094						

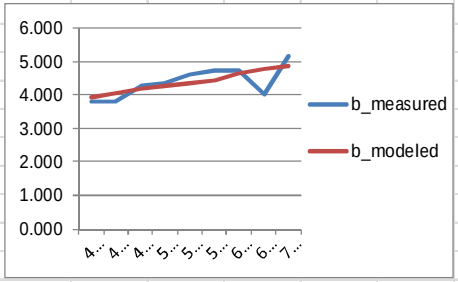

CDOM absorption				
	rms err			0.02063
	G	0.356		
	Sg	0.011		
	a (CDOM	a (CDOM	residue	
412	0.465	0.4846	0.019	0.00037
440	0.377	0.3557	-0.021	0.00045
488	0.250	0.20934	-0.041	0.00166
510	0.152	0.16418	0.012	0.00014
532	0.103	0.12876	0.026	0.00066
555	0.089	0.09988	0.011	0.00012
630	0.049	0.04362	-0.005	2.9E-05
676	0.016	0.02625	0.010	0.00011
715	0.000	0.01706	0.017	########

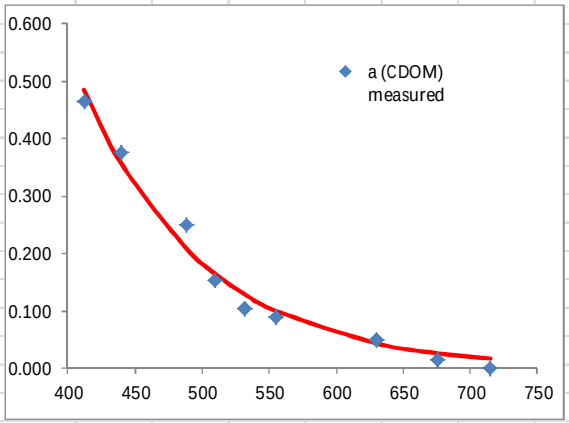

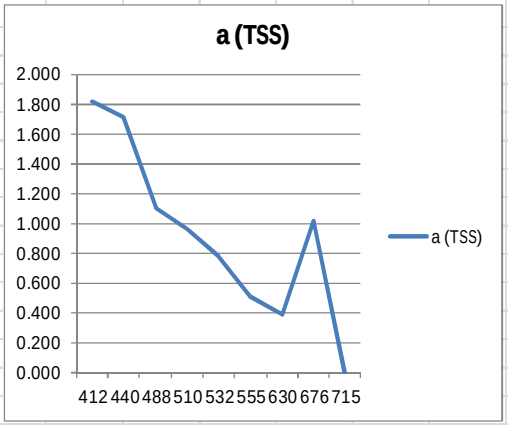

TTS decomposition (Lee, 1994)									
	rms err			0.01633	a_ss(440	0.54182	a_chl(44	1.16243	
					S_ss	0.01821			
	a (TSS) n	a (TSS) n	residue		a (phyto	a (sedim	a (phyto	a0	a1
412	1.823	1.82827	0.006	3.2E-05	0.920	0.90216	0.92611	0.795	0.0113
440	1.717	1.70426	-0.013	0.00017	1.175	0.54182	1.16243	1	0
488	1.105	1.11312	0.008	7.1E-05	0.879	0.22608	0.88703	0.7598	0.0218
510	0.964	0.96996	0.006	3.2E-05	0.813	0.15146	0.8185	0.6911	0.0865
532	0.783	0.76422	-0.019	0.00035	0.681	0.10147	0.66275	0.5557	0.0959
555	0.517	0.52425	0.007	4.6E-05	0.451	0.06675	0.45751	0.3828	0.07155
630	0.387	0.42727	0.040	0.00159	0.370	0.01703	0.41024	0.3421	0.0718
676	1.017	1.00648	-0.010	0.0001	1.009	0.00737	0.99911	0.8362	0.1547
715	0.000	0.00362	0.004	1.3E-05	-0.004	0.00362	0	0	0

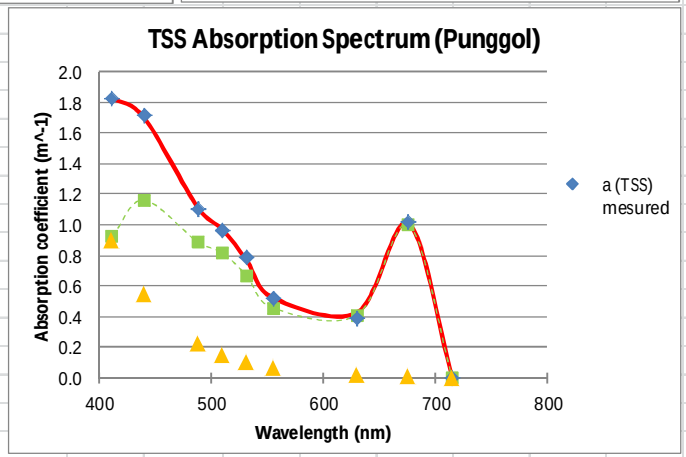

Ubin_E					uncorrected		corrected		**Scattering slope**				b0	9.54075	n	-0.4383	rms	0.188
	c (total)	c (CDOM)	c (TSS)	a (total)	a (CDOM)	a (TSS)	a (CDOM)	a (TSS)	b (TSS)	b_model	residue	residue^2						
412	12.401	0.279	12.121	1.970	0.408	1.562	0.408	1.562	10.559	10.872	-0.313	0.098						
440	11.894	0.262	11.632	1.440	0.353	1.087	0.330	1.110	10.522	10.563	-0.041	0.002						
488	11.171	0.262	10.909	0.858	0.262	0.596	0.223	0.635	10.274	10.094	0.179	0.032						
510	10.892	0.288	10.604	0.657	0.183	0.474	0.149	0.508	10.096	9.901	0.195	0.038						
532	10.760	0.474	10.286	0.517	0.124	0.394	0.098	0.419	9.867	9.719	0.148	0.022						
555	10.235	0.180	10.055	0.359	0.104	0.256	0.095	0.264	9.791	9.541	0.250	0.062						
630	9.236	0.198	9.038	0.218	0.047	0.171	0.023	0.195	8.843	9.025	-0.182	0.033						
676	8.928	0.122	8.805	0.246	0.035	0.211	0.029	0.217	8.589	8.751	-0.162	0.026						
715	8.644	0.184	8.460	0.000	0.000	0.000	0.000	0.000	8.460	8.538	-0.078	0.006						

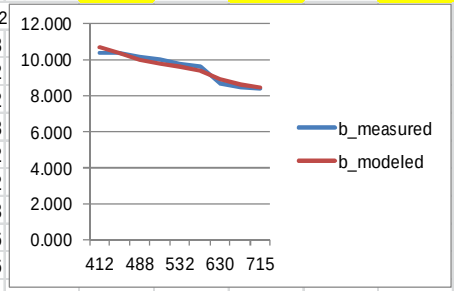

CDOM absorption

	rms err			0.0173
	G	0.316		
	Sg	0.011		
	a (CDOM)	a (CDOM)	residue	
412	0.408	0.42354	0.016	0.00025
440	0.330	0.3156	-0.014	0.0002
488	0.223	0.1906	-0.032	0.00104
510	0.149	0.15126	0.002	4.7E-06
532	0.098	0.12005	0.022	0.00047
555	0.095	0.09428	-0.001	8E-07
630	0.023	0.04287	0.020	0.00041
676	0.029	0.02644	-0.003	8.2E-06
715	0.000	0.01755	0.018	########

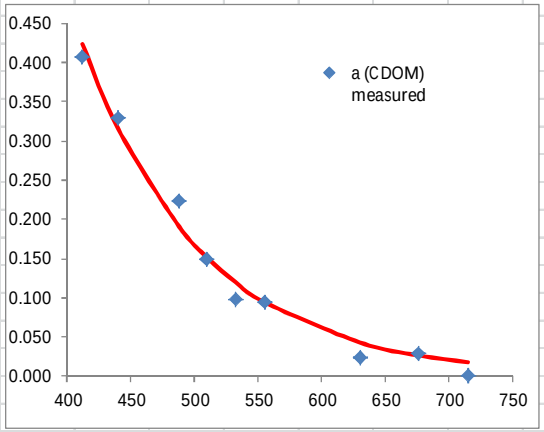

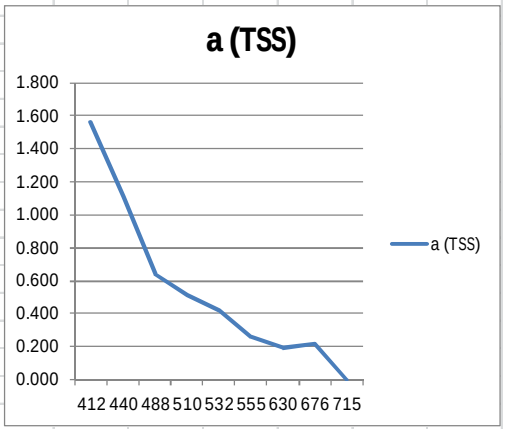

TTS decomposition (Lee, 1994)

	rms err			0.03621	a_ss(440	0.88639	a_chl(44	0.28262	
					S_ss	0.01384			
	a (TSS) m	a (TSS) m	residue		a (phyto)	a (sedime	a (phytop	a0	a1
412	1.562	1.52662	-0.035	0.001	0.256	1.30597	0.22065	0.795	0.0113
440	1.110	1.16901	0.059	0.00344	0.224	0.88639	0.28262	1	0
488	0.635	0.66309	0.028	0.00078	0.179	0.45613	0.20695	0.7598	0.0218
510	0.508	0.50083	-0.007	5E-05	0.171	0.33639	0.16443	0.6911	0.0865
532	0.419	0.3709	-0.048	0.0023	0.171	0.24809	0.12281	0.5557	0.0959
555	0.264	0.26309	-0.001	1E-06	0.084	0.18045	0.08264	0.3828	0.07155
630	0.195	0.13495	-0.060	0.0036	0.131	0.0639	0.07105	0.3421	0.0718
676	0.217	0.2149	-0.002	3E-06	0.183	0.03381	0.18109	0.8362	0.1547
715	0.000	0.01971	0.020	0.00039	-0.020	0.01971	0	0	0

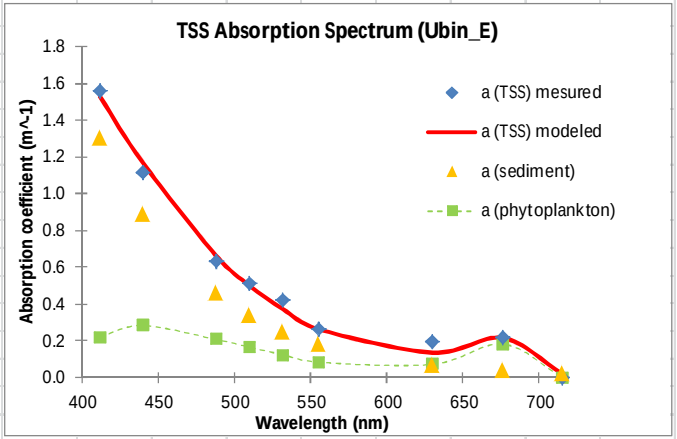

Ubin_N					uncorrected		corrected		**Scattering slope**				b0	8.11052	n	-0.9574	rms	0.173
	c (total)	c (CDOM)	c (TSS)	a (total)	a (CDOM)	a (TSS)	a (CDOM)	a (TSS)	b (TSS)	b_model	residue	residue^2						
412	11.772	0.330	11.442	1.346	0.601	0.746	0.424	0.922	10.535	10.788	-0.253	0.064						
440	10.994	0.292	10.702	0.897	0.448	0.450	0.308	0.589	10.127	10.130	-0.002	0.000						
488	9.904	0.273	9.631	0.467	0.329	0.138	0.179	0.288	9.358	9.174	0.184	0.034						
510	9.495	0.292	9.203	0.321	0.286	0.034	0.103	0.218	9.000	8.794	0.205	0.042						
532	9.249	0.470	8.778	0.325	0.235	0.090	0.086	0.238	8.555	8.446	0.109	0.012						
555	8.593	0.177	8.415	0.232	0.142	0.090	0.056	0.176	8.254	8.111	0.144	0.021						
630	7.246	0.176	7.070	0.217	0.065	0.153	0.023	0.194	6.891	7.184	-0.293	0.086						
676	6.874	0.112	6.761	0.180	0.146	0.034	0.007	0.172	6.604	6.715	-0.111	0.012						
715	6.530	0.163	6.367	0.000	0.208	-0.208	0.000	0.000	6.367	6.364	0.003	0.000						

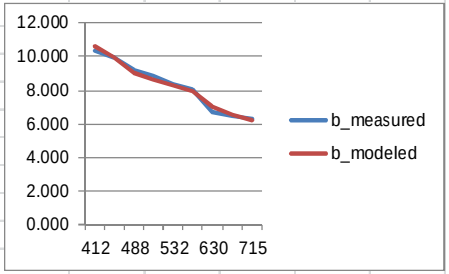

CDOM absorption

	rms err			0.03726
	G	0.341		
	Sg	0.010		
	a (CDOM)	a (CDOM)	residue	
412	0.424	0.45563	0.031	0.00097
440	0.308	0.34095	0.033	0.0011
488	0.179	0.20741	0.029	0.00082
510	0.103	0.16516	0.062	0.00388
532	0.086	0.13151	0.045	0.00203
555	0.056	0.10364	0.047	0.00223
630	0.023	0.04767	0.024	0.00059
676	0.007	0.02961	0.022	0.00049
715	0.000	0.01977	0.020	########

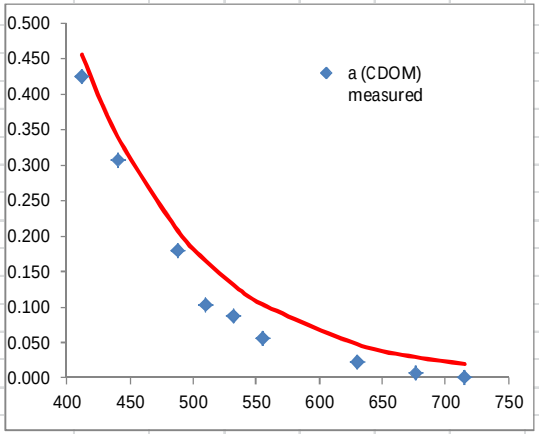

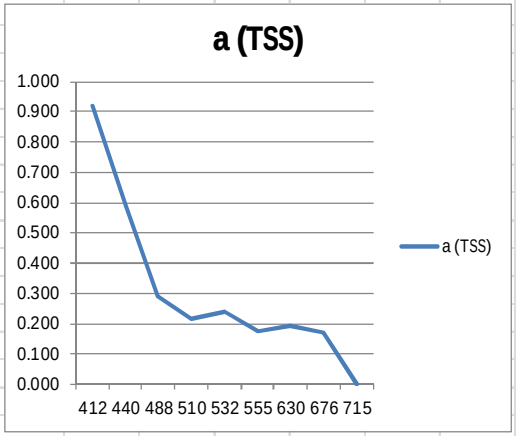

TTS decomposition (Lee, 1994)

	rms err			0.05243	a_ss(440	0.23638	a_chl(44	0.33869		
					S_ss	0.03563				
	a (TSS) m	a (TSS) m	residue		a (phyto)	a (sedime	a (phytop	a0	a1	
412	0.922	0.90623	-0.016	0.00024	0.281	0.64111	0.26511	0.795	0.0113	
440	0.589	0.57507	-0.014	0.00021	0.353	0.23638	0.33869	1	0	
488	0.288	0.29208	0.004	1.5E-05	0.245	0.04273	0.24934	0.7598	0.0218	
510	0.218	0.22187	0.004	1.8E-05	0.198	0.01951	0.20236	0.6911	0.0865	
532	0.238	0.16196	-0.076	0.00579	0.229	0.00891	0.15305	0.5557	0.0959	
555	0.176	0.10735	-0.069	0.0047	0.172	0.00393	0.10342	0.3828	0.07155	
630	0.194	0.08982	-0.104	0.01084	0.194	0.00027	0.08954	0.3421	0.0718	
676	0.172	0.22655	0.054	0.00294	0.172	5.3E-05	0.2265	0.8362	0.1547	
715	0.000	1.3E-05	0.000	7.7E-08	0.000	1.3E-05	0	0	0	

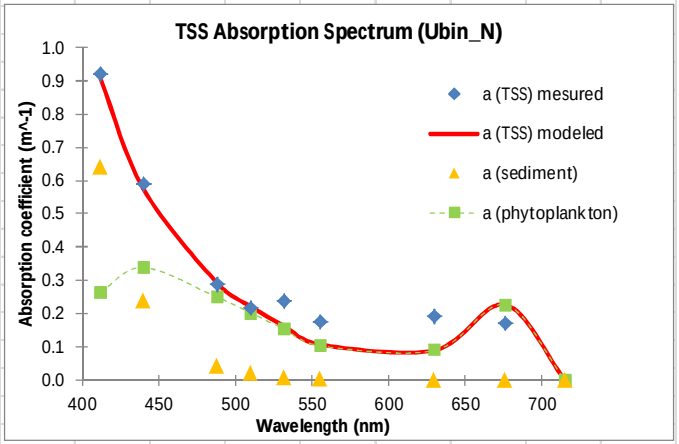

LCK					uncorrected		corrected		Scattering slope				b0	5.32705	n	-0.47482	rms	0.202
	c (total)	c (CDOM)	c (TSS)	a (total)	a (CDOM)	a (TSS)	a (CDOM)	a (TSS)	b (TSS)	b_model	residue	residue^2						
412	7.674	0.735	6.939	2.075	0.968	1.107	0.968	1.107	5.832	6.137	-0.305	0.093						
440	7.221	0.548	6.673	1.563	0.844	0.719	0.791	0.772	5.902	5.948	-0.046	0.002						
488	6.668	0.402	6.266	0.889	0.622	0.267	0.527	0.362	5.904	5.663	0.241	0.058						
510	6.495	0.394	6.101	0.671	0.436	0.235	0.357	0.314	5.787	5.545	0.242	0.058						
532	6.470	0.544	5.925	0.570	0.295	0.275	0.235	0.336	5.590	5.435	0.155	0.024						
555	5.988	0.236	5.752	0.507	0.227	0.280	0.197	0.310	5.443	5.327	0.116	0.013						
630	5.261	0.196	5.065	0.367	0.128	0.239	0.085	0.282	4.783	5.016	-0.233	0.054						
676	5.105	0.126	4.978	0.452	0.094	0.358	0.079	0.373	4.606	4.851	-0.245	0.060						
715	4.957	0.161	4.795	0.000	0.000	0.000	0.000	0.000	4.795	4.723	0.072	0.005						

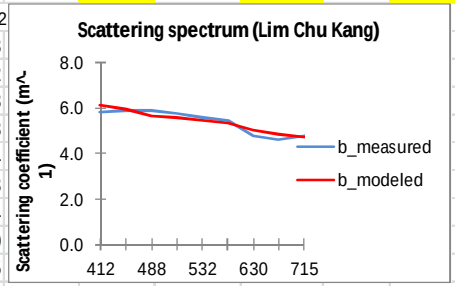

CDOM absorption

	rms err			0.03968
	G	0.750		
	Sg	0.010		
	a (CDOM)	a (CDOM)	residue	
412	0.968	1.00685	0.039	0.00152
440	0.791	0.75045	-0.040	0.00163
488	0.527	0.45343	-0.073	0.00537
510	0.357	0.35993	0.003	9.7E-06
532	0.235	0.28571	0.051	0.0026
555	0.197	0.22443	0.027	0.00075
630	0.085	0.10214	0.017	0.00029
676	0.079	0.06302	-0.016	0.00026
715	0.000	0.04185	0.042	########

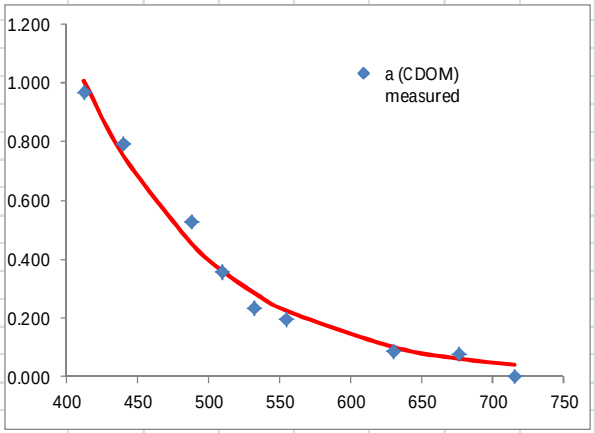

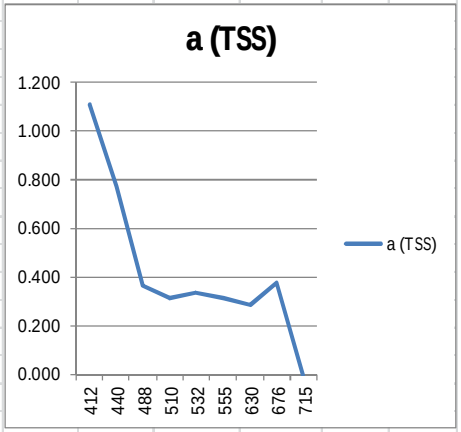

TTS decomposition (Lee, 1994)

	rms err			0.06732	a_ss(440	0.18488	a_chl(44	0.56223		
					S_ss	0.04587				
	a (TSS) mesu	TSS) mode	residue		a (phyto)	(sedimen	hytoplank	a0	a1	
412	1.107	1.1111	0.004	1.8E-05	0.439	0.66779	0.44331	0.795	0.0113	
440	0.772	0.74711	-0.025	0.00061	0.587	0.18488	0.56223	1	0	
488	0.362	0.44058	0.078	0.00612	0.342	0.02045	0.42012	0.7598	0.0218	
510	0.314	0.36802	0.054	0.00289	0.307	0.00746	0.36056	0.6911	0.0865	
532	0.336	0.28411	-0.052	0.00265	0.333	0.00272	0.28139	0.5557	0.0959	
555	0.310	0.19301	-0.117	0.01358	0.309	0.00095	0.19206	0.3828	0.07155	
630	0.282	0.16913	-0.113	0.01266	0.282	3E-05	0.1691	0.3421	0.0718	
676	0.373	0.42007	0.047	0.00225	0.373	3.7E-06	0.42006	0.8362	0.1547	
715	0.000	6.2E-07	0.000	3.8E-13	0.000	6.2E-07	0	0	0	

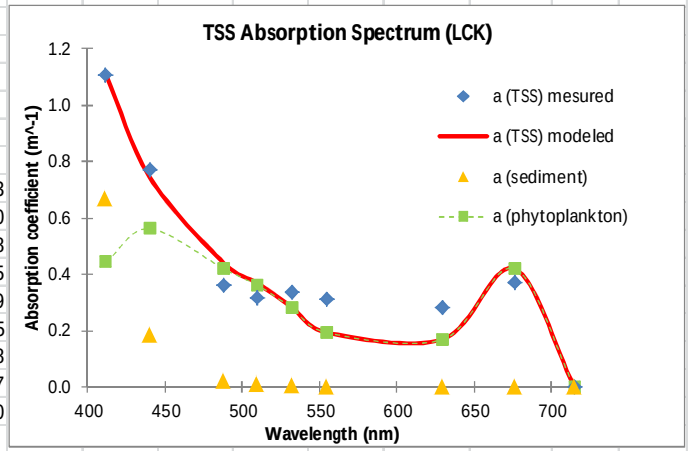

Bedok					uncorrected		corrected		**Scattering slope**				b0	7.09827	n	-0.724	rms	0.237
	c (total)	c (CDOM)	c (TSS)	a(total)	a (CDOM)	a (TSS)	a (CDOM)	a (TSS)	b (TSS)	b_model	residue	residue^2						
412	10.216	0.616	9.600	1.949	0.948	1.001	0.731	1.218	8.382	8.807	-0.426	0.181						
440	9.602	0.488	9.114	1.249	0.863	0.386	0.610	0.639	8.475	8.398	0.077	0.006						
488	8.762	0.404	8.358	0.650	0.716	-0.066	0.431	0.328	8.030	7.791	0.239	0.057						
510	8.460	0.406	8.054	0.456	0.586	-0.130	0.302	0.270	7.784	7.546	0.238	0.056						
532	8.250	0.566	7.684	0.454	0.455	-0.001	0.155	0.212	7.472	7.319	0.153	0.023						
555	7.759	0.275	7.484	0.340	0.349	-0.009	0.070	0.154	7.330	7.098	0.232	0.054						
630	6.729	0.260	6.468	0.307	0.210	0.096	0.005	0.302	6.167	6.476	-0.309	0.096						
676	6.436	0.194	6.242	0.265	0.113	0.152	0.002	0.263	5.979	6.154	-0.175	0.031						
715	6.103	0.235	5.868	0.000	0.000	0.000	0.000	0.000	5.868	5.909	-0.041	0.002						

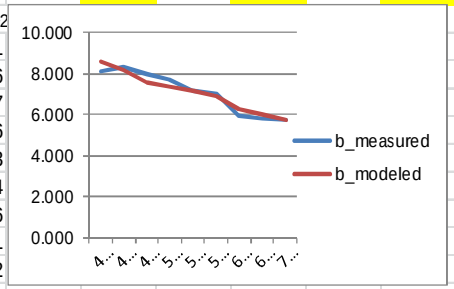

CDOM absorption				
	rms err			0.05914
	G	0.569		
	Sg	0.011		
	a (CDOM	a (CDOM	residue	
412	0.731	0.78248	0.052	0.00268
440	0.610	0.56893	-0.041	0.00165
488	0.431	0.32944	-0.102	0.0104
510	0.302	0.25646	-0.045	0.00206
532	0.155	0.19965	0.045	0.002
555	0.070	0.15366	0.084	0.00707
630	0.005	0.06543	0.060	0.00365
676	0.002	0.03876	0.037	0.00135
715	0.000	0.02487	0.025	########

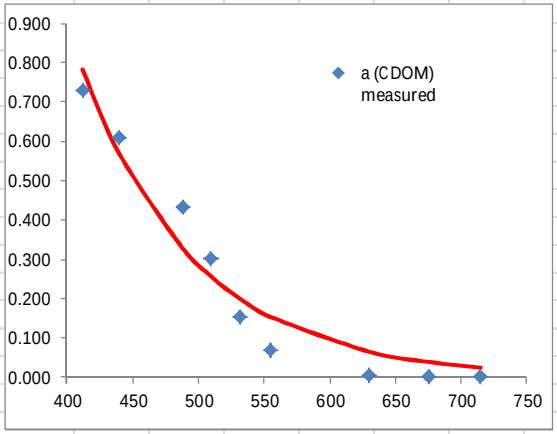

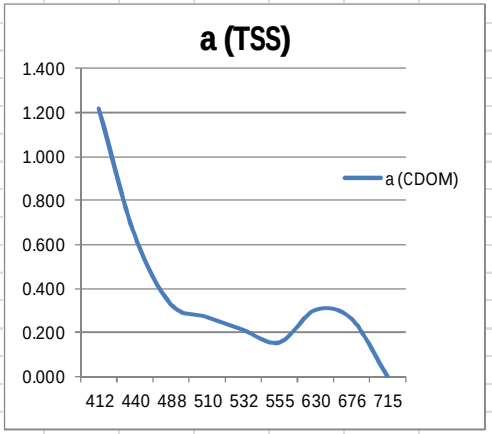

TTS decomposition (Lee, 1994)									
	rms err			0.0615	a_ss(440	0.18878	a_chl(44	0.44604	
					S_ss	0.05449			
	a (TSS) mesu	SS) mode	residue		a (phyto)	sedimen	ytoplank	a0	a1
412	1.218	1.21876	0.001	0.000	0.350	0.86822	0.35054	0.795	0.0113
440	0.639	0.63483	-0.004	1.7E-05	0.450	0.18878	0.44604	1	0
488	0.328	0.34486	0.017	0.00028	0.314	0.0138	0.33106	0.7598	0.0218
510	0.270	0.28128	0.011	0.00013	0.266	0.00416	0.27712	0.6911	0.0865
532	0.212	0.2146	0.003	6.7E-06	0.211	0.00125	0.21334	0.5557	0.0959
555	0.154	0.14535	-0.009	7.5E-05	0.154	0.00036	0.14499	0.3828	0.07155
630	0.302	0.12675	-0.175	0.03059	0.302	6E-06	0.12674	0.3421	0.0718
676	0.263	0.31729	0.054	0.00295	0.263	4.9E-07	0.31729	0.8362	0.1547
715	0.000	5.9E-08	0.000	3.4E-15	0.000	5.9E-08	0	0	0

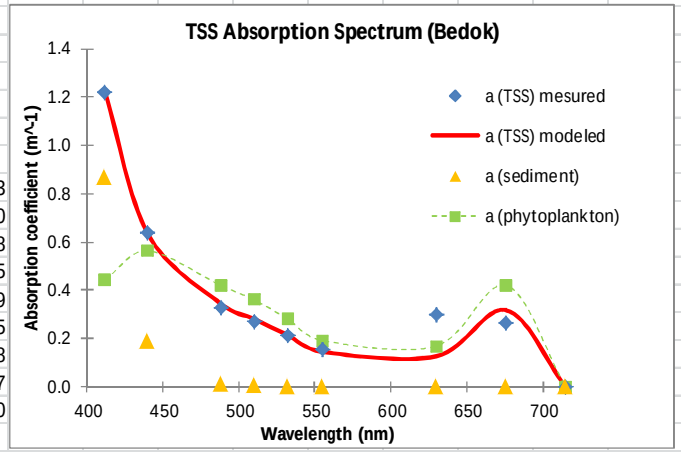

Sembawang					uncorrected		corrected		**Scattering slope**				b0	12.2863	n	-0.5039	rms	0.316
	c (total)	c (CDOM)	c (TSS)	a (total)	a (CDOM)	a (TSS)	a (CDOM)	a (TSS)	b (TSS)	b_model	residue	residue^2						
412	16.745	0.616	16.129	2.963	0.580	2.383	0.580	2.383	13.746	14.277	-0.531	0.282						
440	15.914	0.488	15.426	2.145	0.506	1.639	0.475	1.670	13.756	13.811	-0.055	0.003						
488	14.718	0.404	14.314	1.225	0.377	0.848	0.322	0.903	13.411	13.109	0.302	0.091						
510	14.285	0.406	13.879	0.900	0.256	0.644	0.204	0.696	13.183	12.821	0.362	0.131						
532	13.882	0.566	13.316	0.706	0.173	0.533	0.138	0.568	12.748	12.551	0.196	0.039						
555	13.301	0.275	13.026	0.438	0.137	0.301	0.122	0.316	12.710	12.286	0.423	0.179						
630	11.694	0.260	11.433	0.241	0.059	0.182	0.026	0.215	11.218	11.526	-0.308	0.095						
676	11.358	0.194	11.163	0.263	0.030	0.232	0.018	0.245	10.919	11.124	-0.205	0.042						
715	10.856	0.235	10.621	0.000	0.000	0.000	0.000	0.000	10.621	10.814	-0.193	0.037						

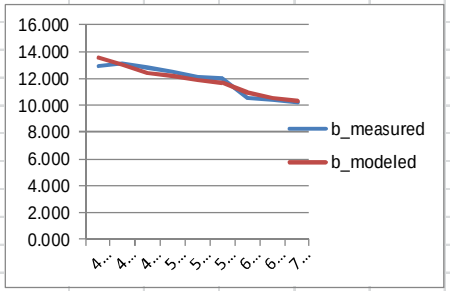

CDOM absorption

	rms err			0.02829
	G	0.449		
	Sg	0.011		
	a (CDOM)	a (CDOM)	residue	
412	0.580	0.6083	0.029	0.00082
440	0.475	0.44854	-0.026	0.00069
488	0.322	0.26606	-0.056	0.00311
510	0.204	0.20942	0.005	2.5E-05
532	0.138	0.16484	0.027	0.00074
555	0.122	0.12834	0.007	4.7E-05
630	0.026	0.05675	0.031	0.00097
676	0.018	0.0344	0.016	0.00027
715	0.000	0.02251	0.023	########

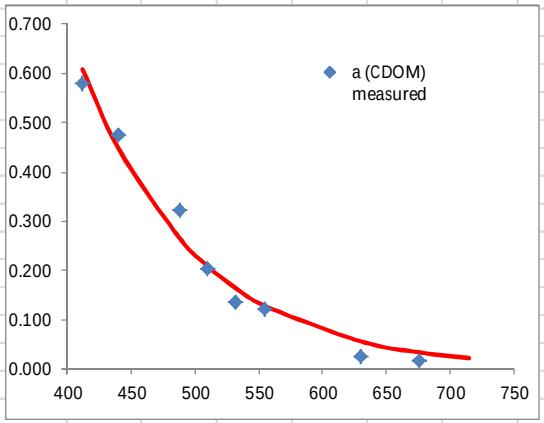

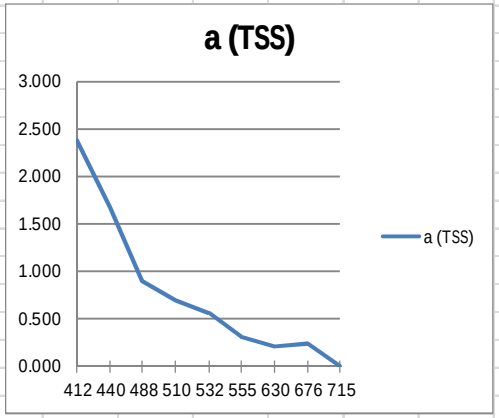

TTS decomposition (Lee, 1994)

	rms err			0.03605	a_ss(440	1.3954	a_chl(44	0.31891		
					S_ss	0.01476				
	a (TSS) m	a (TSS) m	residue		a (phyto)	(sedimen	a (phytop	a0	a1	
412	2.383	2.35865	-0.024	0.00059	0.274	2.10923	0.24942	0.795	0.0113	
440	1.670	1.71431	0.044	0.00195	0.275	1.3954	0.31891	1	0	
488	0.903	0.92161	0.018	0.00034	0.216	0.68724	0.23437	0.7598	0.0218	
510	0.696	0.68563	-0.010	0.0001	0.199	0.49675	0.18888	0.6911	0.0865	
532	0.568	0.50133	-0.067	0.00451	0.209	0.35905	0.14228	0.5557	0.0959	
555	0.316	0.35173	0.036	0.00128	0.060	0.25572	0.09601	0.3828	0.07155	
630	0.215	0.1675	-0.048	0.00227	0.131	0.08456	0.08294	0.3421	0.0718	
676	0.245	0.2532	0.009	7.3E-05	0.202	0.04289	0.21031	0.8362	0.1547	
715	0.000	0.02413	0.024	0.00058	-0.024	0.02413	0	0	0	

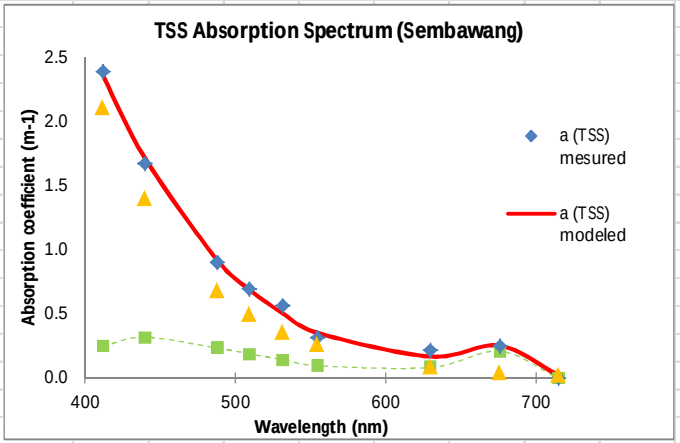

APPENDIX C: PARTICLE SIZE DISTRIBUTION (PSD)

size	radius (µm)	radius(m)	volume (µl/	volume (m³	particles/L	particles/m	Upp Lim (µ	Low Lim (µ	bin size diff	no of partic	logr	logn	cum volume
1.4	0.68	6.8E-07	2.62E-02	2.62E-05	1.986E+13	1.99E+16	1.48	1.25	2.3E-07	8.64E+22	-0.386	52.813	2.62E-05
1.6	0.8	0.0000008	4.42E-02	4.42E-05	2.061E+13	2.06E+16	1.74	1.48	2.6E-07	7.93E+22	-0.223	52.727	7.04E-05
1.9	0.945	9.45E-07	8.62E-02	8.62E-05	2.437E+13	2.44E+16	2.05	1.74	3.1E-07	7.86E+22	-0.057	52.719	1.57E-04
2.2	1.115	1.115E-06	1.64E-01	1.64E-04	2.82E+13	2.82E+16	2.42	2.05	3.7E-07	7.62E+22	0.109	52.688	3.20E-04
2.6	1.315	1.315E-06	2.60E-01	2.60E-04	2.728E+13	2.73E+16	2.86	2.42	4.4E-07	6.20E+22	0.274	52.481	5.80E-04
3.1	1.555	1.555E-06	2.80E-01	2.80E-04	1.778E+13	1.78E+16	3.38	2.86	5.2E-07	3.42E+22	0.441	51.886	8.60E-04
3.7	1.835	1.835E-06	2.57E-01	2.57E-04	9.92E+12	9.92E+15	3.98	3.38	0.0000006	1.65E+22	0.607	51.160	1.12E-03
4.3	2.165	2.165E-06	2.87E-01	2.87E-04	6.743E+12	6.74E+15	4.7	3.98	7.2E-07	9.37E+21	0.772	50.591	1.40E-03
5.1	2.555	2.555E-06	3.07E-01	3.07E-04	4.401E+12	4.40E+15	5.55	4.7	8.5E-07	5.18E+21	0.938	49.999	1.71E-03
6.0	3.015	3.015E-06	3.07E-01	3.07E-04	2.678E+12	2.68E+15	6.55	5.55	0.000001	2.68E+21	1.104	49.339	2.02E-03
7.1	3.555	3.555E-06	3.41E-01	3.41E-04	1.812E+12	1.81E+15	7.72	6.55	1.17E-06	1.55E+21	1.268	48.792	2.36E-03
8.4	4.195	4.195E-06	3.57E-01	3.57E-04	1.153E+12	1.15E+15	9.12	7.72	0.0000014	8.24E+20	1.434	48.160	2.72E-03
9.9	4.95	4.95E-06	4.16E-01	4.16E-04	8.181E+11	8.18E+14	10.8	9.12	1.68E-06	4.87E+20	1.599	47.635	3.13E-03
11.7	5.85	5.85E-06	0.5031411	5.03E-04	6E+11	6.00E+14	12.7	10.8	0.0000019	3.16E+20	1.766	47.202	3.63E-03
13.8	6.9	0.0000069	0.5669566	5.67E-04	4.12E+11	4.12E+14	15	12.7	0.0000023	1.79E+20	1.932	46.635	4.20E-03
16.3	8.15	8.15E-06	0.6082044	6.08E-04	2.682E+11	2.68E+14	17.7	15	0.0000027	9.93E+19	2.098	46.045	4.81E-03
19.2	9.6	0.0000096	0.62826	6.28E-04	1.695E+11	1.70E+14	20.9	17.7	0.0000032	5.30E+19	2.262	45.416	5.44E-03
22.7	11.35	1.135E-05	0.7315277	7.32E-04	1.194E+11	1.19E+14	24.6	20.9	0.0000037	3.23E+19	2.429	44.921	6.17E-03
26.7	13.35	1.335E-05	0.7099296	7.10E-04	7.123E+10	7.12E+13	29.1	24.6	0.0000045	1.58E+19	2.592	44.208	6.88E-03
31.6	15.8	0.0000158	0.6919747	6.92E-04	4.188E+10	4.19E+13	34.3	29.1	0.0000052	8.05E+18	2.760	43.533	7.57E-03
37.2	18.6	0.0000186	0.5320833	5.32E-04	1.974E+10	1.97E+13	40.5	34.3	0.0000062	3.18E+18	2.923	42.605	8.10E-03
43.9	21.95	2.195E-05	0.4147964	4.15E-04	9.364E+09	9.36E+12	47.7	40.5	0.0000072	1.30E+18	3.089	41.709	8.52E-03
51.9	25.95	2.595E-05	0.2946915	2.95E-04	4.026E+09	4.03E+12	56.3	47.7	8.6E-06	4.68E+17	3.256	40.688	8.81E-03
61.2	30.6	0.0000306	0.2466829	2.47E-04	2.055E+09	2.06E+12	66.5	56.3	0.0000102	2.02E+17	3.421	39.845	9.06E-03
72.2	36.1	0.0000361	0.2198853	2.20E-04	1.116E+09	1.12E+12	78.4	66.5	0.0000119	9.38E+16	3.586	39.080	9.28E-03
85.2	42.6	0.0000426	0.1978345	1.98E-04	610920243	6.11E+11	92.6	78.4	0.0000142	4.30E+16	3.752	38.301	9.48E-03
101.0	50.5	0.0000505	0.1489403	1.49E-04	276089231	2.76E+11	109	92.6	0.0000164	1.68E+16	3.922	37.362	9.63E-03
119.0	59.5	0.0000595	0.1125855	1.13E-04	127597702	1.28E+11	129	109	0.00002	6.38E+15	4.086	36.392	9.74E-03
140.0	70	0.00007	0.0813229	8.13E-05	56601815	5.66E+10	152	129	0.000023	2.46E+15	4.248	35.439	9.82E-03
165.0	82.5	0.0000825	0.061046	6.10E-05	25954158	2.60E+10	180	152	0.000028	9.27E+14	4.413	34.463	9.88E-03
195.0	97.5	0.0000975	0.0706015	7.06E-05	18184917	1.82E+10	212	180	0.000032	5.68E+14	4.580	33.974	9.95E-03
230.0	115	0.000115	0.0954121	9.54E-05	14976884	1.50E+10	250	212	0.000038	3.94E+14	4.745	33.608	1.00E-02

d50 calculation						
5.02E-03						
16.3	4.81E-03		mass	60	mg/L	
19.2	5.44E-03		volume	1.00E-02	m3/L	
	2.14E-04		density	**5.97E+03**	**mg/m3**	
	4.63E-08					
d50	**1.63E+01**					

Kranji19

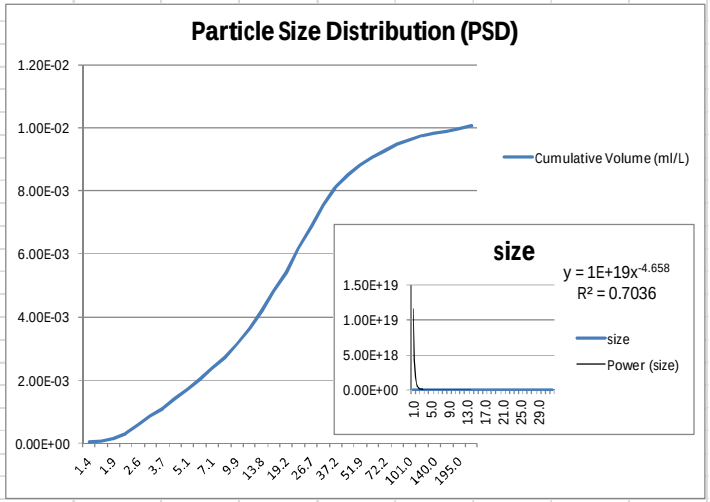

size	radius (µm)	radius(m)	volume (µl/	volume (m³	particles/L	particles/m	Upp Lim (µ	Low Lim (µ	bin size diff	no of partic	logr	logn	cum volume
1.4	0.68	6.8E-07	6.34E-03	6.34E-06	4.811E+12	4.81E+15	1.48	1.25	2.3E-07	2.09E+22	-0.386	51.395	6.34E-06
1.6	0.8	0.0000008	1.38E-02	1.38E-05	6.424E+12	6.42E+15	1.74	1.48	2.6E-07	2.47E+22	-0.223	51.561	2.01E-05
1.9	0.945	9.45E-07	3.64E-02	3.64E-05	1.029E+13	1.03E+16	2.05	1.74	3.1E-07	3.32E+22	-0.057	51.856	5.65E-05
2.2	1.115	1.115E-06	9.37E-02	9.37E-05	1.614E+13	1.61E+16	2.42	2.05	3.7E-07	4.36E+22	0.109	52.130	1.50E-04
2.6	1.315	1.315E-06	1.86E-01	1.86E-04	1.957E+13	1.96E+16	2.86	2.42	4.4E-07	4.45E+22	0.274	52.149	3.37E-04
3.1	1.555	1.555E-06	2.21E-01	2.21E-04	1.405E+13	1.41E+16	3.38	2.86	5.2E-07	2.70E+22	0.441	51.651	5.58E-04
3.7	1.835	1.835E-06	2.05E-01	2.05E-04	7.909E+12	7.91E+15	3.98	3.38	0.0000006	1.32E+22	0.607	50.933	7.63E-04
4.3	2.165	2.165E-06	2.39E-01	2.39E-04	5.614E+12	5.61E+15	4.7	3.98	7.2E-07	7.80E+21	0.772	50.408	1.00E-03
5.1	2.555	2.555E-06	2.66E-01	2.66E-04	3.804E+12	3.80E+15	5.55	4.7	8.5E-07	4.48E+21	0.938	49.853	1.27E-03
6.0	3.015	3.015E-06	2.75E-01	2.75E-04	2.399E+12	2.40E+15	6.55	5.55	0.000001	2.40E+21	1.104	49.229	1.54E-03
7.1	3.555	3.555E-06	3.21E-01	3.21E-04	1.705E+12	1.70E+15	7.72	6.55	1.17E-06	1.46E+21	1.268	48.731	1.86E-03
8.4	4.195	4.195E-06	3.46E-01	3.46E-04	1.12E+12	1.12E+15	9.12	7.72	0.0000014	8.00E+20	1.434	48.131	2.21E-03
9.9	4.95	4.95E-06	4.18E-01	4.18E-04	8.222E+11	8.22E+14	10.8	9.12	1.68E-06	4.89E+20	1.599	47.640	2.63E-03
11.7	5.85	5.85E-06	0.5038192	5.04E-04	6.008E+11	6.01E+14	12.7	10.8	0.0000019	3.16E+20	1.766	47.203	3.13E-03
13.8	6.9	0.0000069	0.5600848	5.60E-04	4.07E+11	4.07E+14	15	12.7	0.0000023	1.77E+20	1.932	46.622	3.69E-03
16.3	8.15	8.15E-06	0.5798127	5.80E-04	2.557E+11	2.56E+14	17.7	15	0.0000027	9.47E+19	2.098	45.997	4.27E-03
19.2	9.6	0.0000096	0.5958788	5.96E-04	1.608E+11	1.61E+14	20.9	17.7	0.0000032	5.02E+19	2.262	45.363	4.87E-03
22.7	11.35	1.135E-05	0.7206389	7.21E-04	1.177E+11	1.18E+14	24.6	20.9	0.0000037	3.18E+19	2.429	44.906	5.59E-03
26.7	13.35	1.335E-05	0.7309531	7.31E-04	7.334E+10	7.33E+13	29.1	24.6	0.0000045	1.63E+19	2.592	44.238	6.32E-03
31.6	15.8	0.0000158	0.7927726	7.93E-04	4.798E+10	4.80E+13	34.3	29.1	0.0000052	9.23E+18	2.760	43.669	7.11E-03
37.2	18.6	0.0000186	0.6548926	6.55E-04	2.43E+10	2.43E+13	40.5	34.3	0.0000062	3.92E+18	2.923	42.812	7.77E-03
43.9	21.95	2.195E-05	0.5497616	5.50E-04	1.241E+10	1.24E+13	47.7	40.5	0.0000072	1.72E+18	3.089	41.991	8.32E-03
51.9	25.95	2.595E-05	0.4090557	4.09E-04	5.588E+09	5.59E+12	56.3	47.7	8.6E-06	6.50E+17	3.256	41.015	8.73E-03
61.2	30.6	0.0000306	0.3377669	3.38E-04	2.814E+09	2.81E+12	66.5	56.3	0.0000102	2.76E+17	3.421	40.159	9.06E-03
72.2	36.1	0.0000361	0.2744684	2.74E-04	1.393E+09	1.39E+12	78.4	66.5	0.0000119	1.17E+17	3.586	39.301	9.34E-03
85.2	42.6	0.0000426	0.2265695	2.27E-04	699655293	7.00E+11	92.6	78.4	0.0000142	4.93E+16	3.752	38.436	9.56E-03
101.0	50.5	0.0000505	0.1631071	1.63E-04	302350095	3.02E+11	109	92.6	0.0000164	1.84E+16	3.922	37.453	9.73E-03
119.0	59.5	0.0000595	0.1196323	1.20E-04	135584173	1.36E+11	129	109	0.00002	6.78E+15	4.086	36.453	9.85E-03
140.0	70	0.00007	0.082272	8.23E-05	57262376	5.73E+10	152	129	0.000023	2.49E+15	4.248	35.451	9.93E-03
165.0	82.5	0.0000825	0.0551589	5.52E-05	23451185	2.35E+10	180	152	0.000028	8.38E+14	4.413	34.361	9.98E-03
195.0	97.5	0.0000975	0.0450096	4.50E-05	11593192	1.16E+10	212	180	0.000032	3.62E+14	4.580	33.523	1.00E-02
230.0	115	0.000115	0.0404475	4.04E-05	6349054.7	6.35E+09	250	212	0.000038	1.67E+14	4.745	32.749	1.01E-02

d50 calculation

5.03E-03	
19.2	4.87E-03
22.7	5.59E-03
	1.68E-04
	3.45E-08
d50	**1.92E+01**

mass	49	mg/L
volume	1.01E-02	m3/L
density	**4.87E+03**	**mg/m3**

Kranji11

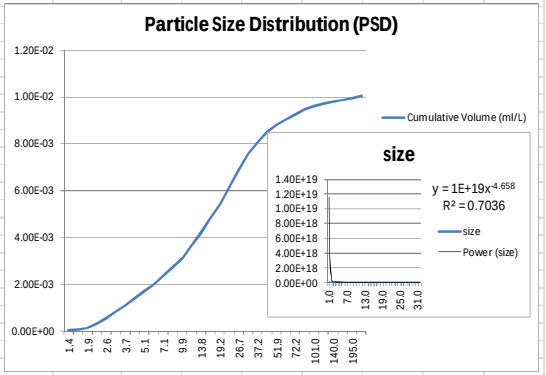

size	radius (µm)	radius(m)	volume (µl/	volume (m³	particles/L	particles/m	Upp Lim (µ	Low Lim (µ	bin size diff	no of partic	logr	logn	cum volume
1.4	0.68	6.8E-07	1.46E-02	1.46E-05	1.106E+13	1.11E+16	1.48	1.25	2.3E-07	4.81E+22	-0.386	52.227	1.46E-05
1.6	0.8	0.0000008	2.76E-02	2.76E-05	1.288E+13	1.29E+16	1.74	1.48	2.6E-07	4.95E+22	-0.223	52.257	4.22E-05
1.9	0.945	9.45E-07	6.08E-02	6.08E-05	1.721E+13	1.72E+16	2.05	1.74	3.1E-07	5.55E+22	-0.057	52.371	1.03E-04
2.2	1.115	1.115E-06	1.27E-01	1.27E-04	2.189E+13	2.19E+16	2.42	2.05	3.7E-07	5.92E+22	0.109	52.435	2.30E-04
2.6	1.315	1.315E-06	2.14E-01	2.14E-04	2.242E+13	2.24E+16	2.86	2.42	4.4E-07	5.09E+22	0.274	52.285	4.44E-04
3.1	1.555	1.555E-06	2.30E-01	2.30E-04	1.463E+13	1.46E+16	3.38	2.86	5.2E-07	2.81E+22	0.441	51.691	6.74E-04
3.7	1.835	1.835E-06	2.08E-01	2.08E-04	8.019E+12	8.02E+15	3.98	3.38	0.0000006	1.34E+22	0.607	50.947	8.82E-04
4.3	2.165	2.165E-06	2.35E-01	2.35E-04	5.535E+12	5.54E+15	4.7	3.98	7.2E-07	7.69E+21	0.772	50.394	1.12E-03
5.1	2.555	2.555E-06	2.70E-01	2.70E-04	3.859E+12	3.86E+15	5.55	4.7	8.5E-07	4.54E+21	0.938	49.867	1.39E-03
6.0	3.015	3.015E-06	3.05E-01	3.05E-04	2.66E+12	2.66E+15	6.55	5.55	0.000001	2.66E+21	1.104	49.333	1.69E-03
7.1	3.555	3.555E-06	4.03E-01	4.03E-04	2.142E+12	2.14E+15	7.72	6.55	1.17E-06	1.83E+21	1.268	48.959	2.09E-03
8.4	4.195	4.195E-06	5.12E-01	5.12E-04	1.656E+12	1.66E+15	9.12	7.72	0.0000014	1.18E+21	1.434	48.522	2.61E-03
9.9	4.95	4.95E-06	6.97E-01	6.97E-04	1.372E+12	1.37E+15	10.8	9.12	1.68E-06	8.17E+20	1.599	48.152	3.30E-03
11.7	5.85	5.85E-06	0.8776219	8.78E-04	1.047E+12	1.05E+15	12.7	10.8	0.0000019	5.51E+20	1.766	47.758	4.18E-03
13.8	6.9	0.0000069	0.9365686	9.37E-04	6.806E+11	6.81E+14	15	12.7	0.0000023	2.96E+20	1.932	47.137	5.12E-03
16.3	8.15	8.15E-06	0.8798926	8.80E-04	3.88E+11	3.88E+14	17.7	15	0.0000027	1.44E+20	2.098	46.414	6.00E-03
19.2	9.6	0.0000096	0.7893704	7.89E-04	2.13E+11	2.13E+14	20.9	17.7	0.0000032	6.66E+19	2.262	45.645	6.79E-03
22.7	11.35	1.135E-05	0.7890547	7.89E-04	1.288E+11	1.29E+14	24.6	20.9	0.0000037	3.48E+19	2.429	44.997	7.58E-03
26.7	13.35	1.335E-05	0.682275	6.82E-04	6.846E+10	6.85E+13	29.1	24.6	0.0000045	1.52E+19	2.592	44.169	8.26E-03
31.6	15.8	0.0000158	0.6108575	6.11E-04	3.697E+10	3.70E+13	34.3	29.1	0.0000052	7.11E+18	2.760	43.408	8.87E-03
37.2	18.6	0.0000186	0.442511	4.43E-04	1.642E+10	1.64E+13	40.5	34.3	0.0000062	2.65E+18	2.923	42.420	9.31E-03
43.9	21.95	2.195E-05	0.313966	3.14E-04	7.087E+09	7.09E+12	47.7	40.5	0.0000072	9.84E+17	3.089	41.431	9.63E-03
51.9	25.95	2.595E-05	0.205183	2.05E-04	2.803E+09	2.80E+12	56.3	47.7	8.6E-06	3.26E+17	3.256	40.326	9.83E-03
61.2	30.6	0.0000306	0.1448541	1.45E-04	1.207E+09	1.21E+12	66.5	56.3	0.0000102	1.18E+17	3.421	39.312	9.98E-03
72.2	36.1	0.0000361	0.1064714	1.06E-04	540284683	5.40E+11	78.4	66.5	0.0000119	4.54E+16	3.586	38.354	1.01E-02
85.2	42.6	0.0000426	0.0805462	8.05E-05	248729792	2.49E+11	92.6	78.4	0.0000142	1.75E+16	3.752	37.402	1.02E-02
101.0	50.5	0.0000505	0.0541642	5.42E-05	100403667	1.00E+11	109	92.6	0.0000164	6.12E+15	3.922	36.351	1.02E-02
119.0	59.5	0.0000595	0.03781	3.78E-05	42851665	4.29E+10	129	109	0.00002	2.14E+15	4.086	35.301	1.03E-02
140.0	70	0.00007	0.0255475	2.55E-05	17781388	1.78E+10	152	129	0.000023	7.73E+14	4.248	34.281	1.03E-02
165.0	82.5	0.0000825	0.0174545	1.75E-05	7420925.2	7.42E+09	180	152	0.000028	2.65E+14	4.413	33.211	1.03E-02
195.0	97.5	0.0000975	0.0164626	1.65E-05	4240294	4.24E+09	212	180	0.000032	1.33E+14	4.580	32.518	1.03E-02
230.0	115	0.000115	0.0215454	2.15E-05	3381996.8	3.38E+09	250	212	0.000038	8.90E+13	4.745	32.120	1.03E-02

d50 calculation

5.17E-03	
13.8	5.12E-03
16.3	6.00E-03
	4.99E-05
	1.76E-08
d50	**1.38E+01**

mass	47	mg/L
volume	1.03E-02	m3/L
density	**4.55E+03**	**mg/m3**

Kranji04

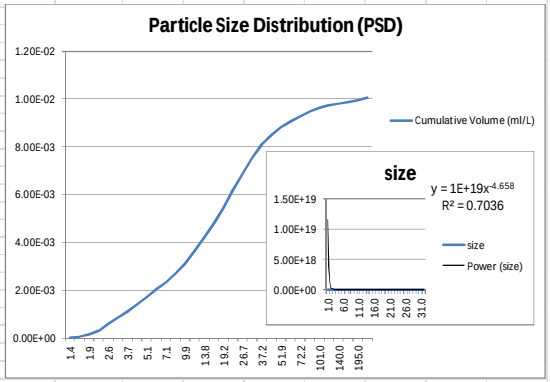

size	radius (µm)	radius(m)	volume (µl/	volume (m³	particles/L	particles/m	Upp Lim (µ	Low Lim (µ	bin size diff	no of partic	logr	logn	cum volume
1.4	0.68	6.8E-07	2.29E-02	2.29E-05	1.737E+13	1.74E+16	1.48	1.25	2.3E-07	7.55E+22	-0.386	52.679	2.29E-05
1.6	0.8	0.0000008	3.25E-02	3.25E-05	1.514E+13	1.51E+16	1.74	1.48	2.6E-07	5.82E+22	-0.223	52.419	5.54E-05
1.9	0.945	9.45E-07	5.08E-02	5.08E-05	1.438E+13	1.44E+16	2.05	1.74	3.1E-07	4.64E+22	-0.057	52.192	1.06E-04
2.2	1.115	1.115E-06	8.45E-02	8.45E-05	1.455E+13	1.45E+16	2.42	2.05	3.7E-07	3.93E+22	0.109	52.026	1.91E-04
2.6	1.315	1.315E-06	1.29E-01	1.29E-04	1.352E+13	1.35E+16	2.86	2.42	4.4E-07	3.07E+22	0.274	51.779	3.19E-04
3.1	1.555	1.555E-06	1.71E-01	1.71E-04	1.088E+13	1.09E+16	3.38	2.86	5.2E-07	2.09E+22	0.441	51.395	4.91E-04
3.7	1.835	1.835E-06	2.15E-01	2.15E-04	8.295E+12	8.30E+15	3.98	3.38	0.0000006	1.38E+22	0.607	50.981	7.05E-04
4.3	2.165	2.165E-06	3.08E-01	3.08E-04	7.248E+12	7.25E+15	4.7	3.98	7.2E-07	1.01E+22	0.772	50.664	1.01E-03
5.1	2.555	2.555E-06	4.13E-01	4.13E-04	5.906E+12	5.91E+15	5.55	4.7	8.5E-07	6.95E+21	0.938	50.293	1.43E-03
6.0	3.015	3.015E-06	5.20E-01	5.20E-04	4.525E+12	4.53E+15	6.55	5.55	0.000001	4.53E+21	1.104	49.864	1.95E-03
7.1	3.555	3.555E-06	6.64E-01	6.64E-04	3.529E+12	3.53E+15	7.72	6.55	1.17E-06	3.02E+21	1.268	49.458	2.61E-03
8.4	4.195	4.195E-06	7.56E-01	7.56E-04	2.443E+12	2.44E+15	9.12	7.72	0.0000014	1.75E+21	1.434	48.911	3.37E-03
9.9	4.95	4.95E-06	8.63E-01	8.63E-04	1.699E+12	1.70E+15	10.8	9.12	1.68E-06	1.01E+21	1.599	48.366	4.23E-03
11.7	5.85	5.85E-06	0.9101453	9.10E-04	1.085E+12	1.09E+15	12.7	10.8	0.0000019	5.71E+20	1.766	47.794	5.14E-03
13.8	6.9	0.0000069	0.8552463	8.55E-04	6.215E+11	6.22E+14	15	12.7	0.0000023	2.70E+20	1.932	47.046	5.99E-03
16.3	8.15	8.15E-06	0.7016967	7.02E-04	3.094E+11	3.09E+14	17.7	15	0.0000027	1.15E+20	2.098	46.188	6.70E-03
19.2	9.6	0.0000096	0.5423576	5.42E-04	1.463E+11	1.46E+14	20.9	17.7	0.0000032	4.57E+19	2.262	45.269	7.24E-03
22.7	11.35	1.135E-05	0.4387974	4.39E-04	7.165E+10	7.16E+13	24.6	20.9	0.0000037	1.94E+19	2.429	44.410	7.68E-03
26.7	13.35	1.335E-05	0.3095129	3.10E-04	3.106E+10	3.11E+13	29.1	24.6	0.0000045	6.90E+18	2.592	43.378	7.99E-03
31.6	15.8	0.0000158	0.2218347	2.22E-04	1.343E+10	1.34E+13	34.3	29.1	0.0000052	2.58E+18	2.760	42.395	8.21E-03
37.2	18.6	0.0000186	0.139417	1.39E-04	5.172E+09	5.17E+12	40.5	34.3	0.0000062	8.34E+17	2.923	41.265	8.35E-03
43.9	21.95	2.195E-05	0.0874472	8.74E-05	1.974E+09	1.97E+12	47.7	40.5	0.0000072	2.74E+17	3.089	40.153	8.44E-03
51.9	25.95	2.595E-05	0.053553	5.36E-05	731615931	7.32E+11	56.3	47.7	8.6E-06	8.51E+16	3.256	38.982	8.49E-03
61.2	30.6	0.0000306	0.0337253	3.37E-05	280997879	2.81E+11	66.5	56.3	0.0000102	2.75E+16	3.421	37.855	8.52E-03
72.2	36.1	0.0000361	0.0230875	2.31E-05	117156406	1.17E+11	78.4	66.5	0.0000119	9.85E+15	3.586	36.826	8.55E-03
85.2	42.6	0.0000426	0.0164835	1.65E-05	50901572	5.09E+10	92.6	78.4	0.0000142	3.58E+15	3.752	35.815	8.56E-03
101.0	50.5	0.0000505	0.0128941	1.29E-05	23901673	2.39E+10	109	92.6	0.0000164	1.46E+15	3.922	34.915	8.57E-03
119.0	59.5	0.0000595	0.0116164	1.16E-05	13165371	1.32E+10	129	109	0.00002	6.58E+14	4.086	34.121	8.59E-03
140.0	70	0.00007	0.0151504	1.52E-05	10544859	1.05E+10	152	129	0.000023	4.58E+14	4.248	33.759	8.60E-03
165.0	82.5	0.0000825	0.0350467	3.50E-05	14900336	1.49E+10	180	152	0.000028	5.32E+14	4.413	33.908	8.64E-03
195.0	97.5	0.0000975	0.1362929	1.36E-04	35105152	3.51E+10	212	180	0.000032	1.10E+15	4.580	34.631	8.77E-03
230.0	115	0.000115	0.7994199	7.99E-04	125485298	1.25E+11	250	212	0.000038	3.30E+15	4.745	35.733	9.57E-03

d50 calculation

4.79E-03	
9.9	4.23E-03
11.7	5.14E-03
	5.57E-04
	2.82E-07
d50	**9.90E+00**

Poly Marina

mass	73.3	mg/L
volume	9.57E-03	m3/L
density	**7.66E+03**	**mg/m3**

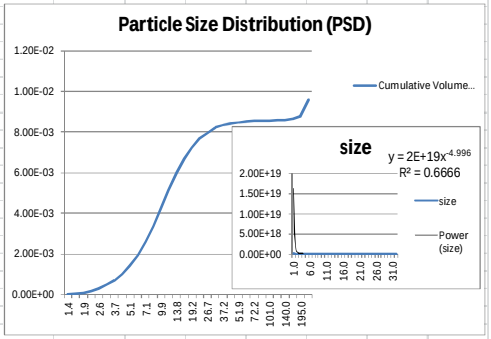

size	radius (µm)	radius(m)	volume (µl/	volume (m³	particles/L	particles/m	Upp Lim (µ	Low Lim (µ	bin size diff	no of partic	logr	logn	cum volume
1.4	0.68	6.8E-07	1.62E-01	1.62E-04	1.232E+14	1.23E+17	1.48	1.25	2.3E-07	5.36E+23	-0.386	54.638	1.62E-04
1.6	0.8	0.0000008	2.04E-01	2.04E-04	9.505E+13	9.50E+16	1.74	1.48	2.6E-07	3.66E+23	-0.223	54.256	3.66E-04
1.9	0.945	9.45E-07	2.72E-01	2.72E-04	7.708E+13	7.71E+16	2.05	1.74	3.1E-07	2.49E+23	-0.057	53.870	6.39E-04
2.2	1.115	1.115E-06	3.79E-01	3.79E-04	6.534E+13	6.53E+16	2.42	2.05	3.7E-07	1.77E+23	0.109	53.528	1.02E-03
2.6	1.315	1.315E-06	5.02E-01	5.02E-04	5.271E+13	5.27E+16	2.86	2.42	4.4E-07	1.20E+23	0.274	53.140	1.52E-03
3.1	1.555	1.555E-06	6.20E-01	6.20E-04	3.934E+13	3.93E+16	3.38	2.86	5.2E-07	7.57E+22	0.441	52.681	2.14E-03
3.7	1.835	1.835E-06	7.47E-01	7.47E-04	2.887E+13	2.89E+16	3.98	3.38	0.0000006	4.81E+22	0.607	52.228	2.89E-03
4.3	2.165	2.165E-06	9.82E-01	9.82E-04	2.309E+13	2.31E+16	4.7	3.98	7.2E-07	3.21E+22	0.772	51.822	3.87E-03
5.1	2.555	2.555E-06	1.20E+00	1.20E-03	1.712E+13	1.71E+16	5.55	4.7	8.5E-07	2.01E+22	0.938	51.357	5.06E-03
6.0	3.015	3.015E-06	1.39E+00	1.39E-03	1.208E+13	1.21E+16	6.55	5.55	0.000001	1.21E+22	1.104	50.846	6.45E-03
7.1	3.555	3.555E-06	1.60E+00	1.60E-03	8.511E+12	8.51E+15	7.72	6.55	1.17E-06	7.27E+21	1.268	50.339	8.05E-03
8.4	4.195	4.195E-06	1.67E+00	1.67E-03	5.4E+12	5.40E+15	9.12	7.72	0.0000014	3.86E+21	1.434	49.704	9.72E-03
9.9	4.95	4.95E-06	1.74E+00	1.74E-03	3.427E+12	3.43E+15	10.8	9.12	1.68E-06	2.04E+21	1.599	49.067	1.15E-02
11.7	5.85	5.85E-06	1.7111675	1.71E-03	2.04E+12	2.04E+15	12.7	10.8	0.0000019	1.07E+21	1.766	48.426	1.32E-02
13.8	6.9	0.0000069	1.5748936	1.57E-03	1.144E+12	1.14E+15	15	12.7	0.0000023	4.98E+20	1.932	47.656	1.47E-02
16.3	8.15	8.15E-06	1.3554912	1.36E-03	5.978E+11	5.98E+14	17.7	15	0.0000027	2.21E+20	2.098	46.846	1.61E-02
19.2	9.6	0.0000096	1.1489242	1.15E-03	3.1E+11	3.10E+14	20.9	17.7	0.0000032	9.69E+19	2.262	46.020	1.73E-02
22.7	11.35	1.135E-05	1.0290482	1.03E-03	1.68E+11	1.68E+14	24.6	20.9	0.0000037	4.54E+19	2.429	45.262	1.83E-02
26.7	13.35	1.335E-05	0.8661151	8.66E-04	8.69E+10	8.69E+13	29.1	24.6	0.0000045	1.93E+19	2.592	44.407	1.91E-02
31.6	15.8	0.0000158	0.755463	7.55E-04	4.572E+10	4.57E+13	34.3	29.1	0.0000052	8.79E+18	2.760	43.621	1.99E-02
37.2	18.6	0.0000186	0.6162798	6.16E-04	2.286E+10	2.29E+13	40.5	34.3	0.0000062	3.69E+18	2.923	42.752	2.05E-02
43.9	21.95	2.195E-05	0.5147706	5.15E-04	1.162E+10	1.16E+13	47.7	40.5	0.0000072	1.61E+18	3.089	41.925	2.10E-02
51.9	25.95	2.595E-05	0.4223007	4.22E-04	5.769E+09	5.77E+12	56.3	47.7	8.6E-06	6.71E+17	3.256	41.047	2.15E-02
61.2	30.6	0.0000306	0.3555548	3.56E-04	2.962E+09	2.96E+12	66.5	56.3	0.0000102	2.90E+17	3.421	40.210	2.18E-02
72.2	36.1	0.0000361	0.3093133	3.09E-04	1.57E+09	1.57E+12	78.4	66.5	0.0000119	1.32E+17	3.586	39.421	2.21E-02
85.2	42.6	0.0000426	0.2677332	2.68E-04	826770263	8.27E+11	92.6	78.4	0.0000142	5.82E+16	3.752	38.603	2.24E-02
101.0	50.5	0.0000505	0.2238883	2.24E-04	415019619	4.15E+11	109	92.6	0.0000164	2.53E+16	3.922	37.770	2.26E-02
119.0	59.5	0.0000595	0.1796417	1.80E-04	203595260	2.04E+11	129	109	0.00002	1.02E+16	4.086	36.859	2.28E-02
140.0	70	0.00007	0.1389256	1.39E-04	96694006	9.67E+10	152	129	0.000023	4.20E+15	4.248	35.975	2.29E-02
165.0	82.5	0.0000825	0.1096102	1.10E-04	46601552	4.66E+10	180	152	0.000028	1.66E+15	4.413	35.048	2.30E-02
195.0	97.5	0.0000975	0.1085436	1.09E-04	27957716	2.80E+10	212	180	0.000032	8.74E+14	4.580	34.404	2.32E-02
230.0	115	0.000115	0.1423704	1.42E-04	22347950	2.23E+10	250	212	0.000038	5.88E+14	4.745	34.008	2.33E-02

d50 calculation

1.16E-02	
9.9	1.15E-02
11.7	1.32E-02
	1.83E-04
	1.74E-07
d50	**9.90E+00**

ECP1

mass	110	mg/L
volume	2.33E-02	m3/L
density	**4.72E+03**	**mg/m3**

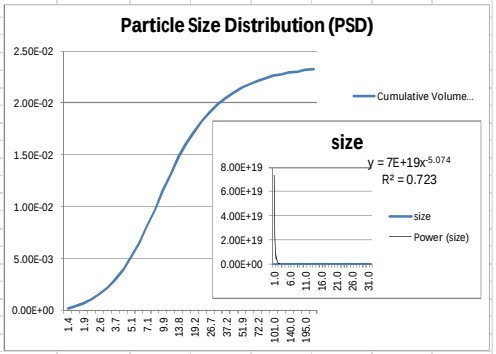

size	radius (µm)	radius(m)	volume (µl/	volume (m³	particles/L	particles/m	Upp Lim (µ	Low Lim (µ	bin size diff	no of partic	logr	logn	cum volume
1.4	0.68	6.8E-07	2.23E-02	2.23E-05	1.695E+13	1.70E+16	1.48	1.25	2.3E-07	7.37E+22	-0.386	52.654	2.23E-05
1.6	0.8	0.0000008	3.30E-02	3.30E-05	1.539E+13	1.54E+16	1.74	1.48	2.6E-07	5.92E+22	-0.223	52.435	5.53E-05
1.9	0.945	9.45E-07	5.46E-02	5.46E-05	1.546E+13	1.55E+16	2.05	1.74	3.1E-07	4.99E+22	-0.057	52.264	1.10E-04
2.2	1.115	1.115E-06	9.70E-02	9.70E-05	1.67E+13	1.67E+16	2.42	2.05	3.7E-07	4.51E+22	0.109	52.164	2.07E-04
2.6	1.315	1.315E-06	1.56E-01	1.56E-04	1.635E+13	1.64E+16	2.86	2.42	4.4E-07	3.72E+22	0.274	51.970	3.63E-04
3.1	1.555	1.555E-06	2.12E-01	2.12E-04	1.344E+13	1.34E+16	3.38	2.86	5.2E-07	2.58E+22	0.441	51.606	5.74E-04
3.7	1.835	1.835E-06	2.59E-01	2.59E-04	1.002E+13	1.00E+16	3.98	3.38	0.0000006	1.67E+22	0.607	51.170	8.34E-04
4.3	2.165	2.165E-06	3.54E-01	3.54E-04	8.33E+12	8.33E+15	4.7	3.98	7.2E-07	1.16E+22	0.772	50.803	1.19E-03
5.1	2.555	2.555E-06	4.38E-01	4.38E-04	6.274E+12	6.27E+15	5.55	4.7	8.5E-07	7.38E+21	0.938	50.353	1.63E-03
6.0	3.015	3.015E-06	5.08E-01	5.08E-04	4.427E+12	4.43E+15	6.55	5.55	0.000001	4.43E+21	1.104	49.842	2.13E-03
7.1	3.555	3.555E-06	6.10E-01	6.10E-04	3.242E+12	3.24E+15	7.72	6.55	1.17E-06	2.77E+21	1.268	49.374	2.74E-03
8.4	4.195	4.195E-06	6.72E-01	6.72E-04	2.174E+12	2.17E+15	9.12	7.72	0.0000014	1.55E+21	1.434	48.794	3.42E-03
9.9	4.95	4.95E-06	7.76E-01	7.76E-04	1.528E+12	1.53E+15	10.8	9.12	1.68E-06	9.10E+20	1.599	48.259	4.19E-03
11.7	5.85	5.85E-06	0.8665556	8.67E-04	1.033E+12	1.03E+15	12.7	10.8	0.0000019	5.44E+20	1.766	47.745	5.06E-03
13.8	6.9	0.0000069	0.9042539	9.04E-04	6.571E+11	6.57E+14	15	12.7	0.0000023	2.86E+20	1.932	47.102	5.96E-03
16.3	8.15	8.15E-06	0.8629106	8.63E-04	3.805E+11	3.81E+14	17.7	15	0.0000027	1.41E+20	2.098	46.395	6.83E-03
19.2	9.6	0.0000096	0.8067102	8.07E-04	2.177E+11	2.18E+14	20.9	17.7	0.0000032	6.80E+19	2.262	45.666	7.63E-03
22.7	11.35	1.135E-05	0.8270456	8.27E-04	1.35E+11	1.35E+14	24.6	20.9	0.0000037	3.65E+19	2.429	45.044	8.46E-03
26.7	13.35	1.335E-05	0.7445575	7.45E-04	7.471E+10	7.47E+13	29.1	24.6	0.0000045	1.66E+19	2.592	44.256	9.21E-03
31.6	15.8	0.0000158	0.6874636	6.87E-04	4.161E+10	4.16E+13	34.3	29.1	0.0000052	8.00E+18	2.760	43.526	9.89E-03
37.2	18.6	0.0000186	0.5370197	5.37E-04	1.992E+10	1.99E+13	40.5	34.3	0.0000062	3.21E+18	2.923	42.614	1.04E-02
43.9	21.95	2.195E-05	0.4128397	4.13E-04	9.319E+09	9.32E+12	47.7	40.5	0.0000072	1.29E+18	3.089	41.705	1.08E-02
51.9	25.95	2.595E-05	0.2938234	2.94E-04	4.014E+09	4.01E+12	56.3	47.7	8.6E-06	4.67E+17	3.256	40.685	1.11E-02
61.2	30.6	0.0000306	0.2146072	2.15E-04	1.788E+09	1.79E+12	66.5	56.3	0.0000102	1.75E+17	3.421	39.705	1.14E-02
72.2	36.1	0.0000361	0.1583702	1.58E-04	803643179	8.04E+11	78.4	66.5	0.0000119	6.75E+16	3.586	38.751	1.15E-02
85.2	42.6	0.0000426	0.1183615	1.18E-04	365504839	3.66E+11	92.6	78.4	0.0000142	2.57E+16	3.752	37.787	1.16E-02
101.0	50.5	0.0000505	0.0850849	8.51E-05	157721043	1.58E+11	109	92.6	0.0000164	9.62E+15	3.922	36.802	1.17E-02
119.0	59.5	0.0000595	0.0613648	6.14E-05	69547203	6.95E+10	129	109	0.00002	3.48E+15	4.086	35.785	1.18E-02
140.0	70	0.00007	0.0447863	4.48E-05	31171809	3.12E+10	152	129	0.000023	1.36E+15	4.248	34.843	1.18E-02
165.0	82.5	0.0000825	0.0340327	3.40E-05	14469240	1.45E+10	180	152	0.000028	5.17E+14	4.413	33.879	1.19E-02
195.0	97.5	0.0000975	0.0321331	3.21E-05	8276577.2	8.28E+09	212	180	0.000032	2.59E+14	4.580	33.186	1.19E-02
230.0	115	0.000115	0.0384316	3.84E-05	6032623.7	6.03E+09	250	212	0.000038	1.59E+14	4.745	32.698	1.19E-02

d50 calculation

5.96E-03	
13.8	5.96E-03
16.3	6.83E-03
	-2.18E-06
	-7.54E-10
d50	**1.38E+01**

mass 80 mg/L
volume 1.19E-02 m3/L
density **6.71E+03 mg/m3**

ECP3

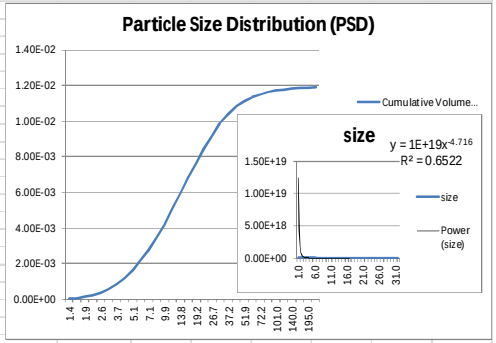

size	radius (µm)	radius(m)	volume (µl/	volume (m³	particles/L	particles/m	Upp Lim (µ	Low Lim (µ	bin size diff	no of partic	logr	logn	cum volume
1.4	0.68	6.8E-07	2.76E-01	2.76E-04	2.092E+14	2.09E+17	1.48	1.25	2.3E-07	9.10E+23	-0.386	55.167	2.76E-04
1.6	0.8	0.0000008	3.33E-01	3.33E-04	1.552E+14	1.55E+17	1.74	1.48	2.6E-07	5.97E+23	-0.223	54.746	6.09E-04
1.9	0.945	9.45E-07	4.23E-01	4.23E-04	1.198E+14	1.20E+17	2.05	1.74	3.1E-07	3.86E+23	-0.057	54.311	1.03E-03
2.2	1.115	1.115E-06	5.61E-01	5.61E-04	9.658E+13	9.66E+16	2.42	2.05	3.7E-07	2.61E+23	0.109	53.919	1.59E-03
2.6	1.315	1.315E-06	7.17E-01	7.17E-04	7.525E+13	7.52E+16	2.86	2.42	4.4E-07	1.71E+23	0.274	53.496	2.31E-03
3.1	1.555	1.555E-06	8.81E-01	8.81E-04	5.595E+13	5.59E+16	3.38	2.86	5.2E-07	1.08E+23	0.441	53.033	3.19E-03
3.7	1.835	1.835E-06	1.08E+00	1.08E-03	4.175E+13	4.18E+16	3.98	3.38	0.0000006	6.96E+22	0.607	52.597	4.27E-03
4.3	2.165	2.165E-06	1.44E+00	1.44E-03	3.384E+13	3.38E+16	4.7	3.98	7.2E-07	4.70E+22	0.772	52.204	5.71E-03
5.1	2.555	2.555E-06	1.78E+00	1.78E-03	2.547E+13	2.55E+16	5.55	4.7	8.5E-07	3.00E+22	0.938	51.754	7.49E-03
6.0	3.015	3.015E-06	2.11E+00	2.11E-03	1.836E+13	1.84E+16	6.55	5.55	0.000001	1.84E+22	1.104	51.264	9.60E-03
7.1	3.555	3.555E-06	2.50E+00	2.50E-03	1.327E+13	1.33E+16	7.72	6.55	1.17E-06	1.13E+22	1.268	50.783	1.21E-02
8.4	4.195	4.195E-06	2.68E+00	2.68E-03	8.671E+12	8.67E+15	9.12	7.72	0.0000014	6.19E+21	1.434	50.178	1.48E-02
9.9	4.95	4.95E-06	2.89E+00	2.89E-03	5.682E+12	5.68E+15	10.8	9.12	1.68E-06	3.38E+21	1.599	49.573	1.77E-02
11.7	5.85	5.85E-06	2.9492239	2.95E-03	3.517E+12	3.52E+15	12.7	10.8	0.0000019	1.85E+21	1.766	48.970	2.06E-02
13.8	6.9	0.0000069	2.8377787	2.84E-03	2.062E+12	2.06E+15	15	12.7	0.0000023	8.97E+20	1.932	48.245	2.35E-02
16.3	8.15	8.15E-06	2.5532326	2.55E-03	1.126E+12	1.13E+15	17.7	15	0.0000027	4.17E+20	2.098	47.480	2.60E-02
19.2	9.6	0.0000096	2.2420594	2.24E-03	6.05E+11	6.05E+14	20.9	17.7	0.0000032	1.89E+20	2.262	46.689	2.82E-02
22.7	11.35	1.135E-05	2.0778704	2.08E-03	3.393E+11	3.39E+14	24.6	20.9	0.0000037	9.17E+19	2.429	45.965	3.03E-02
26.7	13.35	1.335E-05	1.7847349	1.78E-03	1.791E+11	1.79E+14	29.1	24.6	0.0000045	3.98E+19	2.592	45.130	3.21E-02
31.6	15.8	0.0000158	1.5639747	1.56E-03	9.466E+10	9.47E+13	34.3	29.1	0.0000052	1.82E+19	2.760	44.348	3.37E-02
37.2	18.6	0.0000186	1.2591494	1.26E-03	4.671E+10	4.67E+13	40.5	34.3	0.0000062	7.53E+18	2.923	43.466	3.49E-02
43.9	21.95	2.195E-05	1.0139341	1.01E-03	2.289E+10	2.29E+13	47.7	40.5	0.0000072	3.18E+18	3.089	42.603	3.59E-02
51.9	25.95	2.595E-05	0.7923527	7.92E-04	1.082E+10	1.08E+13	56.3	47.7	8.6E-06	1.26E+18	3.256	41.677	3.67E-02
61.2	30.6	0.0000306	0.6399847	6.40E-04	5.332E+09	5.33E+12	66.5	56.3	0.0000102	5.23E+17	3.421	40.798	3.74E-02
72.2	36.1	0.0000361	0.5353651	5.35E-04	2.717E+09	2.72E+12	78.4	66.5	0.0000119	2.28E+17	3.586	39.969	3.79E-02
85.2	42.6	0.0000426	0.4435111	4.44E-04	1.37E+09	1.37E+12	92.6	78.4	0.0000142	9.64E+16	3.752	39.108	3.84E-02
101.0	50.5	0.0000505	0.3518265	3.52E-04	652177554	6.52E+11	109	92.6	0.0000164	3.98E+16	3.922	38.222	3.87E-02
119.0	59.5	0.0000595	0.2688621	2.69E-04	304712354	3.05E+11	129	109	0.00002	1.52E+16	4.086	37.262	3.90E-02
140.0	70	0.00007	0.2029684	2.03E-04	141268646	1.41E+11	152	129	0.000023	6.14E+15	4.248	36.354	3.92E-02
165.0	82.5	0.0000825	0.1590614	1.59E-04	67626082	6.76E+10	180	152	0.000028	2.42E+15	4.413	35.421	3.93E-02
195.0	97.5	0.0000975	0.1618292	1.62E-04	41682552	4.17E+10	212	180	0.000032	1.30E+15	4.580	34.803	3.95E-02
230.0	115	0.000115	0.2153328	2.15E-04	33800887	3.38E+10	250	212	0.000038	8.89E+14	4.745	34.422	3.97E-02

d50 calculation

1.99E-02	
9.9	1.77E-02
11.7	2.06E-02
	2.20E-03
	3.60E-06
d50	**9.90E+00**

mass 123.3 mg/L
volume 3.97E-02 m3/L
density **3.10E+03 mg/m3**

ECP2

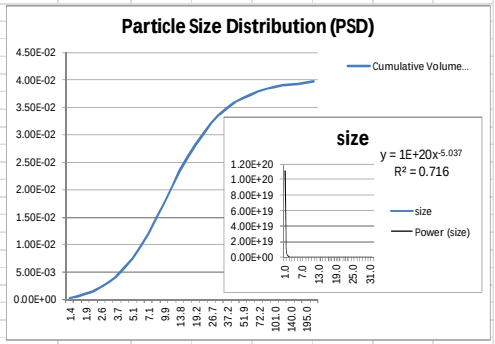

size	radius (µm)	radius(m)	volume (µl/	volume (m³	particles/L	particles/m	Upp Lim (µ	Low Lim (µ	bin size diff	no of partic	logr	logn	cum volume
1.4	0.68	6.8E-07	1.44E-01	1.44E-04	1.093E+14	1.09E+17	1.48	1.25	2.3E-07	4.75E+23	-0.386	54.518	1.44E-04
1.6	0.8	0.0000008	1.49E-01	1.49E-04	6.952E+13	6.95E+16	1.74	1.48	2.6E-07	2.67E+23	-0.223	53.943	2.93E-04
1.9	0.945	9.45E-07	1.55E-01	1.55E-04	4.394E+13	4.39E+16	2.05	1.74	3.1E-07	1.42E+23	-0.057	53.308	4.48E-04
2.2	1.115	1.115E-06	1.66E-01	1.66E-04	2.867E+13	2.87E+16	2.42	2.05	3.7E-07	7.75E+22	0.109	52.704	6.15E-04
2.6	1.315	1.315E-06	1.81E-01	1.81E-04	1.904E+13	1.90E+16	2.86	2.42	4.4E-07	4.33E+22	0.274	52.122	7.96E-04
3.1	1.555	1.555E-06	2.11E-01	2.11E-04	1.341E+13	1.34E+16	3.38	2.86	5.2E-07	2.58E+22	0.441	51.604	1.01E-03
3.7	1.835	1.835E-06	2.62E-01	2.62E-04	1.013E+13	1.01E+16	3.98	3.38	0.0000006	1.69E+22	0.607	51.181	1.27E-03
4.3	2.165	2.165E-06	3.39E-01	3.39E-04	7.975E+12	7.98E+15	4.7	3.98	7.2E-07	1.11E+22	0.772	50.759	1.61E-03
5.1	2.555	2.555E-06	4.05E-01	4.05E-04	5.802E+12	5.80E+15	5.55	4.7	8.5E-07	6.83E+21	0.938	50.275	2.01E-03
6.0	3.015	3.015E-06	4.66E-01	4.66E-04	4.056E+12	4.06E+15	6.55	5.55	0.000001	4.06E+21	1.104	49.755	2.48E-03
7.1	3.555	3.555E-06	5.04E-01	5.04E-04	2.681E+12	2.68E+15	7.72	6.55	1.17E-06	2.29E+21	1.268	49.183	2.98E-03
8.4	4.195	4.195E-06	4.81E-01	4.81E-04	1.557E+12	1.56E+15	9.12	7.72	0.0000014	1.11E+21	1.434	48.461	3.47E-03
9.9	4.95	4.95E-06	4.46E-01	4.46E-04	8.786E+11	8.79E+14	10.8	9.12	1.68E-06	5.23E+20	1.599	47.706	3.91E-03
11.7	5.85	5.85E-06	0.3896683	3.90E-04	4.647E+11	4.65E+14	12.7	10.8	0.0000019	2.45E+20	1.766	46.946	4.30E-03
13.8	6.9	0.0000069	0.3315428	3.32E-04	2.409E+11	2.41E+14	15	12.7	0.0000023	1.05E+20	1.932	46.098	4.63E-03
16.3	8.15	8.15E-06	0.2768764	2.77E-04	1.221E+11	1.22E+14	17.7	15	0.0000027	4.52E+19	2.098	45.258	4.91E-03
19.2	9.6	0.0000096	0.2313482	2.31E-04	6.243E+10	6.24E+13	20.9	17.7	0.0000032	1.95E+19	2.262	44.417	5.14E-03
22.7	11.35	1.135E-05	0.1965788	1.97E-04	3.21E+10	3.21E+13	24.6	20.9	0.0000037	8.67E+18	2.429	43.607	5.34E-03
26.7	13.35	1.335E-05	0.1606552	1.61E-04	1.612E+10	1.61E+13	29.1	24.6	0.0000045	3.58E+18	2.592	42.723	5.50E-03
31.6	15.8	0.0000158	0.1294395	1.29E-04	7.834E+09	7.83E+12	34.3	29.1	0.0000052	1.51E+18	2.760	41.856	5.63E-03
37.2	18.6	0.0000186	0.1011765	1.01E-04	3.754E+09	3.75E+12	40.5	34.3	0.0000062	6.05E+17	2.923	40.945	5.73E-03
43.9	21.95	2.195E-05	0.0757265	7.57E-05	1.709E+09	1.71E+12	47.7	40.5	0.0000072	2.37E+17	3.089	40.009	5.81E-03
51.9	25.95	2.595E-05	0.0548805	5.49E-05	749751548	7.50E+11	56.3	47.7	8.6E-06	8.72E+16	3.256	39.007	5.86E-03
61.2	30.6	0.0000306	0.0396921	3.97E-05	330712721	3.31E+11	66.5	56.3	0.0000102	3.24E+16	3.421	38.018	5.90E-03
72.2	36.1	0.0000361	0.0302847	3.03E-05	153678233	1.54E+11	78.4	66.5	0.0000119	1.29E+16	3.586	37.097	5.93E-03
85.2	42.6	0.0000426	0.0231581	2.32E-05	71513064	7.15E+10	92.6	78.4	0.0000142	5.04E+15	3.752	36.155	5.95E-03
101.0	50.5	0.0000505	0.0180354	1.80E-05	33431967	3.34E+10	109	92.6	0.0000164	2.04E+15	3.922	35.251	5.97E-03
119.0	59.5	0.0000595	0.014066	1.41E-05	15941572	1.59E+10	129	109	0.00002	7.97E+14	4.086	34.312	5.99E-03
140.0	70	0.00007	0.0113314	1.13E-05	7886806.8	7.89E+09	152	129	0.000023	3.43E+14	4.248	33.468	6.00E-03
165.0	82.5	0.0000825	0.0096519	9.65E-06	4103579	4.10E+09	180	152	0.000028	1.47E+14	4.413	32.618	6.01E-03
195.0	97.5	0.0000975	0.0105123	1.05E-05	2707668.8	2.71E+09	212	180	0.000032	8.46E+13	4.580	32.069	6.02E-03
230.0	115	0.000115	0.0163012	1.63E-05	2558801.5	2.56E+09	250	212	0.000038	6.73E+13	4.745	31.841	6.03E-03

d50 calculation

3.02E-03	
7.1	2.98E-03
8.4	3.47E-03
	3.23E-05
	1.21E-08
d50	**7.11E+00**

mass	65	mg/L
volume	6.03E-03	m3/L
density	**1.08E+04**	**mg/m3**

WCP

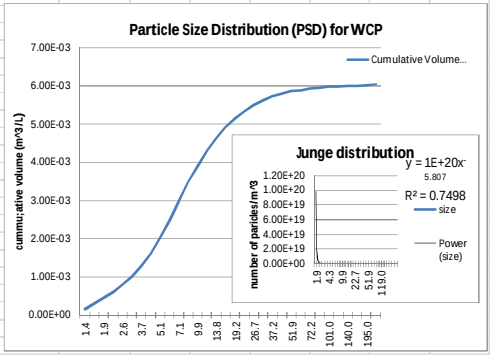

size	radius (µm)	radius(m)	volume (µl/	volume (m³	particles/L	particles/m	Upp Lim (µ	Low Lim (µ	bin size diff	no of partic	logr	logn	cum volume
1.4	0.68	6.8E-07	8.98E-03	8.98E-06	6.819E+12	6.82E+15	1.48	1.25	2.3E-07	2.96E+22	-0.386	51.744	8.98E-06
1.6	0.8	0.0000008	1.71E-02	1.71E-05	7.966E+12	7.97E+15	1.74	1.48	2.6E-07	3.06E+22	-0.223	51.777	2.61E-05
1.9	0.945	9.45E-07	3.90E-02	3.90E-05	1.102E+13	1.10E+16	2.05	1.74	3.1E-07	3.55E+22	-0.057	51.925	6.50E-05
2.2	1.115	1.115E-06	9.67E-02	9.67E-05	1.665E+13	1.67E+16	2.42	2.05	3.7E-07	4.50E+22	0.109	52.161	1.62E-04
2.6	1.315	1.315E-06	2.01E-01	2.01E-04	2.105E+13	2.11E+16	2.86	2.42	4.4E-07	4.78E+22	0.274	52.222	3.62E-04
3.1	1.555	1.555E-06	3.01E-01	3.01E-04	1.914E+13	1.91E+16	3.38	2.86	5.2E-07	3.68E+22	0.441	51.960	6.64E-04
3.7	1.835	1.835E-06	3.70E-01	3.70E-04	1.429E+13	1.43E+16	3.98	3.38	0.0000006	2.38E+22	0.607	51.525	1.03E-03
4.3	2.165	2.165E-06	5.35E-01	5.35E-04	1.258E+13	1.26E+16	4.7	3.98	7.2E-07	1.75E+22	0.772	51.215	1.57E-03
5.1	2.555	2.555E-06	6.98E-01	6.98E-04	9.992E+12	9.99E+15	5.55	4.7	8.5E-07	1.18E+22	0.938	50.819	2.27E-03
6.0	3.015	3.015E-06	8.38E-01	8.38E-04	7.303E+12	7.30E+15	6.55	5.55	0.000001	7.30E+21	1.104	50.343	3.10E-03
7.1	3.555	3.555E-06	1.07E+00	1.07E-03	5.674E+12	5.67E+15	7.72	6.55	1.17E-06	4.85E+21	1.268	49.933	4.17E-03
8.4	4.195	4.195E-06	1.21E+00	1.21E-03	3.91E+12	3.91E+15	9.12	7.72	0.0000014	2.79E+21	1.434	49.381	5.38E-03
9.9	4.95	4.95E-06	1.46E+00	1.46E-03	2.868E+12	2.87E+15	10.8	9.12	1.68E-06	1.71E+21	1.599	48.889	6.84E-03
11.7	5.85	5.85E-06	1.7385136	1.74E-03	2.073E+12	2.07E+15	12.7	10.8	0.0000019	1.09E+21	1.766	48.441	8.58E-03
13.8	6.9	0.0000069	1.9767814	1.98E-03	1.437E+12	1.44E+15	15	12.7	0.0000023	6.25E+20	1.932	47.884	1.06E-02
16.3	8.15	8.15E-06	2.0267503	2.03E-03	8.938E+11	8.94E+14	17.7	15	0.0000027	3.31E+20	2.098	47.249	1.26E-02
19.2	9.6	0.0000096	1.9813199	1.98E-03	5.346E+11	5.35E+14	20.9	17.7	0.0000032	1.67E+20	2.262	46.565	1.46E-02
22.7	11.35	1.135E-05	2.1169292	2.12E-03	3.456E+11	3.46E+14	24.6	20.9	0.0000037	9.34E+19	2.429	45.984	1.67E-02
26.7	13.35	1.335E-05	1.8465528	1.85E-03	1.853E+11	1.85E+14	29.1	24.6	0.0000045	4.12E+19	2.592	45.164	1.85E-02
31.6	15.8	0.0000158	1.691329	1.69E-03	1.024E+11	1.02E+14	34.3	29.1	0.0000052	1.97E+19	2.760	44.426	2.02E-02
37.2	18.6	0.0000186	1.2183527	1.22E-03	4.52E+10	4.52E+13	40.5	34.3	0.0000062	7.29E+18	2.923	43.433	2.14E-02
43.9	21.95	2.195E-05	0.8931276	8.93E-04	2.016E+10	2.02E+13	47.7	40.5	0.0000072	2.80E+18	3.089	42.476	2.23E-02
51.9	25.95	2.595E-05	0.6153583	6.15E-04	8.407E+09	8.41E+12	56.3	47.7	8.6E-06	9.78E+17	3.256	41.424	2.29E-02
61.2	30.6	0.0000306	0.4532093	4.53E-04	3.776E+09	3.78E+12	66.5	56.3	0.0000102	3.70E+17	3.421	40.453	2.34E-02
72.2	36.1	0.0000361	0.3455808	3.46E-04	1.754E+09	1.75E+12	78.4	66.5	0.0000119	1.47E+17	3.586	39.532	2.37E-02
85.2	42.6	0.0000426	0.2681478	2.68E-04	828050663	8.28E+11	92.6	78.4	0.0000142	5.83E+16	3.752	38.605	2.40E-02
101.0	50.5	0.0000505	0.1976631	1.98E-04	366406293	3.66E+11	109	92.6	0.0000164	2.23E+16	3.922	37.645	2.42E-02
119.0	59.5	0.0000595	0.1438304	1.44E-04	163008889	1.63E+11	129	109	0.00002	8.15E+15	4.086	36.637	2.44E-02
140.0	70	0.00007	0.1021986	1.02E-04	71131510	7.11E+10	152	129	0.000023	3.09E+15	4.248	35.668	2.45E-02
165.0	82.5	0.0000825	0.0722552	7.23E-05	30719801	3.07E+10	180	152	0.000028	1.10E+15	4.413	34.631	2.45E-02
195.0	97.5	0.0000975	0.062382	6.24E-05	16067813	1.61E+10	212	180	0.000032	5.02E+14	4.580	33.850	2.46E-02
230.0	115	0.000115	0.0610564	6.11E-05	9584055.6	9.58E+09	250	212	0.000038	2.52E+14	4.745	33.161	2.47E-02

d50 calculation

1.23E-02	
13.8	1.06E-02
16.3	1.26E-02
	1.77E-03
	1.44E-06
d50	**1.38E+01**

mass	69	mg/L
volume	2.47E-02	m3/L
density	**2.80E+03**	**mg/m3**

Ubin E

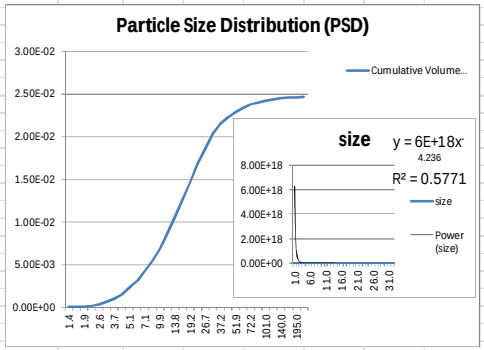

size	radius (µm)	radius(m)	volume (µl/	volume (m³	particles/L	particles/m	Upp Lim (µ	Low Lim (µ	bin size diff	no of partic	logr	logn	cum volume
1.4	0.68	6.8E-07	1.67E-01	1.67E-04	1.272E+14	1.27E+17	1.48	1.25	2.3E-07	5.53E+23	-0.386	54.669	1.67E-04
1.6	0.8	0.0000008	1.84E-01	1.84E-04	8.59E+13	8.59E+16	1.74	1.48	2.6E-07	3.30E+23	-0.223	54.155	3.52E-04
1.9	0.945	9.45E-07	2.07E-01	2.07E-04	5.855E+13	5.86E+16	2.05	1.74	3.1E-07	1.89E+23	-0.057	53.595	5.59E-04
2.2	1.115	1.115E-06	2.35E-01	2.35E-04	4.055E+13	4.06E+16	2.42	2.05	3.7E-07	1.10E+23	0.109	53.051	7.94E-04
2.6	1.315	1.315E-06	2.65E-01	2.65E-04	2.777E+13	2.78E+16	2.86	2.42	4.4E-07	6.31E+22	0.274	52.499	1.06E-03
3.1	1.555	1.555E-06	2.96E-01	2.96E-04	1.879E+13	1.88E+16	3.38	2.86	5.2E-07	3.61E+22	0.441	51.942	1.35E-03
3.7	1.835	1.835E-06	3.39E-01	3.39E-04	1.31E+13	1.31E+16	3.98	3.38	0.0000006	2.18E+22	0.607	51.438	1.69E-03
4.3	2.165	2.165E-06	4.09E-01	4.09E-04	9.616E+12	9.62E+15	4.7	3.98	7.2E-07	1.34E+22	0.772	50.946	2.10E-03
5.1	2.555	2.555E-06	4.67E-01	4.67E-04	6.678E+12	6.68E+15	5.55	4.7	8.5E-07	7.86E+21	0.938	50.416	2.57E-03
6.0	3.015	3.015E-06	5.22E-01	5.22E-04	4.545E+12	4.54E+15	6.55	5.55	0.000001	4.54E+21	1.104	49.868	3.09E-03
7.1	3.555	3.555E-06	5.74E-01	5.74E-04	3.049E+12	3.05E+15	7.72	6.55	1.17E-06	2.61E+21	1.268	49.312	3.66E-03
8.4	4.195	4.195E-06	5.77E-01	5.77E-04	1.865E+12	1.86E+15	9.12	7.72	0.0000014	1.33E+21	1.434	48.641	4.24E-03
9.9	4.95	4.95E-06	5.87E-01	5.87E-04	1.155E+12	1.16E+15	10.8	9.12	1.68E-06	6.88E+20	1.599	47.980	4.83E-03
11.7	5.85	5.85E-06	0.6004226	6.00E-04	7.16E+11	7.16E+14	12.7	10.8	0.0000019	3.77E+20	1.766	47.378	5.43E-03
13.8	6.9	0.0000069	0.6355368	6.36E-04	4.619E+11	4.62E+14	15	12.7	0.0000023	2.01E+20	1.932	46.749	6.06E-03
16.3	8.15	8.15E-06	0.6799524	6.80E-04	2.999E+11	3.00E+14	17.7	15	0.0000027	1.11E+20	2.098	46.157	6.74E-03
19.2	9.6	0.0000096	0.7125191	7.13E-04	1.923E+11	1.92E+14	20.9	17.7	0.0000032	6.01E+19	2.262	45.542	7.46E-03
22.7	11.35	1.135E-05	0.7480031	7.48E-04	1.221E+11	1.22E+14	24.6	20.9	0.0000037	3.30E+19	2.429	44.943	8.20E-03
26.7	13.35	1.335E-05	0.7028868	7.03E-04	7.053E+10	7.05E+13	29.1	24.6	0.0000045	1.57E+19	2.592	44.198	8.91E-03
31.6	15.8	0.0000158	0.649123	6.49E-04	3.929E+10	3.93E+13	34.3	29.1	0.0000052	7.56E+18	2.760	43.469	9.56E-03
37.2	18.6	0.0000186	0.539058	5.39E-04	2E+10	2.00E+13	40.5	34.3	0.0000062	3.23E+18	2.923	42.618	1.01E-02
43.9	21.95	2.195E-05	0.4159364	4.16E-04	9.389E+09	9.39E+12	47.7	40.5	0.0000072	1.30E+18	3.089	41.712	1.05E-02
51.9	25.95	2.595E-05	0.3012329	3.01E-04	4.115E+09	4.12E+12	56.3	47.7	8.6E-06	4.79E+17	3.256	40.709	1.08E-02
61.2	30.6	0.0000306	0.2250548	2.25E-04	1.875E+09	1.88E+12	66.5	56.3	0.0000102	1.84E+17	3.421	39.753	1.10E-02
72.2	36.1	0.0000361	0.1754285	1.75E-04	890204699	8.90E+11	78.4	66.5	0.0000119	7.48E+16	3.586	38.854	1.12E-02
85.2	42.6	0.0000426	0.1365382	1.37E-04	421635104	4.22E+11	92.6	78.4	0.0000142	2.97E+16	3.752	37.930	1.13E-02
101.0	50.5	0.0000505	0.0978186	9.78E-05	181325432	1.81E+11	109	92.6	0.0000164	1.11E+16	3.922	36.942	1.14E-02
119.0	59.5	0.0000595	0.06937	6.94E-05	78619793	7.86E+10	129	109	0.00002	3.93E+15	4.086	35.908	1.15E-02
140.0	70	0.00007	0.0470565	4.71E-05	32751953	3.28E+10	152	129	0.000023	1.42E+15	4.248	34.892	1.16E-02
165.0	82.5	0.0000825	0.0323092	3.23E-05	13736478	1.37E+10	180	152	0.000028	4.91E+14	4.413	33.827	1.16E-02
195.0	97.5	0.0000975	0.0299204	2.99E-05	7706648.6	7.71E+09	212	180	0.000032	2.41E+14	4.580	33.115	1.16E-02
230.0	115	0.000115	0.0382193	3.82E-05	5999302.9	6.00E+09	250	212	0.000038	1.58E+14	4.745	32.693	1.17E-02

d50 calculation

5.83E-03	
11.7	5.43E-03
13.8	6.06E-03
	4.04E-04
	1.22E-07
d50	**1.17E+01**

mass	65	mg/L	
volume	1.17E-02	m3/L	
density	**5.57E+03**	**mg/m3**	

Ubin_N

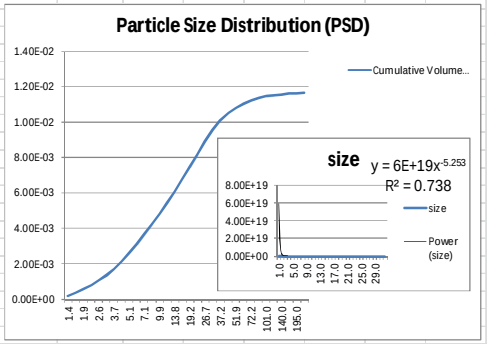

size	radius (µm)	radius(m)	volume (µl/	volume (m³	particles/L	particles/m	Upp Lim (µ	Low Lim (µ	bin size diff	no of partic	logr	logn	cum volume
1.4	0.68	6.8E-07	0.00E+00	0.00E+00	0	0.00E+00	1.48	1.25	2.3E-07	0.00E+00	-0.386	#NUM!	0.00E+00
1.6	0.8	0.0000008	0.00E+00	0.00E+00	0	0.00E+00	1.74	1.48	2.6E-07	0.00E+00	-0.223	#NUM!	0.00E+00
1.9	0.945	9.45E-07	3.15E-03	3.15E-06	8.903E+11	8.90E+14	2.05	1.74	3.1E-07	2.87E+21	-0.057	49.409	3.15E-06
2.2	1.115	1.115E-06	2.08E-02	2.08E-05	3.583E+12	3.58E+15	2.42	2.05	3.7E-07	9.68E+21	0.109	50.625	2.40E-05
2.6	1.315	1.315E-06	9.18E-02	9.18E-05	9.641E+12	9.64E+15	2.86	2.42	4.4E-07	2.19E+22	0.274	51.441	1.16E-04
3.1	1.555	1.555E-06	1.99E-01	1.99E-04	1.261E+13	1.26E+16	3.38	2.86	5.2E-07	2.43E+22	0.441	51.543	3.14E-04
3.7	1.835	1.835E-06	2.46E-01	2.46E-04	9.504E+12	9.50E+15	3.98	3.38	0.0000006	1.58E+22	0.607	51.117	5.60E-04
4.3	2.165	2.165E-06	3.74E-01	3.74E-04	8.81E+12	8.81E+15	4.7	3.98	7.2E-07	1.22E+22	0.772	50.859	9.35E-04
5.1	2.555	2.555E-06	5.07E-01	5.07E-04	7.257E+12	7.26E+15	5.55	4.7	8.5E-07	8.54E+21	0.938	50.499	1.44E-03
6.0	3.015	3.015E-06	6.11E-01	6.11E-04	5.323E+12	5.32E+15	6.55	5.55	0.000001	5.32E+21	1.104	50.026	2.05E-03
7.1	3.555	3.555E-06	8.44E-01	8.44E-04	4.486E+12	4.49E+15	7.72	6.55	1.17E-06	3.83E+21	1.268	49.698	2.90E-03
8.4	4.195	4.195E-06	9.47E-01	9.47E-04	3.064E+12	3.06E+15	9.12	7.72	0.0000014	2.19E+21	1.434	49.137	3.84E-03
9.9	4.95	4.95E-06	1.06E+00	1.06E-03	2.077E+12	2.08E+15	10.8	9.12	1.68E-06	1.24E+21	1.599	48.566	4.90E-03
11.7	5.85	5.85E-06	1.1006465	1.10E-03	1.312E+12	1.31E+15	12.7	10.8	0.0000019	6.91E+20	1.766	47.984	6.00E-03
13.8	6.9	0.0000069	1.0343539	1.03E-03	7.517E+11	7.52E+14	15	12.7	0.0000023	3.27E+20	1.932	47.236	7.03E-03
16.3	8.15	8.15E-06	0.9193169	9.19E-04	4.054E+11	4.05E+14	17.7	15	0.0000027	1.50E+20	2.098	46.458	7.95E-03
19.2	9.6	0.0000096	0.9171114	9.17E-04	2.475E+11	2.47E+14	20.9	17.7	0.0000032	7.73E+19	2.262	45.795	8.87E-03
22.7	11.35	1.135E-05	1.1597594	1.16E-03	1.894E+11	1.89E+14	24.6	20.9	0.0000037	5.12E+19	2.429	45.382	1.00E-02
26.7	13.35	1.335E-05	1.1145187	1.11E-03	1.118E+11	1.12E+14	29.1	24.6	0.0000045	2.49E+19	2.592	44.659	1.11E-02
31.6	15.8	0.0000158	1.2004466	1.20E-03	7.266E+10	7.27E+13	34.3	29.1	0.0000052	1.40E+19	2.760	44.084	1.23E-02
37.2	18.6	0.0000186	0.9153167	9.15E-04	3.396E+10	3.40E+13	40.5	34.3	0.0000062	5.48E+18	2.923	43.147	1.33E-02
43.9	21.95	2.195E-05	0.7619736	7.62E-04	1.72E+10	1.72E+13	47.7	40.5	0.0000072	2.39E+18	3.089	42.317	1.40E-02
51.9	25.95	2.595E-05	0.5827973	5.83E-04	7.962E+09	7.96E+12	56.3	47.7	8.6E-06	9.26E+17	3.256	41.369	1.46E-02
61.2	30.6	0.0000306	0.4973797	4.97E-04	4.144E+09	4.14E+12	66.5	56.3	0.0000102	4.06E+17	3.421	40.546	1.51E-02
72.2	36.1	0.0000361	0.4377172	4.38E-04	2.221E+09	2.22E+12	78.4	66.5	0.0000119	1.87E+17	3.586	39.768	1.55E-02
85.2	42.6	0.0000426	0.3937472	3.94E-04	1.216E+09	1.22E+12	92.6	78.4	0.0000142	8.56E+16	3.752	38.989	1.59E-02
101.0	50.5	0.0000505	0.2974489	2.97E-04	551378254	5.51E+11	109	92.6	0.0000164	3.36E+16	3.922	38.054	1.62E-02
119.0	59.5	0.0000595	0.2224427	2.22E-04	252103343	2.52E+11	129	109	0.00002	1.26E+16	4.086	37.073	1.65E-02
140.0	70	0.00007	0.1416666	1.42E-04	98601775	9.86E+10	152	129	0.000023	4.29E+15	4.248	35.994	1.66E-02
165.0	82.5	0.0000825	0.0843634	8.44E-05	35867714	3.59E+10	180	152	0.000028	1.28E+15	4.413	34.786	1.67E-02
195.0	97.5	0.0000975	0.0618063	6.18E-05	15919523	1.59E+10	212	180	0.000032	4.97E+14	4.580	33.841	1.67E-02
230.0	115	0.000115	0.0492928	4.93E-05	7737506.5	7.74E+09	250	212	0.000038	2.04E+14	4.745	32.947	1.68E-02

d50 calculation

8.40E-03	
16.3	7.95E-03
19.2	8.87E-03
	4.42E-04
	1.40E-07
d50	**1.63E+01**

mass	70	mg/L	
volume	1.68E-02	m3/L	
density	**4.17E+03**	**mg/m3**	

Punggol

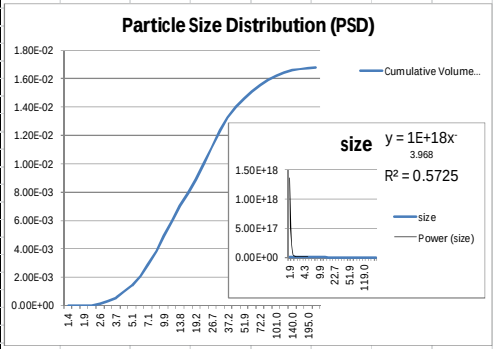

size	radius (µm)	radius(m)	volume (µl/L	lume (m^3/	particles/L	articles/m^3	pp Lim (µm	ow Lim (µm	n size diff	o of particle	logr	logn	m vol (m^3/
1.4	0.68	6.8E-07	2.58E-02	2.58E-05	1.956E+13	1.96E+16	1.48	1.25	2.3E-07	8.51E+22	-0.386	52.798	2.58E-05
1.6	0.8	0.0000008	4.45E-02	4.45E-05	2.074E+13	2.07E+16	1.74	1.48	2.6E-07	7.98E+22	-0.223	52.733	7.02E-05
1.9	0.945	9.45E-07	8.88E-02	8.88E-05	2.511E+13	2.51E+16	2.05	1.74	3.1E-07	8.10E+22	-0.057	52.749	1.59E-04
2.2	1.115	1.115E-06	1.81E-01	1.81E-04	3.121E+13	3.12E+16	2.42	2.05	3.7E-07	8.44E+22	0.109	52.789	3.40E-04
2.6	1.315	1.315E-06	3.13E-01	3.13E-04	3.287E+13	3.29E+16	2.86	2.42	4.4E-07	7.47E+22	0.274	52.668	6.53E-04
3.1	1.555	1.555E-06	3.91E-01	3.91E-04	2.484E+13	2.48E+16	3.38	2.86	5.2E-07	4.78E+22	0.441	52.221	1.04E-03
3.7	1.835	1.835E-06	4.11E-01	4.11E-04	1.587E+13	1.59E+16	3.98	3.38	0.0000006	2.65E+22	0.607	51.630	1.46E-03
4.3	2.165	2.165E-06	5.00E-01	5.00E-04	1.176E+13	1.18E+16	4.7	3.98	7.2E-07	1.63E+22	0.772	51.148	1.96E-03
5.1	2.555	2.555E-06	5.71E-01	5.71E-04	8.168E+12	8.17E+15	5.55	4.7	8.5E-07	9.61E+21	0.938	50.617	2.53E-03
6.0	3.015	3.015E-06	6.24E-01	6.24E-04	5.436E+12	5.44E+15	6.55	5.55	0.000001	5.44E+21	1.104	50.047	3.15E-03
7.1	3.555	3.555E-06	7.38E-01	7.38E-04	3.92E+12	3.92E+15	7.72	6.55	1.17E-06	3.35E+21	1.268	49.563	3.89E-03
8.4	4.195	4.195E-06	8.14E-01	8.14E-04	2.633E+12	2.63E+15	9.12	7.72	0.0000014	1.88E+21	1.434	48.986	4.70E-03
9.9	4.95	4.95E-06	9.70E-01	9.70E-04	1.91E+12	1.91E+15	10.8	9.12	1.68E-06	1.14E+21	1.599	48.482	5.67E-03
11.7	5.85	5.85E-06	1.1403533	1.14E-03	1.36E+12	1.36E+15	12.7	10.8	0.0000019	7.16E+20	1.766	48.020	6.81E-03
13.8	6.9	0.0000069	1.2516586	1.25E-03	9.096E+11	9.10E+14	15	12.7	0.0000023	3.95E+20	1.932	47.427	8.06E-03
16.3	8.15	8.15E-06	1.2504972	1.25E-03	5.515E+11	5.51E+14	17.7	15	0.0000027	2.04E+20	2.098	46.766	9.31E-03
19.2	9.6	0.0000096	1.2348963	1.23E-03	3.332E+11	3.33E+14	20.9	17.7	0.0000032	1.04E+20	2.262	46.092	1.05E-02
22.7	11.35	1.135E-05	1.3555447	1.36E-03	2.213E+11	2.21E+14	24.6	20.9	0.0000037	5.98E+19	2.429	45.538	1.19E-02
26.7	13.35	1.335E-05	1.2881927	1.29E-03	1.293E+11	1.29E+14	29.1	24.6	0.0000045	2.87E+19	2.592	44.804	1.32E-02
31.6	15.8	0.0000158	1.2621718	1.26E-03	7.639E+10	7.64E+13	34.3	29.1	0.0000052	1.47E+19	2.760	44.134	1.45E-02
37.2	18.6	0.0000186	1.0065021	1.01E-03	3.734E+10	3.73E+13	40.5	34.3	0.0000062	6.02E+18	2.923	43.242	1.55E-02
43.9	21.95	2.195E-05	0.805381	8.05E-04	1.818E+10	1.82E+13	47.7	40.5	0.0000072	2.53E+18	3.089	42.373	1.63E-02
51.9	25.95	2.595E-05	0.6005708	6.01E-04	8.205E+09	8.20E+12	56.3	47.7	8.6E-06	9.54E+17	3.256	41.399	1.69E-02
61.2	30.6	0.0000306	0.4735427	4.74E-04	3.946E+09	3.95E+12	66.5	56.3	0.0000102	3.87E+17	3.421	40.497	1.73E-02
72.2	36.1	0.0000361	0.3765828	3.77E-04	1.911E+09	1.91E+12	78.4	66.5	0.0000119	1.61E+17	3.586	39.618	1.77E-02
85.2	42.6	0.0000426	0.3050363	3.05E-04	941963468	9.42E+11	92.6	78.4	0.0000142	6.63E+16	3.752	38.734	1.80E-02
101.0	50.5	0.0000505	0.2290491	2.29E-04	424586205	4.25E+11	109	92.6	0.0000164	2.59E+16	3.922	37.793	1.83E-02
119.0	59.5	0.0000595	0.1704372	1.70E-04	193163432	1.93E+11	129	109	0.00002	9.66E+15	4.086	36.807	1.84E-02
140.0	70	0.00007	0.1206638	1.21E-04	83983531	8.40E+10	152	129	0.000023	3.65E+15	4.248	35.834	1.85E-02
165.0	82.5	0.0000825	0.0844136	8.44E-05	35889034	3.59E+10	180	152	0.000028	1.28E+15	4.413	34.787	1.86E-02
195.0	97.5	0.0000975	0.070702	7.07E-05	18210811	1.82E+10	212	180	0.000032	5.69E+14	4.580	33.975	1.87E-02
230.0	115	0.000115	0.068501	6.85E-05	10752638	1.08E+10	250	212	0.000038	2.83E+14	4.745	33.276	1.88E-02

d50 calculation

9.38E-03	
16.3	9.31E-03
19.2	1.05E-02
	6.87E-05
	2.93E-08
d50	**1.63E+01**

mass	68.9	mg/L
volume	1.88E-02	m3/L
density	**3.67E+03**	**mg/m3**

LCK

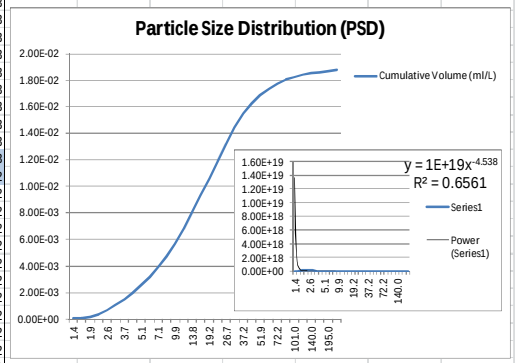

size	radius (µm)	radius(m)	volume (µl/	volume (m^	particles/L	particles/m	Upp Lim (µ	Low Lim (µ	bin size diff	no of partic	logr	logn	cum volume
1.4	0.68	6.8E-07	8.14E-01	8.14E-04	6.183E+14	6.18E+17	1.48	1.25	2.3E-07	2.69E+24	-0.386	56.251	8.14E-04
1.6	0.8	0.0000008	8.12E-01	8.12E-04	3.786E+14	3.79E+17	1.74	1.48	2.6E-07	1.46E+24	-0.223	55.638	1.63E-03
1.9	0.945	9.45E-07	8.07E-01	8.07E-04	2.282E+14	2.28E+17	2.05	1.74	3.1E-07	7.36E+23	-0.057	54.956	2.43E-03
2.2	1.115	1.115E-06	8.23E-01	8.23E-04	1.418E+14	1.42E+17	2.42	2.05	3.7E-07	3.83E+23	0.109	54.303	3.26E-03
2.6	1.315	1.315E-06	8.65E-01	8.65E-04	9.081E+13	9.08E+16	2.86	2.42	4.4E-07	2.06E+23	0.274	53.684	4.12E-03
3.1	1.555	1.555E-06	9.90E-01	9.90E-04	6.288E+13	6.29E+16	3.38	2.86	5.2E-07	1.21E+23	0.441	53.149	5.11E-03
3.7	1.835	1.835E-06	1.21E+00	1.21E-03	4.682E+13	4.68E+16	3.98	3.38	0.0000006	7.80E+22	0.607	52.711	6.32E-03
4.3	2.165	2.165E-06	1.51E+00	1.51E-03	3.55E+13	3.55E+16	4.7	3.98	7.2E-07	4.93E+22	0.772	52.252	7.83E-03
5.1	2.555	2.555E-06	1.74E+00	1.74E-03	2.493E+13	2.49E+16	5.55	4.7	8.5E-07	2.93E+22	0.938	51.733	9.57E-03
6.0	3.015	3.015E-06	2.01E+00	2.01E-03	1.749E+13	1.75E+16	6.55	5.55	0.000001	1.75E+22	1.104	51.216	1.16E-02
7.1	3.555	3.555E-06	2.35E+00	2.35E-03	1.251E+13	1.25E+16	7.72	6.55	1.17E-06	1.07E+22	1.268	50.724	1.39E-02
8.4	4.195	4.195E-06	2.61E+00	2.61E-03	8.448E+12	8.45E+15	9.12	7.72	0.0000014	6.03E+21	1.434	50.152	1.65E-02
9.9	4.95	4.95E-06	2.98E+00	2.98E-03	5.859E+12	5.86E+15	10.8	9.12	1.68E-06	3.49E+21	1.599	49.604	1.95E-02
11.7	5.85	5.85E-06	3.3395012	3.34E-03	3.982E+12	3.98E+15	12.7	10.8	0.0000019	2.10E+21	1.766	49.094	2.29E-02
13.8	6.9	0.0000069	3.6651742	3.67E-03	2.664E+12	2.66E+15	15	12.7	0.0000023	1.16E+21	1.932	48.501	2.65E-02
16.3	8.15	8.15E-06	3.8394536	3.84E-03	1.693E+12	1.69E+15	17.7	15	0.0000027	6.27E+20	2.098	47.888	3.04E-02
19.2	9.6	0.0000096	3.8519741	3.85E-03	1.039E+12	1.04E+15	20.9	17.7	0.0000032	3.25E+20	2.262	47.230	3.42E-02
22.7	11.35	1.135E-05	3.9616392	3.96E-03	6.468E+11	6.47E+14	24.6	20.9	0.0000037	1.75E+20	2.429	46.610	3.82E-02
26.7	13.35	1.335E-05	3.7372828	3.74E-03	3.75E+11	3.75E+14	29.1	24.6	0.0000045	8.33E+19	2.592	45.869	4.19E-02
31.6	15.8	0.0000158	3.4316279	3.43E-03	2.077E+11	2.08E+14	34.3	29.1	0.0000052	3.99E+19	2.760	45.134	4.54E-02
37.2	18.6	0.0000186	2.8640893	2.86E-03	1.063E+11	1.06E+14	40.5	34.3	0.0000062	1.71E+19	2.923	44.288	4.82E-02
43.9	21.95	2.195E-05	2.2102153	2.21E-03	4.989E+10	4.99E+13	47.7	40.5	0.0000072	6.93E+18	3.089	43.382	5.04E-02
51.9	25.95	2.595E-05	1.5886554	1.59E-03	2.17E+10	2.17E+13	56.3	47.7	8.6E-06	2.52E+18	3.256	42.372	5.20E-02
61.2	30.6	0.0000306	1.1678172	1.17E-03	9.73E+09	9.73E+12	66.5	56.3	0.0000102	9.54E+17	3.421	41.399	5.32E-02
72.2	36.1	0.0000361	0.8724511	8.72E-04	4.427E+09	4.43E+12	78.4	66.5	0.0000119	3.72E+17	3.586	40.458	5.41E-02
85.2	42.6	0.0000426	0.649276	6.49E-04	2.005E+09	2.00E+12	92.6	78.4	0.0000142	1.41E+17	3.752	39.489	5.47E-02
101.0	50.5	0.0000505	0.4591287	4.59E-04	851082575	8.51E+11	109	92.6	0.0000164	5.19E+16	3.922	38.488	5.52E-02
119.0	59.5	0.0000595	0.3308204	3.31E-04	374932234	3.75E+11	129	109	0.00002	1.87E+16	4.086	37.470	5.55E-02
140.0	70	0.00007	0.2460735	2.46E-04	171270311	1.71E+11	152	129	0.000023	7.45E+15	4.248	36.547	5.57E-02
165.0	82.5	0.0000825	0.1941941	1.94E-04	82563022	8.26E+10	180	152	0.000028	2.95E+15	4.413	35.620	5.59E-02
195.0	97.5	0.0000975	0.1974875	1.97E-04	50867114	5.09E+10	212	180	0.000032	1.59E+15	4.580	35.002	5.61E-02
230.0	115	0.000115	0.2622217	2.62E-04	41161055	4.12E+10	250	212	0.000038	1.08E+15	4.745	34.619	5.64E-02

d50 calculation

2.82E-02	
13.8	2.65E-02
16.3	3.04E-02
	1.67E-03
	2.56E-06
d50	**1.38E+01**

mass	105.7	mg/L
volume	5.64E-02	m3/L
density	**1.87E+03**	**mg/m3**

Sembawang

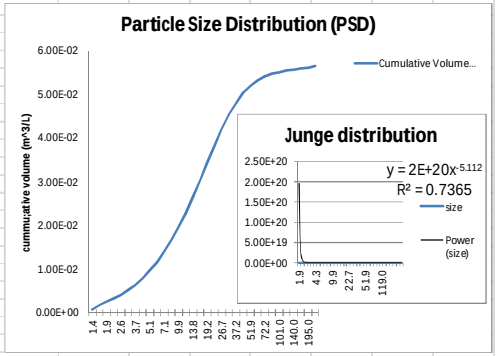

size	radius (µm)	radius(m)	volume (µl/	volume (m³	particles/L	particles/m	Upp Lim (µ	Low Lim (µ	bin size diff	no of partic	logr	logn	cum volume
1.4	0.68	6.8E-07	1.07E-01	1.07E-04	8.134E+13	8.13E+16	1.48	1.25	2.3E-07	3.54E+23	-0.386	54.223	1.07E-04
1.6	0.8	0.0000008	1.35E-01	1.35E-04	6.303E+13	6.30E+16	1.74	1.48	2.6E-07	2.42E+23	-0.223	53.845	2.42E-04
1.9	0.945	9.45E-07	1.81E-01	1.81E-04	5.126E+13	5.13E+16	2.05	1.74	3.1E-07	1.65E+23	-0.057	53.462	4.24E-04
2.2	1.115	1.115E-06	2.50E-01	2.50E-04	4.307E+13	4.31E+16	2.42	2.05	3.7E-07	1.16E+23	0.109	53.111	6.74E-04
2.6	1.315	1.315E-06	3.27E-01	3.27E-04	3.432E+13	3.43E+16	2.86	2.42	4.4E-07	7.80E+22	0.274	52.711	1.00E-03
3.1	1.555	1.555E-06	3.94E-01	3.94E-04	2.502E+13	2.50E+16	3.38	2.86	5.2E-07	4.81E+22	0.441	52.228	1.39E-03
3.7	1.835	1.835E-06	4.66E-01	4.66E-04	1.8E+13	1.80E+16	3.98	3.38	0.0000006	3.00E+22	0.607	51.755	1.86E-03
4.3	2.165	2.165E-06	6.07E-01	6.07E-04	1.428E+13	1.43E+16	4.7	3.98	7.2E-07	1.98E+22	0.772	51.342	2.47E-03
5.1	2.555	2.555E-06	7.48E-01	7.48E-04	1.07E+13	1.07E+16	5.55	4.7	8.5E-07	1.26E+22	0.938	50.887	3.22E-03
6.0	3.015	3.015E-06	8.96E-01	8.96E-04	7.807E+12	7.81E+15	6.55	5.55	0.000001	7.81E+21	1.104	50.409	4.11E-03
7.1	3.555	3.555E-06	1.10E+00	1.10E-03	5.851E+12	5.85E+15	7.72	6.55	1.17E-06	5.00E+21	1.268	49.964	5.21E-03
8.4	4.195	4.195E-06	1.24E+00	1.24E-03	4.005E+12	4.00E+15	9.12	7.72	0.0000014	2.86E+21	1.434	49.405	6.45E-03
9.9	4.95	4.95E-06	1.41E+00	1.41E-03	2.77E+12	2.77E+15	10.8	9.12	1.68E-06	1.65E+21	1.599	48.854	7.86E-03
11.7	5.85	5.85E-06	1.5092042	1.51E-03	1.8E+12	1.80E+15	12.7	10.8	0.0000019	9.47E+20	1.766	48.300	9.37E-03
13.8	6.9	0.0000069	1.4948069	1.49E-03	1.086E+12	1.09E+15	15	12.7	0.0000023	4.72E+20	1.932	47.604	1.09E-02
16.3	8.15	8.15E-06	1.3468308	1.35E-03	5.94E+11	5.94E+14	17.7	15	0.0000027	2.20E+20	2.098	46.840	1.22E-02
19.2	9.6	0.0000096	1.1613257	1.16E-03	3.134E+11	3.13E+14	20.9	17.7	0.0000032	9.79E+19	2.262	46.031	1.34E-02
22.7	11.35	1.135E-05	1.0389665	1.04E-03	1.696E+11	1.70E+14	24.6	20.9	0.0000037	4.58E+19	2.429	45.272	1.44E-02
26.7	13.35	1.335E-05	0.8291799	8.29E-04	8.32E+10	8.32E+13	29.1	24.6	0.0000045	1.85E+19	2.592	44.364	1.52E-02
31.6	15.8	0.0000158	0.6623049	6.62E-04	4.009E+10	4.01E+13	34.3	29.1	0.0000052	7.71E+18	2.760	43.489	1.59E-02
37.2	18.6	0.0000186	0.472226	4.72E-04	1.752E+10	1.75E+13	40.5	34.3	0.0000062	2.83E+18	2.923	42.485	1.64E-02
43.9	21.95	2.195E-05	0.3306368	3.31E-04	7.464E+09	7.46E+12	47.7	40.5	0.0000072	1.04E+18	3.089	41.483	1.67E-02
51.9	25.95	2.595E-05	0.2213475	2.21E-04	3.024E+09	3.02E+12	56.3	47.7	8.6E-06	3.52E+17	3.256	40.401	1.69E-02
61.2	30.6	0.0000306	0.1507893	1.51E-04	1.256E+09	1.26E+12	66.5	56.3	0.0000102	1.23E+17	3.421	39.352	1.71E-02
72.2	36.1	0.0000361	0.1071732	1.07E-04	543846092	5.44E+11	78.4	66.5	0.0000119	4.57E+16	3.586	38.361	1.72E-02
85.2	42.6	0.0000426	0.0762589	7.63E-05	235490271	2.35E+11	92.6	78.4	0.0000142	1.66E+16	3.752	37.347	1.73E-02
101.0	50.5	0.0000505	0.0538274	5.38E-05	99779272	9.98E+10	109	92.6	0.0000164	6.08E+15	3.922	36.344	1.73E-02
119.0	59.5	0.0000595	0.0374661	3.75E-05	42461859	4.25E+10	129	109	0.00002	2.12E+15	4.086	35.292	1.74E-02
140.0	70	0.00007	0.0263832	2.64E-05	18363064	1.84E+10	152	129	0.000023	7.98E+14	4.248	34.314	1.74E-02
165.0	82.5	0.0000825	0.0191591	1.92E-05	8145642.4	8.15E+09	180	152	0.000028	2.91E+14	4.413	33.304	1.74E-02
195.0	97.5	0.0000975	0.018854	1.89E-05	4856242.8	4.86E+09	212	180	0.000032	1.52E+14	4.580	32.653	1.74E-02
230.0	115	0.000115	0.0277542	2.78E-05	4356594.3	4.36E+09	250	212	0.000038	1.15E+14	4.745	32.373	1.74E-02

d50 calculation

8.72E-03	
9.9	7.86E-03
11.7	9.37E-03
	8.63E-04
	7.23E-07
d50	9.90E+00

mass 75 mg/L
volume 1.74E-02 m3/L
density **4.30E+03 mg/m3**

Bedok

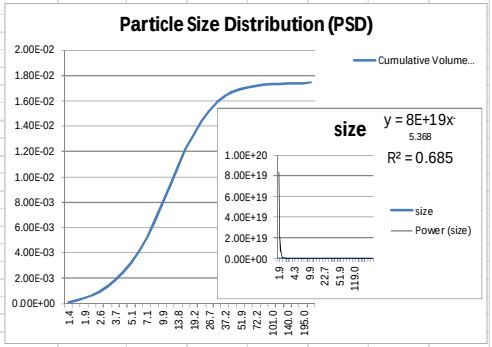

size	radius (µm)	radius(m)	volume (µl/	volume (m³	particles/L	particles/m	Upp Lim (µ	Low Lim (µ	bin size diff	no of partic	logr	logn	cum volume
1.4	0.68	6.8E-07	4.94E-01	4.94E-04	3.751E+14	3.75E+17	1.48	1.25	2.3E-07	1.63E+24	-0.386	55.751	4.94E-04
1.6	0.8	0.0000008	4.87E-01	4.87E-04	2.27E+14	2.27E+17	1.74	1.48	2.6E-07	8.73E+23	-0.223	55.126	9.81E-04
1.9	0.945	9.45E-07	4.67E-01	4.67E-04	1.32E+14	1.32E+17	2.05	1.74	3.1E-07	4.26E+23	-0.057	54.408	1.45E-03
2.2	1.115	1.115E-06	4.16E-01	4.16E-04	7.166E+13	7.17E+16	2.42	2.05	3.7E-07	1.94E+23	0.109	53.620	1.86E-03
2.6	1.315	1.315E-06	3.75E-01	3.75E-04	3.937E+13	3.94E+16	2.86	2.42	4.4E-07	8.95E+22	0.274	52.848	2.24E-03
3.1	1.555	1.555E-06	3.53E-01	3.53E-04	2.241E+13	2.24E+16	3.38	2.86	5.2E-07	4.31E+22	0.441	52.118	2.59E-03
3.7	1.835	1.835E-06	3.89E-01	3.89E-04	1.501E+13	1.50E+16	3.98	3.38	0.0000006	2.50E+22	0.607	51.574	2.98E-03
4.3	2.165	2.165E-06	4.81E-01	4.81E-04	1.131E+13	1.13E+16	4.7	3.98	7.2E-07	1.57E+22	0.772	51.109	3.46E-03
5.1	2.555	2.555E-06	5.65E-01	5.65E-04	8.084E+12	8.08E+15	5.55	4.7	8.5E-07	9.51E+21	0.938	50.607	4.03E-03
6.0	3.015	3.015E-06	6.29E-01	6.29E-04	5.475E+12	5.48E+15	6.55	5.55	0.000001	5.48E+21	1.104	50.055	4.65E-03
7.1	3.555	3.555E-06	6.93E-01	6.93E-04	3.68E+12	3.68E+15	7.72	6.55	1.17E-06	3.15E+21	1.268	49.500	5.35E-03
8.4	4.195	4.195E-06	6.93E-01	6.93E-04	2.242E+12	2.24E+15	9.12	7.72	0.0000014	1.60E+21	1.434	48.825	6.04E-03
9.9	4.95	4.95E-06	6.91E-01	6.91E-04	1.36E+12	1.36E+15	10.8	9.12	1.68E-06	8.10E+20	1.599	48.143	6.73E-03
11.7	5.85	5.85E-06	0.6812083	6.81E-04	8.123E+11	8.12E+14	12.7	10.8	0.0000019	4.28E+20	1.766	47.505	7.41E-03
13.8	6.9	0.0000069	0.6630229	6.63E-04	4.818E+11	4.82E+14	15	12.7	0.0000023	2.09E+20	1.932	46.791	8.08E-03
16.3	8.15	8.15E-06	0.6553804	6.55E-04	2.89E+11	2.89E+14	17.7	15	0.0000027	1.07E+20	2.098	46.120	8.73E-03
19.2	9.6	0.0000096	0.6444177	6.44E-04	1.739E+11	1.74E+14	20.9	17.7	0.0000032	5.43E+19	2.262	45.442	9.38E-03
22.7	11.35	1.135E-05	0.6731861	6.73E-04	1.099E+11	1.10E+14	24.6	20.9	0.0000037	2.97E+19	2.429	44.838	1.00E-02
26.7	13.35	1.335E-05	0.6844003	6.84E-04	6.867E+10	6.87E+13	29.1	24.6	0.0000045	1.53E+19	2.592	44.172	1.07E-02
31.6	15.8	0.0000158	0.7048426	7.05E-04	4.266E+10	4.27E+13	34.3	29.1	0.0000052	8.20E+18	2.760	43.551	1.14E-02
37.2	18.6	0.0000186	0.678267	6.78E-04	2.516E+10	2.52E+13	40.5	34.3	0.0000062	4.06E+18	2.923	42.847	1.21E-02
43.9	21.95	2.195E-05	0.6285088	6.29E-04	1.419E+10	1.42E+13	47.7	40.5	0.0000072	1.97E+18	3.089	42.125	1.27E-02
51.9	25.95	2.595E-05	0.5454379	5.45E-04	7.452E+09	7.45E+12	56.3	47.7	8.6E-06	8.66E+17	3.256	41.303	1.33E-02
61.2	30.6	0.0000306	0.5283939	5.28E-04	4.403E+09	4.40E+12	66.5	56.3	0.0000102	4.32E+17	3.421	40.606	1.38E-02
72.2	36.1	0.0000361	0.5400052	5.40E-04	2.74E+09	2.74E+12	78.4	66.5	0.0000119	2.30E+17	3.586	39.978	1.44E-02
85.2	42.6	0.0000426	0.5488631	5.49E-04	1.695E+09	1.69E+12	92.6	78.4	0.0000142	1.19E+17	3.752	39.321	1.49E-02
101.0	50.5	0.0000505	0.4654705	4.65E-04	862838356	8.63E+11	109	92.6	0.0000164	5.26E+16	3.922	38.502	1.54E-02
119.0	59.5	0.0000595	0.3742768	3.74E-04	424183092	4.24E+11	129	109	0.00002	2.12E+16	4.086	37.593	1.57E-02
140.0	70	0.00007	0.25919	2.59E-04	180399596	1.80E+11	152	129	0.000023	7.84E+15	4.248	36.598	1.60E-02
165.0	82.5	0.0000825	0.1716459	1.72E-04	72976487	7.30E+10	180	152	0.000028	2.61E+15	4.413	35.497	1.62E-02
195.0	97.5	0.0000975	0.1709774	1.71E-04	44038877	4.40E+10	212	180	0.000032	1.38E+15	4.580	34.858	1.63E-02
230.0	115	0.000115	0.268121	2.68E-04	42087063	4.21E+10	250	212	0.000038	1.11E+15	4.745	34.641	1.66E-02

d50 calculation

8.31E-03	
13.8	8.08E-03
16.3	8.73E-03
	2.33E-04
	6.11E-08
d50	1.38E+01

mass mg/L
volume 1.66E-02 m3/L
density **0.00E+00 mg/m3**

Serangoon

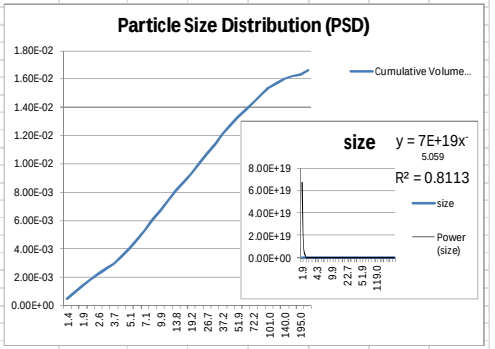

size	radius (µm)	radius(m)	volume (µl/	volume (m³	particles/L	particles/m	Upp Lim (µ	Low Lim (µ	bin size diff	no of partic	logr	logn	cum volume
1.4	0.68	6.8E-07	1.29E+01	1.29E-02	9.811E+15	9.81E+18	1.48	1.25	2.3E-07	4.27E+25	-0.386	59.015	1.29E-02
1.6	0.8	0.0000008	9.32E+00	9.32E-03	4.346E+15	4.35E+18	1.74	1.48	2.6E-07	1.67E+25	-0.223	58.078	2.22E-02
1.9	0.945	9.45E-07	6.03E+00	6.03E-03	1.705E+15	1.70E+18	2.05	1.74	3.1E-07	5.50E+24	-0.057	56.967	2.83E-02
2.2	1.115	1.115E-06	3.82E+00	3.82E-03	6.581E+14	6.58E+17	2.42	2.05	3.7E-07	1.78E+24	0.109	55.838	3.21E-02
2.6	1.315	1.315E-06	2.75E+00	2.75E-03	2.892E+14	2.89E+17	2.86	2.42	4.4E-07	6.57E+23	0.274	54.842	3.48E-02
3.1	1.555	1.555E-06	2.73E+00	2.73E-03	1.731E+14	1.73E+17	3.38	2.86	5.2E-07	3.33E+23	0.441	54.162	3.76E-02
3.7	1.835	1.835E-06	3.41E+00	3.41E-03	1.317E+14	1.32E+17	3.98	3.38	0.0000006	2.20E+23	0.607	53.746	4.10E-02
4.3	2.165	2.165E-06	4.02E+00	4.02E-03	9.464E+13	9.46E+16	4.7	3.98	7.2E-07	1.31E+23	0.772	53.233	4.50E-02
5.1	2.555	2.555E-06	4.39E+00	4.39E-03	6.289E+13	6.29E+16	5.55	4.7	8.5E-07	7.40E+22	0.938	52.658	4.94E-02
6.0	3.015	3.015E-06	4.93E+00	4.93E-03	4.294E+13	4.29E+16	6.55	5.55	0.000001	4.29E+22	1.104	52.114	5.43E-02
7.1	3.555	3.555E-06	5.29E+00	5.29E-03	2.81E+13	2.81E+16	7.72	6.55	1.17E-06	2.40E+22	1.268	51.533	5.96E-02
8.4	4.195	4.195E-06	5.26E+00	5.26E-03	1.702E+13	1.70E+16	9.12	7.72	0.0000014	1.22E+22	1.434	50.852	6.49E-02
9.9	4.95	4.95E-06	5.03E+00	5.03E-03	9.903E+12	9.90E+15	10.8	9.12	1.68E-06	5.89E+21	1.599	50.128	6.99E-02
11.7	5.85	5.85E-06	4.5641357	4.56E-03	5.443E+12	5.44E+15	12.7	10.8	0.0000019	2.86E+21	1.766	49.407	7.45E-02
13.8	6.9	0.0000069	4.0859462	4.09E-03	2.969E+12	2.97E+15	15	12.7	0.0000023	1.29E+21	1.932	48.610	7.86E-02
16.3	8.15	8.15E-06	3.6488503	3.65E-03	1.609E+12	1.61E+15	17.7	15	0.0000027	5.96E+20	2.098	47.837	8.22E-02
19.2	9.6	0.0000096	3.0920664	3.09E-03	8.343E+11	8.34E+14	20.9	17.7	0.0000032	2.61E+20	2.262	47.010	8.53E-02
22.7	11.35	1.135E-05	2.414717	2.41E-03	3.943E+11	3.94E+14	24.6	20.9	0.0000037	1.07E+20	2.429	46.115	8.77E-02
26.7	13.35	1.335E-05	1.8568597	1.86E-03	1.863E+11	1.86E+14	29.1	24.6	0.0000045	4.14E+19	2.592	45.170	8.96E-02
31.6	15.8	0.0000158	1.3258064	1.33E-03	8.025E+10	8.02E+13	34.3	29.1	0.0000052	1.54E+19	2.760	44.183	9.09E-02
37.2	18.6	0.0000186	0.9992926	9.99E-04	3.707E+10	3.71E+13	40.5	34.3	0.0000062	5.98E+18	2.923	43.235	9.19E-02
43.9	21.95	2.195E-05	0.6837176	6.84E-04	1.543E+10	1.54E+13	47.7	40.5	0.0000072	2.14E+18	3.089	42.209	9.26E-02
51.9	25.95	2.595E-05	0.4678581	4.68E-04	6.392E+09	6.39E+12	56.3	47.7	8.6E-06	7.43E+17	3.256	41.150	9.31E-02
61.2	30.6	0.0000306	0.3343602	3.34E-04	2.786E+09	2.79E+12	66.5	56.3	0.0000102	2.73E+17	3.421	40.149	9.34E-02
72.2	36.1	0.0000361	0.2730143	2.73E-04	1.385E+09	1.39E+12	78.4	66.5	0.0000119	1.16E+17	3.586	39.296	9.37E-02
85.2	42.6	0.0000426	0.2276381	2.28E-04	702954943	7.03E+11	92.6	78.4	0.0000142	4.95E+16	3.752	38.441	9.39E-02
101.0	50.5	0.0000505	0.1844856	1.84E-04	341979265	3.42E+11	109	92.6	0.0000164	2.09E+16	3.922	37.576	9.41E-02
119.0	59.5	0.0000595	0.1415346	1.42E-04	160406919	1.60E+11	129	109	0.00002	8.02E+15	4.086	36.621	9.42E-02
140.0	70	0.00007	0.1026131	1.03E-04	71420021	7.14E+10	152	129	0.000023	3.11E+15	4.248	35.672	9.43E-02
165.0	82.5	0.0000825	0.0751851	7.52E-05	31965468	3.20E+10	180	152	0.000028	1.14E+15	4.413	34.671	9.44E-02
195.0	97.5	0.0000975	0.0895071	8.95E-05	23054465	2.31E+10	212	180	0.000032	7.20E+14	4.580	34.211	9.45E-02
230.0	115	0.000115	0.2171806	2.17E-04	34090939	3.41E+10	250	212	0.000038	8.97E+14	4.745	34.430	9.47E-02

d50 calculation

4.73E-02	
4.3	4.50E-02
5.1	4.94E-02
	2.34E-03
	1.32E-05
d50	4.33E+00

Tekong1

mass mg/L
volume 9.47E-02 m3/L
density **0.00E+00 mg/m3**

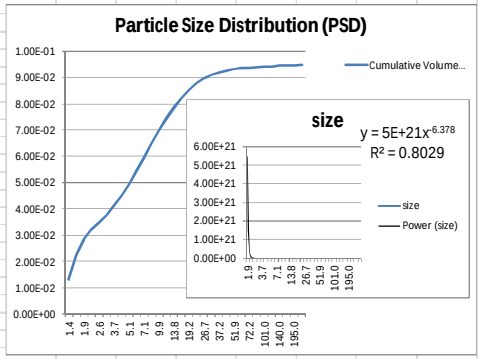

size	radius (µm)	radius(m)	volume (µl/	volume (m³	particles/L	particles/m	Upp Lim (µ	Low Lim (µ	bin size diff	no of partic	logr	logn	cum volume
1.4	0.68	6.8E-07	2.03E-01	2.03E-04	1.538E+14	1.54E+17	1.48	1.25	2.3E-07	6.69E+23	-0.386	54.860	2.03E-04
1.6	0.8	0.0000008	2.04E-01	2.04E-04	9.527E+13	9.53E+16	1.74	1.48	2.6E-07	3.66E+23	-0.223	54.258	4.07E-04
1.9	0.945	9.45E-07	2.05E-01	2.05E-04	5.803E+13	5.80E+16	2.05	1.74	3.1E-07	1.87E+23	-0.057	53.586	6.12E-04
2.2	1.115	1.115E-06	2.06E-01	2.06E-04	3.549E+13	3.55E+16	2.42	2.05	3.7E-07	9.59E+22	0.109	52.918	8.18E-04
2.6	1.315	1.315E-06	2.10E-01	2.10E-04	2.2E+13	2.20E+16	2.86	2.42	4.4E-07	5.00E+22	0.274	52.266	1.03E-03
3.1	1.555	1.555E-06	2.23E-01	2.23E-04	1.416E+13	1.42E+16	3.38	2.86	5.2E-07	2.72E+22	0.441	51.659	1.25E-03
3.7	1.835	1.835E-06	2.52E-01	2.52E-04	9.729E+12	9.73E+15	3.98	3.38	0.0000006	1.62E+22	0.607	51.140	1.50E-03
4.3	2.165	2.165E-06	2.95E-01	2.95E-04	6.935E+12	6.93E+15	4.7	3.98	7.2E-07	9.63E+21	0.772	50.619	1.80E-03
5.1	2.555	2.555E-06	3.32E-01	3.32E-04	4.752E+12	4.75E+15	5.55	4.7	8.5E-07	5.59E+21	0.938	50.075	2.13E-03
6.0	3.015	3.015E-06	3.72E-01	3.72E-04	3.243E+12	3.24E+15	6.55	5.55	0.000001	3.24E+21	1.104	49.531	2.50E-03
7.1	3.555	3.555E-06	4.11E-01	4.11E-04	2.186E+12	2.19E+15	7.72	6.55	1.17E-06	1.87E+21	1.268	48.979	2.91E-03
8.4	4.195	4.195E-06	4.22E-01	4.22E-04	1.365E+12	1.36E+15	9.12	7.72	0.0000014	9.75E+20	1.434	48.329	3.33E-03
9.9	4.95	4.95E-06	4.32E-01	4.32E-04	8.502E+11	8.50E+14	10.8	9.12	1.68E-06	5.06E+20	1.599	47.673	3.77E-03
11.7	5.85	5.85E-06	0.4225778	4.23E-04	5.039E+11	5.04E+14	12.7	10.8	0.0000019	2.65E+20	1.766	47.027	4.19E-03
13.8	6.9	0.0000069	0.3980581	3.98E-04	2.893E+11	2.89E+14	15	12.7	0.0000023	1.26E+20	1.932	46.281	4.59E-03
16.3	8.15	8.15E-06	0.3582307	3.58E-04	1.58E+11	1.58E+14	17.7	15	0.0000027	5.85E+19	2.098	45.516	4.95E-03
19.2	9.6	0.0000096	0.3090553	3.09E-04	8.339E+10	8.34E+13	20.9	17.7	0.0000032	2.61E+19	2.262	44.707	5.25E-03
22.7	11.35	1.135E-05	0.2635315	2.64E-04	4.303E+10	4.30E+13	24.6	20.9	0.0000037	1.16E+19	2.429	43.900	5.52E-03
26.7	13.35	1.335E-05	0.2072977	2.07E-04	2.08E+10	2.08E+13	29.1	24.6	0.0000045	4.62E+18	2.592	42.977	5.73E-03
31.6	15.8	0.0000158	0.1571483	1.57E-04	9.512E+09	9.51E+12	34.3	29.1	0.0000052	1.83E+18	2.760	42.050	5.88E-03
37.2	18.6	0.0000186	0.112464	1.12E-04	4.172E+09	4.17E+12	40.5	34.3	0.0000062	6.73E+17	2.923	41.050	6.00E-03
43.9	21.95	2.195E-05	0.0751432	7.51E-05	1.696E+09	1.70E+12	47.7	40.5	0.0000072	2.36E+17	3.089	40.001	6.07E-03
51.9	25.95	2.595E-05	0.0482285	4.82E-05	658875682	6.59E+11	56.3	47.7	8.6E-06	7.66E+16	3.256	38.878	6.12E-03
61.2	30.6	0.0000306	0.0321755	3.22E-05	268085270	2.68E+11	66.5	56.3	0.0000102	2.63E+16	3.421	37.808	6.15E-03
72.2	36.1	0.0000361	0.023397	2.34E-05	118727283	1.19E+11	78.4	66.5	0.0000119	9.98E+15	3.586	36.839	6.17E-03
85.2	42.6	0.0000426	0.0172682	1.73E-05	53324848	5.33E+10	92.6	78.4	0.0000142	3.76E+15	3.752	35.862	6.19E-03
101.0	50.5	0.0000505	0.0122897	1.23E-05	22781262	2.28E+10	109	92.6	0.0000164	1.39E+15	3.922	34.867	6.20E-03
119.0	59.5	0.0000595	0.0084337	8.43E-06	9558203.3	9.56E+09	129	109	0.00002	4.78E+14	4.086	33.800	6.21E-03
140.0	70	0.00007	0.0054736	5.47E-06	3809666.8	3.81E+09	152	129	0.000023	1.66E+14	4.248	32.741	6.22E-03
165.0	82.5	0.0000825	0.0034379	3.44E-06	1461652.7	1.46E+09	180	152	0.000028	5.22E+13	4.413	31.586	6.22E-03
195.0	97.5	0.0000975	0.0033435	3.34E-06	861180.68	8.61E+08	212	180	0.000032	2.69E+13	4.580	30.924	6.22E-03
230.0	115	0.000115	0.0063623	6.36E-06	998687.07	9.99E+08	250	212	0.000038	2.63E+13	4.745	30.900	6.23E-03

d50 calculation

3.12E-03	
7.1	2.91E-03
8.4	3.33E-03
	2.02E-04
	6.67E-08
d50	7.11E+00

Tekong2

mass mg/L
volume 6.23E-03 m3/L
density **0.00E+00 mg/m3**